**Astrophysics and Space Science Proceedings** 

André Moitinho João Alves *Editors* 

# Star Clusters in the Era of Large Surveys

Proceedings of Symposium 5 of JENAM 2010





# Star Clusters in the Era of Large Surveys

Proceedings of Symposium 5 of JENAM 2010

**Editors** 

André Moitinho João Alves







Editors
André Moitinho
SIM
Fac. de Ciências da Univ. de
Lisboa
Campo Grande, Edifício C8
1749-016 Lisbon
Portugal
andre@sim.ul.pt

João Alves Institute of Astronomy Türkenschanzstrasse 17 1180 Vienna Austria joao.alves@univie.ac.at

ISSN 1570-6591 ISBN 978-3-642-22112-5 DOI 10.1007/978-3-642-22113-2

e-ISSN 1570-6605 e-ISBN 978-3-642-22113-2

Springer Heidelberg Dordrecht London New York

Library of Congress Control Number: 2011939489

© Springer-Verlag Berlin Heidelberg 2012

This work is subject to copyright. All rights are reserved, whether the whole or part of the material is concerned, specifically the rights of translation, reprinting, reuse of illustrations, recitation, broadcasting, reproduction on microfilm or in any other way, and storage in data banks. Duplication of this publication or parts thereof is permitted only under the provisions of the German Copyright Law of September 9, 1965, in its current version, and permission for use must always be obtained from Springer. Violations are liable to prosecution under the German Copyright Law.

The use of general descriptive names, registered names, trademarks, etc. in this publication does not imply, even in the absence of a specific statement, that such names are exempt from the relevant protective laws and regulations and therefore free for general use.

Cover design: eStudio Calamar S.L.

Printed on acid-free paper

Springer is part of Springer Science+Business Media (www.springer.com)

#### **Preface**

Stars form mainly in clustered mode. Over time, these clusters evaporate and/or disrupt, enriching the general field population. Cluster lifetimes can vary enormously, ranging from a large population of short lived individuals that get shattered in a few Myr while emerging from their parent clouds, to old globular clusters that have been inhabiting the halo of Milky Way for more than 12 Gyr.

These characteristics confer multiple roles to the star cluster population. As stellar birth sites they are laboratories for studying local and large scale star formation processes, and later on, stellar evolution. Emergence from their gaseous and dusty cocoons highlights the interaction of stellar systems with the interstellar medium (ISM): If on one side, stellar winds will blow away the surrounding medium, on the other side, this sweeping of the ISM will have dramatic consequences on the kinematics of cluster stars, affect a cluster's morphology, star loss to the field and even its survival. Analysis of the Galactic cluster population, either as a whole or in age groups has already provided a wealth of insight on the morphology and dynamics of spiral arms, the various scales of Milky Way (disk heights, distance to Galactic centre, extension of the warp, flare, and others), Galactic rotation, formation and development of the Milky Way.

Estimates indicate that the Milky Way has around 200 billion stars (number growing every few years) and presently hosts  $\sim 10^5$  or more star clusters. However, only about 2,500 open clusters have been identified and constitute a sample affected by several well known selection effects. Less than a half of these clusters has actually been studied, and this subset suffers from further selection biases.

Given the estimated number of present day clusters, one would expect that available all sky surveys would have produced many thousands of identifications. Yet, only  $\sim$ 1,300 clusters, i.e. 1/3 of the optically visible clusters ( $\sim$ 600 of 1,800) and most of the infrared clusters ( $\sim$ 700), have been discovered through automatic or semi-automatic searches on large scale survey data products from ground based (mainly DSS, 2MASS and GLIMPSE), and space (Hipparcos) endeavours. Expectations are that the new generation of all sky surveys (UKIDSS, the VISTA-based VHS and VVV, and Gaia) will add many more.

vi Preface

The symposium "Star Clusters in the Era of Large Surveys" was held in Lisbon on Sep 9–10 during JENAM 2010. It has been a meeting point for discussing what and how can recent, on-going and planned large area surveys from ground and space, availability of efficient reduction pipelines, development of analysis algorithms and access to databases around the world, contribute to produce a leap in this research field that has a strong European history.

Science topics addressed included:

- Cluster searches
- Clustered vs isolated star formation, large scale star formation, enrichment of the field population
- Structure, populations and evolution of the Milky Way
- Cluster dynamics (internal and within the Milky Way)
- Variability of stars in clusters (from time resolved surveys)
- Analysis techniques for large samples
- Archiving

By any measure the meeting was a great success, proving that the time was right for it. The credit for this goes to all the participants who made the meeting reach beyond the mere presentation into a forum of prolific discussions. The "official provokers" appointed by the SOC helped immensely by stimulating hours of lively and fruitful debate. We thank the SOC for this and for enforcing a very focused program which generated the good level of discussion during the meeting. It was hard to leave well known researchers outside of the program, but in hindsight it was the right decision. Finally, if only one thought remains from the meeting it is that stellar clusters are indeed unique and fundamental tools to investigate a series of important astrophysical problems, from planet formation to galaxy evolution. And that the time to study clusters is *now*.

The invited "provokers" were Coryn Bailer-Jones, Emmanuel Bertin, Eli Bressert, Laurent Eyer, Simon Goodwin, Simon Hodgkin, David Martínez-Delgado, Giusi Micela, Nickolas Moeckel, Estelle Moraux, Tim Naylor, Martin Netopil, Sofia Randich, John Stauffer, Paolo Ventura, Günther Wuchterl and Hans Zinnecker.

We would like to thank the tireless help of staff at the SIM laboratory and the Faculty of Science of the University of Lisbon. Very special thanks to the LOC and its extremely helpful and kind crew of student volunteers: Alexandra Guerreiro, Ana Matos, Andreia Ribeiro, André Viana, Daniela Bolrão, Diogo Pereira, Gil Marques, Gustavo Mil-Homens, Gustavo Sousa, Joana Oliveira, Joana Pires, João Calhau, João Resende, João Retrê, Mariana Vargas, João Faria, Raul Mendes, Pedro Carvas, Salomé Matos and Susana Fernandes.

The meeting would have not been possible without the support of the European Astronomical Society, the Portuguese Astronomical Society and the Portuguese Foundation for Science and Technology.

Lisbon, André Moitinho
Vienna João Alves

Preface vii

#### **Scientific Organising Committee**

André Moitinho (Portugal) Chair João Alves (Austria) Co-Chair Joana Ascenso (Portugal) Jerôme Bouvier (France) Giovanni Carraro (ESO) Wilton S. Dias (Brazil) Janet Drew (UK) Mark Gieles (UK) Valentin Ivanov (ESO)

#### **Local Organising Committee**

André Moitinho (SIM- U. Lisbon) Eduardo Amôres (SIM - U. Lisbon) Joana Ascenso (CAUP) Ângela Antunes (SIM- U. Lisbon) Raquel Brito (SIM- U. Lisbon)

#### **Sponsors**









#### FCT Fundação para a Ciência e a Tecnologia

MINISTÉRIO DA CIÊNCIA, TECNOLOGIA E ENSINO SUPERIOR

viii Preface



#### **Contents**

#### Part I Recent, On-going and Planned Surveys: Cluster **Searches: Technical Challenges** Optical Digital Galactic Plane Surveys and Star-Cluster Science ...... 3 Janet E. Drew, Roberto Raddi, and the EGAPS Consortia Census of Milky Way Star Clusters from Infrared Surveys..... 13 Valentin D. Ivanov Time-Resolved Surveys of Stellar Clusters 21 Laurent Eyer, Patrick Eggenberger, Claudia Greco, Sophie Saesen, Richard I. Anderson, and Nami Mowlavi SDSS-III/APOGEE: Detailed Abundances of Galactic Star Clusters..... 31 Peter M. Frinchaboy, Gail Zasowski, Kelly Jackson, Jennifer A. Johnson, Steven R. Majewski, Matthew Shetrone, Aaron Rocha, and the SDSS-III collaboration Processing Data from Large Infrared Surveys..... 39 Simon Hodgkin, Mike Irwin, Jim Lewis, Eduardo Gonzalez-Solares, and Aybüke Küpcü Yoldaş **Properties of Star Clusters Found and Investigated by Data** from Large Surveys ..... 47 Elena V. Glushkova, Sergey E. Koposov, Ivan Yu. Zolotukhin, and Ramakant S. Yadav Developments of the Open Cluster Database WEBDA ..... 53 Martin Netopil, Ernst Paunzen, and Christian Stütz **Inferring Stellar Properties Using Colours, Parallaxes** and an HRD Prior 63 Coryn A.L. Bailer-Jones

x Contents

<b>Astr</b> <i>O</i> matic Software in the Era of Large Stellar Photometric Surveys Emmanuel Bertin, Philippe Delorme, and Hervé Bouy	71
Cluster Parameter Determinations for Large Datasets	79
Open Clusters Science in the Virtual Observatory Era	87
GALExtin: A VO-Service for Estimating Galactic Interstellar Extinction Eduardo Amôres, André Moitinho, Vladan Arsenijevic, and Laerte Sodré	93
YSO Clusters on Galactic Infrared Loops Gábor Marton, Zoltán Tamás Kiss, L. Viktor Tóth, Sarolta Zahorecz, László Pásztor, Munateka Ueno, Yoshimi Kitamura, Motohide Tamura, Akiko Kawamura, and Toshikazu Onishi	97
VVV Search for New Young Clusters Towards the Star Forming Regions in Our Galaxy: First Results  Jura Borissova, Radostin Kurtev, Stuart Folkes, Étienne Artigau, Valentin Ivanov, Dante Minniti, Philip Lucas, Francisco Penaloza, Stuart Sale, Eduardo Bica, Charles Bonatto, Márcio Catelan, Maren Hempel, Monica Zoccali, Ignacio Toledo, Douglas Geisler, Christian Moni Bidin, Andrea Ahumada, Rodolfo Barba, Richard de Grijs, Andrés Jordán, and Gustavo Baume	101
New Milky Way Star Cluster Candidates from DSS and 2MASS	105
VVV Study of the Young Milky Way Star Clusters: Mercer 35, 69 and 70	109
Part II Star Formation & Evolution. The Milky Way and Beyond	
Optical Surveys of Young Open Clusters	115
Probing the Low-Mass End of the IMF in Star-Forming Regions: A WIRCam/CFHT Survey  Catarina Alves de Oliveira, Estelle Moraux, Jerôme Bouvier,  Andrew Burgess, Hervé Bouy, Chiara Marmo, and Patrick Hudelot	125

<b>Dynamics in the Embedded Phase: Accretion, Collisions, Contraction</b> Nickolas Moeckel	131
Unraveling the Initial Conditions of Star Formation in Serpens North  Ana Duarte-Cabral, Nicolas Peretto, Gary A. Fuller, and Clare L. Dobbs	139
<b>Do All Stars in the Solar Neighbourhood Form in Clusters?</b> Eli Bressert, Nate Bastian, and Robert Gutermuth	147
Uncertainties in the Age Scale for Young Open Clusters and Moving Groups  John R. Stauffer	155
Are There Age Spreads in Star Forming Regions?  Rob D. Jeffries	163
The Relevance of X-ray Surveys for the Study of the Properties of Young Open Clusters	171
Chandra Observations of Cygnus OB2	179
Young Massive Stellar Clusters in the Milky Way: the Cl1813-178 and GLIMPSE 9 Clusters  Maria Messineo, Ben Davies, Donald F. Figer, Christine Trombley, Elena Valenti, Francisco Najarro, John MacKenty, Karl Menten, R. Michael Rich, Rolf P. Kudritzki, Simon Clark, and Valentiv Ivanov	185
Multiple Populations in Globular Clusters: The Role of AGB and Super-AGB Stars	191
Chemical Properties of the Open Cluster Population	199
Deep and Extended Multiband Photometry of the Galactic Globular Cluster M71  Alessandra Di Cecco, Giuseppe Bono, Matteo Monelli, Peter B. Stetson, Rosa Becucci, Scilla Degl'Innocenti, Pier G. Prada Moroni, and Roberto Buonanno	207
Chromospheric Activity and Lithium Abundance in NGC2516	211
A Deep Photometric Survey of the Double Cluster h & χ Per	213

xii Contents

A Detailed Spectroscopic Analysis of the Open Cluster NGC 5460  Luca Fossati, Colin P. Folsom, Stefano Bagnulo, Jason Grunhut,  John Landstreet, Oleg Kochukhov, Claudia Paladini,  and Gregg A. Wade	215
A Kinematic Study of Open Clusters: Implications for Origin	217
The Luminosity Function of Globular Clusters Used As a Distance Indicator	219
Chemical Properties of the Hipparcos Red Clump	221
Chemical Composition of a Kinematically Identified Stellar Group in the Milky Way  Edita Stonkutė, Gražina Tautvaišienė, Birgitta Nordström, and Renata Ženovienė	223
Star Disk Interaction in T Tauri Stars: Analysis of the MgII Lines	225
Indication of Mass Segregation in LMC Star Clusters	227
Carbon and Nitrogen As Tracers of Stellar Evolution in Red Clump Stars of Open Clusters Gražina Tautvaišienė and Šarūnas Mikolaitis	229
Observations of the IMF in Clusters  Joana Ascenso and João Alves	231
Dynamical Evolution of Rotating Globular Clusters with Embedded Black Holes Jose Fiestas and Rainer Spurzem	235
Stellar Populations in the Super Star Clusters NGC 3603 and 30 Doradus  Loredana Spezzi, Giacomo Beccari, Guido De Marchi, Francesco Paresce, Marco Sirianni, Morten Andersen, Nino Panagia, and the WFC3 SOC	239
Dynamical Expansion of Star Clusters	241
The Metallicity Gradient in the Galactic Disk Revealed by Cepheids and Open Clusters  Patricia Cruz and Jacques R.D. Lépine	245

Contents xiii

Spitzer's View of NGC2264's Circumstellar Disk Population	249
Super Star Clusters in IR-Luminous Interacting Galaxies: The NIR Luminosity Function Petri Väisänen, Zara Randriamanakoto, Stuart Ryder, and Seppo Mattila	251
Populations of Variable Stars in Open Clusters	255
Tracing the Structure of the Perseus Arm with IPHAS	259
Setting up the T35 Telescope at Sierra Nevada Observatory for Detecting Variable Stars in Open Clusters  Susana Martín-Ruiz, Francisco J. Aceituno, and Juan Gutiérrez Soto	261
<b>The Substellar Population of the</b> σ <b>Orionis Cluster</b>	263

### Part I Recent, On-going and Planned Surveys: Cluster Searches: Technical Challenges

Coverage of proper motion surveys of the Pleiades. From E. Bertin et al., this volume.

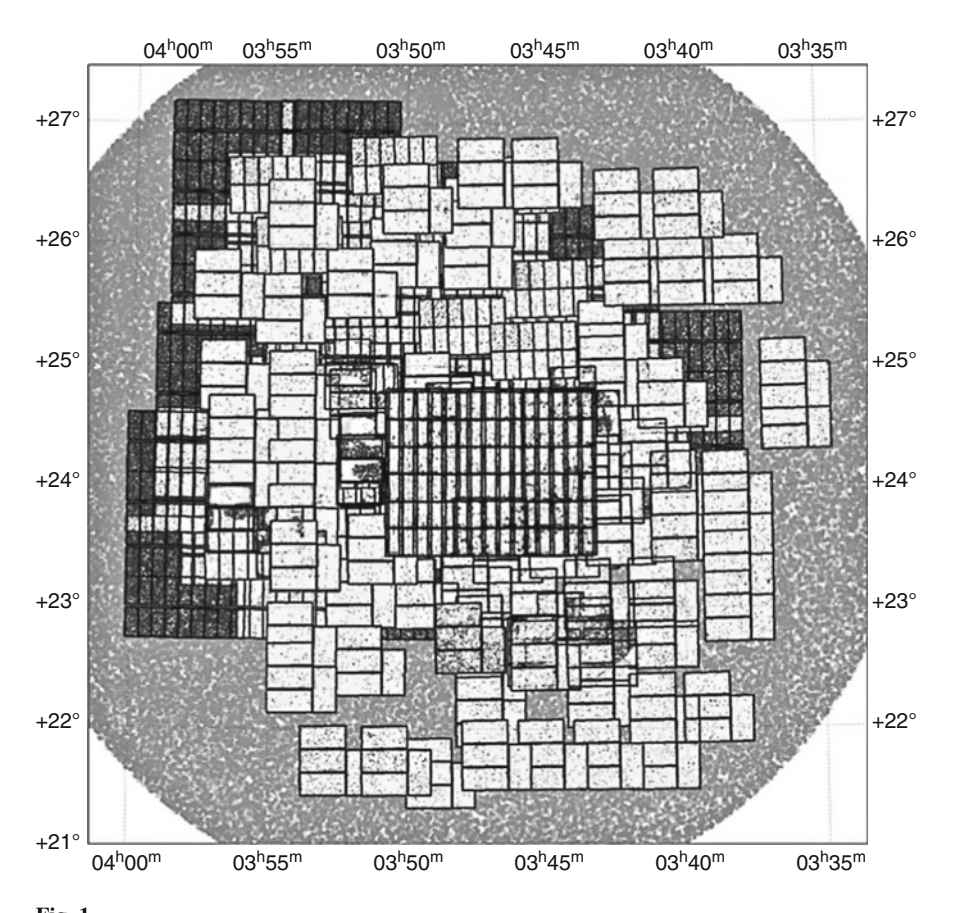


Fig. 1

# Optical Digital Galactic Plane Surveys and Star-Cluster Science

Janet E. Drew, Roberto Raddi, and the EGAPS Consortia

**Abstract** Over the next few years, the optical surveys IPHAS, UVEX and VPHAS+ will provide complete photometric coverage of the Galactic Plane within the latitude range  $-5^{\circ} < b < +5^{\circ}$ . Of these surveys, IPHAS is the most complete. Drawing on the work that has already been embarked upon using IPHAS r, i and narrowband  $H\alpha$  data, examples of the application of these very wide area surveys to the study of star clusters and the structure of the Milky Way disc are outlined.

#### 1 Introductory Remarks

The acronym EGAPS stands for "European Galactic Plane Surveys", and refers to a collection of optical Galactic Plane surveys that have their roots in the forming of a consortium in 2003 to pursue a digital H $\alpha$  survey at  $\sim$ 1 arcsec spatial resolution across the entire northern Galactic Plane. This first survey, the INT/WFC H $\alpha$  Survey of the Northern Galactic Plane (IPHAS, [1]). is now very close to completion. Because it has also seen some exploitation already, that illustrates aspects of the science we may expect from this set of interlinked surveys, it is the focus here. The other surveys making up the set are UVEX [4] – underway since 2006 – and VPHAS+ which is likely to begin in earnest during the southern Galactic Plane season of 2012, after the VLT Survey Telescope has been confirmed as fully operational.

IPHAS was itself inspired by the example of the last Siding Spring UK Schmidt photographic survey which began the process of updating the known stock of

J.E. Drew  $(\boxtimes) \cdot R$ . Raddi

CAR/STRI, University of Hertfordshire, Hatfield, Hertfordshire, UK

e-mail: j.drew@herts.ac.uk

EGAPS Consortia

www.iphas.org; www.astro.ru.nl/uvex; www.vphas.org

J.E. Drew et al.

compact  $H\alpha$  emission line objects [11] across the southern Galactic Plane. Beyond hemisphere, the key difference of course is the superior linear character of the digital detectors over a wide dynamic range that are available as the Wide Field Camera (WFC) on the Isaac Newton Telescope (INT): IPHAS is accordingly subject to reliable photometric calibration, transforming the science opportunities.

The IPHAS survey footprint spans all Galactic longitudes north of the celestial equator, and reaches to  $\pm 5^{\circ}$  in Galactic latitude, amounting to a total area of 1,800 square degrees. This strip has been observed in double pass down to a limiting magnitude of ~20th in 3 filters: Sloan r and i, contemporaneously with narrowband  $H\alpha$ . The FWHM of the  $H\alpha$  transmission profile is 95 Å. The core observing concept is that each field is observed through the three survey filters in unbroken succession, and the telescope is then offset 5 arcmin in both right ascension and declination and the sequence of exposures is repeated. This is to ensure that the derived survey colours,  $r - H\alpha$  and r - i are unaffected by secular variation and hence are valid. None of the EGAPS constituent surveys is constructed as a variability survey: the aim instead is assured SED information.

The median seeing obtaining in IPHAS data regarded as reaching the required standard is 1.1 arcsec. Since the WFC imaging area is only  $\sim$ 0.25 square degrees, the total number of exposures collected has been  $7635 \times 2 \times 3 = 45810$ . The whole translates to a database containing of the order of 100 million distinct objects (mainly unresolved point sources). A preliminary release of data was made in late 2007 [3]. Just how all the detected sources are spread across the Galactic Plane is shown in Fig. 1. The next release, during 2011 in all likelihood, will cover almost

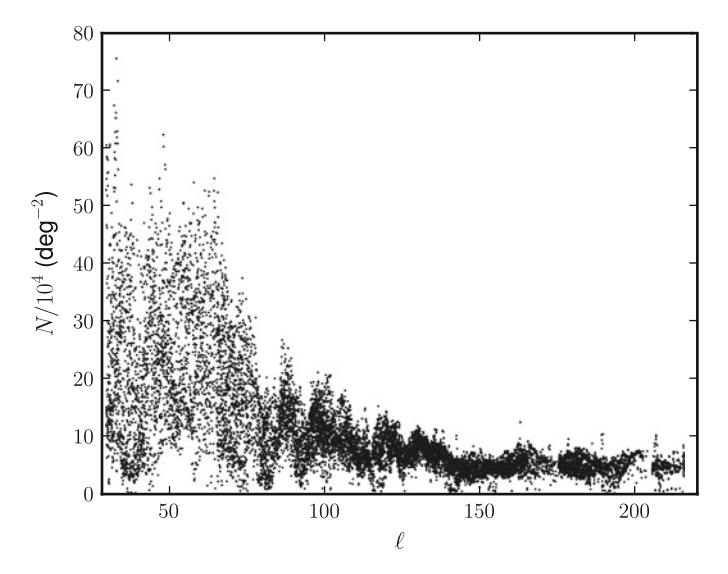


Fig. 1 IPHAS point source density across the northern Galactic Plane, as a function of Galactic latitude. Each data point is the mean r source density for a single IPHAS field. At lower longitude, fields in the Galactic midplane and towards the survey latitude bounds at  $b=\pm 5^{\circ}$  exhibit the lowest source densities typically. From [3]

the entire survey area. Some new observations are still needed to patch up limited locations, particularly in the anticentre region of the Plane.

UVEX is the northern hemisphere blue complement to IPHAS, in that it uses the same telescope, instrument and observing strategy. Like IPHAS it is pipelined at the Cambridge Astronomical Survey Unit. The differences are in the filter set, which is U, g, r and narrowband HeI 5876 and dates of execution. The filter sets of the two surveys overlap in the r band for two reasons: (a) to facilitate the eventual construction of optical SEDs, safely combining the data from both surveys; (b) to provide the basis for proper motion studies of nearby unreddened – and typically low luminosity – compact objects and low mass stars. In support of aim (b), it is a deliberate policy for UVEX data-taking to lag IPHAS by at least 3 years (often 5).

#### 2 IPHAS Science Goals: The Roles of Narrowband Hα

The distinguishing feature of IPHAS is the narrowband H $\alpha$  data. This yields the traditional capability to select among the general stellar population of the Galactic Plane for the presence of H $\alpha$  emission. But the fact of the photometric precision bestowed by CCD detector technology also allows narrowband H $\alpha$ , in combination with the r,i broad band filters to provide good intrinsic colour (or, more loosely, spectral type) discrimination. This flows from the sensitivity of the H $\alpha$  narrowband measurements to *absorption* equivalent width differences at the level of  $\sim 2$  Å on objects brighter than  $\sim 19$ th magnitude. We discuss these two modes of use of the survey data in the next two sections, restricting the discussion to applications relevant to star-cluster science.

#### 2.1 Hunting Emission Line Stars

Among stars, the very young and the very old are prone to present spectra with  $H\alpha$  emission either because they are accreting from or returning matter to the circumstellar environment. In addition, the beginning/end states are generally associated with heightened luminosity, which often implies the availability of ionising photons. A survey such as IPHAS is thus expected to pick out: young stars (T Tau and Herbig stars); relatively more evolved classical Be and some B[e] stars, and Wolf–Rayet stars (where the  $H\alpha$  line is substituted by HeII or even carbon-line emission); a variety of compact interacting binaries; and of course both spatially resolved and unresolved emission line nebulae.

IPHAS, in principle, provides a harvest of all types of emission line star across all of the northern Galactic Plane. The photometric marker delivered by the survey for line emission is an "excess" in  $r - H\alpha$  relative to the "normal" value for this colour. What is "normal" strongly depends on spectral type, and indeed reddening – so in practice,  $r - H\alpha$  is best plotted as a function of r - i in order to define an

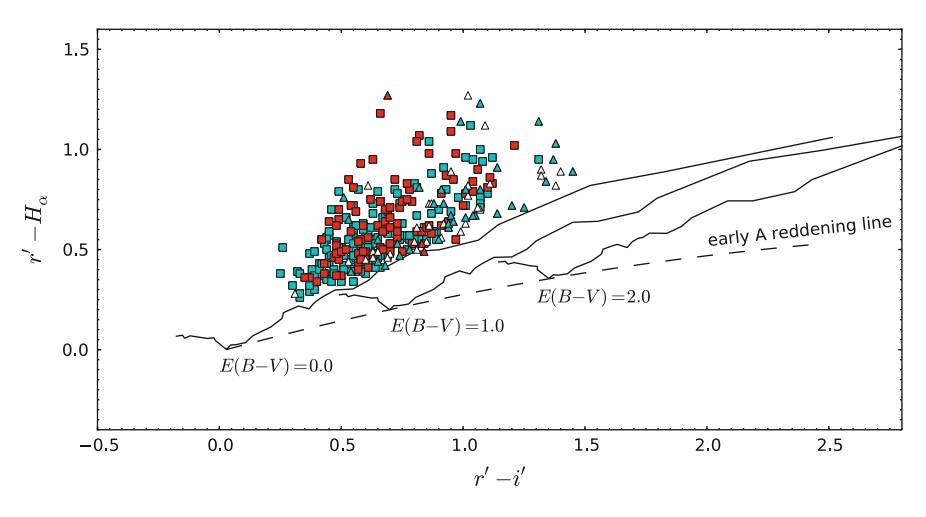


Fig. 2 The IPHAS colour–colour plane, and its use in the selection of candidate emission line stars. The three tracks shown are main sequence tracks calculated for 3 different reddenings: E(B-V)=0, 1, and 2. Most stars in the Galactic Plane fall on or to the right of the unreddened main sequence, and on or above the early-A reddening line (see [1]). Objects located above the unreddened main sequence are, at a probability typically exceeding 90%, emission line objects. The 338 data points plotted are the colours of stars in the Perseus Arm region shown in Fig. 3 – 306 have been followed up spectroscopically (coloured symbols), and only 9 have *not* been confirmed as emission line stars

area of the colour–colour plane in which the combination of colours identifies the presence of  $H\alpha$  emission. An example of this is shown as Fig. 2: all the coloured data points are confirmed emission line objects, lying above the track defining the unreddened main sequence. Non-emission line stars, if plotted in this same diagram, lie on, to the right of, or below the unreddened main sequence. Notice that reddened main sequence stars with weak line emission may show too little excess in  $r-H\alpha$  to rise above the unreddened main sequence in the colour–colour diagram. So whilst it is true that IPHAS candidate emission line stars convert at an extremely high rate to spectroscopically-confirmed emission line stars, it is also true that some reddened emission line objects are likely to remain hidden in the main stellar locus (see [1] for more discussion, including how more refined searches for candidate emission line stars may be conducted).

The most populous categories of emission line objects are the classical Be stars (early-mid B stars that are commonly near the terminal-age main sequence), and young TTau/Herbig stars. The latter would be expected to cluster in and around star forming regions. As relatively luminous objects drawn from the sparsely populated top end of the stellar IMF, the classical Be stars will less often appear as clustered. This is indeed what is seen – expressing itself as a tendency for the brighter emission line objects to be more evenly distributed across the sky. These properties are illustrated in Fig. 3 which shows how IPHAS emission line candidates from the [18] catalogue are distributed along the Perseus Arm, in the longitude range

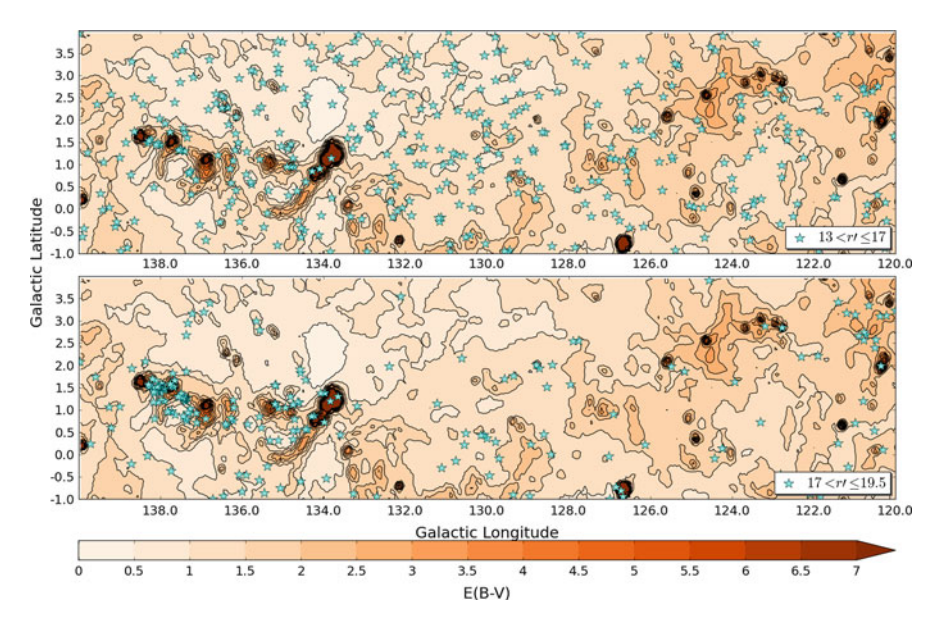


Fig. 3 The top panel places candidate emission line stars brighter than r=17 on an integrated extinction map for a section of the Perseus Arm  $(120^{\circ} < \ell < 140^{\circ})$ . The lower panel shows instead the candidate emission line stars fainter than r=17. The emission line candidates are derived from the catalogue of [18]. The contours and colour scale underlying the stars, represent integrated line-of-sight extinction (data are from [15])

 $120^{\circ} < \ell < 140^{\circ}$ , if brighter or fainter than r=17 (from Raddi et al., in prep. – see also Raddi et al., this volume). A relatively small proportion of the brighter sources in the example shown are likely to be YSOs – and if they are YSOs, they will be Herbig Ae/Be stars, mainly in the Perseus Arm, about 2–2.5 kpc away. Only at fainter magnitudes is there a switch to a more clustered spatial distribution, as the clustered YSO population starts to dominate.

A long-term IPHAS goal is to use the newly detected mainly classical Be stars as a means to a (limited) mapping of the outer reaches of the northern Galactic Plane. The feasibility is demonstrated by noting that a 16th magnitude classical Be star, behind even 3 magnitudes of extinction is likely to be 6 kpc away from the Sun. There are many hundreds of these, for which spectra have begun to be collected, and around which we may search for faint relatively distant clusters. This endeavour will be aided by the 3-D extinction mapping that IPHAS photometry is able to support – to be discussed in the next section.

The gathering of statistics of emission line stars on more limited angular scales is also an option for more focused studies of individual OB associations. An example of this was presented by [17], in which deep spectroscopy of candidate emission line stars in and around Cyg OB2 was obtained and examined. It was found there that the centre of Cy OB2 has a rather meagre Herbig/T Tau population, while DR 15 over a degree away to the south bristles with them. The comprehensive collection of data of this kind can inform discussions of triggering and/or sequential star formation.

#### 2.2 Narrowband Hα As an Intrinsic Stellar Colour Discriminant

It is well-known that the equivalent width of the  $H\alpha$  line in absorption in the spectra of main sequence stars reaches a maximum at early-A spectral type: in F, G and early K stars the feature slowly weakens. Passing through late K and M stars, narrowband  $H\alpha$  observations yield a continuing trend in that the weakening  $H\alpha$  absorption, that promotes a rise in  $r-H\alpha$  from A through to early K types, is replaced by the appearance of a growing pseudo-emission, in band, created by TiO absorption eating away stellar continuum to either side of the narrowband  $H\alpha$ . The net result is a steady growth in  $r-H\alpha$  index as a function of intrinsic colour working along the main sequence from early-A to M. Significantly, the dependence of  $r-H\alpha$  on interstellar extinction is actually very much less. This contrast in sensitivity, when combined with the undoubted sensitivity of broadband r-i to interstellar reddening, results in a useful near-orthogonality in the IPHAS colour-colour diagram, such that a progressively reddened main sequence track moves almost at right angles to itself. This is evident from the tracks shown in Fig. 2.

This general pattern of behaviour has two useful consequences. First, the way in which  $H\alpha$  absorption equivalenet width peaks in the early-A spectral type range renders the selection of A stars an easy thing to do. Examples of the science this enables will be summarised in Sect. 2.3.

Secondly, the way in which the reddening main sequence sweeps out area in the colour–colour diagram allows any point within the swept-out region to be uniquely associated with a reddening and an intrinsic colour (or spectral type). This opens the door to 3D extinction mapping, *provided* we know how to convert intrinsic colour into an absolute magnitude. If we do, it permits photometric parallax on an industrial scale. The challenge is how to do this for magnitude limited sightlines passing through the Galactic Plane at low latitude: it is a very different proposition from the one faced by the Sloan project targeting high galactic latitude. That it turns out to be possible at all has a lot to do with the first sparse guess provided by the A stars falling along the lower edge of the main stellar locus in the IPHAS colour–colour plane. It is also helpful that it is true for many sightlines that most stars picked up by IPHAS are indeed main sequence stars. Nevertheless there is no avoiding the need to be able to devise an algorithm that allows intelligent luminosity class assignments, drawing on colour–magnitude information. This step was taken in the work published by [13].

One of the ways in which the 3D mapping algorithm was tested was against published parameters for a number of well-studied star clusters. And the comparisons were successful. But it remains the case that this capability remains under review and development – with the intention in the long run to achieve a 3-D mapping of the entire Galactic Plane (after the completion of VPHAS+ in the southern hemisphere) at a spatial resolution of 10 arcmin or better. With the incorporation of g photometry, either from UVEX or VPHAS+, the technique becomes more powerful because of the greater sensitivity of g-i colour to reddening (compared with r-i). Before leaving this topic it is worth the comment that extinction-distance curves derived from IPHAS photometry are typically most useful beyond a minimum distance of

0.8–1 kpc. Inside this radius the surface density of useful (faint enough) stars is too low for what, in the end, is a fundamentally statistical method.

#### 2.3 Applications of A Star Selection

A detailed presentation of how to select early (A0-5) stars was given by [2]. This particular work is half an appraisal of the "why" and "how" of A star selection from IPHAS photometry, culminating in a couple of tests against classical photometry of open clusters, and half an examination of the early A star content of Cyg OB2 and environs.

The practicalities of A star selection amount to a trade off between precision of outcome and the scale of the sample needed to achieve the desired science: this arises from the simple fact that contamination of the selection will increase sharply as more and more stars are skimmed off the lower edge of the main stellar locus in the (r-Ha,r-i) colour–colour diagram. Experience suggests that the width of the selection in  $r-H\alpha$  about the early-A reddening line (see Fig. 2) is best kept to 0.05 or less for IPHAS data of a representative standard. Increasing the width of the selection band beyond this value progressively drags in later-A and then F-type stars with the consequence that the inferred mean distance of the selected objects tends towards an over-estimate. The test-of-concept comparisons were made with existing results on NGC 7510 and NGC 7791, and were satisfactory.

The selection technique was then applied to Cyg OB2 and its surroundings, across a sky area of about 5 square degrees, taking in the area that has in the past been claimed to all be part of the same high mass clustering [6]. A challenge in doing this was to take into account how the absolute magnitude,  $M_r$ , of early A stars is likely to be age-dependent, given the young age (1–3 Myrs; [5]) of the well-known compact clustering of O and early B stars around the trapezium, VI Cyg no. 8. Data on age versus absolute magnitude for early-A stars were obtained from [16]. A further point to take on board is that the youngest, essentially pre main sequence A stars (defined by intrinsic colour) are emission line objects, expected to join the main sequence as B stars: these are not selected by this technique – only those approaching, on or moving off the early-A stretch of the main sequence are. In line with this reasoning, very few early A stars were found mixed in among the concentration of OB stars. Instead, most were distributed over a 1–2 square-degree region to the south and west, and needed to 5–7 Myrs old if they are to be at the same distance as the OB stars.

This finding amounts to a strong indication that Cyg OB2 is the latest of two or more phases of star formation activity in the area, the A stars perhaps being the products of the last but one phase. This result is consonant with the finding that the similarly massive cluster R136, in the LMC, has experienced at least 2 star-forming phases [8], and also with the analysis of W3/W4 in the Perseus Arm, and the large scale shell structure associated with it, where 3 closely-spaced generations have been identified [10]. The older slightly-evolved early B stars found by [5],

J.E. Drew et al.

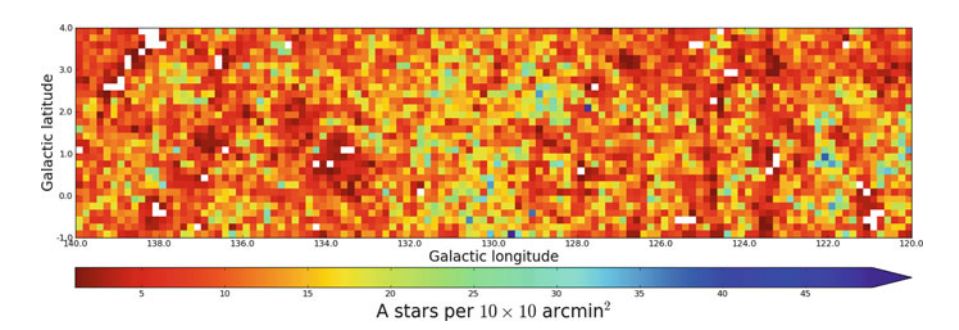


Fig. 4 The IPHAS-derived surface density of early A stars across the same part of the Perseus Arm as shown in Fig. 3. The region is broken up into  $10 \times 10 \, \text{arcmin}^2$  elements that are colour coded according to the number of early-A stars contained with that sky area

that she wondered might be foreground objects, may very well belong to the same star-forming event as the early A stars.

An even wider-area selection of A stars has since been undertaken [14] – in the Galactic Anticentre, with the aim of revisiting the claim that the stellar disc of the Milky Way is truncated ([12], based on DENIS data). As this is not an application directly relevant to star-cluster research, the reader is referred to this work for further details. Suffice it to say, the reach of this study was out to a Galactocentric radius of  $\sim$ 15 kpc, which was sufficient to reveal that the disk is not so much truncated as subject to a steepening decline in the early-A stellar density beyond  $\sim$ 13 kpc.

From the perspective of searching for clusters by selecting early-A stars from IPHAS data, we are at the beginning. Linked to the study of the emission line stars of the Perseus Arm (see Fig. 3), we are starting to construct direct maps of the surface density of early-A stars for the region. The current version of this, is shown as Fig. 4 (some small changes for the future can't be ruled out as we continue to replace some of the lowest quality data in a few locations). The outstanding points of note are how the general surface densities tend to be low in the regions of current vigorous star formation – clusters are to be found there, of course, but are too young for significant concentrations of near main sequence A stars to be present. The most prominent density spikes are indeed associated with known clusters, such as NGC  $663 \ (\ell = 129.5^{\circ}, b = -0.9^{\circ})$  and NGC  $609 \ (\ell = 127.7^{\circ}, b = 2.1^{\circ})$ : both clusters are plausible hosts for near main sequence A stars, and are given in the literature at distances that plausibly link them to the Perseus Arm [7,9].

#### 3 Concluding Remarks

IPHAS is all but complete and UVEX is underway. After repeated delays, the VLT Survey Telescope (VST) is now under construction and may go into service in the second half of 2011. VPHAS+ the southern hemisphere merger of the

IPHAS/UVEX concept has recently been reapproved as a Public Survey for the VST. The concept for this survey is the contemporaneous collection of u, g, r, i and  $H\alpha$  images and photometry across the southern Plane, down to AB limiting magnitudes in the range 21–22. In addition, it has been agreed that the  $|b| < 5^\circ$  survey limit should be expanded to  $|b| < 10^\circ$  around the Galactic Centre region, in order to capture most of the Galactic Bulge. This change will also ensure VPHAS+ covers that part of the Bulge that VVV (see the article in this volume by V.Ivanov) will cover at near-infrared wavelengths. The hoped-for window of execution of this survey is 2012–2014. Given that there is also the prospect of a shallow  $H\alpha$  survey by Skymapper, the future is rosy for uniform photometric coverage of the southern Milky Way.

In short, essentially all the science becoming possible with UVEX and IPHAS in the north should become possible in the south a modest number of years further on. It was mentioned in the introduction that, during 2011, it is intended to make a further release of IPHAS data that will incorporate a global photometric calibration (Miszalski et al, in preparation). The final goal for the absolute error and spatial variation in the applied photometric scale is 0.02-0.03. This is likely to only be achieved after a range of astrophysical tests have been applied across the database, given that there is no similarly large overlapping digital optical survey available that supplies a reliable pre-existing photometric framework. In this respect, near-infrared survey astronomy is clearly ahead of the optical. In the 2011 release, the error in the photometric scale may be  $\sim$ twice final target, whilst point-source random errors will of course range from entirely negligible just inside the 13th-magnitude bright limit up to  $\sim 0.1$  at the 20th magnitude faint limit.

For the astronomy of Galactic star clusters, the EGAPS surveys offer the opportunity for a uniform, essentially, all-sky approach to finding and characterising the Milky Way's cluster population. Allied to NIR survey data, and to the important revelatory flood of Gaia astrometry coming in the next 5–10 years, this is surely the threshold to a golden age.

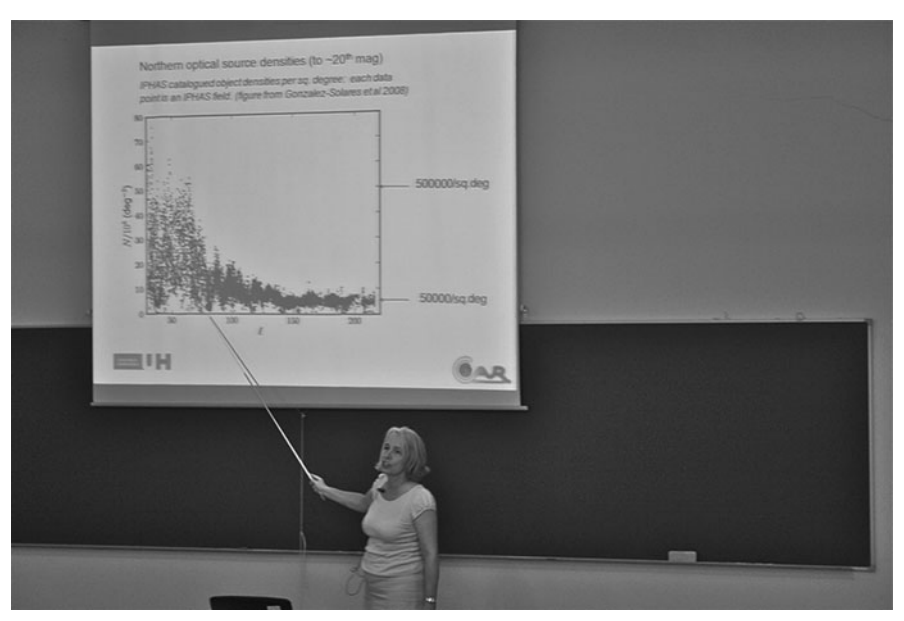
**Acknowledgements** RR acknowledges the support of a University of Hertfordshire studentship. IPHAS and UVEX observations are all obtained using the Isaac Newton Telescope (INT). The INT is operated on the island of La Palma by the Isaac Newton Group in the Spanish Observatorio del Roque de los Muchachos of the Instituto de Astrofisica de Canarias. All data are processed by the Cambridge Astronomical Survey Unit, at the Institute of Astronomy in Cambridge.

#### References

- 1. Drew, J.E., et al.: Mon. Not. R. Astron. Soc. **362**, 753 (2005)
- 2. Drew, J.E., Greimel, R., Irwin, M.J., Sale, S.E.: Mon. Not. R. Astron. Soc. 386, 1761 (2008)
- 3. Gonzalez-Solares, E.A., et al.: Mon. Not. R. Astron. Soc. 388, 89 (2008)
- 4. Groot, P.J., et al.: Mon. Not. R. Astron. Soc. 399, 323 (2009)
- 5. Hanson, M.M., Astrophys. J. 597, 957 (2003)
- 6. Knödlseder, J. Astron. Astrophys. 360, 539 (2000)

J.E. Drew et al.

- 7. Lee, V.L., Burkhead, M.S.: Astron. J. 76, 467 (1971)
- 8. Massey, P.: ARA&A 41, 15 (2003)
- 9. Moffat, A.F.J.: A&AS **160**, 139 (1972)
- 10. Oey, M.S., Watson, A.M., Kern, K., Walth, G.L.: Astron. J. 129, 393 (2005)
- 11. Parker, Q.A., et al.: Mon. Not. R. Astron. Soc. **362**, 689 (2005)
- 12. Ruphy, S., et al.: Astron. Astrophys. 313, L21 (1996)
- 13. Sale, S.E., et al.: Mon. Not. R. Astron. Soc. 392, 497 (2009)
- 14. Sale, S.E., et al.: Mon. Not. R. Astron. Soc. 402, 713 (2009)
- 15. Schlegel, D.J., Finkbeiner, D.P., Davis, M.: Astrophys. J. 500, 525 (1998)
- 16. Siess, L., Dufour, E., Forestini, M.: Astron. Astrophys. 358, 593 (2000)
- 17. Vink, J.S., Drew, J.E., Steeghs, D., Wright, N.J., Martin, E.L., Gänsicke, B.T., Greimel, R., Drake, J.: Mon. Not. R. Astron. Soc. 387, 308 (2008)
- 18. Witham, A.R., Knigge, C., Drew, J.E., Greimel, R., Steeghs, D., Gänsicke, B.T., Groot, P.J., Mampaso, A.: Mon. Not. R. Astron. Soc. 384, 1277 (2008)



Janet Drew

#### **Census of Milky Way Star Clusters from Infrared Surveys**

Valentin D. Ivanov

**Abstract** Recent near- and mid-infrared wide-field sky surveys are reviewed, and their applicability for Milky Way star cluster studies are discussed. The on-going VISTA Variables in Via Lactea survey is described. Finally, the first results from a simulation addressing the completeness of cluster searches are presented.

# 1 Infrared Surveys Relevant for Milky Way Star Cluster Studies

Cluster studies are hampered by extinction – clusters concentrate in the plane of the Galaxy, and the optical surveys have been able to provide us with reasonably complete cluster census only for the nearest 1–2 kpc (see Fig. 15 in [25]). Until a decade ago it was impossible to carry out a wide-field infrared (IR) surveys that would "see" through the dust (i.e.,  $A_{K_S} = 0.112 \times A_V$ ; [30]) because of technological limitations. However, the recent advances of the IR detectors made it possible to carry out homogeneous observations of wide areas of the sky, comparable with the state of the art wide-field optical surveys, and the new space missions such as *Spitzer*, opened to us the mid-IR wavelength range. For the first time the Milky Way cluster studies could rely on excellent quality preexisting data to find and characterize clusters. Table 1 describes the near- and mid-IR surveys with depth and sky coverage that make them suitable for these purposes.

The strategies of these surveys can be summarized as follows:

- 2MASS simultaneous *JHK<sub>S</sub>* observations [32]
- DENIS semi-simultaneous  $I_{Gunn}JK_S$  [11]

V.D. Ivanov (⊠)

European Southern Observatory, Ave. Alonso de Córdova 3107, Casilla 19, Santiago 19001, Chile

e-mail: vivanov@eso.org

14 V.D. Ivanov

<b>Table 1</b> Near- and mid-infrared surveys, relevant for 1	Milky way	cluster studies
---	-----------	-----------------

Survey	Area	Bands /	Cluster searches	Status and data products
	$deg^2$	$5\sigma$ -limit		
			Hundreds of new clus-	
			ters: Dutra and Bica	
			[8,9], Ivanov et al.	
			[17], Bica et al. [1],	Completed (1997–2001);
		$J/16.5 \mathrm{mag}$	Borissova et al. [7],	last DR Mar 2003;~471
		$H/15.8  {\rm mag}$	Dutra et al. [10],	million PSC + 2 arcsec
2MASS	All sky	$K_S/15.1 \text{ mag}$	Froebrich et al. [12, 13]	resolution $JHK_S$ atlas
				Completed (1995–2001);
		Gunn I/18.5 mag		as of DR3 from Sept
		$J/16.5 \mathrm{mag}$	Two new clusters (Reylé	2005:~355 million
DENIS	16700	$K_S/14.0\mathrm{mag}$	and Robin [29])	$PSC + IJK_S$ atlas
				In progress (2006–2013),
		$J/19.8 \mathrm{mag}$		as of DR6 (Oct 2009):
		$H/19.0{\rm mag}$		$\sim$ 604 million PSC +
UKIDSS	1800-JHK	K/18.1 mag	$\sim$ 170 new clusters	~1 arcsec resolution
GPS	$300 - H_2$	H <sub>2</sub> /	(Lucas et al., in prep.)	JHK atlas
		$Z/21.5 \mathrm{mag}$		Raw paw-prints public via
		Y/20.7 mag		the ESO Data
		$J/20.2 \mathrm{mag}$		Archive; first v. 1.0
		H/19.3  mag		tiles+catalogs recently
	300-bulge	K/19.3 mag		available to the team via
VVV	220 - disk	(disk)	Search in progress	CASU
				In progress (2003–2012);
		[3.6]/0.2 mJy		$\sim$ 100 million PSC
GLIMPSE	220+60+	[4.5]/0.2 mJy		(up to GLIMPSE 3D)
I+II+3D	134 + 290	[5.8]/0.6 mJy	59 new clusters (Mercer	+ ≤2 arcsec resolution
+360	$= \sim 700$	[8.0]/4.0 mJy	et al. [22])	atlas

- UKIDSS GPS semi-simultaneous *JHK* imaging, and two more *K*-band re-visits for proper motion and variability purposes [20]
- VVV two visits during which semi-simultaneous YZ and  $JHK_S$  images are taken, and multiple (50–80)  $K_S$  re-visits separated by up to 5 yrs (see Sect. 2 for details) [27]
- GLIMPSE simultaneous [3.6] and [5.8], and simultaneous [4.5] and [8.0] imaging; two visits, separated by 20 s to 3 h [7]

The relative depth of the various surveys and a sensitivity versus area plot are shown in Fig. 1. The sky footprints are shown in Figs. 2 and 3. While the depth and the spatial resolution of the 2MASS allowed detailed study only of the closest star clusters, the new generation of near-IR surveys (UKIDSS and VVV) lets us to characterize the clusters, at least to some extent. For example, VVV revealed the pre-main sequence population of some young clusters that would have been invisible in 2MASS. Of course, studies of most clusters require spectroscopy which is typically the most reliable method for measuring their distances, and all parameters

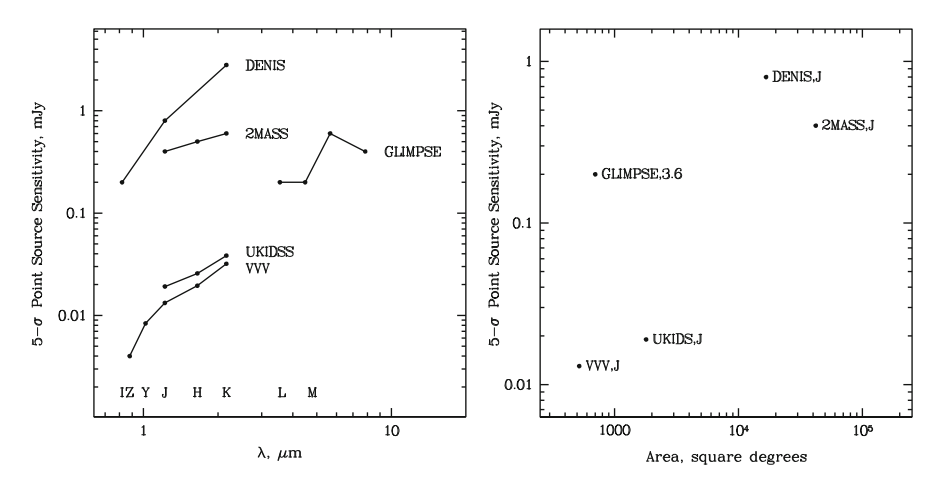


Fig. 1 Relative depth of the various surveys (*left*), and sensitivity versus area plot (*right*)

that scale with distance, including their mass, total luminosity, and even the age – for the clusters with no main sequence turn off point.

#### 2 VISTA Variables in Via Lactea Survey

The VISTA Variables in Via Lactea (VVV) Survey was designed to probe the time axis – producing a large-scale 3-dimensional map of the Milky Way with the RR Lyr and Cepheid variables. The survey has two sub-components: the bulge  $(-10 < l < 10\deg, -10 < b < 5\deg)$  and the disk  $(-65 < l < -10\deg, -2 < b < 2\deg)$ , observed with nearly identical strategies, but with mildly different integration times and depths. The total footprint spans  $520\deg^2$  (green on Fig. 3), and the final point source catalog is expected to contain  $10^9$  sources, including  $10^6$  variable stars of different types. Proper motion measurements with  $\geq 5$  yr baseline will also be obtained.

The VVV has a broad range of corollary science goals related to clusters: distances to some of them, based on their variable star members, and most importantly – providing a broad new census of clusters including, in particular, young ones containing obscured pre-main sequence stars. The VVV team has broad experience in cluster identification and characterization [2–6, 14–18,23–25], and we will search for clusters on the deepest ever  $K_S$ -band sub-arc-second image of the Galaxy that will be created stacking together all multi-epoch VVV observations.

The yearly strategy of VVV involves a complicated timing schedule for randomized sampling of light curves, and for proper motion studies:

• 1 year : quasi-simultaneously  $ZYJHK_S$  and 6 separate epochs in  $K_S$  of the entire survey area

16 V.D. Ivanov

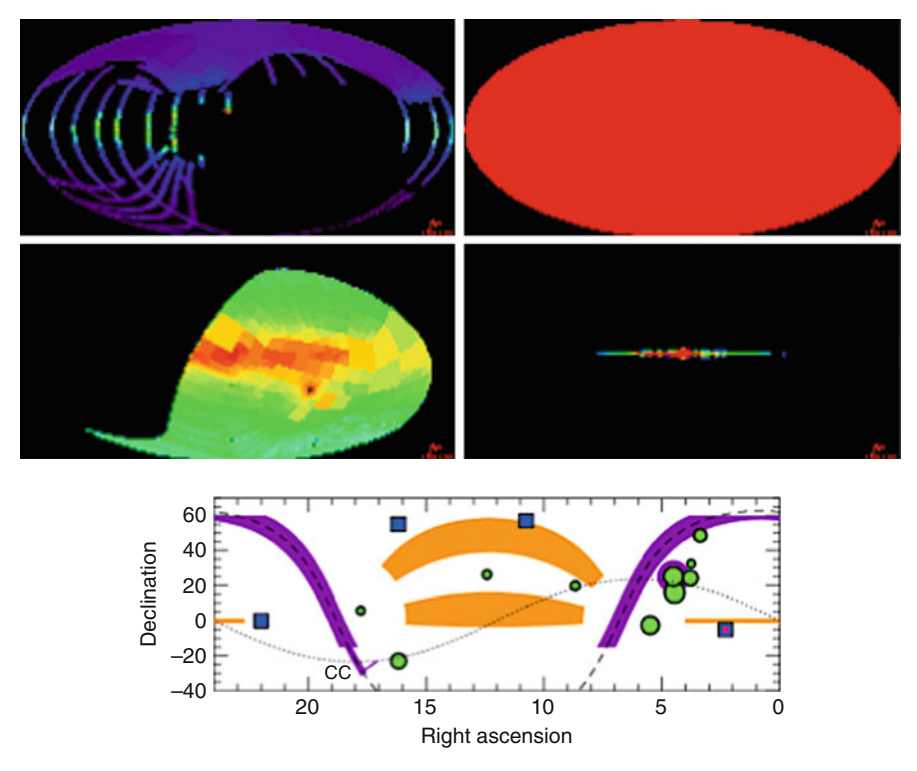


**Fig. 2** Sky footprints of various surveys: *top left* – SDSS (large optical CCD survey, shown here for comparison), *top right* – 2MASS, *middle left* – DENIS, *middle right* – GLIMPSE, without the recent extensions are (all four maps are in Galactic coordinates), and *bottom* – UKIDSS (in Equatorial coordinates; GPS is shown in *violet*, GCS in *green*, LAS in *yellow*, DXS in *blue*, and USD in *red*). The top for plots are courtesy of the VizieR database, the bottom is courtesy of the UKIDSS team (*http://www.ukidss.org*)

- 2 years : 6 separate epochs in  $K_S$  of the entire survey area
- 3 years: 80 separate epochs in  $K_S$  of the bulge main bulge variability campaign
- 4 years : 70 separate epochs in  $K_S$  of the disk main disk variability campaign
- 5 years : 20 epochs in  $K_S$  of the bulge and 9 of the disk; subset of pointings will be observed more frequently; provides the large baseline for the proper motion studies

The survey is on-going. Observations started in the first half of 2010, and high level data products are being generated as of mid-2010, but they are still undergoing quality control and verification, and have not yet been released to the general users. For example, the entire data set from the first half a year of observations has been re-reduced three times, to improve the data quality.

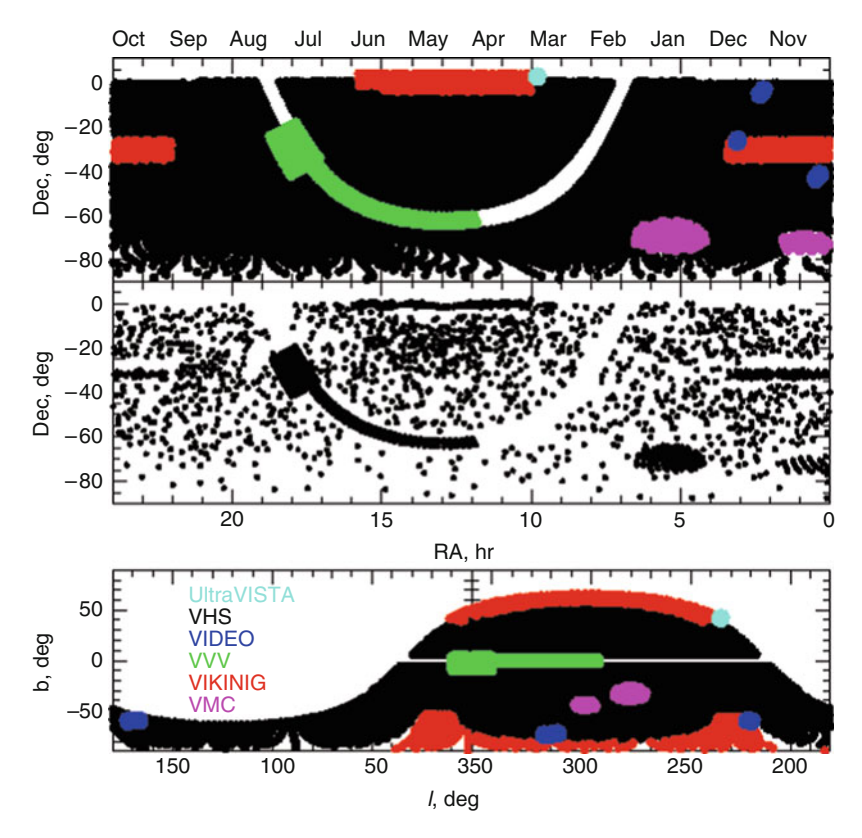


**Fig. 3** Sky footprints of the original VISTA surveys. The *top* and the *bottom panels* show all telescope pointings necessary to cover the areas of the surveys, in Equatorial and Galactic coordinates. The middle panel shows the subset of the pointings excepted to be observed during the first year of VISTA operation

# 3 Incompleteness of the Milky Way Cluster Census from the 2MASS

Finding and characterizing new clusters can be an exciting challenge, but the discovery of yet a few more objects, as interesting and important as they may be, does not help to address the question of the total population's size – dust obscuration makes the Milky Way cluster census incomplete for distances larger than a few kpc. GLIMPSE demonstrated that even mid-IR surveys have difficulties in detecting distant clusters because the [3.6] band is still noticeably affected by extinction ( $A_L = 0.058 \times A_V$ ; [30]), and the longer wavelengths are more sensitive to extended dust emission than to stars.

To address the issue of completeness we began a project [19] to simulate the cluster population of the Galaxy, to merge it with a real point-source catalog, and to run a cluster search using various algorithms. It became clear form the beginning,

18 V.D. Ivanov

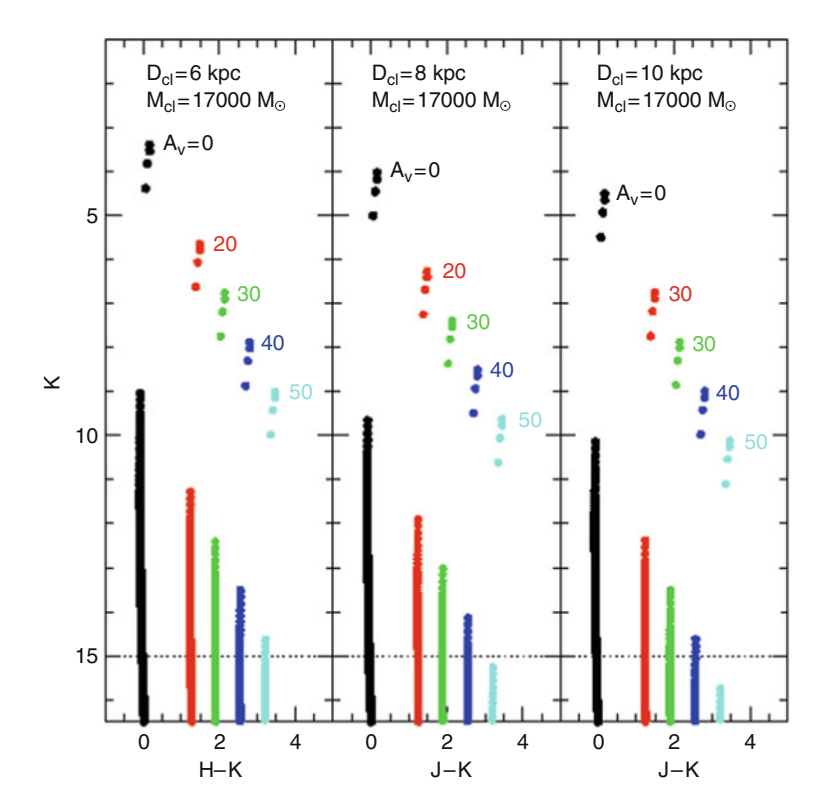


Fig. 4 Color-magnitude diagrams for a cluster with total mass  $M_{cl}$ =17,000  $M_{\odot}$ ) and age of 10 Myr for various distances and optical extinctions  $A_V$ , generated from the Padova isochrones [21]. The *horizontal dotted line* shows the approximate 2MASS completness limit in the most crowded regions of the Galaxy

that we can hope to derive incompleteness corrections for distances beyond a few kpc for the most massive clusters only. Therefore, for now we will consider only supermassive clusters ( $M_{cl}=17,000\,M_{\odot}$ ) with age of 10 Myr. The young age makes the member stars intrinsically brighter, and somewhat alleviates the question of the infant mortality. Synthetic color-magnitude diagrams for such clusters at different distances and values of  $A_V$  are shown in Fig. 4 to illustrate the depth necessary for detecting their member stars.

We assumed that the clusters follow a spatial distribution close to that of the stars in the Milky Way disk, and generated  $10^5$  clusters in na exponential disk-like distribution (Fig. 5) with scale length  $R_0^{cl} = 1.8$  kpc and scale height  $Z_0^{cl} = 55$  pc. The obscuring dust also has exponential distribution, with  $R_0^{dust} = 3$  kpc and  $Z_0^{dust} = 200$  pc. These values were adopted from the Besançon Milky Way model [31]. The spatial distribution of the stars within the clusters was taken directly from MASSCLEAN (Massive Cluster Evolution and Analysis Package; [28]).

Let us consider a "pencil" beam  $(3\times3\deg)$  at  $l=+60\deg b=0\deg$  (red dots in Fig. 5). It contains 286 of all generated clusters. It is clear from the synthetic

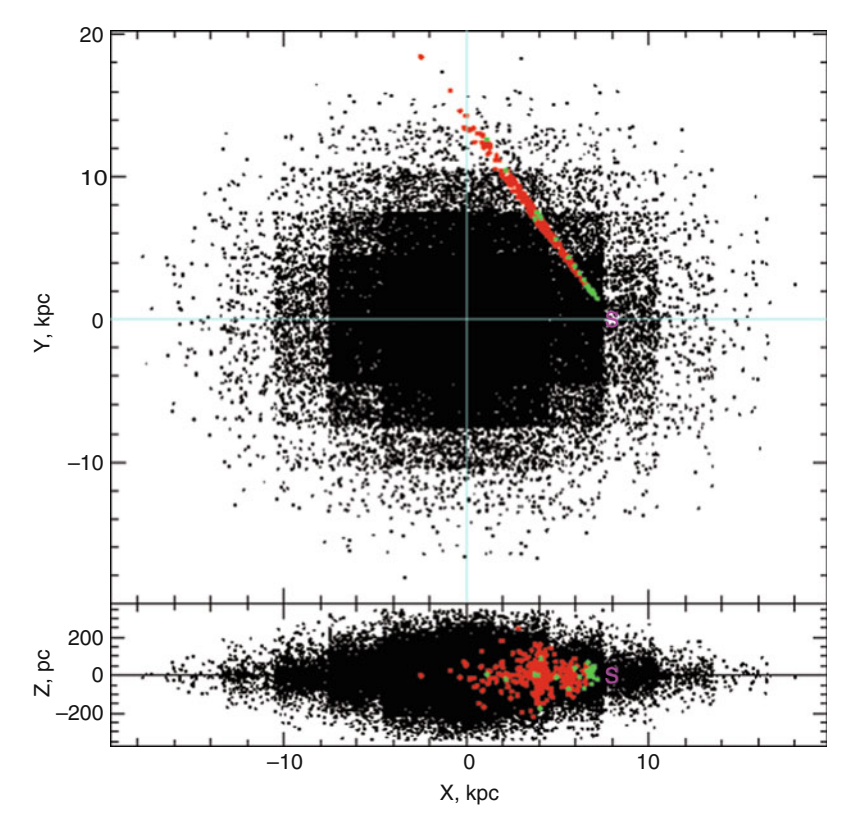


Fig. 5 Cluster simulation [19]. The *green dots* are potentially detectable clusters, the *red dots* are undetectable clusters. The Sun's position is marked with the letter "S"

color-magnitude diagram (Fig. 4) that four stars at the red supergiant stage dominate the cluster. We exclude from the sample the clusters for which more than one of these four member star is rendered undetectable by the proximity to bright foreground stars (taken from the real 2MASS point-source catalog [32]) because the stars on the main sequence are too faint to be detected in the glare of the bright cluster members, and therefore, the cluster can only be detected by the red supergiants. This "cleaning" left us with only 24 clusters, or  $\sim 8\%$ , that remain potentially detectable as groups of three or more stars with similar colors and magnitudes. Note that 17 of these clusters are "local", i.e. reside within 5 kpc from the Sun.

The potential detectability does not guarantee that a cluster will be detected because of the fore- and background star density variation, and the clumpy structure of the dust. Therefore, the  $\sim\!8\%$  is an optimistic upper limit for the 2MASS cluster search in that direction. In reality, the detection rate even for supermassive red supergiant phase clusters (that are the easiest to detect) in this direction will be lower. Note that the better spatial resolution and depth of VVV with respect to the 2MASS will increase somewhat the detection rate.

20 V.D. Ivanov

#### 4 Summary

The modern near- and mid-infrared surveys provide observational bases for detailed cluster census and characterization but the completeness rate of the cluster searches even for the deepest surveys is likely to remain low.

#### References

- 1. Bica, E., Dutra, C.M., Soares, J., & Barbuy, B., A&A, 404, 223 (2003)
- Borissova, J., Pessev, P., Ivanov, V.D., Saviane, I., Kurtev, R., Ivanov, G.R.: Astron. Astrophys. 411, 83 (2003)
- Borissova, J., Ivanov, V.D., Minniti, D., Geisler, D., Stephens, A.W.: Astron. Astrophys. 435, 95 (2005)
- 4. Borissova, J., Ivanov, V.D., Minniti, D., Geisler, D.: Astron. Astrophys. 455, 923 (2006)
- Borissova, J., Ivanov, V.D., Stephens, A.W., Catelan, M., Minniti, D., Prieto, G.: Astron. Astrophys. 474, 121 (2007)
- Borissova, J., Ivanov, V.D., Hanson, M.M., Georgiev, L., Minniti, D., Kurtev, R., Geisler, D.: Astron. Astrophys. 488, 151 (2008)
- 7. Benjamin, R.A., Churchwell, E., Babler, B.L. et al.: Publ. Astron. Soc. Pac. 115, 953 (2003)
- 8. Dutra, C.M., & Bica, E., A&A, **359**, 9 (2000)
- 9. Dutra, C.M., & Bica, E., A&A, **376**, 434 (2001)
- 10. Dutra, C.M., Bica, E., Soares, J., & Barbuy, B., A&A, **400**, 533 (2003)
- 11. Epchtein, N., Deul, E., Derriere, S., et al.: Astron. Astrophys. 349, 236 (1999)
- 12. Froebrich, D., Scholz, A., & Raftery, C.L., MNRAS, **374**, 399 (2007)
- 13. Froebrich, D., Schmeja, S., Samuel, D., & Lucas, P.W., MNRAS, 409, 1281 (2010)
- 14. Hanson, M.M.: Astrophys. J. **597**, 957 (2003)
- 15. Hanson, M.M., Bubnick, B.F.: Publ. Astron. Soc. Pac. 120, 150 (2008)
- Hanson, M.M., Kurtev, R., Borissova, J., Georgiev, L., Ivanov, V.D., Hillier, D.J., Minniti, D.: Astron. Astrophys. 516, 35 (2010)
- Ivanov, V.D., Borissova, J., Pessev, P., Ivanov, G.R., Kurtev, R.: Astron. Astrophys. 394, L1 (2002)
- 18. Ivanov, V.D., Kurtev, R., Borissova, J.: Astron. Astrophys. **442**, 195 (2005)
- 19. Ivanov, V.D., Popescu, B., Hanson, M.M., et al.: (in preparation) (2011)
- 20. Lucas, P.W., Hoare, M.G., Longmore, A., et al.: Mon. Not. R. Astron. Soc. 391, 136 (2008)
- Marigo, P., Girardi, L., Bressan, A., Groenewegen, M.A.T., Silva, L., Granato, G.L.: Astron. Astrophys. 482, 833 (2008)
- 22. Mercer, E.P., et al., ApJ, 635, 560 (2005)
- 23. Messineo, M., Petr-Gotzens, M.G., Schuller, F., et al.: Astron. Astrophys. 472, 471 (2007)
- 24. Messineo, M., Figer, D.F., Davies, B., et al.: Astrophys. J. 683, L155 (2008)
- 25. Messineo, M., Davies, B., Ivanov, V.D., et al.: Astrophys. J. 697, 701 (2009)
- 26. Messineo, M., Figer, D.F., Davies, B., et al.: Astrophys. J. **708**, 1241 (2010)
- 27. Minniti, D., Lucas, P.W., Emerson, J.P., et al.: New Astron. 15, 433 (2010)
- 28. Popescu, B., Hanson, M.M.: Astron. J. 138, 1724 (2009)
- 29. Reylé, C., & Robin, A.C., A&A, **384**, 403 (2002)
- 30. Rieke, G.H., Lebofsky, M.J.: Astrophys. J. 288, 618 (1985)
- 31. Robin, A.C., Reylé, C., Derriére, S., Picaud, S.: Astron. Astrophys. 409, 523 (2003)
- 32. Skrutskie, M.F., Cutri, R.M., Stiening, R., et al.: Astron. J. 131, 1163 (2006)

#### **Time-Resolved Surveys of Stellar Clusters**

Laurent Eyer, Patrick Eggenberger, Claudia Greco, Sophie Saesen, Richard I. Anderson, and Nami Mowlavi

**Abstract** We describe the information that can be gained when a survey is done multi-epoch, and its particular impact in open cluster research. We first explain the irreplaceable information that multi-epoch observations are giving within astrometry, photometry and spectroscopy. Then we give three examples of results on open clusters from multi-epoch surveys, namely, the distance to the Pleiades, the angular momentum evolution of low mass stars and asteroseismology. Finally we mention several very large surveys, which are ongoing or planned for the future, Gaia, JASMINE, LSST, and VVV.

#### 1 Introduction

The organizers of the conference asked us to present the following subject: What can time-resolved surveys of stellar clusters teach us? We show that time is an essential dimension to gain knowledge in astronomy when we want to learn about stars, clusters and the Galaxy. In this article, we focus on open clusters.

Astrophysics has some limited avenues to explore the Universe and its content. Some main trends for survey strategies are to observe:

- Deeper/fainter
- Wider areas of the sky (with the whole sky as upper limit)
- "Sharper", i.e., with a better resolution
- In different wavelenghts
- Multi-epoch, i.e., to observe many times the same region of the sky

L. Eyer (☑) · P. Eggenberger · C. Greco · S. Saesen · R.I. Anderson Geneva Observatory, University of Geneva, CH-1290 Sauverny, Switzerland e-mail: laurent.eyer@unige.ch

N. Mowlavi

ISDC, Geneva Observatory, University of Geneva, CH-1290 Versoix, Switzerland

22 L.Eyer et al.

Meas. type	Single-epoch	Multi-epoch
	position	parallax, proper motion
Astrometry	optical doubles	(projected) binary orbits
	AstroParam (Teff, logg)	variation of AstroParam
	metallicity	
	extinction <sup>a</sup>	
Photometry	age <sup>a</sup> , distance <sup>a</sup>	
•		variability types:
		ecl. Bin/ planetary transits
		pulsation
		rotation
		eruptive phenomena, etc.
	AstroParam	variation of AstroParam
	elemental abundance	line-profile variations
Spectroscopy	radial velocity	radial-velocity variations
. 17	stellar rotation	•

**Table 1** Information from single- and multi-epoch surveys.

<sup>a</sup>Clusters

In this text we explore the last item, noting that different astronomical subjects/objects may be explored/discovered depending on the above choices for a survey.

The three main pillars of astrophysics are astrometry, photometry and spectroscopy. We show in Table 1 what can be gained by doing a multi-epoch survey with respect to single-epoch survey.

We obtain the best astrophysical constraints when several observables are combined. For example bringing together the astrometric orbit and radial-velocity measurements, allows to solve entirely a binary system (inclination, masses, radii, semi-major axis, eccentricity); bringing together photometric and radial-velocity observations allows the determination of the radius of certain pulsating stars such as the Cepheids by the Baade–Wesselink method, etc.

It should be noted that even in single-epoch surveys, it is advisable to take multiepoch data of some regions as it allows to establish the precision (internal errors) of the survey. For example, this has been done in SDDS and 2MASS.

#### 2 Use of Multi-Epoch Observations for Open Clusters

We have shown above that multi-epoch observations allow to derive many astrophysical quantities. Some of these quantities require fairly elaborated work, like the modelling of eclipsing binaries. How do we know whether the models are correct? If we consider that all stars of an open cluster have the same age and initial chemical composition, we can compare astrophysical quantities derived from measurements of different stars. Any significant difference between a star's property

and the property of another star within the cluster or the cluster property is of interest and may point towards problems in stellar models or in the method employed to derive the quantity. Open clusters are therefore unique tools to test the astrophysical models.

Another interest of multi-epoch observations of open clusters is that a given property can be compared for clusters of different ages and metallicities. The idea is to see whether there is a dependence on metallicity or age, e.g., for the properties of variable star populations. Of particular interest are the instability strip boundaries, the fraction of variables within the instability strips, the variability amplitudes and periods, etc. (cf. Anderson et al., these proceedings).

We present in the following sections three applications of multi-epoch surveys for open clusters.

#### 2.1 Example 1: The Distance to the Pleiades

Thanks to its multi-epoch astrometric observations and derived parallaxes, Hipparcos data allowed to precisely determine and compare the distance of the Pleiades with the one obtained through the usual main sequence fitting technique. It resulted in a well-known mismatch: Hipparcos locates the Pleiades at  $118.3 \pm 3.5$  pc [21], and with the new reduction at  $120 \pm 3.5$  [22] closer than usually quoted results  $(132 \pm 4$  pc, see e.g. [10]).

Various attempts have been undertaken to determine the distance, using the interferometric binary Atlas [14, 20], the eclipsing binary HD 23642 discovered thanks to Hipparcos (cf. [5, 13, 17, 19]) and the Hubble Space Telescope to derive parallaxes of three star members of the Pleiades [16]. These studies give a distance between 132 and 139 pc, so larger than the Hipparcos result. We will not debate these results, but point out that all the methods were using multi-epoch observations, indeed most methods to derive distances are using the time domain. Finally we note that the Gaia mission should resolve this debate.

# 2.2 Example 2: Angular Momentum Evolution of Low Mass Stars

The angular momentum evolution of low mass stars can be studied thanks to multiepoch photometric observations of open clusters. One cause for the variability of low mass stars is the presence of spots on their surfaces. The period of the photometric variations thus directly yields the stellar rotation period. Observing open clusters of different ages (as derived from isochrone fitting) allows to describe the angular momentum evolution. For a review of the subject we refer to [8] and Moraux and Bouvier (these proceedings). We therefore briefly present here the results of the HATNet project (Hungarian-made Automated Telescope network, cf. [1]) dedicated to the search of transiting exo-planets. These data allow other scientific investigations, such as period determinations of F, G, K Pleiades stars [6], or general variability of K and M dwarf stars [7]. Thanks to HATNet data, 14 new Pleides members were discovered, and the number of known periods for the Pleiades stars has been increased by a factor of 5. The HATNet results confirm previous indications that the spin-down stalls at  $\simeq 100$  Myr for the slowest rotating stars. The HATNet results also reveal that inconsistencies remain for the radii, spectroscopic and photometric stellar spin rates for low mass stars. With this example we also want to show that large surveys with small telescopes (11-cm) can be scientifically very productive for open cluster science.

## 2.3 Example 3: Observations of Solar-Like Oscillations in Stellar Clusters

By directly obtaining observational constraints on the internal properties of stars, the study of stellar oscillation modes or asteroseismology is a valuable technique to improve our knowledge of the complex physical processes that take place in stellar interiors and to progress thereby in their modelling. The study of solar oscillations has provided a wealth of information on the internal structure of the Sun and stimulated various attempts to obtain similar observations for other stars. In past years, the spectrographs developed for exoplanet searches have achieved the accuracy needed to detect solar-like oscillations in other stars from the ground, while photometric measurements of solar-like oscillations are obtained from space thanks to the CoRoT (CNES/ESA) and the *Kepler* (NASA) missions. Solar-like oscillations are of course not restricted to solar-type stars but are expected in any star exhibiting a convective envelope able to excite acoustic waves. In particular, beautiful observations of solar-like oscillations in red giant stars have been recently obtained.

The wealth of information contained in these detections of solar-like oscillations for numerous red giants stimulated the theoretical study of the asteroseismic properties of red giants and also population studies aiming at reproducing the distribution of global asteroseismic properties for a large number of these stars. Red giants in clusters are particularly interesting targets since they enable to combine the capability of asteroseismic studies to probe stellar interiors with the valuable additional constraints resulting from the common origin of stars in clusters (same age and initial chemical composition). The first clear detection of solar-like oscillations for red giants in an open cluster has been recently reported [18]. These observations were obtained for the open cluster NGC 6819 during the first 34 days of continuous science observations by *Kepler* using the spacecrafts long-cadence mode of about 30 min. These observations led to the determination of the global asteroseismic properties and oscillation amplitudes for red-giant stars with different

luminosities, which gives valuable constraints on the predicted scaling relations of these quantities with global stellar parameters. The asteroseismic measurements provide also additional tests for cluster membership. These preliminary results, based on data sampled at the spacecraft's long cadence during about 1 month, illustrate the valuable potential of solar-like observations in stellar clusters. Longer time series using the spacecraft's short cadence mode of about 1 min will yield detections of oscillation modes in subgiant and turnoff stars. This should allow testing important aspects of stellar evolution such as the mass-loss rate on the red giant branch [11]. Since the rotational history of a star has a large impact on its global and asteroseismic properties during the red giant phase [4], these observations will also provide valuable constrains on transport processes during the main sequence. Moreover, NGC 6819 is not the only cluster that will be observed by Kepler, since there are four open clusters in Kepler's field of view with different ages and metallicities. The observation of solar-like oscillations for stars in stellar clusters promise therefore great prospects for testing stellar evolution models and to progress in our knowledge of stellar physics.

#### 3 Some Surveys

There is an extremely large number of photometric surveys, past, present and planned. Here, we will do a somewhat unfair selection and consider only a few of them. First we discuss the Geneva open cluster survey aiming at the detection of stellar variability and we continue with four very large surveys with broader science cases. Open cluster science will probably benefit most when the data of these several projects will be combined.

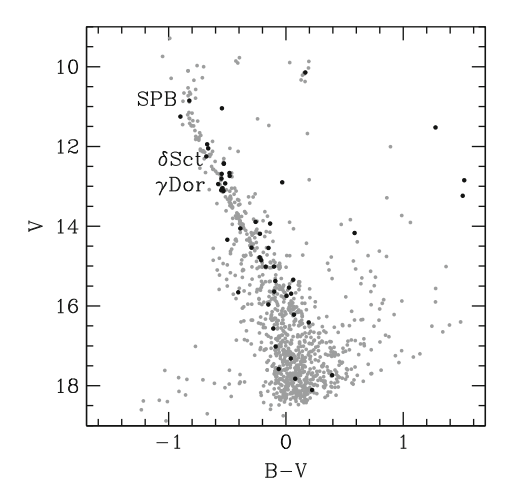
## 3.1 Geneva Open Cluster Survey

A long-term project devoted to the systematic search for variable stars in Galactic open clusters, was started at Geneva Observatory in 2002. Between 2002 and 2010, we observed 30 open clusters in both hemispheres using the 1.2-m Euler Swiss Telescope at La Silla and the 1.2-m Mercator Flemish telescope at La Palma, Spain. The open clusters in our sample range from metal-poor<sup>1</sup> (e.g.  $\langle [Fe/H] \rangle = -0.52 \, dex$ , NGC 2324) to metal-rich (e.g.  $\langle [Fe/H] \rangle = 0.10 \, dex$ , IC 4651), and from very young (e.g. 14 Myr, NGC 3766) to "old" (e.g. 2 Gyr, NGC 7789). Euler and Mercator share the same design, but have different fields of view: 11.5′ × 11.5′ for Euler and 6.5′ × 6.5′ for Mercator. The photometric observations were done in the Geneva U, B, and V filters. The observations were scheduled so that the

<sup>&</sup>lt;sup>1</sup>Literature data taken from WEBDA, http://www.univie.ac.at/webda/.

26 L.Eyer et al.

Fig. 1 Colour-Magnitude diagram of NGC 2447. We detect variability on time scales going from tens of minutes to tens of days in 54 variable stars in total. Below 14 V-mag, we find one slowly pulsating B star, one ellipsoidal binary, seven  $\delta$  Sct stars, six  $\gamma$  Dor stars and one hybrid  $\delta$  Sct –  $\gamma$  Dor pulsator



detection and phase coverage of both long and short period variables was optimized. All clusters were observed at least once per night during runs of 2 weeks, two to three times per year. We aimed to improve our coverage for short period variables by monitoring two clusters at higher cadence during each run. Observations of three of the southern clusters were limited to a 2-month baseline. In total, we obtained more than 2000 multi-band observations for each cluster.

Preliminary results have been published for NGC 1901 [3], NGC 5617 [2], and additional publications are in preparation for IC 4651, NGC 2447, and NGC 2437. A preliminary colour magnitude diagram for NGC 2447 including identified variables is shown in Fig. 1. We reach a precision of 5 mmag in V for the brightest constant stars. Reductions for the remaining clusters are ongoing. The methods used for data reduction and variability investigation are described in Greco et al. (in preparation) and [15].

#### 3.2 Gaia

Gaia is a space mission of the European Space Agency (for further information we refer to http://www.rssd.esa.int/Gaia). It will observe all objects brighter than  $V \sim 20$ , recording the position, brightness, spectrophotometric and spectroscopic measurements, to determine distances, proper motions, stellar basic parameters and radial velocities. The mission duration is 5 years (with a possible extension of 1 year), during which the satellite will observe the entire sky an average of 70 times. One billion stars will be observed, with a tentative estimate of 100 million variables. The satellite will be launched from French Guyana in 2012. There will be intermediate data releases (although it is too early to develop the details of these releases) and the final results will be published in 2020–2021.

The scientific impact of Gaia will be tremendous in many fields of stellar physics, Galactic structure and Galactic history. Since it combines all the fundamental measurement types (astrometry, photometry, spectroscopy), it will also impact the subject of time-resolved science, particularly for open clusters.

Furthermore, if we want to unravel the formation history of our Galaxy, it has become clear that also detailed abundances play a crucial role. This is why across Europe there is an effort to get vast amounts of observing time from ESO spectrographs (which is included in the GREAT<sup>2</sup> initiative).

#### 3.3 JASMINE

JASMINE is an acronym for Japan Astrometry Satellite Mission for INfrared Exploration. This project was planned in three phases of three satellites: Nano-JASMINE, Small-JASMINE, and JASMINE.

Nano-JASMINE (N-J), the first astrometric Japan satellite, should be launched in 2011 from Brazil by a Cyclone-4 rocket. N-J is fully funded by NAOJ (National Astronomical Observatory of Japan). The flight model will be completed this December. The N-J catalogue will be opened after about 2 years of operation. The observing strategy, whole sky scanning satellite, and method of the data analysis for N-J are similar to those for Gaia. N-J should reach in a zw-band (0.61  $\mu m$ ) an astrometric precision of 2–3 mas. It will observe more than 10 million stars, complete to zw  $\simeq$  12.

Small-JASMINE (S-J) is a project that will observe in an infrared band (Hwband:1.1–1.7 micron). S-J will determine positions and parallaxes accurate to  $10\,\mu as$  and will have proper-motion errors of  $9\,\mu as$ /year for stars brighter than Hw=11.5 mag. It will observe small areas of the Galactic bulge with a single-beam telescope whose primary mirror diameter is around 30 cm. If selected by JAXA (Japan Aerospace Exploration Agency), the target launch date would be around 2016.

JASMINE is an extended mission of the S-J mission. It is designed to perform a survey towards the Galactic bulge region (20 by  $10\,\mathrm{deg^2}$ ) around the Galactic center with a single-beam telescope whose primary mirror diameter is around  $80\,\mathrm{cm}$ . It will determine positions and parallaxes accurate to  $10\,\mu\mathrm{as}$  and will have propermotion errors of  $4\,\mu\mathrm{as}$ /year for stars brighter than Kw=11 mag. JASMINE would detect about one million bulge stars with the parallax uncertainty better than 10%. If selected, JASMINE will be launched in the first half of the 2020s.

These projects should complement very well the Gaia mission, since Gaia will observe in the visible G-band and will be more sensitive to extinction. S-J and JASMINE will have J- and H-band photometry besides Hw-band, and Kw-band for astrometry, but the detailed design for photometry has not been determined yet.

<sup>&</sup>lt;sup>2</sup>http://www.ast.cam.ac.uk/GREAT/.

28 L.Eyer et al.

#### 3.4 LSST

LSST (cf. [9] and http://www.lsst.org) stands for Large Synoptic Survey Telescope. It is an ambitious project of an 8.4-m telescope that will be situated in Chile (Cerro Pachon). Observations will consist of measurements of positions and fluxes using the 5 ugriz sloan+ y bands. During the 10 years of the project length, LSST will measure 1,000 times half of the sky. The beginning of the observations is foreseen in 2017. The magnitude limit will attain 24.5 in a single image and 27 in stacked images. The number of objects that will be observed by LSST is estimated to be 10 billion stars and 10 billion galaxies. When performance and magnitude ranges are compared between Gaia and LSST, we remark there are many synergies.

#### 3.5 VVV

We mention this ESO-survey because of its importance, but as it has been presented by Ivanov (details in these proceedings, see also [12]), we will therefore not develop it in this text.

**Acknowledgements** We would like to thank for their helpful comments Dr G.Bakos on Sect. 2.2 and Prof. N.Gouda on Sect. 3.3.

#### References

- 1. Bakos, G., et al.: Publ. Astron. Soc. Pac. 116, 266 (2004)
- 2. Carrier, F., et al.: Commun. Asteroseismol. **158**, 199 (2009)
- 3. Cherix, M., et al.: Memorie della Societa Astronomica Italiana 77, 328 (2006)
- 4. Eggenberger, P., et al.: Astron. Astrophys. 509, A72 (2010)
- 5. Groenewegen, M.A.T., et al.: Astron. Astrophys. **463**, 579 (2007)
- 6. Hartman, J.D., et al.: Mon. Not. R. Astron. Soc. 408, 475 (2010)
- 7. Hartman, J.D., Bakos, G.Á., Noyes, R.W., Sipöcz, B., Kovács, G., Mazeh, T., Shporer, A., Pál, A.: arXiv0907.2924 (2009)
- 8. Irwin, J., Bouvier, J.: In: Mamajek, E.E., Soderblom, D.R., Wyse, R.F.G. (eds.)The Ages of Stars. IAU Symposium, vol. 258, pp. 363. Cambridge University Press, Cambridge (2009)
- 9. LSST Science Collaborations, et al.: arXiv0912.0201 (2009)
- 10. Meynet, G., et al.: Astron. Astrophys. Suppl. 98, 477 (1993)
- 11. Miglio, A., et al.: In: Guzik, J.A., Bradley, P.A. (eds.) American Institute of Physics Conference Series. AIPCS, vol. 1170, pp. 132. (2009)
- 12. Minniti, D., et al.: New Astron. 15, 433 (2010)
- 13. Munari, U., et al.: Astron. Astrophys. 418, L31 (2004)
- 14. Pan, X., et al.: Nature 427, 326 (2004)
- 15. Saesen, S., et al.: Astron. Astrophys. **515**, A16+ (2010)
- 16. Soderblom, D.R., et al.: Astron. J. 129, 1616 (2005)
- 17. Southworth, J., et al.: Astron. Astrophys. **429**, 645 (2005)
- 18. Stello, D., et al.: Astrophys. J. Lett. **713**, L182 (2010)

- Valls-Gabaud, D.: In: Hartkopf, W.I., Guinan, E.F., Harmanec, P. (eds.) Binary Stars as Critical Tools & Tests in Contemporary Astrophysics. IAU Symposium, vol. 240, pp. 281. (2007)
- 20. Zwahlen, N., et al.: Astron. Astrophys. 425, L45 (2004)
- 21. van Leeuwen, F.: Astron. Astrophys. 341, L71 (1999)
- 22. van Leeuwen, F.: Astron. Astrophys. 497, 209 (2009)



Laurent Eyer sets the strategy

30 L.Eyer et al.



Jerôme Bouvier and Giusi Micela



What's in Jayne Birkby's laptop?

## SDSS-III/APOGEE: Detailed Abundances of Galactic Star Clusters

Peter M. Frinchaboy, Gail Zasowski, Kelly Jackson, Jennifer A. Johnson, Steven R. Majewski, Matthew Shetrone, Aaron Rocha, and the SDSS-III collaboration

Abstract The Sloan Digital Sky Survey III/Apache Point Observatory Galactic Evolution Experiment (SDSS-III/APOGEE) is a large-scale spectroscopic survey of Galactic stars and star clusters. The SDSS-III/APOGEE survey is designed to produce high-S/N, R = 27.500-31.000 spectra that cover a wavelength range of 1.51–1.68  $\mu$ m. By utilizing APOGEE's excellent kinematics (error  $< 0.5 \,\mathrm{km \, s^{-1}}$ ) and abundances (errors = 0.1 dex), we will be able to study star cluster kinematics and chemical properties in detail. Over the course of the 3-year survey beginning in 2011, APOGEE will target 25-30 key open and globular clusters. In addition, the large area coverage of the SDSS focal plane will also allow us to target stars in 100–200 additional star clusters during the main survey observations. We present the strength of APOGEE for both open and globular star cluster studies and the methods of identifying probable clusters members utilizing 2MASS and IRAC/WISE data.

P.M. Frinchaboy (⋈) · K. Jackson · A. Rocha

Department of Physics & Astronomy, Texas Christian University, TCU Box 298840, Fort Worth, TX 76129, USA

e-mail: p.frinchaboy@tcu.edu; kelly.m.jackson@tcu.edu; a.a.rocha@tcu.edu

G. Zasowski · S.R. Majewski

Department of Astronomy, University of Virginia, P.O. Box 400325, Charlottesville, VA 22904-4325, USA

e-mail: gz2n@virginia.edu; srm4n@virginia.edu

J.A. Johnson

Department of Astronomy, The Ohio State University, 140 West 18th Avenue, Columbus, OH 43210, USA

e-mail: jaj@astronomy.ohio-state.edu

M. Shetrone

McDonald Observatory, University of Texas at Austin, HC75 Box 1337-MCD, Fort Davis, TX 79734, USA

e-mail: shetrone@astro.as.utexas.edu

#### 1 Introduction

Star clusters represent a key tracer for the dynamical and chemical evolution of galaxies. The one galaxy for which we can investigate *in detail* is our own Milky Way galaxy. While there have been wide ranging studies of Galactic star clusters, there remains a key problem with studying Galactic evolution: lack of large uniform samples. For photometric studies, this is starting to be possible with large-area surveys (e.g., 2MASS, SDSS-I, VVV, Skymapper, LSST). Large kinematic samples have begun to be derived utilizing proper motions (e.g., [1, 4, 5, 7, 12]) and radial velocities (e.g., [9]). However, high-resolution spectroscopy studies, yielding high accuracy radial velocities and detailed chemical abundances, are still limited to small sets of clusters. The soon to be commissioned Sloan Digital Sky Survey III/Apache Point Observatory Galactic Evolution Experiment (SDSS-III/APOGEE) will provide for uniform data and analysis for a survey of up to 200 star clusters.

#### 2 SDSS-III/APOGEE

The SDSS-III/APOGEE project is 3-year high-resolution spectroscopic survey that will cover all major Galactic populations (thin disk, thick disk, bulge/bar, and halo). The project utilizes a new 300-fiber-fed H-band (1.51–1.68  $\mu$ m) spectrograph [23]. The spectrograph will yield R=27,500–31,000 spectra with  $S/N\sim100$  per pixel for stars with H=12.3. The goal of the survey is to derive precision radial velocities ( $\sigma_{v}\leq0.5~{\rm km~s^{-1}}$ ) and abundances ( $\sigma_{[X/Fe]}\leq0.1~{\rm dex}$ ) for  $\sim100,000$  stars. The survey has planned to study 15 different elements (including Fe, C, N, O,  $\alpha$ -elements, odd-Z elements, iron peak elements, possibly even neutron capture). The survey will coordinate observations with another SDSS-III survey, the Multi-object APO Radial Velocity Exoplanet Large-area Survey (SDSS-III/MARVELS) survey, which will necessitate that 75% of the observing time be spent in 58 key fields (which contain  $\sim$ 60 star clusters). The total APOGEE survey plans to target 220–230 unique field centers covering  $\sim$ 1, 200 deg $^2$  of the sky.

#### 2.1 APOGEE Calibration Clusters

One area of APOGEE science and calibration is the study of key star clusters listed in Table 1, with parameters taken from Harris catalog [14] for globular clusters and the Dias catalog [6] for the open clusters. These key clusters will have at least one 7 deg<sup>2</sup> plate configuration, up to 250 fibers, dedicated to likely cluster member stars.

<sup>&</sup>lt;sup>1</sup>High-resolution studies of up to ten open clusters are starting to be published using CTIO/WIYN Hydra (e.g., [8, 16]) and VLT/Flames+UVES (e.g., [2, 20, 21]).

Table 1 A	PUGEE	candidate c	andrauc	ni ciustei	8			
Name		Type	Diam	[Fe/H]	$\sigma_{[Fe/H]}$	Age (years)	Log(Age)	Dist(pc)
NGC 188		Open Cl	17'	-0.01	0.09	4.2 Gyr	9.632	2047
Pleiades		Open Cl	110'	-0.03	0.06	135 Myr	8.131	150
Hyades	M45	Open Cl	330'	+0.13	0.06	787 Myr	8.896	45
NGC 2168	M35	Open Cl	25'	-0.16	0.09	95 Myr	7.979	816
NGC 2243		Open Cl	5'	-0.49	0.05	1.1 Gyr	9.032	4458
Melotte 71		Open Cl	7'	-0.30	0.06	235 Myr	8.371	3154
NGC 2420		Open Cl	5'	-0.40		2.8 Gyr	9.45	2290
NGC 2682	M67	Open Cl	25'	-0.15	0.05	2.5 Gyr	9.409	908
NGC 6171	M107	Globular	17'	-0.90	0.10	GC	GC	6400
NGC 6205	M13	Globular	25'	-1.51	0.10	GC	GC	7700
IC 4725	M25	Open Cl	29'	+0.17	0.06	92 Myr	7.965	620
NGC 6791		Open Cl	10'	+0.35	0.02	4.4 Gyr	9.643	5853
NGC 6819		Open Cl	5'	+0.07		3.1 Gyr	9.490	2360
NGC 6838	M71	Globular	9'	-0.79	0.10	GC	GC	6700
NGC 7078	M15	Globular	21'	-2.20	0.10	GC	GC	10300
NGC 7089	M2	Globular	21'	-1.62		GC	GC	11500
NGC 7789		Open Cl	25'	-0.20		1.7 Gyr	9.230	1820

 Table 1
 APOGEE candidate calibration clusters

For some of the open clusters (e.g., M67, NGC 188, NGC 6819) we have kinematic membership and binary information available from the WIYN Open Cluster Study (WOCS; [10, 15, 19])

We will explicitly target many stars which have already been observed at high resolution (R > 30,000) in the optical or near infrared to be used to compare SDSS-III/APOGEE to other high-resolution studies. For these "calibration" cluster targets, we will obtain large numbers of members that will be used to fully characterize the clusters bulk chemical properties, but also allow science ranging for looking for abundance variations on the individual element level to investigating isotopic abundance variations as keys to understanding evolution along the red giant branch.

## 3 APOGEE Candidate Cluster Analysis

## 3.1 Photometry Analysis

The APOGEE project requires this cleaning for most clusters for two reasons: (1) most open clusters are found at low Galactic latitude and thereby are heavily contaminated with field stars. (2) Due to the large SDSS telescope field of view [13], the minimum fiber-to-fiber distance is fairly large  $\geq 1$  arcmin, which only allows for the targeting of a handfull of stars ( $\sim 5-10$ ) per cluster for the most poorly studied, distant, and reddened clusters. The only all-sky photometry that will be available for APOGEE targeting will come from two sources Two-Micron All-Sky Survey (2MASS  $JHK_S$ ; [22]) and the soon to be released *Wide-field Infrared* 

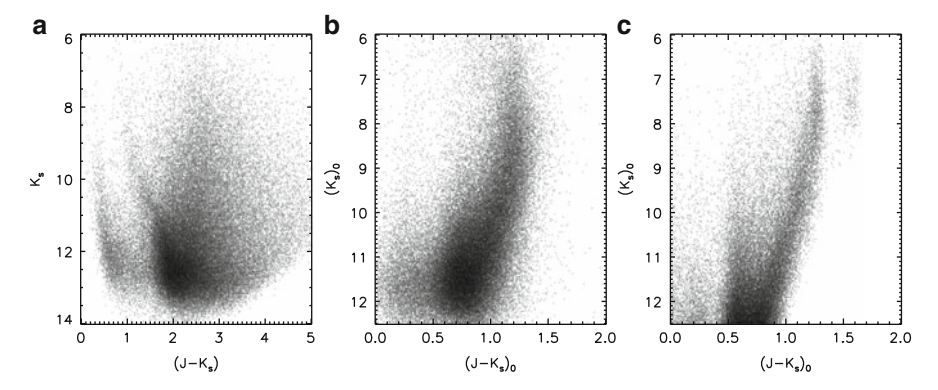


**Fig. 1** Demostration of the RJCE technique. (a) Raw 2MASS CMD for a  $4 deg^2$  field at (l, b) = (42,0). (b) Field dereddened using the RJCE technique. (c) TRILEGAL [11] simulation of the Galaxy for a field at (l, b) = (42,0)

Survey Explorer (WISE; [24]) mission. However, since many of the targets will be in the Galactic midplane, and WISE has poor resolution (~6 arcsec), we will also supplement our data set with *Spitzer/IRAC* Galactic Legacy Infrared Mid-Plane Survey Extraordinaire (GLIMPSE I, II, 3D, 360; [3]) surveys, which provide better resolution in the needed [3.6] and [4.5] micron bandpasses.

These surveys will provide five-band photometry  $JHK_S[3.6][4.5]$  data which allow us to derive star-by-star extinctions utilizing the Rayleigh–Jeans Color Excess (RJCE) method (see Fig. 1), fully described in Majewski et al. [17]. The RJCE method allows us to explicitly determine the  $A_{K_S}$  extinction to each star by using the observed H-[4.5] color that is nearly constant for a large range of common spectral types. The ability to derive extinctions and correct to relative distance ranges is essential for a survey of the Galactic plane and bulge, and we can utilize this tool to isolate potential cluster stars from the field population.

## 3.2 Cluster Analysis

In order to distinguish and isolate star cluster stars from foreground and background contamination, we utilize the  $A_{K_S}$  values derived from the RJCE technique described above. We isolate a region of approximately twice the clusters catalog radius [6] and divide it into 5 regions (see Fig. 2a). We utilize four "background" regions and the cluster region (radius =  $R_{Dias}$ ). The background is divided in order to account for dust clouds, clusters near the edge of the GLIMPSE survey region, and any other source of background variability. We difference the mean field/background star numbers to the "cluster" star numbers within a given  $A_{K_s}$  range, and scan this range across all available  $A_{K_s}$  values that have at least 15 stars (Mean field + cluster stars  $\geq 15$ ; see Fig. 2b). The window of extinction

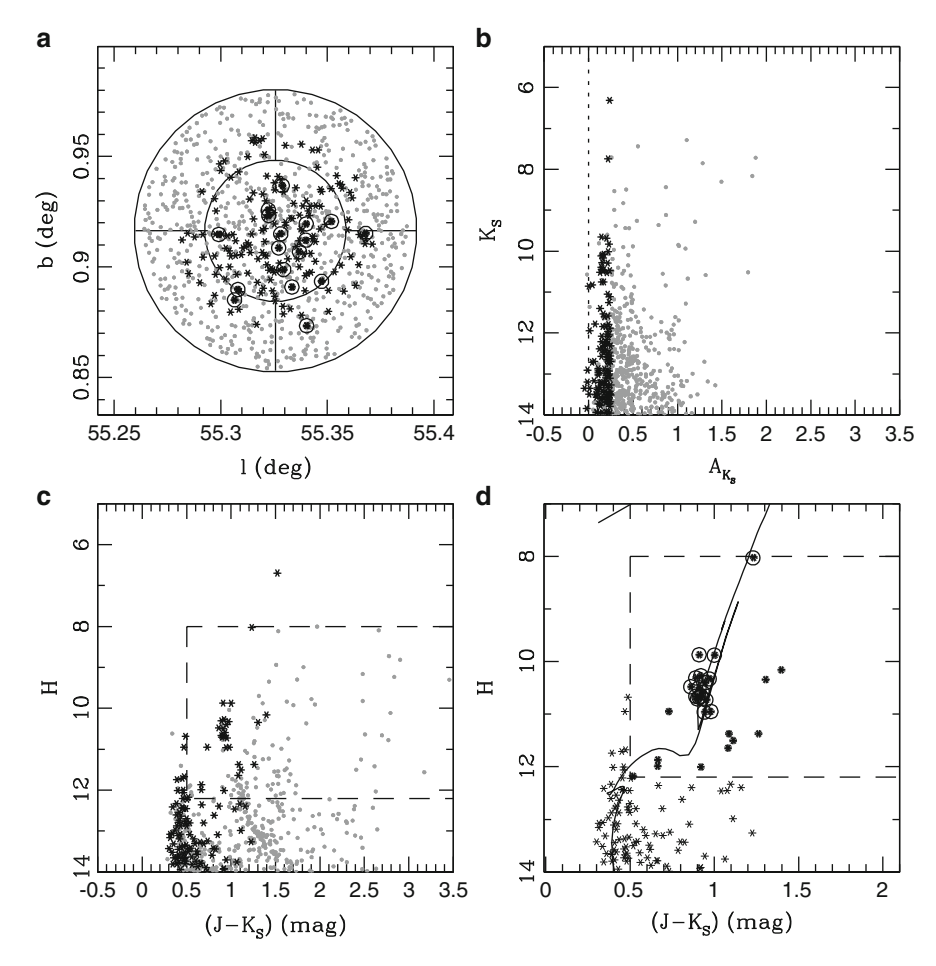


Fig. 2 Sample analysis for the cluster NGC 6802 utilizing 2MASS+GLIMPSE data. (a) Galactic latitude and longitude for all stars (gray) within the  $2R_{cl}$  area to be analyzed, stars selected to be likely members from the photometry extinction analysis are shown in *black*. Prime APOGEE targets are circled. (b) Distribution of  $A_{K_s}$  for all stars in the NGC 6802 sample area, black points denote stars with  $1.1R_{cl}$  within the determined mean cluster  $A_{K_s}$  range. (c) Color-magnitude diagram (CMD) for all stars in the analysis area (gray). The *dashed box* denotes the SDSS-III/APOGEE target selection region. *Black points* denote stars selected as likely members from their  $A_{K_s}$ . (d) CMD of only likely cluster members overplotted with the Padova Isochrone [18] using the clusters parameters from [6]. *Circled stars* denote identified high-probability stars for APOGEE target selection (also see the on-sky distribution in (a))

with the highest concentration of stars within the inner radius will reveal the cluster (Fig. 2c, d). We then work to optimize the cluster isolation surveying a grid of  $A_{K_s}$  width,  $A_{K_s}$  stepsize, and allowed  $\sigma_{A_{K_s}}$  values.

#### 3.3 Preliminary Results

We present a first analysis for the cluster NGC 6802 to demonstrate the technique, shown in Fig. 2. Figure 2a first shows the area explored by our analysis in Galactic latitude and longitude. As described above, we selected likely cluster members utilizing the  $A_{K_s}$  as shown in Fig. 2b. For NGC 6802 we find a low, but nonnegligible extinction or reddening to the cluster. A color magnitude diagram (CMD) of the clusters (Fig. 2c) is generated which highlights the member stars with  $A_{K_s}$  values within the window of extinction, where the dashed box in the center denotes the area where the upcoming SDSS-III/APOGEE project will be targeting (8.0 < H < 12.3 and H = 13.4 is compare our "cleaned" cluster CMD to the Padova isochrone utilizing catalog values [6] for NGC 6802 and find a good match. By comparing the CMD with isochrone values, when available, we are able to isolate candidate cluster stars with a high probablility for membership needed for APOGEE targeting and science.

Acknowledgements SDSS-III is managed by the Astrophysical Research Consortium for the Participating Institutions of the SDSS-III Collaboration including the University of Arizona, the Brazilian Participation Group, Brookhaven National Laboratory, University of Cambridge, University of Florida, the French Participation Group, the German Participation Group, the Institute de Astrofisica de Canarias, the Michigan State/Notre Dame/JINA Participation Group, Johns Hopkins University, Lawrence Berkeley National Laboratory, Max Planck Institute for Astrophysics, New Mexico State University, New York University, the Ohio State University, University of Portsmouth, Princeton University, University of Tokyo, the University of Utah, Vanderbilt University, University of Virginia, University of Washington, and Yale University. This work is based in part on observations made with the Spitzer Space Telescope, which is operated by the Jet Propulsion Laboratory, California Institute of Technology under a contract with NASA. Support for this work was provided by NASA through an award issued by JPL/Caltech. Additionally KJ was supported by an NSF REU grant (NSF 0851558) and funding from Texas Christian University, including a Science and Engineering Research Center (TCU-SERC) grant.

#### References

- 1. Baumgardt, H., Dettbarn, C., Wielen, R.: Astron. Astrophys. Suppl. 146, 251 (2000)
- Bragaglia, A., Sestito, P., Villanova, S., Carretta, E., Randich, S., Tosi, M.: Astron. Astrophys. 480, 79 (2008)
- 3. Churchwell, E., et al.: Publ. Astron. Soc. Pac. 121, 213, (2009)
- 4. Dias, W.S., Lépine, J.R.D., Alessi, B.S.: Astron. Astrophys. 376, 441 (2001)
- 5. Dias, W.S., Lépine, J.R.D., Alessi, B.S.: Astron. Astrophys. 388, 168 (2002)
- 6. Dias, W.S., Alessi, B.S., Moitinho, A., Lepine, J.R.D.: Astron. Astrophys. 389, 871 (2002)
- 7. Dias, W.S., Assafin, M., Flório, V., Alessi, B.S., Líbero, V.: Astron. Astrophys. 446, 949 (2006)
- 8. Friel, E.D., Jacobson, H.R., Pilachowski, C.A.: Astron. J. 139, 1942 (2010)
- 9. Frinchaboy, P.M., Majewski, S.R.: Astron. J. 136, 118 (2008)
- 10. Geller, A.M., Mathieu, R.D., Harris, H.C., McClure, R.D.: Astron. J. 135, 2264 (2008)
- Girardi, L., Groenewegen, M.A.T., Hatziminaoglou, E., da Costa, L.: Astron. Astrophys. 436, 895 (2005)

- 12. Glushkova, E.V., Zabolotskikh, M.V., Rastorguev, A. S., Uglova, I. M., Fedorova, A.A.: Astron. Lett. 23, 71 (1997)
- 13. Gunn, J.E., et al.: Astron. J. 131, 2332 (2006)
- 14. Harris, W.E.: Astron. J. 112, 1487 (1996)
- Hole, K.T., Geller, A.M., Mathieu, R.D., Platais, I., Meibom, S., Latham, D.W.: Astron. J. 138, 159 (2009)
- 16. Jacobson, H.R., Friel, E.D., Pilachowski, C.A.: Astron. J. 137, 4753 (2009)
- 17. Majewski, S.R., Zasowski, G., Nidever, D.L.: Astron. J. (submitted) (2010) arXiv:1106.2542
- Marigo, P., Girardi, L., Bressan, A., Groenewegen, M.A.T., Silva, L., Granato, G.L.: Astron. Astrophys. 482, 883 (2008)
- 19. Mathieu, R.D., Latham, D.W., Griffin, R.F., Gunn, J.E.: Astron. J. 92, 1100 (1986)
- Sestito, P., Bragaglia, A., Randich, S., Carretta, E., Prisinzano, L., Tosi, M.: Astron. Astrophys. 458, 121 (2006)
- 21. Sestito, P., Bragaglia, A., Randich, S., Pallavicini, R., Andrievsky, S.M., Korotin, S.A.: Astron. Astrophys. **488** 943, (2008)
- 22. Skrutskie, M.F., et al.: Astron. J. 131, 1163 (2006)
- 23. Wilson, J.C., et al.: SPIE 7735, 46 (2010)
- 24. Wright, E.L., et al., AJ, 140, 1868 (2010)



André Moitinho, Simon Hodgkin and Peter Frinchaboy



Simon Hodgkin



Coffee break

## **Processing Data from Large Infrared Surveys**

Simon Hodgkin, Mike Irwin, Jim Lewis, Eduardo Gonzalez-Solares, and Aybüke Küpcü Yoldaş

**Abstract** At the Cambridge Astronomical Survey Unit (CASU<sup>1</sup>) we are responsible for the development and implementation of a number of pipelines for the routine processing of large area near-infrared surveys. In this paper, we discuss some of the challenges we face when tackling the large volumes of data generated nightly from WFCAM on UKIRT and VIRCAM on VISTA.

#### 1 Introduction

VISTA alone requires 3 distinct pipelines, run in 3 different places:

- 1. *Paranal pipeline:* data from VISTA are assessed for quality control (QC) in real time at the summit using a simplified data reduction pipeline. Because these reductions have to happen very rapidly and in a causal sequence, this pipeline relies on previously prepared library calibration information.
- 2. Garching pipeline: the raw data are then collected onto USB discs, which are shipped to Garching and ingested into the ESO raw data archive. A second pipeline is run, used to monitor instrumental health, generate calibration information and to provide library calibration frames for the summit pipeline. More up-to-date calibration information is applied and the quality control results are correspondingly better.
- 3. *Cambridge pipeline:* once the archive ingestion is done, the same USB discs are forwarded to Cambridge for science data processing. When running the science

<sup>1</sup>http://casu.ast.cam.ac.uk/

S. Hodgkin (⊠) · M. Irwin · J. Lewis · E. Gonzalez-Solares · A.K. Yoldaş Institute of Astronomy, Madingley Road, Cambridge CB3 0HA, UK e-mail: sth@ast.cam.ac.uk; mike@ast.cam.ac.uk; jrl@ast.cam.ac.uk; eglez@ast.cam.ac.uk

40 S. Hodgkin et al.

pipeline we are able to consider an entire night of data (or indeed a whole week of data) as a single entity and hence we can use information which is not available to the ESO pipelines. This leads to a much better result than can be obtained with the QC pipelines.

The Cambridge pipeline products (astrometrically and photometrically calibrated images and catalogues) can then be accessed by the survey participants either directly from Cambridge, or via the VISTA and WFCAM Science Archives (VSA, WSA) both hosted at the Royal Observatory in Edinburgh.

## 2 Processing of VIRCAM and WFCAM Images

Observing in the near infrared is a little like observing in the daytime, the vast majority of interesting sources are much fainter than the bright and variable night-time sky. Modern infrared detectors are now very sensitive, but they do tend to suffer from significant instrumental features. The most pernicious of these are described below, together with a short outline of how they are removed.

- Reset correction: this is similar but not the same as a debias operation in CCD processing. Reset frames are taken for each exposure and are subtracted in the data acquisition system. Although this is not a pipeline reduction step per se, it is important to realise that this happens as it has an impact when estimating the linearity of the detectors.
- *Dark correction:* the dark current is estimated from a series of exposures taken with a dark filter inserted. Subtracting a mean dark frame also corrects several other additive electronic effects, such as residual reset correction anomalies.
- Linearity correction: although the WFCAM detectors are linear, the VIRCAM detectors do not have a linear response. To estimate the non-linearity of each detector we need information on the readout timing, the exposure time and the reset image timing (this is because there is no shutter on the camera and in double-correlated sampling mode, the default, the reset frame is subtracted prior to writing images to disk).
- Flat field correction: dividing by a mean twilight flatfield image removes the small scale QE variations in the detector as well as the large scale vignetting profile of the camera. We also use the global flatfield properties of each detector to gain-normalise each detector to a common (median) system.
- Sky background correction: this removes the large scale spatial background emission that comes from the atmosphere as well as several remaining additive effects. The 2-D background map is estimated using several different algorithms that combine the science images themselves with rejection or masking. Sometimes when large extended objects are present it is necessary to use offset sky exposures to get a background map. Automating this correctly is one of the most difficult parts of near-infrared image processing. Figure 1 shows an example of a WFCAM image with and without sky subtraction.

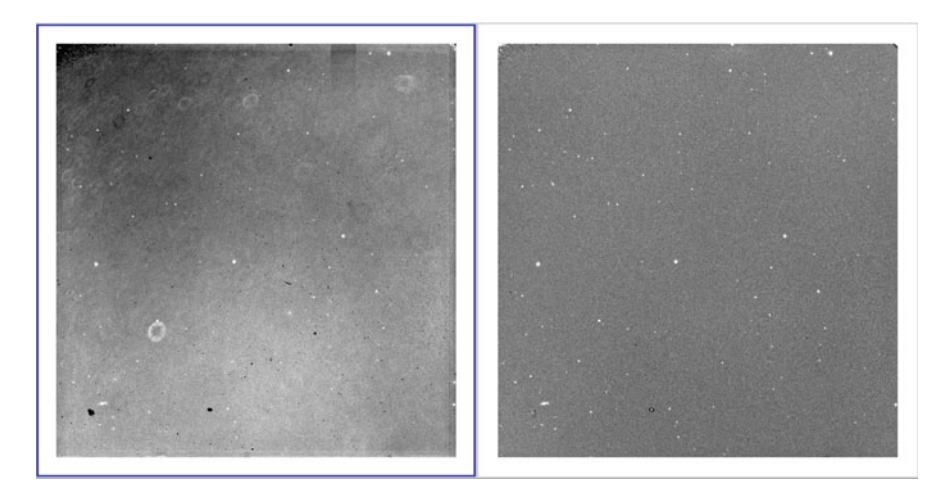


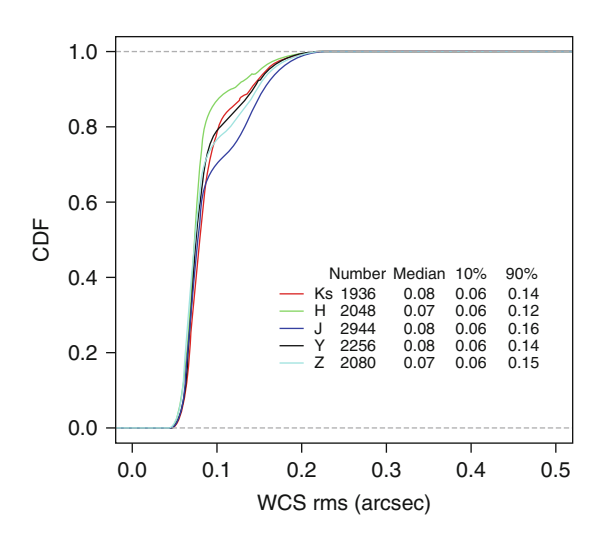
Fig. 1 Images from WFCAM with and without the skysubtraction applied

- Destripe: the readout electronics for the VIRCAM detectors introduce a low-level horizontal stripe pattern into the background. Every exposure yields a different pattern, but groups of four detectors, readout through the same IRACE controllers, have the same pattern on a given exposure. This means there a great deal of redundancy when it comes to estimating the stripe pattern. WFCAM shows a similar pattern, but with a different symmetry due to the detector properties.
- Jitter stacking: infrared detectors often have large numbers of cosmetic defects implying infrared imaging is invariably done in a jitter mode, whereby an observation of a region is broken up into several shorter exposures and the telescope moved slightly between them. At this point in the reduction the jitter series is shifted and combined to form a single image stack, using positions of detected objects on all the detectors to compute the shifts. This allows bad pixel regions in one exposure to be rejected in favour of good pixels in other exposures.

Two corrections not discussed above and not implemented for either VIRCAM and WFCAM are: a *fringe correction* which is at a very low level for both instruments and is automatically dealt with during sky subtraction, and a *crosstalk correction* which is very significant in WFCAM (and very hard to remove without compromising the images), and not seen with VIRCAM. We also looked for evidence of persistence, which manifests itself as a glow on a detector where a bright object was recently observed. For both the WFCAM and VIRCAM detectors this turned out to be a very small and unpredictable effect which only occurred when extremely bright stars (which are rare) are observed. In practice this effect is negligible and is therefore ignored during pipeline processing.

42 S. Hodgkin et al.

Fig. 2 The cumulative density function of VIRCAM WCS *rms* values on each filter for all chips, using seven nights of science verification data from Oct 2009. For each filter the number of chips used, median and 10 and 90% quantiles are shown



#### 3 Astrometric Calibration

The astrometric solution for each image taken with VIRCAM or WFCAM is derived from 2MASS. The WCS distortion model used for both instruments is based on the ZPN projection. For a purely radial distortion, this relates the true on-sky radial distance from the optical axis to the measured radial distance in the focal plane in the form:

$$r' = k1r + k3r^3 + k5r^5 + \dots$$
(1)

where k1 is the plate scale at the centre, and k3, k5 etc describe the distortion relative to the angular distance on the focal plane. For WFCAM, k5 is negligable. For VIRCAM  $k1 = 0.3413 \, \text{arcsec/pixel}$  (i.e. 17.065 arcsec/mm) and in angular units the distortion coefficients are given quite accurately by k3/k1 = 44 and k5/k1 = -10300 (using angular measures in radians). Higher order terms are negligible. After distortion correction the residuals from individual detector linear fits can be used to monitor the quality of the 2MASS-based astrometric solution which has a rms of around 80 milliarcseconds for both WFCAM and VIRCAM, dominated by the 2MASS errors (see Fig. 2).

#### 4 Photometric Calibration

The photometric calibration, like the astrometric calibration, is derived from 2MASS, following the methods outlined in [2]. The unsaturated 2MASS stars that are observed in every VIRCAM/WFCAM exposure can be used to derive a single photometric zeropoint for every image (after correcting the 2MASS photometry into the appropriate observing filter system, see Fig. 3).

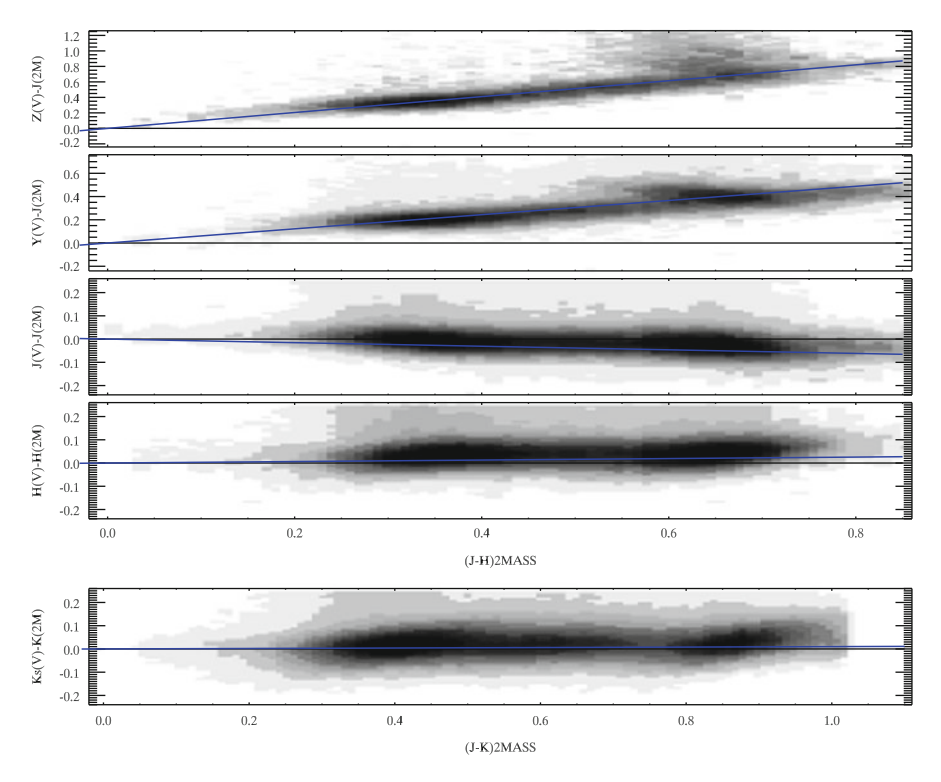


Fig. 3 Hess diagrams to show the measurements of VISTA-2MASS colours for data taken on clear nights in regions of low reddening. The *blue lines* show the colour equations currently in use

Stacking 2MASS zeropoints over long timescales allows us to measure residual spatially-dependent illumination corrections in the data and, for WFCAM, to reach accuracies of 2% in ZY and 1.5% for the JHK bands. With VIRCAM, the illumination corrections look significantly smaller, and we are currently quanitfying the accuracy of the calibration. Obvious benefits of this strategy include a reduction in the observing time required to monitor photometric standards, and the ability to recover the calibration for data taken through thin cirrus. A caveat is that the photometric calibration becomes less robust for regions of extremely high reddening, though this is a relatively small fraction of the sky.

In addition to astrometric effects the change in scale as a function of radius also creates photometric complications. The aim of conventional flatfielding is to create a flat background by normalising out perceived variations from uniformly illuminated frames. If the sky area per pixel changes then this is reflected in a systematic error in the derived photometry. However, since it is much simpler to deal with "flat" backgrounds, this problem is either usually ignored or corrected during later processing stages, together with other systematic photometry effects. The amount of photometric distortion amounts to a 3.5% effect at the edge of the field for VIRCAM, and 1.2–1.7% (wavelength-dependent) for WFCAM.

44 S. Hodgkin et al.

#### 5 From Pawprints to Tiles

A standard VIRCAM tile image is made up from 6 stacked pawprints each containing 16 detector-level images. The sky level on all 96 component images is adjusted to the same level and the components are then projected (drizzled) onto a single Tangent Plane WCS image. During the projection the pixel intensities with respect to sky are adjusted to account for the spatially-dependent photometric distortion within the original ZPN pawprints. Thus no additional photometric distortion correction is necessary for tiled products with VIRCAM (This is not the case for WFCAM where the final products are pawprint based, because the overlaps are not required to achieve full survey depth). Creating tiled images in this simple way has the advantange of preserving edge structures and other artefacts to aid in visual inspection of, say, candidate rare objects and enables most large scale structures to be retained for further investigation (Fig. 4).

The drawback from a catalogue generating point of view is that edges between detectors can often introduce spurious structures and also subsequent spurious objects in the catalogues. For more reliable catalogue generation from tiles we prefilter each stacked pawprint image using a nebulosity filter (see below) to remove all structure on scales of 30 arcsec and over. This filter is also fairly adept at reducing edge effects between pawprints. These filtered images are tiled in exactly the same

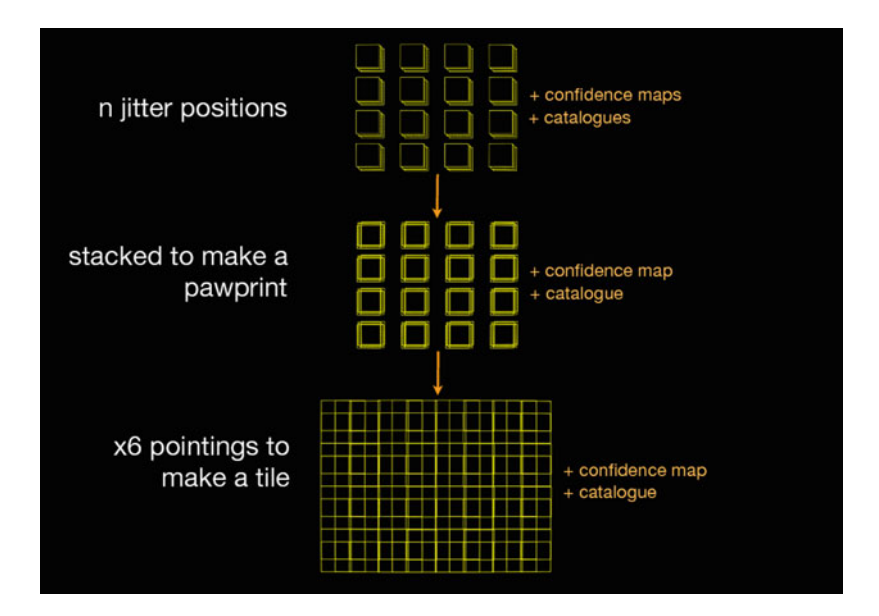
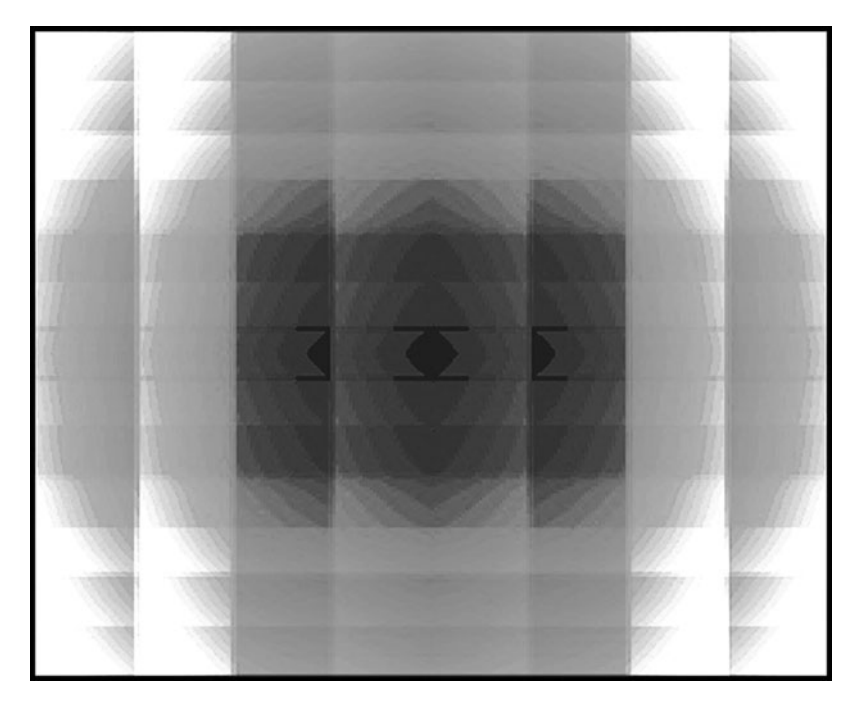


Fig. 4 VIRCAM comprises  $16.2k \times 2k$  Ratheon detectors, each with a Field of view of  $11.6 \times 11.6$  arcmin. 6 pointings are required for continuous uniform coverage. A single pointing is called a pawprint (it made sense when we had 4 array devices with WFCAM), and 6 make a tile with a combined field of view of  $1 \times 1.5$  deg



**Fig. 5** The image shows the systematics in photometry arising from a standard VISTA 6 pointing tile. The systematics vary from 0% in the centre (*dark*) up to 3% toward the corners (*light*)

way as previously but since the background is guaranteed to be completely flat for each detector image, the resulting tile image is much more uniform, since it is by design devoid of any large-scale background structure. The tile catalogues are then created from these images (Fig. 4).

Each detector potentially has a different PSF and together with the varying seeing conditions that can happen during the observation of a tile this means that there are normally 96 different PSFs which contribute to a single tile (some of which are combined in the overlap areas). In order to compute the corrections for the aperture fluxes we assume that the PSF does not vary across the tile. This will inevitably introduce spatial photometric distortions at the level of at least 1–2% over the tile, and we are currently investigating ways of correcting this for VISTA tiles (Fig. 5).

#### 6 The Nebuliser

Traditional methods for source detection first model the background with a singlepass smoothly varying map. Sources are then detected as significant connected pixels above the local background estimate (see e.g. [1,3]). This works well for most of the sky, however in regions of bright, spatially-varying nebulosity, traditional 46 S. Hodgkin et al.

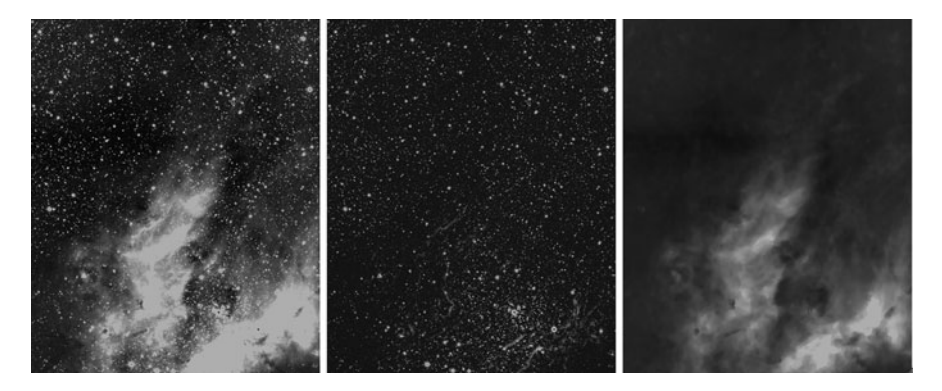


Fig. 6 Spatially splitting the WFCAM image of M17 (*left*) into small-scale features (*the stars*, *centre*) and large-scale features (the background and nebulosity, right) using iteratively clipped non-linear filtering

background following is insufficient, even after increasing the resolution of the background map. An example of such a region is illustrated in Fig. 6, which shows WFCAM K-band observations of M17, taken as part of the UKIDSS Galactic Plane Survey. To handle such data we are using a new aproach, nicknamed the Nebuliser [4]. The Nebuliser works by constructing a non-linear iteratively smoothed version of the image, which attempts to decouple objects from background on the basis of their spatial frequency and hence generate a usable background map. The results of running the algorithm on the M17 data are shown in Fig. 6

The algorithm is also extremely useful in the construction of tiles (see above). The code for this algorithm is now available to the community in the CASUTools package, which can be obtained from our website.<sup>2</sup> For more information and additional support, please contact us via email.<sup>3</sup>

#### References

- 1. Bertin, E., Arnouts, S.: Astron. Astrophys. Suppl. 117, 393 (1996)
- Hodgkin, S.T., Irwin, M.J., Hewett, P.C., Warren, S.J.: Mon. Not. R. Astron. Soc. 394, 675 (2009)
- 3. Irwin, M.J.: Mon. Not. R. Astron. Soc. 214, 575 (1985)
- 4. Irwin, M.J.: UKIRT Newsl. 26, 14 (2010)

<sup>&</sup>lt;sup>2</sup>http://casu.ast.cam.ac.uk/surveys-projects/software-release/software-release/view.

<sup>&</sup>lt;sup>3</sup>email:casuhelp@ast.cam.ac.uk.

## **Properties of Star Clusters Found and Investigated by Data from Large Surveys**

Elena V. Glushkova, Sergey E. Koposov, Ivan Yu. Zolotukhin, and Ramakant S. Yadav

**Abstract** An automated method capable of searching for star clusters in large surveys has been applied to J, H,  $K_s$  data from 2MASS catalog. Totally, we found and verified 168 new clusters; for 142 of them, we evaluated ages, distances and color excesses using photometric data from the 2MASS and UKIDSS surveys. Most of new clusters are older than 100 Myr and have distances within the range 1–4 kpc. 26 newly discovered objects are embedded clusters. An independent check against UBVI photometric data obtained at a 104-cm Sampurnanad telescope demonstrated a very good agreement of our results with these observational data. Some known, but doubted or poorly studied clusters were also investigated using the 2MASS catalog.

#### 1 Introduction

Some literature estimates put the total number of open clusters in the Galaxy at 10<sup>5</sup>. But 2095 clusters only were cataloged by Dias et al. in the latest version of their catalog http://www.astro.iag.usp.br/~wilton. That is why the task of searching for

E.V. Glushkova (⊠)

Sternberg Astronomical Institute, Universitetsky pr. 13, Moscow 119992, Russia e-mail: elena@sai.msu.ru

S.E. Koposov

Institute of Astronomy, University of Cambridge, Madingley road, CB3 0HA, Cambridge, UK e-mail: koposov@ast.cam.ac.uk

I. Yu. Zolotukhin

Sternberg Astronomical Institute, Universitetsky pr. 13, Moscow 119992, Russia e-mail: iz@sai.msu.ru

R.S. Yadav

Aryabhatta Research Institute of Observational Sciences, Manora Peak, Nainital 263129, India e-mail: rkant@aries.ernet.in

A. Moitinho and J. Alves (eds.), *Star Clusters in the Era of Large Surveys*, Astrophysics and Space Science Proceedings, DOI 10.1007/978-3-642-22113-2\_6, © Springer-Verlag Berlin Heidelberg 2012

48 E.V. Glushkova et al.

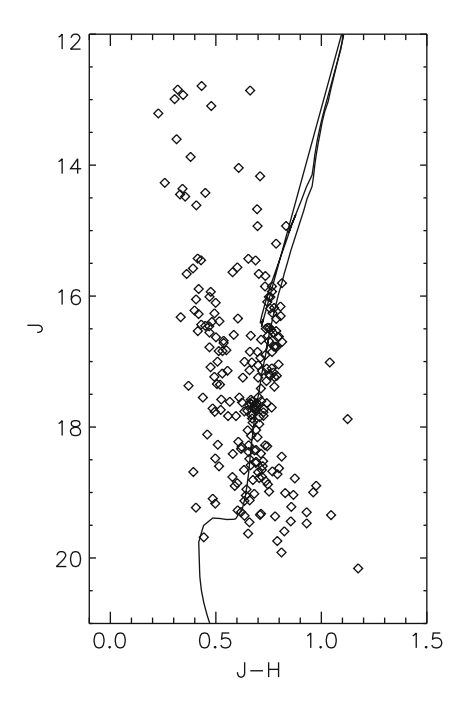
new clusters seems to be promising. As most open clusters are concentrated near the Galactic plane where extinction by interstellar dust is most severe, then the search of infrared surveys should be most perspective. We performed such an investigation using  $JHK_s$  data from the 2MASS point source catalog by an efficient automated method of searching stellar catalogs for star clusters of various radii. To decide whether stellar groups detected by our method are real star clusters, we extended our technique with a special verification method. The results of this investigation have been published in two papers and on the special web site <a href="http://ocl.sai.msu.ru">http://ocl.sai.msu.ru</a>.

#### 2 Discovery of New Clusters and Their Properties

Shortly, the method of searching is based on the convolution of cataloged density maps with the filter of a special shape. In this case, a flat or even slowly changing background produces a zero signal, whereas concentrations of stars exhibit a high signal. We detected 11186 overdensities with the significance level of more than 4.5  $\sigma$  in the region of Milky Way within the interval of the galactic latitude  $-24^{\circ} < b < 24^{\circ}$ . All these overdensities were checked with a special verification procedure, and it was demostrated that most of them are not real clusters, but fast background variations especially in the direction of the galactic center. The verification procedure implies building the Hess-diagram for every overdensity peak and then fitting an isochrone to (J, J - H) diagram in such a way that the radial density distribution for stars lying on the isochrone shows a noticeable concentration toward the center, whereas the distribution for all other stars is almost flat. We verified 168 new clusters among those 11186 overdensities. The known objects have also been found: we detected and identified 565 open and 114 globular clusters.

So, 10339 overdensities turned to be nonclusters. However, this pattern may contain real clusters - we simply could not verify them, because they are in the region where the background varies too quickly, especially in the direction of the galactic center. The second reason for which we cannot confirm all real clusters from the list of overdensities is the magnitude limit (about  $16^m$  in J-filter) of the 2MASS catalog. We could not fit isochrones and verify a number of clusters, because only the upper part of their main sequence or red giant branch can be seen in color-magnitude diagrams. If one uses the deeper survey UKIDSS GPS, then one may confirm more clusters. The limiting magnitude in the J-filter is greater by approximately  $3.5^m$  for UKIDSS GPS than that for 2MASS. For example, in Fig. 1, the color-magnitude diagram for SAI 50 is shown. This CMD was built with data from UKIDSS GPS and is reduced to the red giant branch only. If we cut this diagram at the  $16^m$  which corresponds to limits in 2MASS, we will not detect any cluster here. We investigated 22 cluster candidates found with data from 2MASS in UKIDSS GPS. The reality of nine clusters has been confirmed, and we derived their parameters such as the age, distance and color-excess. Four of these nine objects can not be confirmed as real clusters using 2MASS data only.

Fig. 1 Color-magnitude diagram of the new cluster SAI 50 built with data from UKIDSS GPS



Among our new clusters, 26 are embedded clusters. As a rule, they can not be seen in visual passbands. Unfortunately, we could not fit isochrones for such clusters and find their parameters.

For all other new clusters, we fitted isochrones and found their main parameters: the age, distance to the cluster and extinction to the cluster direction. In Fig. 2, we see the distribution of the clusters in the projection onto the galactic plane. The clear lack of clusters in the direction to the galactic center should be attributed to the discussed impossibility to distinguish a real stellar concentration from rapid variations of the background. Most of the newly discovered clusters are situated at distances ranging from 1 to 4 kpc from the Sun. The sample is complete for open clusters closer than 800–1,000 pc. That is why we did not search for such objects. More distant clusters can be detected, but cannot be verified with data from 2MASS only.

It is clear that most of the new clusters are old ones or clusters of moderate ages with log(t) > 8.0. The reason for that is pretty simple: all young and bright clusters have already been discovered.

As a by-product of our work with data from 2MASS, we confirmed the reality of 14 open clusters known earlier but labelled doubtful (according to the Dias et al. catalog) and evaluated their parameters.

50 E.V. Glushkova et al.

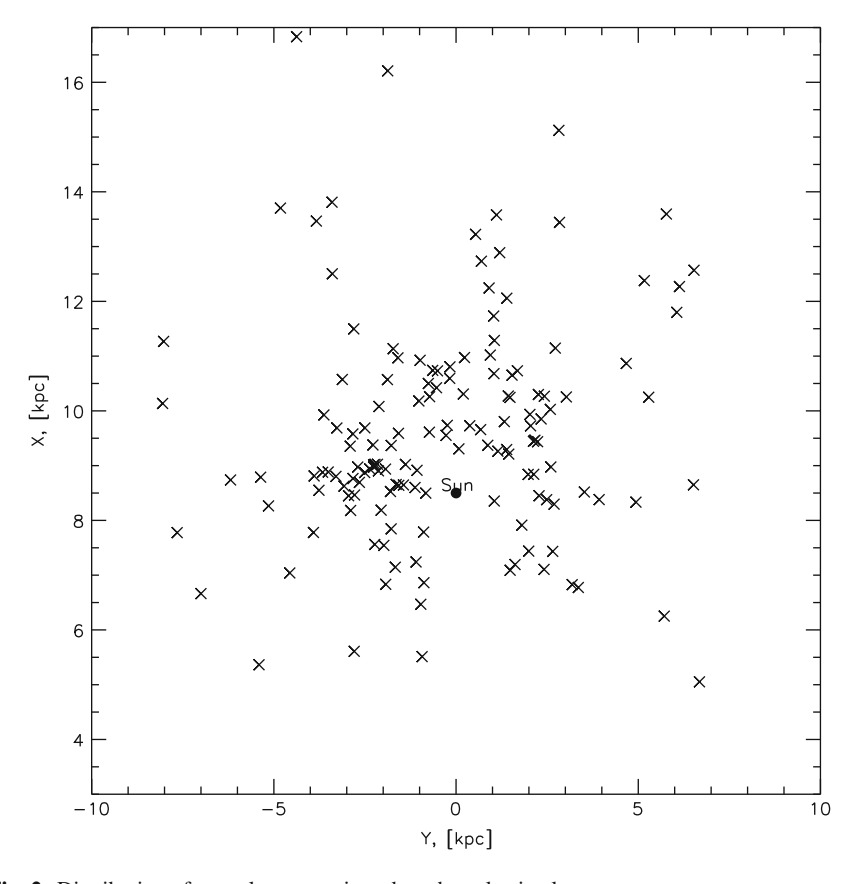


Fig. 2 Distribution of new clusters projected on the galactic plane

## 3 Verification of New Clusters by Optical Observations

Most of new clusters are poor or projected against a rich background and can not be detected "by eye", but we may confirm them by our procedure of verification. In addition, we are carrying out optical observations of a number of the new clusters at different sites, in particular, at the 104-cm Sampurnanand telescope of ARIES institute in India. At this site, we obtained UBVI CCD data for 6 new clusters. Using these data, we derived ages, distances, color excesses and metallicities of the clusters. Figure 3 shows the isochrones fitted to color–color and color–magnitude diagrams for cluster Koposov 12 built using optical UBVI data and  $JHK_s$  data from 2MASS. In the Table 1 the comparison of the parameters derived by 2MASS data only and by UBVI CCD are shown. The accordance is quite good for less distant clusters: 5% for Koposov 12 and 20% for Koposov 53, and there is a noticeable difference of 50% for the more distant and poor cluster Koposov 77. For Koposov 12

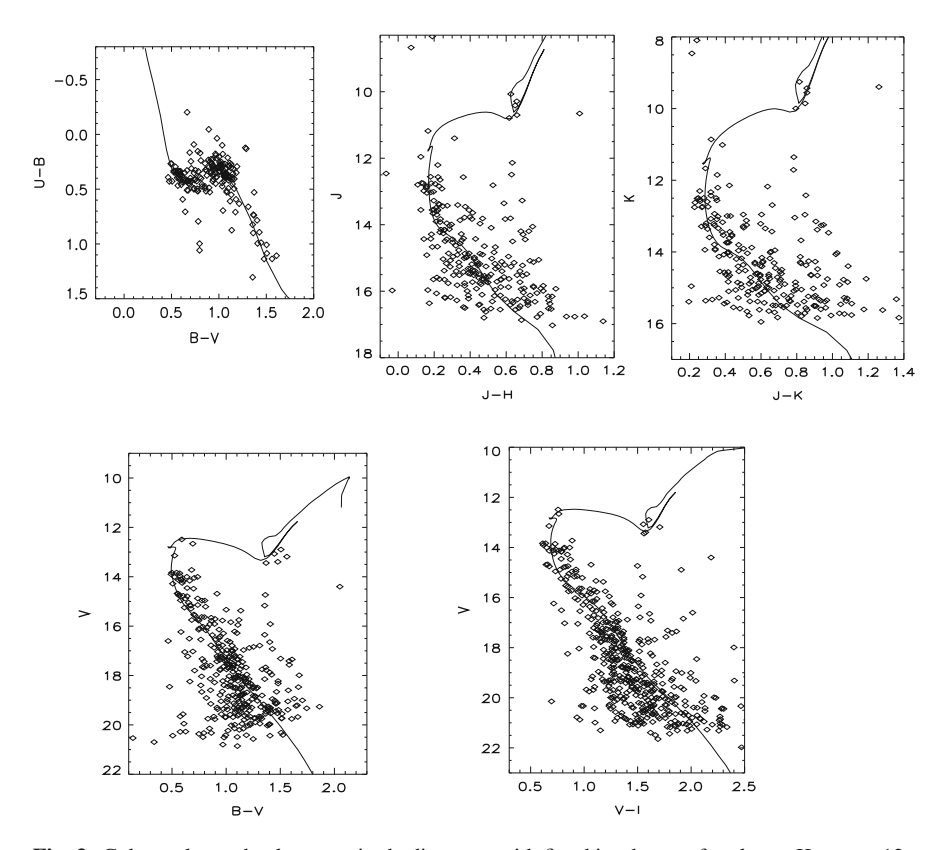


Fig. 3 Color-color and color-magnitude diagrams with fitted isochrones for cluster Koposov 12

Table 1 Comparison of the cluster parameters derived from optical data with those obtained with 2MASS data

Name	E(B-V)	Dist, pc	log(t)	Z	$E(B-V)_K$	$Dist_K$	$log(t)_K$
Koposov 12	0.53	1950	8.65	0.008	0.30	2050	8.90
Koposov 53	0.40	4250	7.90	0.008	0.34	3450	< 8.50
Koposov 77	0.63	3400	9.35	0.004	0.57	1750	9.65

and Koposov 53, we also investigated their mass functions with optical data and calculated their proper motions using UCAC 3 catalog.

### 4 Conclusions

We performed an automated search of star clusters in the 2MASS catalog and found 168 new clusters. Their parameters have been evaluated by  $JHK_s$  data from 2MASS and UKIDSS GPS. Most of the new clusters are situated at the distances

52 E.V. Glushkova et al.

ranging from 1 to 4 kpc from the Sun, have diameters from 1 to 10 arcmin, and their ages are greater than  $100\,\mathrm{Myr}$ . Many new clusters can not detected "by eye", but we could verify them using a specially developed method and UBVI CCD observational data.

**Acknowledgements** This publication makes use of data products from the Two Micron All Sky Survey, which is a joint project of the University of Massachusetts and the Infrared Processing and Analysis Center/California Institute of Technology, funded by the National Science Foundation. This work is partially based on data obtained as part of the UKIRT Infrared Deep Sky Survey.



Elena Glushkova taking notes

# **Developments of the Open Cluster Database WEBDA**

Martin Netopil, Ernst Paunzen, and Christian Stütz

Abstract The database WEBDA offers a significant amount of data concerning open clusters. It is intended to provide a reliable picture of the available data and knowledge on open clusters and to offer a wide access to the existing observations for professional as well as amateur astronomers. It includes astrometric data in the form of coordinates, rectangular positions, and proper motions, photometric data in the major systems in which star clusters have been observed, but also spectroscopic data like spectral classification, radial velocities, and rotational velocities. It also contains miscellaneous types of supplementary data like membership probabilities, orbital elements of spectroscopic binaries, and periods for different kinds of variable stars. We present the upcoming new interface and tools, which are needed to visualise and analyse the increasing amount of data from wide field imagers, all-sky surveys, and deeper investigations. Furthermore, we discuss the prospects of WEBDA in the era of large sky surveys and its extension to star forming regions as well as stellar associations.

#### 1 Introduction

The potential of astronomical archives and databases is enormous, but sometimes underestimated. The efficiency of the scientific output can be significantly increased by using archives and catalogues. Not only does one avoid duplicity of work, but they also provide collections of data, which in their sheer quantity cannot be gathered by one researcher or group on his own.

The amount of published data is huge and is still growing annually with the employment of the CCD technique and the use of more efficient instruments at

M. Netopil (⋈) · E. Paunzen · C. Stütz Institut für Astronomie der Universität Wien, Türkenschanzstr. 17, A-1180 Wien, Austria e-mail: martin.netopil@univie.ac.at; ernst.paunzen@univie.ac.at; christian.stuetz@univie.ac.at

54 M. Netopil et al.

larger telescopes. This includes observations, theoretical data (e.g. stellar atmospheres, isochrones, atomic data), but also all kinds of catalogues. However, these data are reduced and calibrated in different ways by the different authors. So, one has to be cautious, if applying data without a critical assessment of the used methods and reduction algorithm.

It is essential to have several sets of photometric and additional data (e.g. membership probabilities and proper motions) available for a significant number of star clusters. Currently, the only valuable database in this respect we know is WEBDA. It is accessible via a web-interface, which has been developed at the former Institute for Astronomy at the University of Lausanne (now EPFL), Switzerland by Jean-Claude Mermilliod [2]. Since the 1st of October 2005 we are maintaining and developing WEBDA on the WWW-Server of the University of Vienna.

The database is intended to provide a reliable picture of the available data and knowledge on open clusters and to offer a wide access to the existing observations for professional as well as amateur astronomers. WEBDA offers astrometric data in the form of coordinates, rectangular positions, and proper motions, photometric data in the major systems in which star clusters have been observed, as well as data originating from spectroscopy, like spectral classifications, radial velocities, and rotational velocities (see Table 1). It also contains miscellaneous types of supplementary data like membership probabilities, orbital elements of spectroscopic binaries, and periods for different kinds of variable stars. About four million individual measurements of objects, data for more than 1,000 open clusters, are already included in the database. Finally, a whole set of bibliographic references allows the community to easily locate the relevant publications for each individual cluster.

#### 2 The Past

The DataBase for Stars in Open Clusters (BDA) has been developed since 1987. In the year 1995, the extensive collection of observational data covered already about 100 000 stars in some 500 NGC, IC, and anonymous clusters. Maps for about 200 clusters were already scanned and included in the database.

The database contained at that time about 6,000 files and its size was about 35 MByte. Due to its specific structure, it was more convenient to have a copy installed on a local workstation. It was maintained on a Sun Sparc workstation, but copies were also available for DEC stations from the Meudon observatory in Paris.

The database has been planned not only to store data, but also to offer a versatile working environment covering many aspects of the study of open clusters. It provided facilities to compare the data and to plot photometric diagrams.

<sup>&</sup>lt;sup>1</sup>http://www.univie.ac.at/webda.

Table 1 Excerpt of the content of WEBDA from the 25th of September 2010 with the total amount of measurements of individual stars

le 1	le 1 Except of the content of WEBDA from the 25th of September 2010 with the total amount of measurements of individual stars	EBDA Irom	me 25m or septer	nber 2010 w	ith the total amount of mea	surements	of individual stars	
	Data description	Clusters	Measurements	Stars	Data description	Clusters	Measurements	Stars
	Fundamental				Spectroscopy			
	Identifications	729		17 625	MK types	979	16910	12347
	Transit tables	454		1 163 168	HD types	327	15 878	14 573
	Coordinates J2000	935	1 095 086	1 046 706	$v \sin i$	130	6 4 6 9	4 5 0 6
	Coordinates B1950	484	139 711	130 247	$V_r$ (mean)	407	697.7	6167
	Coordinates (round off)	484		137 685	$V_r$ (individual)	310	70 506	8 1 1 9
	Positions (x,y)	1 048		1637058	$V_r$ (GPO)	10	702	669
	Double stars	196	1 662	1 236	Orbits	70	772	389
	Photometry				Miscellaneous			
	UBV (photographic)	299	137 596	109 591	Proper motion (abs)	544		165 458
	UBV (photoelectric)	449	34 522	23 224	Proper motion (rel)	10	6 038	9809
	UBV(CCD)	424	1 084 083	934 648	Probability $(\mu)$	589		75858
	VRI (Cousins)	43	1571	1462	Probability (phot)	331		24 050
	VRI (Cousins; CCD)	160	323 677	311711	Periods (Var)	72	4 113	3 182
	RI (Cousins; CCD)	19	7 646	7411	X-ray flux	31	4 040	3 481
	VI (Cousins; CCD)	347	883 706	791 626	WR stars	20		42
	VRI (Johnson)	94	2 440	1 987	gK stars	260		4 972
	uvby (photoelectric)	220	7 309	4 889	Am stars	34		110
	uvby (CCD)	37	42 091	40 641	Ap stars	94		243
	$\beta$ (photoelectric)	250	7 191	4 647	Be stars	96		401
	$\beta$ (CCD)	25	13 604	13 189	Blue stragglers	209		939
	Geneva 7-colour	187	4 3 4 5	4 223	Spectroscopic binaries	133		1323
	RGU (photographic)	92	10305	10 268	Non-members	233		13 687
	JHK	169	319353	313 257				

56 M. Netopil et al.

Independently of the application software proposed, the main utility of the database was prioritised to bring the extensive data collection into a uniform numbering system, which allows to compare different datasets easily.

It was not only organized as a traditional relational database management system, but also as an advanced file management system. Clusters instead of stars formed the basic unit of the database. The structure, designed to provide a natural working environment, uses the directory hierarchy supported by the Unix system. Each cluster defined an independent directory identified by its name, containing the available data in distinct files. The records in the various data files have the same structure: star identification, source, data. They were organised sequentially and compressed. The entries are sorted by star number and source reference. The commands executing data requests presented a Unix style, with several options. Their names were identical to the data type they handle.

Finally, in 1997 the WWW version of BDA was made available on-line under the name of WEBDA.

#### 3 The Present

The efficient and successful structure of the database is still the same as developed in 1987. Around 100 individual worldwide accesses and data retrievals per day and about 600 publications referring to WEBDA within the last 11 years demonstrate the acceptance of the database within the scientific community.

Technically, WEBDA is located on the WWW-Server at the University of Vienna. This guarantees a high bandwidth and an excellent availability. The current version of WEBDA is based on cgi scripts using Perl within a frame layout. Furthermore, the waiving of Browser Plug-ins like Java-Applets and the server-side preparation of live data, allows easy and fast access to all available data, on all platforms with all common browsers, even if using lower Internet bandwidths.

The complete database with all archived data, scripts, tables, bibliographic files and maps has currently a size of 650 Mbyte.

The database engine WEBDA is a relational database built upon the package "/rdb" developed by [1], which is a high performance relational database management and application development system designed for Unix environments. With the implementation on the new server in Vienna, several additional commands from the Starbase 3.2.3 environment are also in use.

The Plot-routines are mainly based on Gnuplot 4.2.4 with some additional programmes written in the GD Graphics Library, which is part of the local Perl environment. The graphic files are prepared on the fly in the .png format. All these packages are Open Source, available for widely different Operating Systems with a large developing community.

The database is in a dynamic growing process as new data are published and included. Table 1 lists an excerpt of the content of WEBDA based on the status from the 25th of September 2010. In Fig. 1 one can see the number of clusters

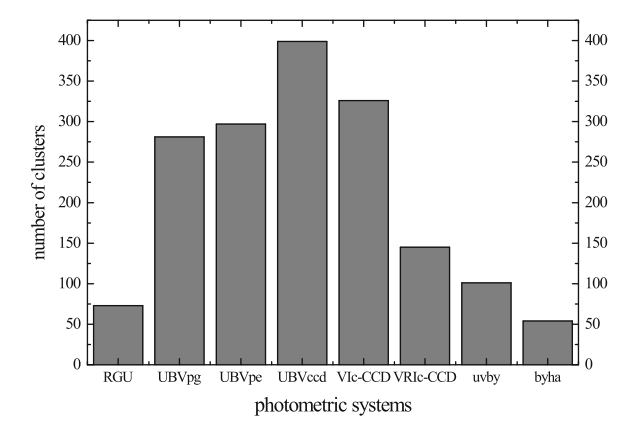


Fig. 1 The number of clusters included in WEBDA, studied in the major photometric systems. We considered only clusters with more than 20 stars observed

observed in the main photometric systems. If considering only clusters with more than 20 stars observed, in total about 650 different clusters are covered. A further restriction to CCD data only, whereby one can expect a deeper investigation, not much more than 400 individual clusters remain. Hence, sky surveys, especially those concentrating on the galactic plane, are providing a valuable contribution to obtain a more profound picture.

#### 4 The Future

The published data in the research area of open clusters are growing almost exponentially in the last years (see e.g. Fig. 2). Unfortunately, the quality of the published data is not always satisfactory. This includes e.g. a not correct consideration of bad CCD lines/columns, resulting in additionally identified "wrong" stars, but more often an apparent wrong standardisation of the photometry. Since the main philosophy of WEBDA is "Quality instead of quantity", the published data are *not* just included in a "copy and paste" way. The inclusion of new data and the inevitably following quality assessment are still carried out manually with the help of semiautomatic tools. In the scope of the ongoing development of the position and coordinate assignment routines and the user interface (see below), also fully automatic on demand quality assessment and maintenance routines are developed.

Another important point is the data mining of published and especially unpublished data, which are not yet included in the database. "Unpublished" data in this respect are results and data listed in a thesis and/or conference proceedings (e.g. American Astronomical Society Meeting) which were never published in a peer-reviewed journal. Starting point for the data mining is the highly efficient Smithsonian/NASA ADS service, which allows sophisticated queries in three large

58 M. Netopil et al.

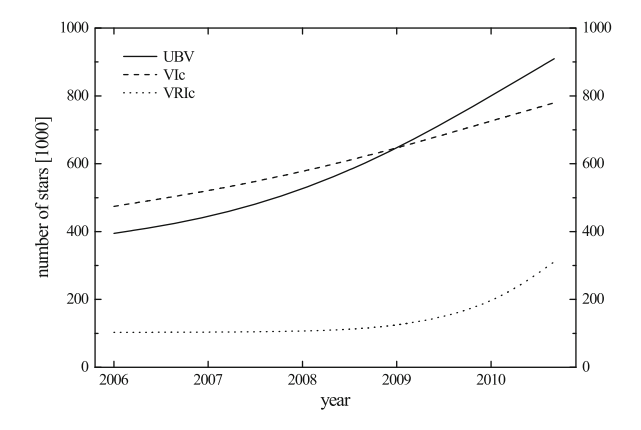


Fig. 2 The increase of stars in WEBDA during the last years in some major photometric systems

bibliographic databases. The results can then be cross checked with the bibliography of WEBDA to find the missing references and data.

The availability of large surveys like SDSS or IPHAS, but even data from individual studies using e.g. wide field imagers are causing problems to represent the data still in a meaningful manner. Hence, new plotting routines are needed, what regards especially to colour-magnitude diagrams, where a restriction to specific colour ranges or diameters can be often necessary (see Fig. 3). An example of such a new plotting routine, to be under way, can be found in Fig. 4. Additionally, also the chart plots and the tool to compare different datasets will be improved, to offer new capabilities with a more user-friendly interface.

Looking at the content of WEBDA (Table 1) it is obvious that it includes about a factor of two more rectangular positions than equatorial coordinates. To close this gap, the following tasks will be performed:

- 1. Transform B1950 into J2000 coordinates
- 2. Average equatorial coordinates
- 3. Transform rectangular positions into equatorial coordinates and vice versa
- 4. Find bad columns/rows and ghosts, wrongly identified as true stars in the literature, with the help of IRAF routines
- 5. Find misidentified objects across different data sets
  - Apply known proper motions to the objects
  - · Check known magnitudes and colours for duplicate entries
  - Simple pattern recognition analysis
- 6. Documentation and publication of the original as well as revised identifications/coordinates together with all transformation coefficients/errors

With the help of the cleaned datasets and then available equatorial coordinates for all objects, further data can be easily integrated such as those from catalogues and

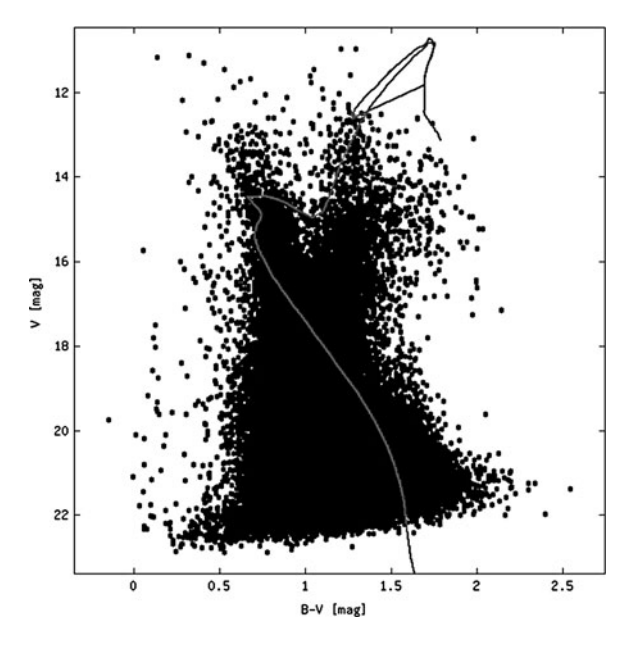


**Fig. 3** The colour-magnitude diagram and plotted isochrone taken from WEBDA for the open cluster NGC 6253 using the data by [3]. It is obvious that new plotting routines are needed to present such large datasets still in a meaningful manner

all-sky surveys, for example UCAC3, 2MASS, SDSS, or IPHAS, only to mention a few.

As a next step, star forming regions and stellar associations will be included in the same manner as open clusters. This can be easily done on the basis of existing catalogues of these aggregates.

With the success of the AstroGrid environment, it becomes obvious to transform the WEBDA database into a Virtual Observatory (VO) compatible format. The technical transformation of the present content into the VO format is rather easy, since there is only a need to generate XML tables from /rdb ones. But to keep the current quality standards as they are, and to find common identifiers is not a straightforward process. However, for an efficient use of the comprehensive capabilities of VO, the aforementioned transformation to equatorial coordinates for all included objects is required. Still, numerous recent publications provide rectangular positions only. Furthermore, for more than 100 open clusters no single star with an equatorial coordinate entry is available in WEBDA. Therefore, also rather time consuming identifications by eye and a comparison to e.g. UCAC3 is necessary to close this gap.

Parallel, the WEBDA user interface still has to be maintained and developed. As mentioned before, all available data can be accessed without preparing the client side in any other way than installing some web-browser. The VO Project does not intend to reach this state at any point in the future. A challenge for the future will be

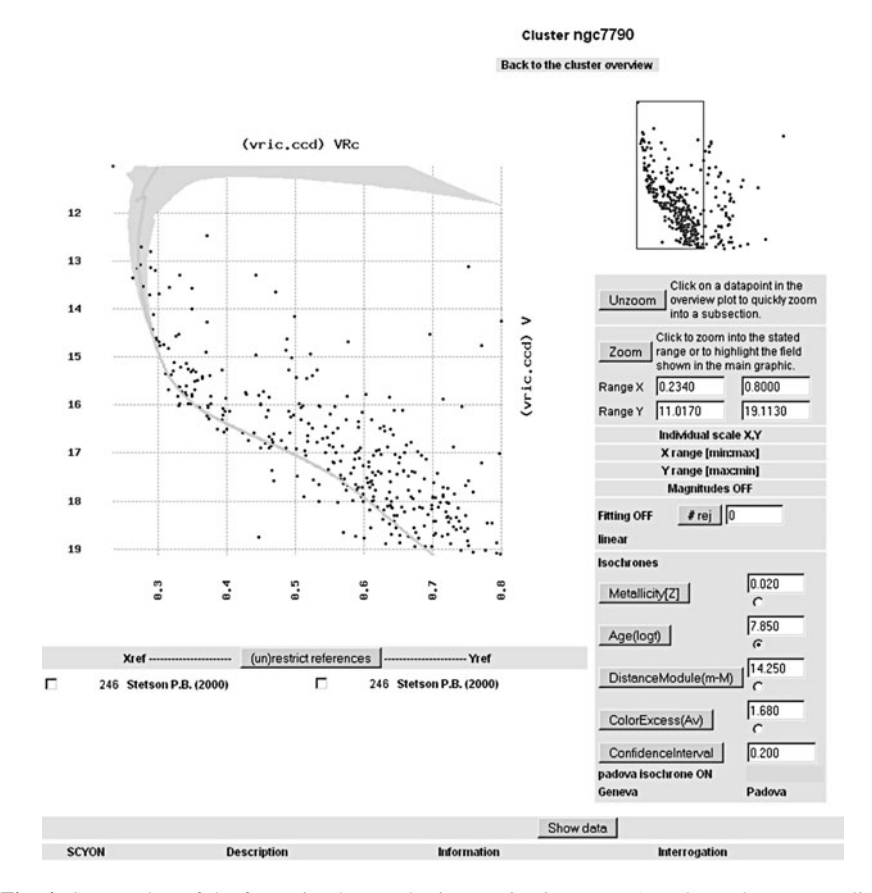


**Fig. 4** Screen shot of the future isochrone plotting routine in WEBDA, to be under way, applied to data of NGC 7790 by [4]. One will be able to restrict the display to specific colour/magnitude ranges, but also to diameters. Furthermore, errors of the given cluster parameters can be displayed, in this case the error in age

the on demand analysis of the ever growing amount of data. Since WEBDA manages with very little cross reference tables, we are in an excellent position to cope with the expected accretion of data. Already the database engine is fast enough to service requests on the webserver quicker than the time required to receive the data and to display the webpage containing the results. However, it will become increasingly important to visualise primarily relevant datapoints. Thus, intelligent and intuitive filter routines have to be generated. Most pleasantly, this will concurrently also reduce the amount of the transfered datastreams.

**Acknowledgements** This work was supported by the financial contributions of the Austrian Agency for International Cooperation in Education and Research (WTZ CZ-10/2010 and HR-14/2010). MN acknowledges the support by the ÖFG under MOEL grants #388 and #446.

#### References

- Manis, R, Schaffer, E., Jorgensen, R.: Unix Relational Database Management. Prentice Hall, Englewood Cliffs (1988)
- 2. Mermilliod, J.-C.: In: Egret, D., Albrecht, M. (eds.) Information & On-line Data in Astronomy, pp. 127. Kluwer, Dordrecht (1995)
- 3. Montalto, M., Piotto, G., Desidera, S., Platais, I., Carraro, G., Momany, Y., de Marchi, F., Recio-Blanco, A.: Astron. Astrophys. **505**, 1129 (2009)
- 4. Stetson, P.B.: Publ. Astron. Soc. Pac. 112, 925 (2000)

## **Inferring Stellar Properties Using Colours, Parallaxes and an HRD Prior**

Coryn A.L. Bailer-Jones

**Abstract** Stellar parameters – effective temperature, metallicity, interstellar extinction etc. – are typically estimated from a spectrum or multiband photometry. I outline a probabilistic method for estimating stellar parameters which uses not only the spectral energy distribution but also the apparent magnitude, parallax (if available) and the strong constraints provided by the Hertzsprung-Russell Diagram. This (a) improves the accuracy and precision over use of just the spectrum, and (b) ensures that the inferred parameters are both physically realistic and are consistent with the distance, apparent magnitude and stellar physics. The method provides full covariate probability distributions over the parameters, i.e. it provides not just parameter estimates but also confidence intervals and the correlations between the estimates. The latter is particularly important given the degeneracies between some parameters, such as temperature and extinction. These degeneracies are shown to be reduced by use of this method. Here I provide a short summary of the method and show some results of its application to 85 000 Hipparcos-2MASS stars and to the Hyades clusters. A full description and further results can be found in Bailer-Jones (Mon. Not. R. Astron. Soc. arXiv:1009.2766, 2011).

#### 1 Introduction

If we are lucky enough to have high resolution spectra of stars, then we can normally measure their parameters with some precision. But obtaining such detailed information on a large number of stars ( $10^7$  or more) is currently out of the question, and we have to resort to low resolution spectroscopy or multiband photometry. This is the case with surveys such as SDSS, Pan-STARRS and LSST (five band

C.A.L. Bailer-Jones  $(\boxtimes)$ 

Max Planck Institute for Astronomy, Königstuhl 17, 69117 Heidelberg, Germany e-mail: calj@mpia.de

64 C.A.L. Bailer-Jones

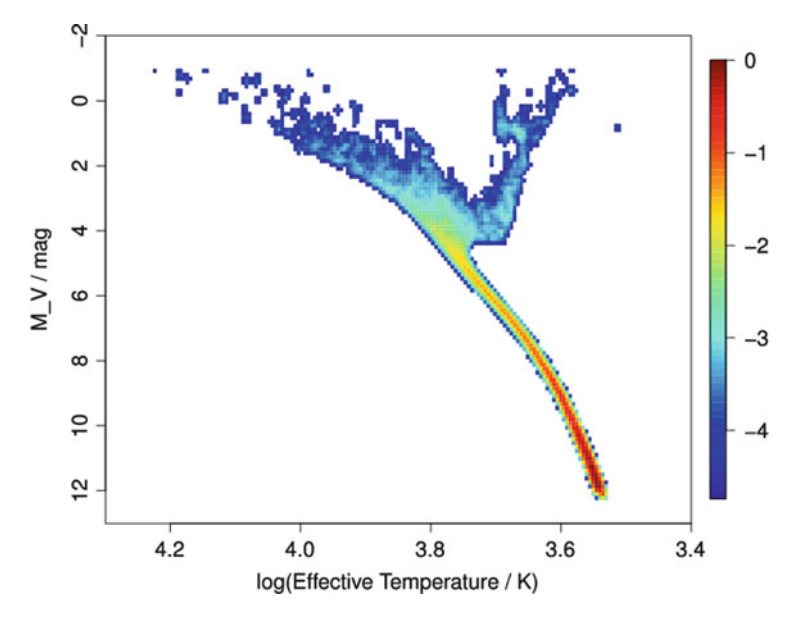


Fig. 1 HRD prior. The colour scale shows  $\log P(M_{\rm V},T)$  normalized to have zero at its maximum. Unoccupied areas are shown in *white* 

photometry), and Gaia (very low resolution spectrophotometry). The parameter accuracy we can achieve with such data alone is limited.

What other information is available to help improve performance? The Hertzsprung–Russell Diagram (HRD) describes the location of stars in the  $(M_{\rm V},T)$  (absolute magnitude, effective temperature) plane, and for virtually any stellar population it is very sparsely and non-uniformly populated (see Fig. 1). That is, a priori we can place strong and plausible constraints on the relative probability of different combinations of the stellar parameters.

Stellar parametrization in large, deep surveys faces another problem, namely interstellar extinction  $(A_{\rm V})$ . In principle this can also be estimated from the photometry, but it is frequently degenerate with  $T_{\rm eff}$  (see Fig. 2, explained further in the next section). This problem is sometimes ignored in survey projects by assuming that the stars have negligible extinction (e.g. at high Galactic latitudes), or by using an extinction map. The first solution is inadmissible for surveys near the Galactic plane or near molecular clouds, and extinction maps often have low spatial resolution or are not three-dimensional (they may only give the integrated extinction to the edge of the modelled Galaxy).

Extinction is a major issue for the all-sky Gaia survey. Yet herein also lies an opportunity. Gaia will measure positions, parallaxes  $(\varpi)$  and proper motions with an accuracy of up to 10 microarcseconds for almost all  $10^9$  stars in our Galaxy brighter than G=20. It will also obtain low resolution optical spectrophotometry and apparent magnitudes in the G band (a "white-light" band much broader than

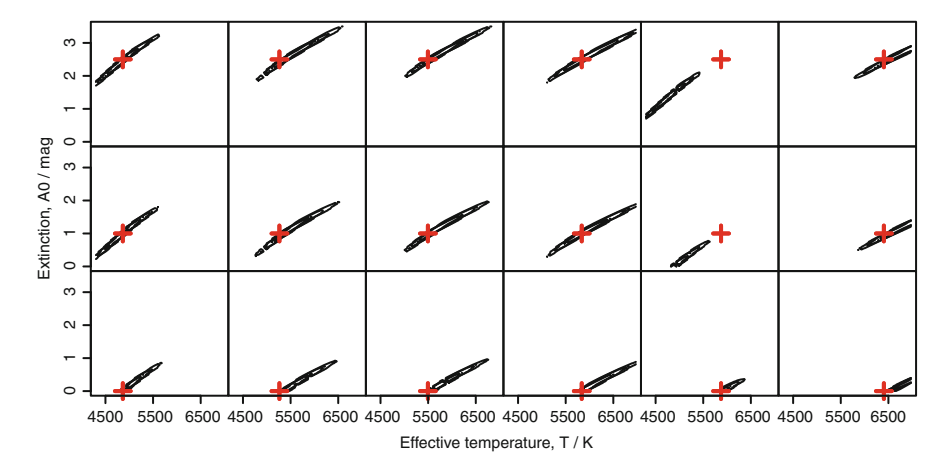


**Fig. 2** Posterior probability density function (PDF) from the p-model (colours only) over 18 stars with 6 different true temperatures (columns) and three different true extinctions (rows). Three contours are shown for each star, enclosing 90, 99 and 99.9% of the total posterior probability. For comparison, the true parameter values are shown with the *red cross* 

the V band). If we knew  $A_{\rm V}$  then we could estimate the absolute stellar magnitude  $(M_{\rm V})$ , a fundamental stellar property, via the relation

$$V + 5\log \varpi = M_{\rm V} + A_{\rm V} - 5. \tag{1}$$

However, we also have to estimate  $A_V$  from the data. How can we do this?

#### 2 Method

The solution is to approach the problem probabilistically. Where we have noise we have uncertainties; these are best represented by probability density functions (PDFs). The Bayesian approach allows one to include all available information as PDFs in a self-consistent manner, and to propagate these PDFs through the calculation to provide not only parameter estimates but confidence intervals on these estimates.

Let us consider the problem of estimating just the two parameters  $\phi = (A_V, T)$ . We have three pieces of information:

- 1. The spectrum (p), which constrains T and  $A_V$
- 2. The quantity  $q = V + 5 \log \varpi$ , which constrains  $M_V + A_V$  from (1)
- 3. The HRD, which constrains  $M_V$  and T (Fig. 1)

The goal is to determine  $P(\phi|p,q)$ . The spectrum we can predict given  $\phi$  using a forward model, which is the result of a fit to a set of labelled data [2]. This is the "training" phase in machine learning speak. Combined with a suitable photometric

66 C.A.L. Bailer-Jones

noise model, the forward model provides  $P(p|\phi)$ . Adopting a noise model for the apparent magnitude and parallax measurement allows us to write item (2) as  $P(q|\phi, M_V)$ . Applying Bayes' theorem we can then arrive at an expression for  $P(\phi|p,q)$  in terms of these quantities. It involves marginalizing over the unknown  $M_V$  to give a (non-parametric) two-dimensional PDF over  $\phi$  for given measurements p and q.

## 3 Demonstration and Application to 85 000 Hipparcos-2MASS Stars

This method has been tested by using it to estimate  $A_V$  and T for 5280 FGK stars with known "true" parameters using BVJHK photometry and Hipparcos parallaxes. These data are derived from a set of 880 stars with T estimated from high resolution spectroscopy by [4], to which I have applied artificial reddening to provide variance in  $A_{\rm V}$ . First I use just the four colours to determine  $P(p|\phi)$  for each star and take the mean of this distribution as the parameter estimates (the *p-model*). The parameter accuracy (mean of absolute residuals) is 5.5% in T and 0.3 dex in  $A_V$ . The probabilities of different solutions for these parameters for 18 example stars were shown in Fig. 2. Note the significant degeneracy between the parameters. When introducing the parallax, apparent magnitude and an HRD prior (to give the pqmodel), these errors are reduced to 3.5% and 0.2 dex respectively, an increase in accuracy of around 40%. (We can also apply the method using just the colours and HRD prior but no measurement of q. Even this improves accuracy by 13% over the p-model.) Posterior probability distributions from this model are plotted in Fig. 3. Note how much smaller the confidence ellipses are, which reflects the increase in the precision of the parameter estimates.

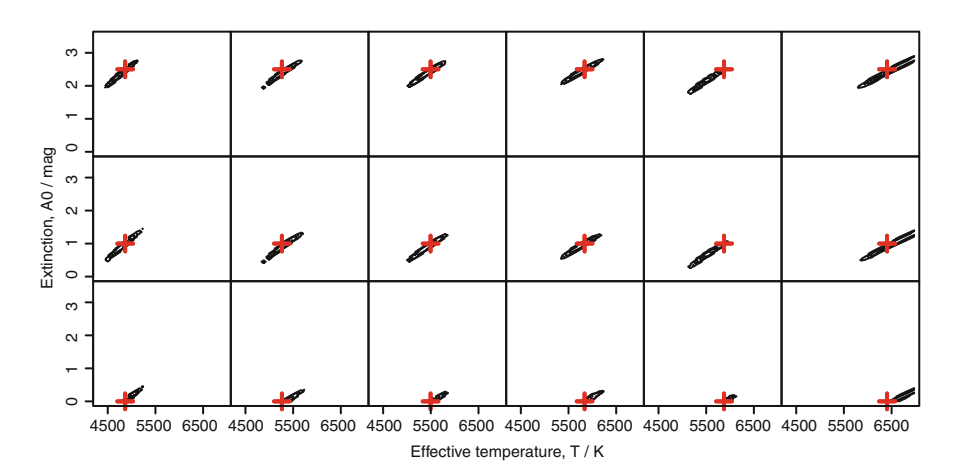
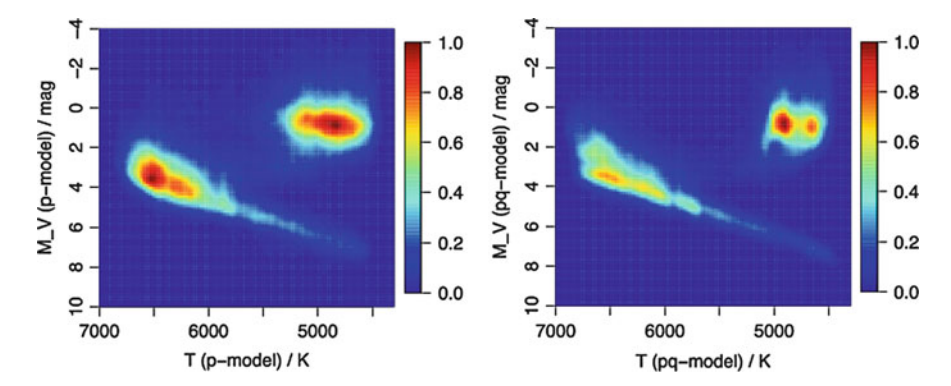


Fig. 3 Posterior probability distribution for the pq-model (i.e. including the HRD prior, parallax and apparent magnitude) for the same stars as shown in Fig. 2



**Fig. 4** HRD for the Hipparcos–2MASS stars derived from the p-model (*left*) and pq-model (*right*) shown as a density plot (achieved via smoothing with a Gaussian kernel). The number of stars per unit area is normalized to a value of 1.0 at the maximum density (separate normalization in each plot)

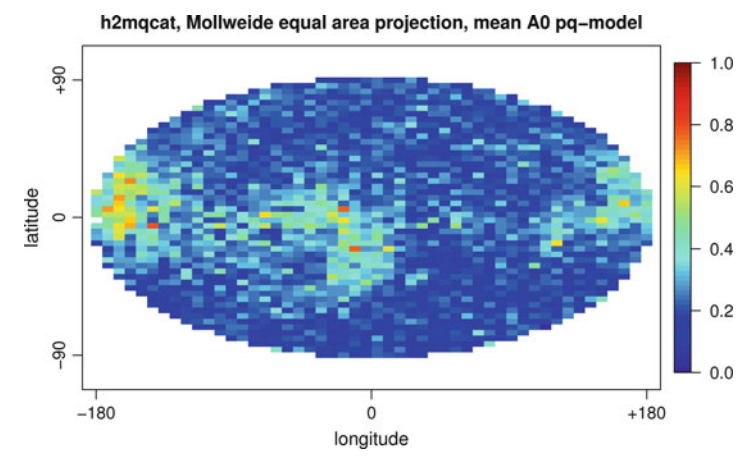


Fig. 5 The mean extinction  $(A_{\rm V})$  from the pq-model along the line of sight to the Hipparcos stars, plotted in Galactic coordinates

I then applied the method to a set of 85 000 Hipparcos stars for which I obtained a reliable astrometric cross match with 2MASS (to give BVJHK photometry), but for which the "true" parameters are unknown. Many of these stars (42%, it turns out) are not FGK stars, so their parameters cannot be estimated reliably by this method. (I identify these stars by their inferred PDF peaking at or very close to the edge of the parameter space.) Once we have estimated  $A_V$  and T we can estimate  $M_V$  (or rather a PDF over it) from (1) and so plot the stars in an HRD: see Fig. 4. These are discussed in more detail in [1]. As the Hipparcos sample covers the whole sky, we can also combine the individual extinction measurements to produce an extinction map; a 2D map is shown in Fig. 5. The median distance to these stars is 170 pc (90% have distances between 40 and 730 pc).

68 C.A.L. Bailer-Jones

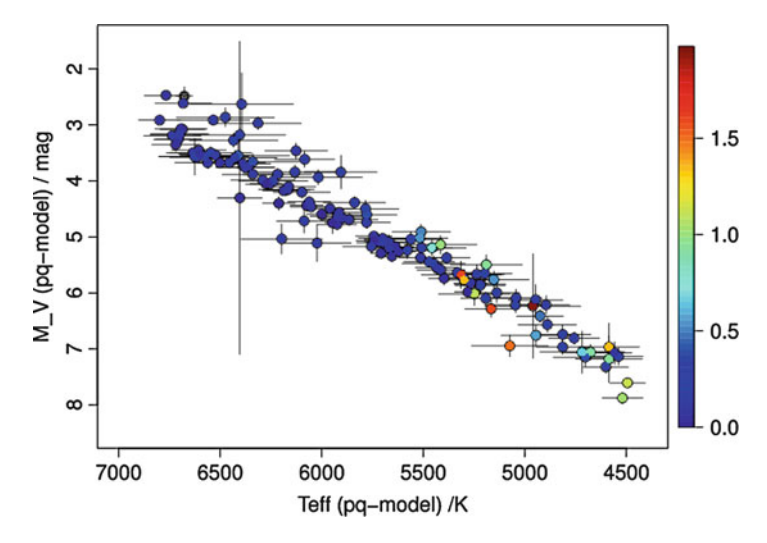


Fig. 6 HRD for 137 Hyades stars with parameters determined using colours, parallaxes and apparent magnitudes. Individual stars are coloured according to their estimated extinction,  $A_V$ 

As an additional test, I identified 137 stars in my sample in the list of 218 Hipparcos Hyades members from [3]. The HRD diagram (pq-model) for these objects is plotted in Fig. 6. As expected, the majority of these have very low extinctions, yet a significant number of the cooler stars have relatively large extinctions. Further investigation of this is beyond the space available in this paper.

A catalogue of parameter estimates (plus uncertainties) from both the p-model and pq-model for 46 900 stars is available online<sup>1</sup> or from CDS, Strasbourg. More results and discussion of the method can be found in [1].

## 4 Why You Shouldn't Use Conventional Methods

I finish this brief article with some arguments against using conventional machine learning methods (e.g. neural networks, support vector machines) for estimating stellar parameters. By "conventional" I mean multidimensional, nonlinear regression algorithms which attempt to model the parameters as a function of the input data, i.e. fit a function  $f(\phi|p)$ . These methods can give overall good performance in some applications – and I have published work using them – but here are some drawbacks

<sup>&</sup>lt;sup>1</sup>http://www.mpia.de/homes/calj/qmethod.html.

- $f(\phi|p)$  is an inverse function and so may not be unique. Especially at low spectral resolution or low SNR, a single p may correspond to a broad range of  $\phi$ , or even isolated islands of parameter space.
- This function is likely to be cumbersome and difficult to fit when *p* is heterogeneous, i.e. includes not only colours/fluxes but also a parallax or something based on it
- Support vector machines, neural networks and related methods are fundamentally non-probabilistic for continuous parameter estimation, so they cannot recognise degeneracies, multiple solutions or naturally deliver meaningful error bars. (Techniques exist for forcing probabilities out of these methods, but these are convenient fixes rather rigourous solutions.)
- These methods cannot naturally or explicitly include domain knowledge or
  prior information. This could lead to inconsistent or non-physical solutions,
  plus misses an opportunity to include additional information which could
  improve performance. Probabilistic methods are much more flexible, for example
  allowing a simple combination of independent solutions based on different pieces
  of information.
- These methods are not robust to missing information: setting an input to zero is not the same thing! With a probabilistic method, on the other hand, you can usually marginalize over missing input data.

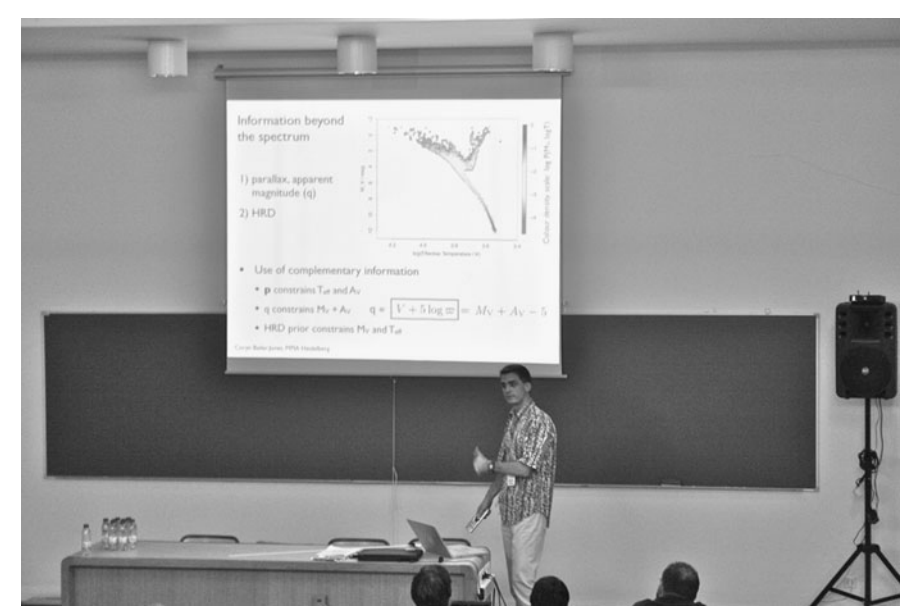
The only real advantage of conventional method is that they are generally much faster, i.e. are cheaper.

**Acknowledgements** I would like to thank Jo Bovy, Ron Drimmel, David Hogg, Dustin Lang and Antonella Vallenari for useful discussions of this work, and Antonella Vallenari for providing me with output from her stellar population models. I am grateful to Chris Stubbs and the LPPC group at Harvard for support during a sabbatical stay. This work makes use of Hipparcos and 2MASS data and has used Simbad and Vizier at CDS, Strasbourg and IRSA at NASA.

#### References

- 1. Bailer-Jones, C.A.L., Mon. Not. R. Astron. Soc. 411, 435 (2011)
- 2. Bailer-Jones, C.A.L.: Mon. Not. R. Astron. Soc. 403, 96 (2010)
- Perryman, M.A.C., Brown, A.G.A., Lebreton, Y., Gomez, A., Turon, C., Cayrel de Strobel, G., Mermilliod, J.C., Robichon, N., Kovalevsky, J., Crifo, F.: Astron. Astrophys. 331, 81 (1998)
- 4. Valenti, J.A., Fischer, D.A.: Astrophys. J. Suppl. 159, 141 (2005)

70 C.A.L. Bailer-Jones



Coryn Bailer Jones



General discussion

# AstrOmatic Software in the Era of Large Stellar Photometric Surveys

Emmanuel Bertin, Philippe Delorme, and Hervé Bouy

**Abstract** AstrOmatic software packages have been developed through the years for processing and analysing large quantities of astronomical imaging data in a consistent and fully automated way. I discuss the performance of the latest generation of AstrOmatic software from the angle of wide-field stellar studies, and present ongoing development efforts to overcome some limitations of the current algorithms.

#### 1 Introduction

The AstrOmatic software suite originated as a set of companion tools to the SEXTRACTOR source extraction package. Since the first public availability of SEXTRACTOR in 1995, a total of 10 packages have been released, dealing with various aspects of the management of photometric data, such as image analysis, calibration, and weighting. The companion packages have been developed in the framework of several projects such as DeNIS [9], EIS [7], TERAPIX [4], EFIGI [1], and more recently, DESDM [16].

E. Bertin (⊠)

Institut d'Astrophysique de Paris, UMR 7095 CNRS, Université Pierre et Marie Curie, 98bis Boulevard Arago, Paris 75014, France

e-mail: bertin@iap.fr

P. Delorme

Laboratoire d'Astrophysique de Grenoble, UMR 5571 CNRS, Université Joseph Fourier, 38041 Grenoble Cedex 09, France

e-mail: Philippe.Delorme@obs.ujf-grenoble.fr

H. Bouv

Centro de Astrobiologia INTA-CSIC, PO BOX 78, E-28691, Villanueva de la Cañada,

Madrid, Spain

e-mail: hbouy@cab.inta-csic.es

A. Moitinho and J. Alves (eds.), *Star Clusters in the Era of Large Surveys*, Astrophysics and Space Science Proceedings, DOI 10.1007/978-3-642-22113-2\_9, © Springer-Verlag Berlin Heidelberg 2012

72 E. Bertin et al.

SEXTRACTOR and other Astr*O*matic packages were originally meant to operate at high galactic latitude, primarily for extragalactic surveys. Stellar imaging surveys rely entirely on photometric and astrometric measurements done in fields with a much wider range of source densities. Open cluster surveys are often affected by contamination with nebulous features and halos around bright stars, especially for wide-field instruments with refractive field correctors. Crowding, irregular backgrounds, extended artefacts: this is not the environment SEXTRACTOR has originally been designed for.

Nevertheless, over the past years, collaboration with stellar astronomers has made it possible to implement certain features that make AstrOmatic software better suited to photometric stellar surveys, while retaining processing efficiency and full automation. In the following sections we present two examples of such experimental (but already operational) software features: Point Spread Function (PSF)-fitting and automated proper-motion measurements. In the conclusion, we draw a list of other potential improvements to AstrOmatic software that are relevant to the processing of stellar photometric surveys.

#### 2 PSF Fitting

Contrary to more specialised packages such as DAOPHOT [18], SEXTRACTOR is meant to deal with any kind of astronomical object, and therefore imposes very few constraints on the shape of detected sources. In SEXTRACTOR, detection is based on the principle of matched filtering and image segmentation [11], not on local peakfinding. Moreover, the extraction engine must take a fairly conservative approach to deblending overlapping sources. For instance, SEXTRACTOR identifies close pairs of stars as elongated objects instead of actual blends of point sources. This makes source extraction in crowded stellar fields unreliable.

To address this problem, an experimental PSF-fitting module has been added to SEXTRACTOR; it has been used for several studies in various regimes of stellar density [6,8,13,14,17]. Given a point-source model, the module makes the assumption that every detection is a point-source, or a group of point sources, and finds the combination of point-source models that fits best (in the  $\chi^2$  sense) the data. Adjustable parameters for each point-source are simply the flux and the two coordinates.

## 2.1 Modelling the PSF with PSFEX

The point source model (the local PSF) is derived at an earlier step of the processing. The modelling of the PSF is managed by a separate package: PSFEX (PSF Extractor)<sup>1</sup>, which uses a specific type of SExtractor catalogue as input.

<sup>&</sup>lt;sup>1</sup>available at http://astromatic.net/software/psfex.

PSFEx starts by identifying detections that are likely to be point-sources, based on heuristics such as finding the position of the stellar locus in a magnitude vs half-light-radius diagram [12]. PSFEx models the PSF as a linear combination of basis vectors (actually small images). The basis vectors are tabulated at a resolution chosen to minimise aliasing, which makes it possible to recover the PSF even in severely undersampled images. The vector basis may be the pixel basis, the Gauss-Laguerre basis [15], the Karhunen-Loève basis derived from a set of actual point-source images, or any user-provided basis. PSFEx fits the image of every point-source  $\mathbf{p}_s$  with a projection on the local pixel grid of the linear combination of basis vectors  $\phi_b$  by minimising the  $\chi^2$  function of the coefficients  $c_b$ 

$$\chi^{2}(\mathbf{c}) = \sum_{s} \left( \mathbf{p}_{s} - f_{s} \mathbf{R}(\mathbf{x}_{s}) \sum_{b} c_{b} \phi_{b} \right)^{T} \mathbf{W}_{s} \left( \mathbf{p}_{s} - f_{s} \mathbf{R}(\mathbf{x}_{s}) \sum_{b} c_{b} \phi_{b} \right), \quad (1)$$

where  $f_s$  is the flux within some reference aperture, and  $\mathbf{W}_s$  the inverse of the pixel noise covariance matrix for point-source s.  $\mathbf{R}(\mathbf{x}_s)$  is a resampling operator that depends on the image grid coordinates  $\mathbf{x}_s$  of the point-source centroid:

$$\mathbf{R}_{ij}(\mathbf{x}_s) = h\left(\mathbf{x}_j - \eta.(\mathbf{x}_i - \mathbf{x}_s)\right),\tag{2}$$

where h is a 2-dimensional interpolant (interpolating function),  $\mathbf{x}_i$  is the coordinate vector of image pixel i,  $\mathbf{x}_j$  the coordinate vector of model sample j, and  $\eta$  is the image-to-model sampling step ratio (oversampling factor). PSFEX is able to model smooth PSF variations by making the  $c_b$  coefficients (1) themselves a linear combination of polynomial functions of the source position within the image.

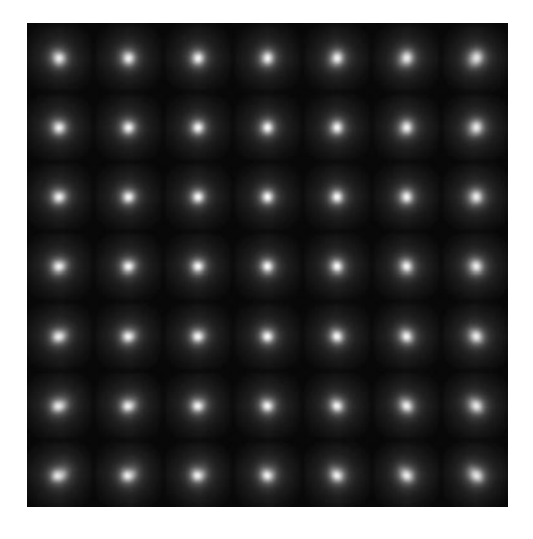
 $\chi^2$  minimisation is fast, but restricts the current modelling process to images with noise in the Gaussian regime. The point-source selection and modelling process is iterated several times to minimise contamination of the sample by image artefacts, multiple stars and compact galaxies. An example of a variable PSF model derived from an image with PSFEx is shown Fig. 1. More details about the working of PSFEx can be found in [3].

## 2.2 Fitting Multiple PSFs to a Single Detection

PSF models are fitted to source images using non-linear  $\chi^2$  minimisation, based on a simple error gradient descent. The fitting algorithm starts with adjusting the position and amplitude of a single model, and examines the residuals of the fit to identify the largest peak that lies away from that position by a fraction of the PSF Full Width at Half Maximum. A new fit is then performed, which involves an extra PSF initially located at the position of the residual peak. The process is iterated, and new PSFs are progressively incorporated until the lowest PSF amplitude drops below some fraction of the background noise or until a maximum number of PSFs is reached (2–10 depending on the data and the science case). Figure 2 shows an example of fit residuals on a star field after PSF-fitting.

74 E. Bertin et al.

Fig. 1 Reconstruction of the PSF at regular intervals over the 1° field of view of the Megaprime imager, from the CFHTLS "D4" field



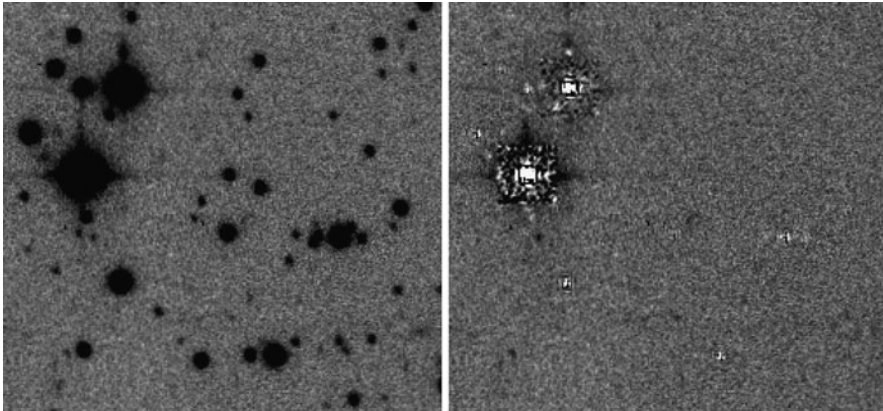


Fig. 2 Example of multiple-PSF fitting on a star field. *Left:* original image data. *Right:* residual image after all PSF models have been subtracted from the original data

## 3 Stellar Proper Motions

An increasing number of high quality, wide-field astronomical images are becoming publicly available on archive servers. The time base covered by these data is now exceeding 10 years, which makes it a very valuable medium to conduct Proper Motion (PM) studies on large scales. Unfortunately archive data come unequally calibrated, both for photometry and astrometry; this is a serious issue when trying to combine data from different epochs, taken through different instruments and filters and in various observing conditions.

#### 3.1 Astrometric Calibration with SCAMP

The SCAMP package<sup>2</sup> [2] is the AstrOmatic tool for astrometric and photometric calibration of astronomical images. SCAMP operates on SEXTRACTOR catalogues, and has been designed from the start to derive a "global" astrometric solution for several instruments at the same time, taking advantage of multiple detections in overlapping exposures to improve relative accuracy. Early versions of SCAMP would consider proper motions rather a nuisance. However it quickly became evident that the software could at the same time be used to directly generate catalogues with relative proper motions computed for every source entering the solution.

Under favourable conditions, systematics in the relative calibration of ground-based wide-field images can be kept at the level of a few milliarcsec (mas). At these angular scales, Differential Chromatic Refraction (DCR) is often a dominant source of disturbance for ground-based observations done through broadband optical filters. Hopefully, SCAMP can correct for the systematic shifts with colour of stars that have been observed in at least two different passbands, provided that the average colour does not vary too much over the field of view (Fig. 3).

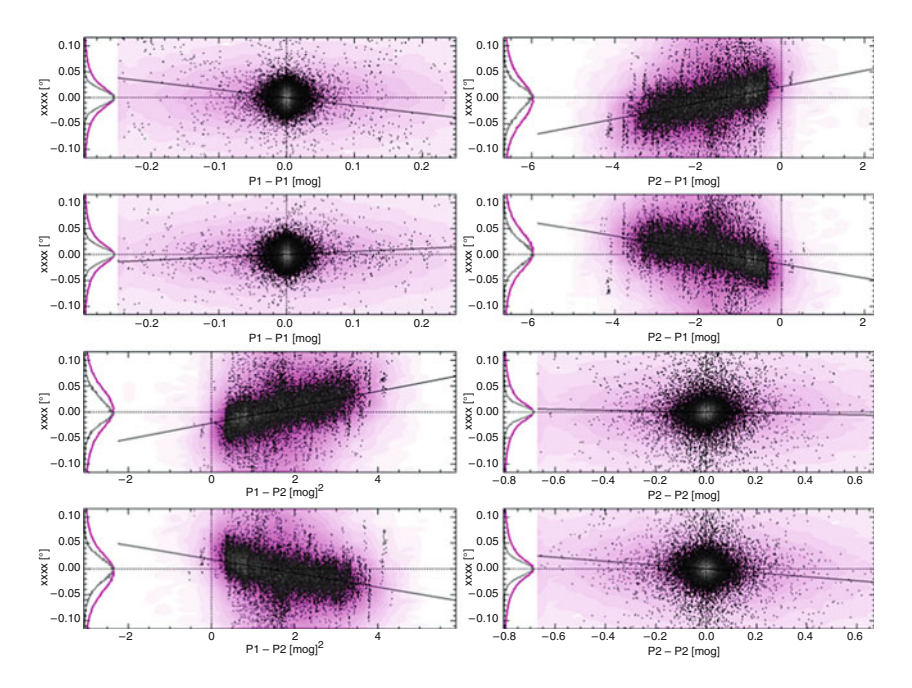


Fig. 3 Correcting for Differential Chromatic Refraction (DCR) in SCAMP: the figure shows residuals in the relative x and y positions of stars as a function of magnitude difference (colour index) for two sets of MEGACAM exposures taken at relatively high airmass ( $\approx 1.6$ ) through different filters (P1 and P2). Regression lines define the colour-dependent correction applied by SCAMP to correct for DCR

<sup>&</sup>lt;sup>2</sup>available at http://astromatic.net/software/scamp.

76 E. Bertin et al.

### 3.2 Computing Proper Motions

Relative PMs are estimated after calibration and reprojection to a common coordinate system, by fitting a straight line to the positions of the detections of every source as a function of time. An example of a preliminary proper motion diagram obtained with SCAMP from the dataset of Fig. 4 is plotted Fig. 5.

Deriving PMs that are consistent over large survey areas, when a substantial fraction of the detected sources have significant proper motions, requires an iterative approach in SCAMP: identify a set of objects with known PMs, or background (extragalactic) sources at rest [10], correct all source coordinates for PMs calibrated with respect to this set, recompute a new astrometric solution, and refine the initial

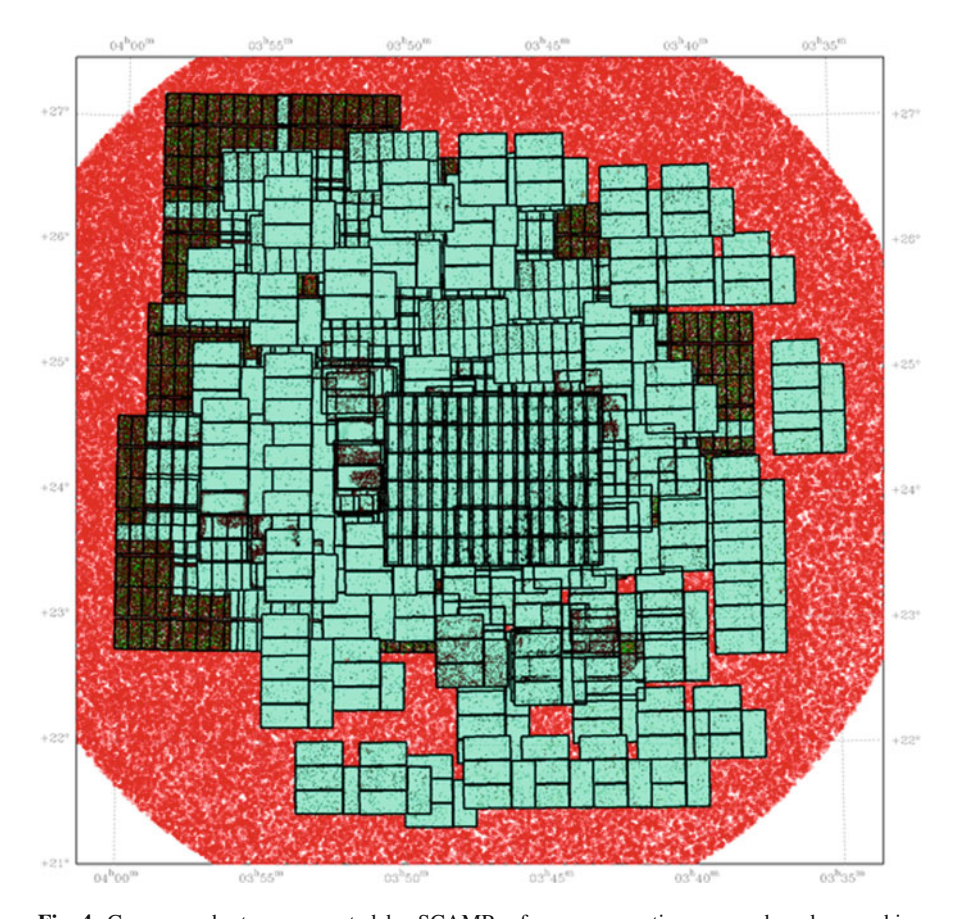
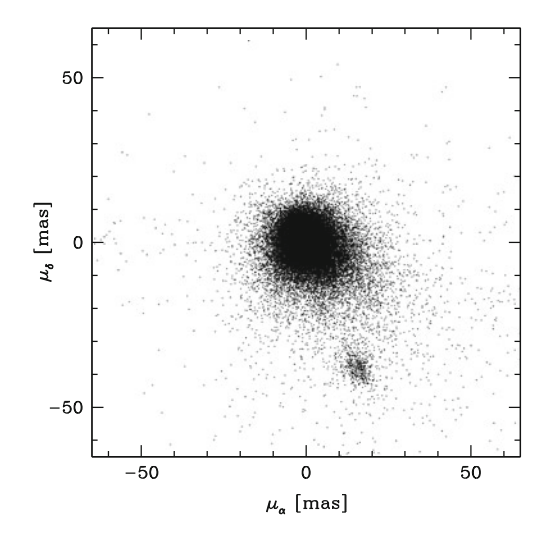


**Fig. 4** Coverage chart, as generated by SCAMP, of a proper motion survey based on archive data in the Pleiades region [5]. Polygons represent the footprints of 646 exposures taken over 11 years with the CFH12k, MEGACAM, SuprimeCam, and WFC instruments. The large disk in the background is the imprint of 2MASS catalogue sources downloaded automatically from the CDS server

Fig. 5 Relative proper motions computed by SCAMP from the Pleiades region archive data of Fig. 4. The clump on the *lower right side* is from stars in the Pleiades group



proper motion estimates. This is a tricky task for deep surveys conducted in stellar cluster fields, because of large coherent motions, high galactic extinction, and a lack of unsaturated catalogued sources with reliable PM measurements. We are currently developing heuristics to automatise the process in such demanding environments.

#### 4 Conclusion and Outlook

Both examples above – although still somewhat experimental – illustrate our current efforts to implement new features that will make AstrOmatic software a more powerful tool for stellar cluster studies. Other improvements in SEXTRACTOR planned for the near future will concern the background subtraction in crowded/nebulous regions and adaptive deblending. On the astrometric side, and based on the wealth of information gathered on various mosaic cameras over the past years, we plan on offering the possibility to derive astrometric solutions by adjusting pre-computed distortion models. This will make the results more robust in the most confused sky regions, where the large fraction of source mismatches between overlapping catalogues can cause "kicks" in the solution on the smaller scales.

**Acknowledgements** EB gratefully acknowledges the organisers of this symposium for offering financial support, and for their patience and understanding as editors of these proceedings.

#### References

 Baillard, A., Bertin, E., Mellier, Y., McCracken, H.J., Géraud, T., Pelló, R., Leborgne, F., Fouqué, P.: In: Gabriel, C., Arviset, C., Ponz, D., Enrique, S. (eds.) Astronomical Data Analysis Software and Systems XV. Astronomical Society of the Pacific Conference Series, vol. 351, pp. 236 (2006) 78 E. Bertin et al.

 Bertin, E.: In: Gabriel, C., Arviset, C., Ponz, D., Enrique, S. (eds.) Astronomical Data Analysis Software and Systems XV. Astronomical Society of the Pacific Conference Series, vol. 351, pp. 112 (2006)

- 3. Bertin, E., et al.: Modelling and characterising the PSF with PSFEx, PSFEx User's Guide available at https://www.astromatic.net/pubsvn/software/psfex/trunk/doc/psfex.pdf
- 4. Bertin, E., Mellier, Y., Radovich, M., Missonnier, G., Didelon, P., Morin, B.: In: Bohlender, D.A., Durand, D., Handley, T.H. (eds.) Astronomical Data Analysis Software and Systems XI. Astronomical Society of the Pacific Conference Series, vol. 281, pp. 228 (2002)
- 5. Bouy, H., et al. (in preparation)
- 6. Cuillandre, J., Lequeux, J., Allen, R.J., Mellier, Y., Bertin, E., Astrophys. J. 554, 190 (2001)
- da Costa, L., Bertin, E., Deul, E., Erben, T., Freudling, W., Guarnieri, M.D., Hook, I., Hook, R., Mendez, R., Nonino, M., Olsen, L., Prandoni, I., Renzini, A., Savaglio, S., Scodeggio, M., Silva, D., Slijkhuis, R., Wicenec, A., Wichmann, R., Benoist, C.: The Messenger 91, 49 (1998)
- 8. Delorme, P., Willott, C.J., Forveille, T., Delfosse, X., Reylé, C., Bertin, E., Albert, L., Artigau, E., Robin, A.C., Allard, F., Doyon, R., Hill, G.J.: Astron. Astrophys. **484**, 469 (2008)
- 9. Epchtein, N., de Batz, B., Capoani, L., Chevallier, L., Copet, E., Fouqué, P., Lacombe, P., Le Bertre, T., Pau, S., Rouan, D., Ruphy, S., Simon, G., Tiphène, D., Burton, W.B., Bertin, E., Deul, E., Habing, H., Borsenberger, J., Dennefeld, M., Guglielmo, F., Loup, C., Mamon, G., Ng, Y., Omont, A., Provost, L., Renault, J., Tanguy, F., Kimeswenger, S., Kienel, C., Garzon, F., Persi, P., Ferrari-Toniolo, M., Robin, A., Paturel, G., Vauglin, I., Forveille, T., Delfosse, X., Hron, J., Schultheis, M., Appenzeller, I., Wagner, S., Balazs, L., Holl, A., Lépine, J., Boscolo, P., Picazzio, E., Duc, P., Mennessier, M.: The Messenger 87, 27 (1997)
- 10. Gould, A., Kollmeier, J.A.: Astrophys. J. Suppl. 152, 103 (2004)
- 11. Irwin, M.J.: Mon. Not. R. Astron. Soc. 214, 575 (1985)
- 12. Kaiser, N., Squires, G., Broadhurst, T.: Astrophys. J. 449, 460 (1995)
- Kalirai, J.S., Richer, H.B., Fahlman, G.G., Cuillandre, J., Ventura, P., D'Antona, F., Bertin, E., Marconi, G., Durrell, P.R.: Astron. J. 122, 266 (2001)
- Kendall, T.R., Bouvier, J., Moraux, E., James, D.J., Ménard, F.: Astron. Astrophys. 434, 939 (2005)
- 15. Massey, R., Refregier, A.: Mon. Not. R. Astron. Soc. 363, 197 (2005)
- Mohr, J.J., Adams, D., Barkhouse, W., Beldica, C., Bertin, E., Cai, Y.D., da Costa, L.A.N., Darnell, J.A., Daues, G.E., Jarvis, M., Gower, M., Lin, H., Martelli, L., Neilsen, E., Ngeow, C., Ogando, R.L.C., Parga, A., Sheldon, E., Tucker, D., Kuropatkin, N., Stoughton, C.: In: Society of Photo-Optical Instrumentation Engineers (SPIE) Conference Series, vol. 7016, 17 (2008)
- 17. Moraux, E., Bouvier, J., Stauffer, J.R., Cuillandre, J.: Astron. Astrophys. 400, 891 (2003)
- 18. Stetson, P.B.: Publ. Astron. Soc. Pac. 99, 191 (1987)

## **Cluster Parameter Determinations for Large Datasets**

**Tim Naylor** 

**Abstract** I review the current methods of extracting parameters from cluster colour-magnitude diagrams, and compare them with the requirements for extracting the new information available from the next generation of optical and infrared sky surveys. I conclude that the basic statistical tools are beginning to emerge, but that there are significant problems with optical pre-main-sequence isochrones which will severely limit our ability to determine parameters for pre-main-sequence populations. In addition we need better tools to use the information relating background and foreground contamination which the sky surveys will provide.

#### 1 Introduction

The new generation of sky surveys give us some remarkable opportunities, but also some testing challenges for extracting astrophysical parameters from their colour-magnitude diagrams (CMDs). The main advantages of these surveys for cluster work are the very large number of clusters surveyed, the fact all the clusters are observed in the same, well constrained photometric system, and that all the clusters have large areas around them which can be used to measure fore- and background contamination. If we can use these advantages to effect, we should be able to make significant improvements in the measurements of age, distance, metallicity and mass functions for these clusters. In addition we will be able to measure radial profiles and examine mass segregation, though it is not clear these will be significantly improved by the new data.

Modern CMD fitting tools, such as those discussed below have the potential to give precise answers, in the sense that they yield small formal uncertainties.

T. Naylor (⊠)

T. Naylor

However, the accuracy of those answers, i.e. the degree to which they reflect the true underlying parameters can be undermined by three factors.

- (1) The photometric calibration. This offers two potential advantages for large surveys. First how well the calibration is understood, which determines how accurately we can move from the flux distributions of models to predicted magnitudes. This involves understanding both the bandpass of the instrument, and the photometric zero point. With the large surveys currently being undertaken, both these are well characterised, giving us a significant advantage over work undertaken by an individual observer over, say, the two weeks of a classical observing run. However, its is almost certain that at the level of precision we can achieve from the fitting tools will exceed the remaining systematic uncertainties from either the calibration or the models. This brings us to the second important advantage of large survey photometry, that the comparability between clusters should be excellent, allowing us to be more confident of differences in parameters between clusters.
- (2) The isochrones themselves. As I shall show later, in some circumstances the models are very poor fits to the data. In straight (frequentist) statistical terms this is a major problem, as one must first fit the dataset allowing (at least) the parameters of interest to vary. Then having obtained a good fit, one can determine the uncertainties in those parameters. If the fit is not a good one (as it often is not in isochrone work) one cannot make a determination of either the parameters or their uncertainties.
- (3) Finally, if working with purely photometric data, there will inevitably be some contamination by non-members. The obvious way of dealing with this is to estimate the background contamination, but as yet there is no general way including this in the fitting methods, yet it is crucial if we are to remove any bias it introduces, and to ensure our parameter uncertainties allow for the effects of background contamination.

## 2 Fitting Isochrones to Colour-Magnitude Diagrams

An isochronal population of single stars in a CMD should lie along a line represented by the isochrone. In principle this could then be fitted by a model, using classical  $\chi^2$  fitting, which would then yield a quality of fit statistic, and uncertainties in any parameters fitted. In practice there are two major problems with such an approach. First, any real cluster population contains multiple stars, which smear the sequence to brighter magnitudes. Second, the datapoints have uncertainties in both colour and magnitude. The second issue can be dealt with, provided the curvature of the isochrone is not too large, using an approximation which makes the problem similar to that for fitting a straight line to data with uncertainties in both dimensions [8]. (Interestingly the details of this approach have recently been revived [10] in a method to use the density of stars along the isochrone as a fitting parameter.)

However, the first issue cannot be addressed with  $\chi^2$  fitting. The traditional answer to this problem has been to simply overlay a series of isochrones on the data, and pick the one which appears to give the best description, and perhaps select two extreme examples which might just fit the data to illustrate the range of a given parameter. Clearly this method lacks in objectivity and the precise meaning of the uncertainties is unclear. Crucially, however, for our purposes, it will clearly be unsuitable for large numbers of clusters, due to its lack of automation.

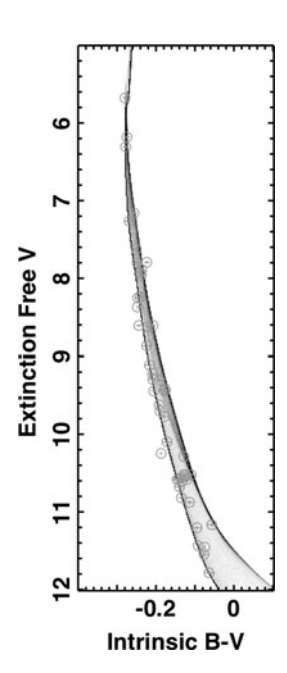
The obvious line of attack for this problem is to bin datapoints into CMD pixels, creating what is sometimes referred to as a Hess diagram. The values in each pixel can then be compared with a model using Poissionion statistics. Such a technique is widely used in extra-galactic work (see review [7]) and is also successful when determining star formation histories for populations with relatively smooth star formation as a function of time (e.g. [16]). The problem with applying such a technique to an isochronal population is that these populations have a very well defined, narrow, single-star sequence. Binning the data smears the sequence, throwing away much of the potential for precision parameter determination. This situation is exacerbated by the fact that the best samples for cluster work are often spectroscopically selected, reducing still further the number of stars, and often making binning impractical.

To solve this problem, one has to leave the data unbinned. There have been various attempts to solve this problem by creating simulated CMDs, which have a similar number of stars in them as the data, and then compare the distributions on a point-by-point basis.

The best known of these is that of Tolstoy and Saha [27]. Whilst having the advantage of leaving the data unbinned, such an approach has the disadvantage that the model is now sampled in a sparse manner, compared with the binning approaches, which can sample the model in a continuous manner.

There is now a new generation of methods which keep the data unbinned, and compare it with a continuously sampled CMD generated from the model. The most widely used for these for cluster work is probably my own  $\tau^2$  technique [20, 21] which in addition to our own work [13, 18, 20] has been used by several other groups [3, 4, 15]. The basic philosophy of these techniques can be illustrated by reference to Fig. 1. The colour scale in the background is the model, created by simulating a cluster of a million stars, and then binning them onto a fine grid in CMD space. Thus this represents the expected density of stars in the CMD. The green circles enclose the error bars for the data. A minimalist version of  $\tau^2$  (which would not take the uncertainties of the datapoints into account) would consider the values of the model at the position of each datapoint, and then multiply these together to give a goodness of fit parameter. One can then conceive of varying (say) the distance modulus by moving the colour scale up and down with respect to the datapoints, choosing the best fit value as the highest value of the goodness of fit parameter. There are two changes needed to make this into  $\tau^2$ . First one must allow for the uncertainties by, for each datapoint, multiplying the model by a twodimensional Gaussian representing the uncertainties, and then integrating under the resulting function. Second, rather than simply taking the product of these integrals, T. Naylor

**Fig. 1** An example of a  $\tau^2$  fit to main-sequence data. The model is the colour scale, which represents the expected density of datapoints, and the data are represented by encircled error bars. In this case the fit is in both distance modulus (which moves the model up and down) and age (which moves the upper part of the sequence left or right). The data are for NGC6530, and yield a probability that the data are explained by the model of 67%, an age of  $5.5\pm0.6$  Myr and a distance of 1.42 kpc with an uncertainty (which is dominated by systematics) of 2%. See [20] for details



one uses the sum of the twice the negative logarithms. This results on a statistic which behaves in a very similar way to  $\chi^2$ ; indeed  $\chi^2$  turns out to be special case of  $\tau^2$ .

There are two other methods in the literature which should give very similar answers to  $\tau^2$ , given the similarity of their underlying mathematics, but this has yet to be proved. Jørgensen and Lindegren [14] consider each star in the CMD, and ask the question what range of physical parameters could produce a star at that point; producing a likelihood distribution for that parameter (in Bayesian terms a posterior probability distribution). The likelihood distributions for each star for a given parameter can then be multiplied together to produce a likelihood distribution for the whole cluster. A similar Bayesian approach has been taken for cluster parameters by von Hippel and collaborators [6,28], and the underlying statistics (though not the implementation) are the same for the Hernandez, Valls-Gabaud and Gilmore method [9] of determining star formation histories for non-isochronal populations.

#### 3 The Isochrone Models

The most serious problems with model isochrones are for pre-main-sequence stars in the optical. Figure 2 shows the Pleiades, where the stars beyond about V - I = 2 are still in their pre-main-sequence phase. The cluster is known to be about 125 Myr old from the I-band luminosity of the most luminous pre-main-sequence stars not to show lithium depletion [26], and from fitting the upper main-sequence stars around

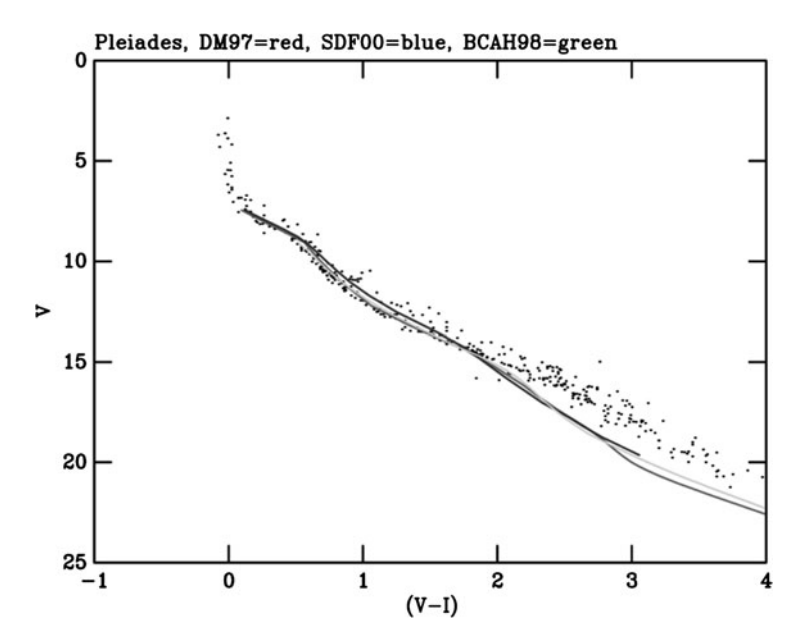


Fig. 2 The V vs V-I colour magnitude diagram for the Pleiades, with various 100 Myr models. (At V-I=3 the models are, from *top* to *bottom*: SDF00, BACH98 and DAM97.) The data are from the compilation of [25]. The isochrones are from [5, 24] and [1]

 $100\,\mathrm{Myr}$  [19] or more precisely perhaps  $115\,\mathrm{Myr}$  [20]. However, as can be seen, all the  $100\,\mathrm{Myr}$  pre-main-sequence models lie below the sequence redward of V-I=2. This problem is well known, and has been previously illustrated nicely for the Pleiades [25] and is discussed in [1]. It is thought to be a problem with the opacities in the optical, but it remains a significant limitation as (a) the largest separation of the isochrones with age (and hence potentially the greatest sensitivity to age) is in the optical and (b) using IR colours and luminosities can be problematic for premain-sequence stars due to the presence of discs. The classical way of countering this problem is to empirically correct the effective temperature – colour relationship, but this destroys any ability to determine masses using the isochrone.

In [12] and [18] we assigned ages to clusters in a relative sense, using the fact that the luminosity of the pre-main-sequence declines with age, but this does not give sequences that can be used for fitting. Given that there seems to be little prospect of the theory improving, it is clear that better empirical corrections must be determined for fitting the pre-main-sequences in the large optical surveys.

## 4 Foreground and Background Star Subtraction

Both  $\tau^2$  and von Hippel's Bayesian method have only been used for samples which are very likely to be composed entirely of members of their respective clusters, there being no contamination from foreground or background stars. The reason for this

is that any star which lies off the predicted sequence (and is presumably a nonmember) will return a probability of zero, which will then lead to probability for the whole model of zero.

There is, therefore, a superficial intellectual attraction in a process which will remove background and foreground stars from the CMD, leaving one with a clean CMD to fit with the above tools. A commonly used method to attempt this is to construct a CMD for a region of sky away from the cluster, which is representative of contamination. One then removes from the cluster CMD the star which is closest to each star in the "background" CMD [22]. More recently, more sophisticated versions of this technique have been developed which divide the CMD into boxes and then remove from the cluster CMD the same number of stars as are found in a background box (e.g. [23]). "Boxless" versions of this examine the number and location of near neighbours of stars in the cluster CMD, in the background field to assign them membership probabilities [2, 17].

Which of these methods is most appropriate depends upon exactly what one requires the background subtraction to achieve. If it is simply to identify a sequence by eye, probably the nearest neighbour removal is adequate. Where one is looking for over densities in the colour magnitude diagram which might indicate a cluster, the box techniques should work, provided the boxes are not larger than the structure in CMD one is looking for. The real issue is for formal fitting, where if one is to be statistically correct, one should simultaneously fit a model of both the background and the cluster to the data. To achieve this one would need to be able to sample the background onto an arbitrary grid, and add this to a model for the cluster such as that given in Fig. 1. In the absence of such a method, it may be that the techniques which derive the probability that a star is a non-member may provide a route forward. When fitting using Bayesian techniques it is possible to introduce a "safety net" which hypothesises that our model is entirely wrong for some unspecified reason (see Sect. 4.4 of [11]), which is given a very low prior probability. One can deal with individual datapoints in a similar way, and in a sense this is what the  $\tau^2$  soft clipping [21] of datapoints achieves. However, von Hippel and collaborators express this more explicitly [6] with a binary switch which allocates a star to the field or the cluster. If this could be extended so one looked at the distribution of membership probabilities (determined from the background data) for those stars assigned to the field, and compared it with an expected distribution there may be a way of disfavouring models which allocate either too many or too few stars to the background.

#### 5 Conclusions

Many of the techniques required to make the best use of the next generation of sky surveys for parameter determinations for clusters are in place. In particular the statistical techniques for fitting isochrones to the data are now maturing. However, there are still problems with the isochrones themselves, particularly for optical CMDS of pre-main-sequence clusters. The largest gap is probably in using

determinations of background and foreground contamination in cluster CMDs to improve our fitting. The large surveys give us much better data for determining the contamination than we have had heretofore, which should provide the impetus for us to develop the techniques to use this information properly

**Acknowledgements** My thanks go to Rob Jeffries, Nathan Mayne, Stuart Littlefair and Cameron Bell with whom I have spent many productive hours developing techniques in this field.

#### References

- 1. Baraffe, I., Chabrier, G., Allard, F., Hauschildt, P.H.: Astron. Astrophys. 337, 403 (1998)
- 2. Bonatto, C., Bica, E.: Mon. Not. R. Astron. Soc. 377, 1301 (2007)
- 3. Cargile, P.A., James, D.J.: Astron. J. 140, 677 (2010)
- 4. Da Rio, N., Gouliermis, D.A., Gennaro, M.: Astrophys. J. 723, 166 (2010)
- 5. D'Antona, F., Mazzitelli, I.: Memor. Soc. Astron. Ital. **68**, 807 (1997)
- De Gennaro, S., von Hippel, T., Jefferys, W.H., Stein, N., van Dyk, D., Jeffery, E.: Astrophys. J. 696, 12 (2009)
- 7. Dolphin, A.E.: Mon. Not. R. Astron. Soc. 332, 91 (2002)
- 8. Flannery, B.P., Johnson, B.C.: Astrophys. J. **263**, 166 (1982)
- 9. Hernandez, X., Valls-Gabaud, D., Gilmore, G.: Mon. Not. R. Astron. Soc. 304, 705 (1999)
- 10. Hernandez, X., Valls-Gabaud, D.: Mon. Not. R. Astron. Soc. 383, 1603 (2008)
- 11. Jaynes, E.T.: Probability Theory: The Logic of Sicence. Cambridge University Press, Cambridge (2004)
- 12. Jeffries, R.D., Oliveira, J.M., Naylor, T., Mayne, N.J., Littlefair, S.P.: Mon. Not. R. Astron. Soc. 376, 580 (2007)
- 13. Jeffries, R.D., Naylor, T., Walter, F.M., Pozzo, M.P., Devey, C.R.: Mon. Not. R. Astron. Soc. **393**, 538 (2009)
- 14. Jørgensen, B.R., Lindegren, L.: Astron. Astrophys. **436**, 127 (2005)
- Joshi, H., Kumar, B., Singh, K.P., Sagar, R., Sharma, S., Pandey, J.C.: Mon. Not. R. Astron. Soc. 391, 1279 (2008)
- 16. Kerber, L.O., Girardi, L., Rubele, S., Cioni, M.-R.: Astron. Astrophys. **499**, 697 (2009)
- 17. Kerber, L.O., Santiago, B.X., Castro, R., Valls-Gabaud, D.: Astron. Astrophys. 390, 121 (2002)
- 18. Mayne, N.J., Naylor, T.: Mon. Not. R. Astron. Soc. 386, 261 (2008)
- 19. Meynet, G., Mermilliod, J.-C., Maeder, A.: Astron. Astrophys. Suppl. 98, 477 (1993)
- 20. Naylor, T.: Mon. Not. R. Astron. Soc. **399**, 432 (2009)
- 21. Naylor, T., Jeffries, R.D.: Mon. Not. R. Astron. Soc. **373**, 1251 (2006)
- 22. Nelson, M., Hodge, P.: Publ. Astron. Soc. Pac. 95, 5 (1983)
- 23. Sanner, J., Geffert, M., Brunzendorf, J., Schmoll, J.: Astron. Astrophys. 349, 448 (1999)
- 24. Siess, L., Dufour, E., Forestini, M.: Astron. Astrophys. 358, 593 (2000)
- Stauffer, J.R., Hartmann, L.W., Fazio, G.G., Allen, L.E., Patten, B.M., Lowrance, P.J., Hurt, R.L., Rebull, L.M., Cutri, R.M., Ramirez, S.V., Young, E.T., Rieke, G.H., Gorlova, N.I., Muzerolle, J.C., Slesnick, C.L., Skrutskie, M.F.: Astrophys. J. Suppl. 172, 663 (2007)
- 26. Stauffer, J.R., Schultz, G., Kirkpatrick, J.D.: Astrophys. J. 499, L199 (1998)
- 27. Tolstoy, E., Saha, A.: Astrophys. J. 462, 672 (1996)
- von Hippel, T., Jefferys, W.H., Scott, J., Stein, N., Winget, D.E., De Gennaro, S., Dam, A., Jeffery, E.: Astrophys. J. 645, 1436 (2006)

T. Naylor



General discussion

# Open Clusters Science in the Virtual Observatory Era

Ivan Zolotukhin and Elena Glushkova

Abstract We present http://ocl.sai.msu.ru, a modern web application with an integrated rich set of third-party analysis tools aimed at facilitating astrophysical research with the Open Cluster Catalog of the Sternberg Astronomical Institute (Koposov et al. Astron. Astrophys. 486:771, 2008; Glushkova et al. Astron. Lett. 36:75, 2010). Discovered using Virtual Observatory (VO) technologies, almost 200 new open clusters are presented in a way that allows further exploitation of the multiple VO-compatible datasets through the single web site serving as an entry point. As more datasets become available (e.g. UCAC3 with proper motions Zacharias et al. Astron. J., 139:2184, 2010), new research perspectives arise with this set of open clusters making it possible to do quick-look science online, which have successfully been demonstrated during several VO-Science tutorials. If populated with a more comprehensive set of open clusters, this tool may become a new WEBDA prototype in the VO era. In this manuscript we also briefly describe steps of a demonstration shown as a contributed talk at JENAM-2010 conference to give an overlook of what kind of original research studies it is now possible to do online

Observatoire de Paris-Meudon, LERMA, UMR 8112, 61 Av. de l'Observatoire, 75014 Paris, France

Sternberg Astronomical Institute, Universitetsky pr. 13, Moscow 119992, Russia

Observatoire de Paris, VO-Paris Data Centre, 61 Av. de l'Observatoire, 75014 Paris, France e-mail: iz@sai.msu.ru

E. Glushkova

Sternberg Astronomical Institute, Universitetsky pr. 13, Moscow 119992, Russia e-mail: elena@sai.msu.ru

I. Zolotukhin (⊠)

#### 1 Introduction

For many years the astronomical community has been using public databases to organize and share scientific data. Researchers that deal with open clusters were among the pioneers of this work. Well-known WEBDA service [5, 6] available since early 1990s is the brightest example of this kind and its value is deservedly acknowledged by hundreds of refereed publications that made use of its content.

Since that time an amount of various data products, analysis environments and scientific applications has grown up significantly and an international effort has been launched to coordinate these advances, named Virtual Observatory. Broadly speaking, this is an interoperability infrastructure between all parties involved in the research process, aimed at facilitating it by making routine operations transparent. The goal is to free more researcher's time for essentially creative stages of his/her everyday work and to increase the number of publications per gigabyte of a data (which is the equivalent to processing a steadily growing data volume by a research community of the constant size at the same completeness level, important point in the era of data intensive astronomy). After several years of technological development the VO is ready for a scientific exploitation which is obviously characterized by an increasing number of VO-based scientific projects (see e.g. [2,9] for recent ones).

Following these trends we have developed a VO mash-up application with the main purpose to facilitate dissemination and scientific usage of the results of our studies, Open Cluster Catalog of the Sternberg Astronomical Institute, developed in [4] and [3]. The web application provides continuous publication of ongoing catalog compilation, and is available as a dedicated web site at http://ocl.sai.msu.ru. Besides the standard access via a web browser to the catalog of individual cluster pages with Hess-diagrams, color-magnitude diagrams (CMDs), 2MASS or DSS cluster images, and catalogs of photometric data (for clusters with CCD observations), the web site offers the catalog exported to CSV, DAT, and VOTable formats as well and implements a standard VO programmatic access interface for positional queries called *ConeSearch*. Moreover, it is possible to start VO client applications, such as TOPCAT<sup>2</sup> or CDS ALADIN<sup>3</sup>, by a single click in a web browser with the catalog preloaded for quick-look analysis of the whole sample and all accompanying data we provide for individual clusters. Special built-in module smoothly integrates web browser with VO applications transparently for a user, essentially forming online data analysis environment.

In the next section we define major blocks of the described web application with some level of technical details important for reusing our experience. In the last section we briefly outline the steps of the demonstration shown live at the

<sup>&</sup>lt;sup>1</sup>http://www.ivoa.net/Documents/latest/ConeSearch.html.

<sup>&</sup>lt;sup>2</sup>http://www.star.bris.ac.uk/~mbt/topcat/.

<sup>&</sup>lt;sup>3</sup>http://aladin.u-strasbg.fr/.

JENAM-2010 meeting in order to showcase the scientific potential of this prototype application.

### 2 Web Application Internals

The web application itself is built on a standard stack of popular open source technologies, namely DJANGO<sup>4</sup> framework, written in PYTHON<sup>5</sup> programming language, and POSTGRESQL<sup>6</sup> database management system.

The fact of PYTHON usage gives the application enhanced extensibility because of the modular structure of the language and availability of many third-party astronomical modules. In particular, the application makes use of MATPLOTLIB<sup>7</sup> module for drawing diagrams, ASTROLIB COORDS<sup>8</sup> – for coordinates conversions, and  $ATPY^9$  – for table manipulations.

We also intensively employ DJANGO automated testing system to detect possible regressions that could be introduced in the course of the code development. Apart from this good practice, we emphasize strong benefits of using DJANGO administrator's interface as it solves most of the problems of content management by non-technical staff, which are probably familiar to almost any research group trying to maintain its own data published online.

Another important block of the presented web application is its advanced cross-platform client toolkit which comprises 2 open source components: browser JAVA plugin WEBSAMPCONNECTOR<sup>10</sup> and a wrapping JAVASCRIPT library SAMP-WEBTOOLS.<sup>11</sup> Technically, JAVA plugin, when loaded, makes browser a SAMP<sup>12</sup> client able to intercommunicate with other applications by means of SAMP, Simple Application Messaging Protocol. JAVASCRIPT wrapper is used to conveniently control JAVA plugin behaviour from within user interface (utilizing JAVA-JAVASCRIPT interaction). It loads/unloads the JAVA plugin after user switches on/off VO mode, gets from it and displays in a browser list of connected SAMP applications or launches them with WEBSTART technology (if detects that necessary tools have not been started), also sends them datasets from the web site through SAMP upon user request. In this scenario web browser acts like a data browser, which is used to locate necessary datasets on a web site and then easily send them to dedicated VO

<sup>&</sup>lt;sup>4</sup>http://www.djangoproject.com.

<sup>&</sup>lt;sup>5</sup>http://www.python.org.

<sup>&</sup>lt;sup>6</sup>http://www.postgresql.org.

<sup>&</sup>lt;sup>7</sup>http://matplotlib.sourceforge.net.

<sup>8</sup>http://www.scipy.org/AstroLib/.

<sup>&</sup>lt;sup>9</sup>http://atpy.sourceforge.net.

<sup>&</sup>lt;sup>10</sup>http://vo.imcce.fr/webservices/samp/.

<sup>&</sup>lt;sup>11</sup>http://github.com/iz-sai/samp-webtools.

<sup>&</sup>lt;sup>12</sup>http://www.ivoa.net/Documents/latest/SAMP.html.

applications prudently launched before, where in turn all scientific analysis takes place.

The purpose of this subsystem is to actually form a VO environment ready for scientific analysis by automated launch of third-party applications TOPCAT and ALADIN and tight integration of a browser into this environment. Initially developed in [1, 8], this technology helps to overcome important problem of the present day Virtual Observatory: too steep entrance for researchers. On the contrary, in a proposed solution with the minimal technical requirements (a web browser and a JAVA installed) within several mouse clicks everybody is able to conduct his/her own research online, transparently using forefront VO infrastructure without necessity to know and understand its internals.

#### 3 Scientific Usage

This section presents concise series of steps necessary to repeat the demonstration shown at JENAM-2010 conference. It is aimed to give an overlook of what science is possible with the system described above by example of determining a proper motion of previously unstudied open cluster.

- 1. Point a web browser to <a href="http://ocl.sai.msu.ru">http://ocl.sai.msu.ru</a>. At the time of writing, JAVA applet we make use of is known to have problems working in SAFARI browser on MAC OS due to deficiencies of their JAVA implementation, but authors of WEBSAMPCONNECTOR will likely be able to solve these issues in future. All other browsers are supported, though we recommend using MOZILLA FIREFOX to follow these steps.
- 2. Click on *VO mode: turn on* link in the VO menu at the top right corner of the browser screen. Then press *Open* and *OK* in every window raising. Small (500 KB) JAVA applet will be loaded into the browser and will check if there are necessary VO applications (ALADIN and TOPCAT) running in the system. If not, the applet will offer to launch TOPCAT. When TOPCAT is downloaded and launched, the green icon will appear in the VO menu at the top right, indicating that the system is ready. After that, click on the *start* link in the VO menu just below the *Aladin* item to launch ALADIN. Now it is possible to conveniently interact with VO applications through the web browser. Note that reload of the JAVA applet after every web page reload takes some moments, so user has to wait until green icon in the VO menu is on before start working with a web page. It indicates that a web browser is connected to the SAMP hub and one can go on with his/her actions. Do not click on a web page when the status is *connecting*. Please also work in one tab; do not open many.
- 3. Go to Catalog page. In a moment the catalog will be loaded automatically in all running VO tools. The table displayed in a browser window will change in VO mode as well: there are checkboxes appeared on the left of every row, RA-Dec coordinates became clickable, and by moving cursor over the table rows one can

- now highlight them. Make sure that catalog was loaded by choosing  $Graphics \rightarrow Sky$  in TOPCAT menu. You should see a cloud of points along the Galactic plane. Note that highlighting rows in the web browser (by mouse movement or by ticking checkboxes on the left) also highlights points on a spherical plot.
- 4. We pick some nearby clusters to analyze their proper motions using UCAC3 catalog [7]. Clusters should not be too distant as UCAC3 magnitude limit implies that there are no stars with measured proper motions further than about 2 kpc. Sort the catalog by distance clicking on *Distance* column header in the web browser. Then examine clusters' CMDs to choose more rich cluster as these are easier to deal with. Press *Activation action: no action* button in the main TOPCAT window, then choose *View URL as Image* → *set Image Location Column* to cluster\_cmd\_file\_url → *Image Format: PNG*. cluster\_cmd\_file\_url is a precomputed CMD based on 2MASS data we used when constructed the Catalog. Then press *OK* button in the bottom of the window. Once you select a row or some point, a window with additional plot will appear. You can move mouse cursor slowly over the table in the web browser and see changing diagrams in a dedicated window. We shall continue with SAI 57 cluster, but one may want to go along with another ones (SAI 61, SAI 137, or SAI 27 are good illustrations also).
- 5. Load UCAC3 data for this cluster. To do so, click on underscored coordinates of SAI 57 in the cluster list on the web page and ALADIN will automatically load DSS2 cluster image, over-plotting UCAC3 objects within cluster's radius. Then right click on UCAC3, SAI 57 plane in a stack list in ALADIN and choose Broadcast selected tables to... → topcat to send UCAC3 data to TOPCAT.
- 6. Plot proper motion diagram for SAI 57 in TOPCAT. Select UCAC3, SAI 57 table in *Table List*. Press *Scatter Plot* toolbar button. Then select pmRA and pmDE columns as X and Y axes, correspondingly. Press *Add auxiliary axis* button in the plot window and add brightness as a third axis, e.g. Jmag column. Add uncertainties to the diagram: press *Toggle X error bars on/off*, and same for Y axis. Note that error columns were recognized automatically. You should now see a colored cloud of points with error bars that is effectively meaningless: there is no dominant proper motion visible on this diagram. The reason for that is presence of many background stars that blur weak cluster's signal in their noise. Press *Display statistics for each column* toolbar button and examine mean and standard deviation for proper motion columns. We now attempt to increase the contrast and to discern open cluster proper motion signal from background noise.
- 7. Go to SAI 57 individual web page by clicking on its name in the web browser. Locate the photometric data available for this cluster at the bottom of the page ((J, J-H) precomputed isochrones derived with [4] method and 2MASS data are available for all clusters). If you move the cursor over isochrone data link, the *Broadcast* button will appear next to it. Click on it to send (J, J-H) isochrone data to VO applications. In TOPCAT select UCAC3, SAI 57 table in *Table List* and press *Scatter Plot* toolbar button. Type the following expressions in axes specifications: Jmag-Hmag for X and Jmag for Y. Tick *Flip* checkbox just next to Y axis expression for the diagram to look conventionally. Then overplot an

- isochrone: press Add a new data set button on a toolbar below the plot and choose SAI 57: (J, J-H) isochrone as a Table and J-H and J as an axes. Click on the blue square in Row Subsets and make these points smaller in the raised window (Size I is convenient).
- 8. We aim to increase contrast on proper motion diagram for cluster's stars. For this purpose pick up those stars that lie in the vicinity of an isochrone. Press Draw a region on the plot to define a new row subset button on a Scatter Plot main toolbar and draw the region along the isochrone. Then press this toolbar button again and type the name of a subset we have just defined, e. g. isochrone\_stars, then press Add Subset button. Points of this subset will be denoted with new symbols at proper motions diagram. Turn off error bars there and see if the selected stars tend to group to some particular place on a diagram. Click on isochrone\_stars symbol inside Row Subsets section of the scatter plot window and change symbols to open circles of Size 5 for convenience. Examine subset's statistics by pressing *Display statistics for each column* toolbar button and choosing isochrone\_stars subset there. If mean value and its standard deviation do not indicate steadily detected proper motion of the cluster, try to exclude or include some points paying attention at CMD. Basically, one should examine both plots and find the place on the proper motion diagram where stars that lie nearby isochrone at the CMD huddle together. You should then be able to see the cluster's proper motion "signal" in the statistics of well defined subset.

More detailed version of these steps as well as other recipes for quick-look online research possible with given web application are published in the VO section of its web site at http://ocl.sai.msu.ru/vo/.

**Acknowledgements** IZ participation in the JENAM-2010 meeting was supported by VO-Paris Data Centre and a grant of European Astronomical Society.

#### References

- Chilingarian, I., Zolotukhin, I.V.: In: Argyle, R.W., Bunclark, P.S., Lewis, J.R.: Astronomical Data Analysis Software and Systems XVII. Astronomical Society of the Pacific Conference Series, vol. 394, pp. 351 (2008)
- 2. Chilingarian, I., Cayatte, V., Revaz, Y., Dodonov, S., Durand, D., Durret, F., Micol, A., Slezak, E.: Science 326, 1379 (2009)
- 3. Glushkova, E.V., Koposov, S.E., Zolotukhin, I.V., Beletsky, Y.V., Vlasov, A.D., Leonova, S.I.: Astron. Lett. **36**, 75 (2010)
- 4. Koposov, S.E., Glushkova, E.V., Zolotukhin, I.Y.: Astron. Astrophys. 486, 771 (2008)
- 5. Mermilliod, J.-C., Paunzen, E.: Astron. Astrophys. **410**, 511 (2003)
- Mermilliod, J.-C.: In: Egret, D., Albrecht, M.A. (eds.) Information & On-Line Data in Astronomy. Astrophysics and Space Science Library, vol. 203, pp. 127–138 (1995)
- 7. Zacharias, N., Finch, C., Girard, T., Hambly, N., Wycoff, G., et al.: Astron. J. 139, 2184 (2010)
- 8. Zolotukhin, I.V., Chilingarian, I.: In: Argyle, R.W., Bunclark, P.S., Lewis, J.R. (eds.) Astronomical Data Analysis Software and Systems XVII. Astronomical Society of the Pacific Conference Series, vol. 394, pp. 393 (2008)
- 9. Zolotukhin, I.V., & Revnivtsev, M., MNRAS, 411, 620 (2011)

## GALExtin: A VO-Service for Estimating Galactic Interstellar Extinction

Eduardo Amôres, André Moitinho, Vladan Arsenijevic, and Laerte Sodré

**Abstract** The distribution of interstellar matter is a fundamental aspect of the structure of our Galaxy. Its knowledge is critical for determining distances and color corrections, for star counts and brightness models of the Galaxy, and also for extinction corrections of spectra, among other applications. In this context, we are developing a *VO*-Service called GALExtin that provides interstellar extinction estimates for any direction in the sky using available 2D maps, 3D models, catalogs with extinction and diffuse emission measurements. The service is naturally useful for estimating interstellar extinction toward star clusters.

#### 1 Interstellar Extinction

One of the critical steps in the study of both individual objects and Galactic structure consists in the determination of interstellar extinction. However, due to the clumpiness of the distribution of interstellar dust, it is difficult to model its distribution. Several works have been produced aiming at modeling the distribution of interstellar extinction in the Galaxy, such as [1,3,7,11,13] (see<sup>1</sup>), [9,10,12] among others. In addition, maps have been elaborated which provide integrated extinction along lines of sight, such as those of [4,5,14] for the whole Galaxy, [15] and [6] for the Galactic center region, as well as map of  $A_V$  of [8] for the whole Galaxy ( $|b| < 40^\circ$ ) based on the star counts.

The resolution and coverage of the different models and maps must be taken into account in studies of extinction. There are models that provide good estimates in the

E. Amôres (⋈) · A. Moitinho · V. Arsenijevic SIM, U. of Lisbon, Campo Grande, Edifício C8, Piso 5, 1749-016 Lisboa, Portugal e-mail: amores@sim.ul.pt; andre@sim.ul.pt; arsenije@sim.ul.pt

¹http://www.astro.iag.usp.br/~amores.

94 E. Amôres et al.

solar neighborhood up to distances  $\sim 1.0$  kpc, while they fail to describe extinction beyond that distance. Conversely, there are models that provide better values at 3.0 kpc being imprecise at smaller distances. Depending on the assumptions used in their elaboration, some models can be used only for a given region of the sky.

For star cluster studies, reliable extinction estimates toward globular and open clusters is essential for obtaining accurate distances, among other properties.

#### 2 GALExtin

Interstellar extinction has a transverse importance across all fields of astronomy, from stellar studies in which one wants to know the extinction toward given objects from their coordinates and distances (3D Models), to extragalactic astronomy where the contribution of the extinction of our Galaxy along the line of sight must be taken into account.

In the context of providing a useful tool for estimating interstellar extinction, we are developing a VO-Service called GALExtin which provides 3D estimates of interstellar extinction along any direction and distance in the sky. The engine behind GALExtin is based on available 2D maps, 3D models and catalogs of measurements of extinction and diffuse emission, such as CO, HI, near and far-infrared, among others.

Since GALExtin is available as a service, users are relieved of installing the programs and large files required by most of the models and maps.

Users provide a list of coordinates and distances for which GALExtin then produces an output list with extinction estimates for each object for a chosen model. GALExtin will be available on-line at the website <a href="http://www.galextin.org">http://www.galextin.org</a>.

**Acknowledgements** E. Amôres and V. Arsenijevic acknowledge support from FCT under grants no. SFRH/BPD/42239/2007 and SFRH/BPD/47498/2008, respectively. This work has been partially funded by FCT project PDCTE/CTE-AST/81711/2003.

#### References

- 1. Amôres, E.B., Lépine, J.R.D.: Astron. J. 130, 679 (2005)
- 2. Amôres, E B., Lépine, J.R.D.: Astron. J. 133, 1519 (2007)
- 3. Arenou, F., Grenon, M., Gómez, A.: Astron. Astrophys. 258, 104 (1992)
- 4. Burstein D., Heiles, C.: Astrophys. J. 225, 40 (1978)
- 5. Burstein D., Heiles, C.: Astron. J. 210, 341 (1982)
- Dutra, C.M., Santiago, B.X., Bica, E.L.D., Barbuy, B.: Mon. Not. R. Astron. Soc. 338, 253 (2003)
- 7. Drimmel, R., Cabrera-Lavers, A., López-Corredoira, M.: Astron. Astrophys. 409, 205 (2003)
- 8. Dobashi, K., Uehara, H., Kandori, R., Sakurai, T., Kaiden, M., Umemoto, T., Sato, F.: Publ. Astron. Soc. Jpn. 57, 1 (2005)
- 9. Froebrich, D., Ray, T.P., Murphy, G.C., Scholz, A.: Astron. Astrophys. 432, L67 (2005)

- Froebrich, D., Murphy, G.C., Smith, M.D., Walsh, J., Del Burgo, C.: Astron. Astrophys. 378, 1447 (2007)
- 11. Hakkila, J., Myers, J., Stidham, B.: Astron. J. 114, 2043 (1997)
- 12. Marshall, D.J., Robin, A.C., Reylé, C., Schultheis, M., Picaud, S.: Astron. Astrophys. 453, 635 (2006)
- 13. Méndez, R.A., van Altena, W.F.: Astron. Astrophys. Suppl. 330, 910 (1997)
- 14. Schlegel, D.J., Finkbeiner, D.P., Davis, M.: Astrophys. J. **500**, 525 (1998)
- 15. Schultheis, M., Ganesh, S., Simon, G., Omont, A., Alard, C., Borsenberger, J., Copet, E., Epchtein, N. Fouqué, P., Habing, H.: Astron. Astrophys. **349**, L69 (1999)

# **YSO Clusters on Galactic Infrared Loops**

Gábor Marton, Zoltán Tamás Kiss, L. Viktor Tóth, Sarolta Zahorecz, László Pásztor, Munateka Ueno, Yoshimi Kitamura, Motohide Tamura, Akiko Kawamura, and Toshikazu Onishi

**Abstract** The AKARI all sky survey (Murakami et al. Publ. Astron. Soc. Jpn. 59:369, 2007) was investigated for YSO candidates. Distribution of candidate sources have been analysed and compared to that of galactic CO and medium scale structures. Clustering and other inhomogenities have been found.

## 1 YSO Candidate and Area Selection

Exploring the AKARI FIS BSC [11] was started by checking the colours of known objects. AKARI FIS colour-magnitude diagram was used to select YSO candidates, where  $[\lambda] = logF_{\lambda}$ . YSOs were taken from SIMBAD, [4] (Spitzer obs.) and [4] (AKARI IRC obs.). For 66% of the known YSOs: 0 < [90] - [140] < 0.5, and [90] > 1.0, see Fig. 1. 86% of extragalactic objects of SIMBAD were fallen into the black parallelogram. We have found YSO number density ( $N_{YSO}$ ) fluctuation relative to the CO line intensity [3]. In the Tau-Aur-Per region (TAP, 157 < l < l

G. Marton  $(\boxtimes) \cdot L$ . Viktor Tóth  $\cdot$  S. Zahorecz

Department of Astronomy, Eötvös University, Budapest, Hungary

e-mail: g.marton@astro.elte.hu

Z.T. Kiss · L. Pásztor

MTA KTM CSKI, Budapest, Hungary

MTA RISSAC, Budapest, Hungary

M. Ueno · Y. Kitamura

Institute of Space and Astronautical Science, Sagamihara, Kanagawa, Japan

M. Tamura · A. Kawamura · T. Onishi

National Astronomical Observatory of Japan, Mitaka, Japan

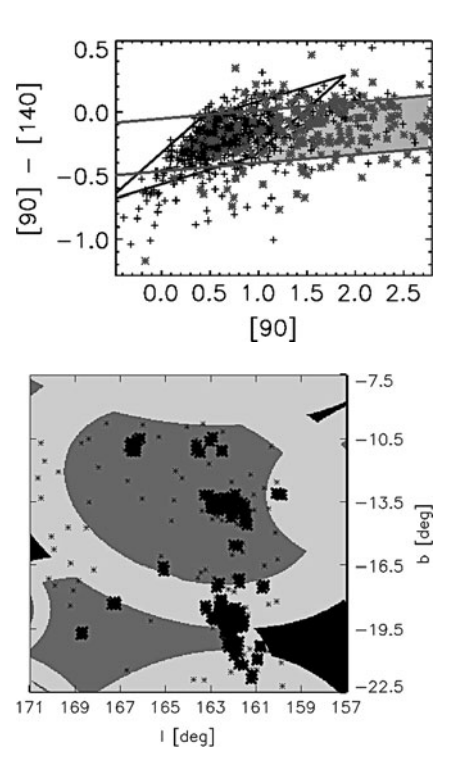
University of Nagoya, Nagoya, Japan

Osaka Prefecture University, Osaka, Japan

98 G. Marton et al.

Fig. 1 Magnitude-colour diagram of known YSOs and extragalactic objects. Gray area is populated by known YSOs. \*: identified YSOs, +: extragalactic objects.

Fig. 2 Small embedded groups of AKARI FIS YSO candidates in the TAP region with Galactic Infrared Loops (GIRLs) in the background. Small dots YSOs that are not members of groups, big asterisks group members. 16 of the 29 identified groups are located on the GIRL shells.



171, -22.5 < b < -7.5) we found  $100 < N_{YSO}/W(CO) < 150$  instead of the average values of 20. The surface distribution ( $\sigma_{YSO}$ ) of the AKARI YSO candidates has also been compared to that of the GIRLs [5]. Groups were identified by the minimum spanning tree method, as described by [4], using a cut-off distance of 16 arcmin (that corresponds to 0.64 pc at a distance of 140 pc).

# 2 Results

We found 236 AKARI YSO candidates with the described selection method in the TAP region.  $\sigma_{YSO}/E(B-V)$  was found to be 1.5, 2.24, 1.86 for inside loop, on loop and between loop areas, respectively.

29 groups were found, 136 YSO candidates are group members. 10 groups have more than 3 elements, 5 groups have more than 10 elements. 16 groups are located on the GIRL shells, see Fig. 2. The biggest group has 28 elements. The centre of this group is at (l,b): (160.15, 18.6), and it is part of the widely studied IC 348 open cluster, which contains more than 300 confirmed members [1] with a mass and age distribution peak at  $0.2~M_{\odot}$  and 2~Myr, respectively [2, 6–8, 10].

**Acknowledgements** This research was partly found by: The European Union and the European Social Fund have provided financial support to the project under the grant agreement no. TÁMOP-4.2.1/B-09/1/KMR-2010-0003. JSPS-HAS collaboration project 2009/2010

# References

- 1. Cambrésy, L., Petropoulou, V., Kontizas, M., Kontizas, E.: Astron. Astrophys. 445, 999 (2006)
- 2. Carpenter, J.M.: Astron. J. 124, 1593 (2002)
- 3. Dame, T.M., Hartmann, D., Thaddeus, P.: Astrophys. J. 547, 792 (2001)
- 4. Gutermuth, R.A., Megeath, S.T., Myers, P.C., Allen, L.E., Pipher, J.L., Fazio, G.G.: Astrophys. J. Suppl. 184, 18 (2009)
- 5. Könyves, V., Kiss, Cs., Moór, A., Kiss, Z.T., Tóth, L.V.: Astron. Astrophys. 463, 1227 (2007)
- 6. Luhman, K.L.: Astrophys. J. 525, 466 (1999)
- 7. Luhman, K.L., Stauffer, J.R., Muench, A.A., et al.: Astrophys. J. 593, 1093 (2003)
- 8. Muench, A.A., Lada, E.A., Lada, C.J., et al.: Astron. J. 125, 2029 (2003)
- 9. Murakami, H., Baba, H., Barthel, P., Clements, D.L., Cohen, M., Doi, Y., Enya, K., Figueredo, E., Fujishiro, N., Fujiwara, H., et al. Publ. Astron. Soc. Jpn. **59**, 369 (2007)
- 10. Preibisch, T., Stanke, T., Zinnecker, H.: Astron. Astrophys. 409, 147 (2003)
- Yamamura, I., Makiuti, S., Ikeda, N., Fukuda, Y., Oyabu, S., Koga, T., White, G.J.: AKARI/FIS All-Sky Survey Point Source Catalogues, ISAS/JAXA, VizieR Online Data Catalog, 2298, 0 (2010)



Ivan Zolotukhin

G. Marton et al.



Tim Naylor is really focused



Estelle Moraux is out of focus

# VVV Search for New Young Clusters Towards the Star Forming Regions in Our Galaxy: First Results

Jura Borissova, Radostin Kurtev, Stuart Folkes, Étienne Artigau, Valentin Ivanov, Dante Minniti, Philip Lucas, Francisco Penaloza, Stuart Sale, Eduardo Bica, Charles Bonatto, Márcio Catelan, Maren Hempel, Monica Zoccali, Ignacio Toledo, Douglas Geisler, Christian Moni Bidin, Andrea Ahumada, Rodolfo Barba, Richard de Grijs, Andrés Jordán, and Gustavo Baume

**Abstract** One of the main goals of the "VVV – Vista Variables in the Via Lactea" ESO Large Survey is to search for new star clusters of different ages. In order to trace the early stages of star clusters formation we carrying out a survey of infrared star cluster candidates and stellar groups in the directions of known massive star formation regions. To date, we have identified 47 candidates. Most of them appear compact (with small angular sizes) and very young.

J. Borissova (⋈) · R. Kurtev · S. Sale · S. Folkes · F. Penaloza Facultad de Ciencias, Departamento de Fisíca y Astronomía, Universidad de Valparaíso, Chile

D. Minniti · M. Catelan · M. Hempel · M. Zoccali · I. Toledo · A. Jordán · S. Sale Pontificia Universidad Catolica, Chile

C. Bonatto · E. Bica Universidade Federal do Rio Grande do Sul, Brazil

V. Ivanov · A. Ahumada ESO, Chile

D. Geisler · C. M. Bidin Universidad de Concepcion, Chile

R. Barba Universidad de La Serena, Chile

É. Artigau Université de Montréal, Canada

P. Lucas University of Hertsfordshire, UK

R. de Grijs KIAA, Peking University, China

G. Baume Universidad de La Plata, Argentina J. Borissova et al

VISTA Variables in the Vía Láctea (VVV) is one of the six ESO Public Surveys selected to operate with the new 4-m Visible and Infrared Survey Telescope for Astronomy (VISTA). VVV is scanning the Milky Way bulge and an adjacent section of the mid-plane, where star formation activity is high. The survey will take 1,929 h of observations during 5 years and will cover an area of 520 deg<sup>2</sup>. The final product will be a deep near-IR atlas in five pass bands, a catalogue of more than 10<sup>6</sup> variable point sources and a 3-D map of the inner Milky Way [4].

In order to trace the early epochs of cluster formation, we are carrying out a survey of infrared star clusters and stellar groups. Our search will focus on sight lines towards known massive star formation regions associated with: methanol maser emission; hot molecular cores [3]; Galactic bubbles outlined by GLIMPSE [1,2]. The pipeline processed and calibrated J,H,Ks images were obtained from the Cambridge Astronomical Survey Unit (CASU). The Ks-band images were inspected by eye to identify any stellar overdensities. The composite J,H,Ks color images were subsequently examined for each candidate cluster. Prior to any color-magnitude investigation one of the main criterions to define the star cluster candidates was to find at least 10 candidate members with similar colors.

To date, we have inspected 21 tiles (1.5×1.1 deg each) associated with known HII regions from the VVV disk area and 4 tiles from the VVV bulge area. We have identified 47 candidate star clusters or young stellar groups. Most of the newly identified candidate star clusters and stellar groups appear compact with small angular sizes (few arcmin). It seems that almost all the candidates are very young, as most of the mass is still concentrated in the gas (Fig. 1, left). Indeed, the color-magnitude diagram of VVV-CL028 (Fig. 1, right) shows well populated Main Sequence and some stars with infrared excess.

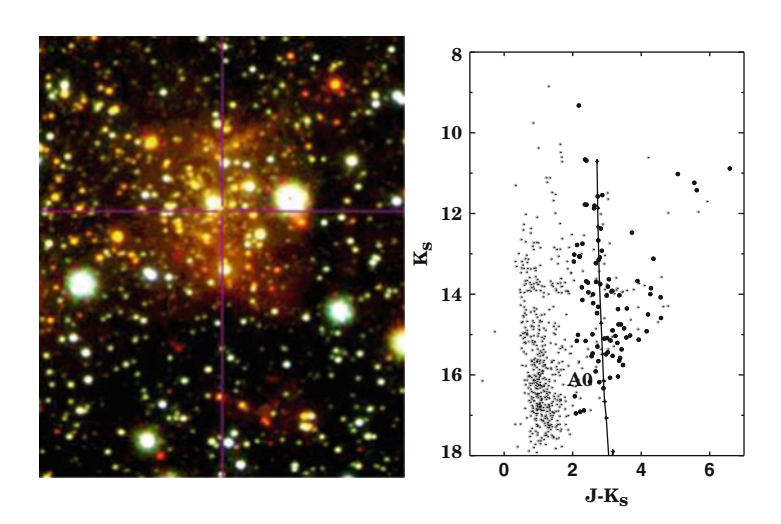


**Fig. 1** Left: The VVV composite J,H,Ks color image of VVV-CL028. The field of view is approximately 2.2 × 1.8 arcmin. Right: The Color-magnitude diagram of the cluster. The solid circles are for radius 0.6 arcmin around cluster center. The solid lines is [5] Main sequence

**Acknowledgements** JB is supported by FONDECYT No.1080086 and MIDEPLAN ICM Nucleus P07-021-F and received partial support from BASAL CATA PFB-06. The VVV Survey is supported by ESO, by BASAL Center for Astrophysics and Associated Technologies PFB-06, by FONDAP Center for Astrophysics 15010003, and by MIDEPLAN's Milky Way Millennium Nucleus P07-021-F. DM is supported by FONDECYT No. 1090213.

#### References

- 1. Churchwell, E., et al.: Astrophys. J. **649**, 759 (2006)
- 2. Churchwell, E., et al.: Astrophys. J. 670, 428 (2007)
- 3. Longmore, S.N., Burton, M.G.: Publ. Astron. Soc. Aust. 26, 439 (2009)
- 4. Minniti, D., et al.: New Astron. 15, 433 (2010)
- 5. Schmidt-Kaler, T., in Landolt-Börnstein, Group VI, Vol. 2b, Stars and Star Clusters, page 15 (editors: K. Schaifers; H. Voigt), Berlin: Springer-Verlag (1982)

# New Milky Way Star Cluster Candidates from DSS and 2MASS

Matthias Kronberger, Piet Reegen, Bruno Sampaio Alessi, Dana Patchick, and Philipp Teutsch

**Abstract** We present 27 open cluster candidates, including 24 previously unknown, that were found during an ongoing visual inspection of First and Second Generation Digitized Sky Survey (DSS) and Two Micron All Sky Survey (2MASS) images. Employing 2MASS and UKIDSS photometry, 10 of these candidates and three earlier published objects have physical parameters determined by isochrone fitting of their [J,J-H] and [J,J-K] colour-magnitude diagrams (CMDs) and [J-H, J-K] colour-colour diagrams. In order to decontaminate the cluster CMDs from stars belonging to the Milky Way fore- and background, a statistical approach is applied that determines the statistical significance of the density differences between the cluster CMD and the CMD of the Milky Way background. The studied clusters have ages ranging from a few Myr to  $\approx$ 1 Gyr, are only moderately reddened ( $E(B-V) \leq 1.1$ ) and are situated at distances between 0.95 and 5.5 kpc.

The availability of deep all-sky surveys in the visual and near infrared has lead to a renaissance of the search for new star clusters. Most of these efforts are based on automated methods that survey for overdensities in star density maps [1–4]. Quite obviously, such approaches are very efficient in detecting clusters with good contrast

M. Kronberger (⋈) CERN, 1211 Geneva 23, Switzerland,

Deepskyhunters Collaboration e-mail: matthias.kronberger@cern.ch

P. Reegen

Institute of Astronomy, University of Vienna, Türkenschanzstrasse 17, 1180 Vienna, Austria

Tricentis Technology and Consulting, Saturn Tower, Leonard-Bernstein-Strasse 10, 1220 Vienna, Austria

B.S. Alessi · D. Patchick · P. Teutsch Deepskyhunters Collaboration 106 M. Kronberger et al.

Table 1 List of open cluster candidates

ID	RA J2000		Size'	log(t)	E(B-V)	d (kpc)	Type <sup>b</sup>
Teutsch 175	01:11:22.0	+57:33:12	5.5	≤7.2	$0.60 \pm 0.40$	$0.95 \pm 0.15$	prob.
Teutsch 176	01:18:47.5	+59:26:38	1.3				poss.
Teutsch 177	01:43:43.5	+60:59:12	4.5	<b>≤</b> 7.5	$0.54 \pm 0.08$	$1.75 \pm 0.30$	poss.
Kronberger 88	01:52:33.0	+53:02:36	5.25	≥9	$0.32 \pm 0.09$	≥4	poss.
Kronberger 89	05:11:06.0	+28:07:24	2.5				poss.
Kronberger 90	05:37:56.0	+41:26:42	1.5				poss.
Teutsch 134	05:50:17.9	+28:10:27	1.5				emb.
Alessi 122	06:36:21.0	+10:54:19	1.75				emb.
Kronberger 91	06:44:23.5	+19:24:06	4.5				poss.
Kronberger 92	06:52:12.4	+02:13:21	1.75				emb.
Alessi 59 <sup>a</sup>	06:52:18.8	+02:11:27	2.5	<b>≤</b> 7.6	$0.59 \pm 0.05$	$3.50 \pm 0.30$	prob.
Teutsch 178	07:38:06.7	-21:33:48	2.0	$8.35\pm0.35$	$0.20 \pm 0.10$	$2.25\pm0.25$	poss.
Teutsch 179	07:45:30.3	-20:49:42	2.0				emb.
Teutsch 180	10:32:02.4	-57:00:18	3.5	$8.70 \pm 0.20$	$0.60 \pm 0.10$	$1.35 \pm 0.25$	poss.
Patchick 57	12:17:09.0	-62:57:24	3.5	$9.05 \pm 0.10$	$0.45\pm0.05$	$1.70 \pm 0.20$	prob.
Teutsch 181	15:54:45.0	-54:22:48	3.75	$8.80 \pm 0.15$	$0.75 \pm 0.05$	$0.98 \pm 0.07$	poss.
Teutsch 182	15:58:29.0	-53:39:18	3.75	$8.55 \pm 0.10$	$1.10 \pm 0.10$	$1.50 \pm 0.15$	prob.
Teutsch 183	18:26:57.7	-14:06:12	5.0	$8.80\pm0.05$	$0.59 \pm 0.06$	$2.65 \pm 0.10$	prob.
Kronberger 93	19:30:49.2	+18:59:21	0.5				emb.
Kronberger 94	19:31:08.8	+18:28:26	1.25				emb.
Kronberger 68 <sup>a</sup>	20:00:36.4	+30:35:23	2.25	$8.65\pm0.10$	$0.95 \pm 0.05$	$5.50 \pm 0.80$	prob.
Kronberger 95	21:18:01.5	+60:05:13	4.25				emb.
Teutsch 158	21:22:36.8	+56:03:16	1.3				poss.
Kronberger 96	22:16:29.6	+55:30:48	2.5	$9.05 \pm 0.05$	$0.80\pm0.06$	$5.00 \pm 0.10$	prob.
Kronberger 97	22:18:38.8	+56:10:57	2.0				emb.
Teutsch 127 <sup>a</sup>	22:18:59.3	+56:07:25	7.0	<b>≤</b> 6.8	$0.85\pm0.10$	$3.50 \pm 0.50$	prob.
Kronberger 98	22:29:08.9	+64:50:16	0.75				emb.
Kronberger 96 Kronberger 97 Teutsch 127 <sup>a</sup>	22:16:29.6 22:18:38.8 22:18:59.3 22:29:08.9	+55:30:48 +56:10:57 +56:07:25 +64:50:16	2.5 2.0 7.0 0.75	≤6.8			prob. emb. prob.

<sup>&</sup>lt;sup>a</sup>Previously classified as possible cluster candidate [5]

to the surrounding field. However, they may fail in finding clusters with a low star density relative to the Milky Way fore- and background, and clusters with only little coverage of their member stars in the underlying star catalogue.

Table 1 presents 27 objects that have been missed by recent open cluster surveys and thus, probably fall into these categories. 24 of them represent new open cluster candidates; the remaining three objects (Alessi 59, Teutsch 127 and Kronberger 68) were listed in an earlier publication [5] but had not been verified yet as open clusters. All objects were discovered in the course of an ongoing visual inspection of the Milky Way using DSS and 2MASS [6] images. Candidates bright enough to be studied with 2MASS or, if available, UKIDSS [7] photometry were analysed using [J,J-H] and [J,J-K] CMDs, [J-H,J-K] colour–colour diagrams, and Padova solar metallicity isochrones calculated for the JHK photometric bands [8]. The influence of pollution of the cluster CMDs by field stars was minimized by applying a statistical approach employing [J,J-H] and [J,J-K] Hess diagrams of the cluster

<sup>&</sup>lt;sup>b</sup>prob. probable cluster; poss. possible cluster; emb. probable embedded cluster

candidate and the surrounding Milky Way field. This approach is based on the assumption that the number of field stars in an infinitesimally small region of a CMD represents a Poisson distribution  $P_{\lambda}$ . If the cluster and field star densities  $\rho_C$  and  $\rho_F$  are now different from each other, the statistical significance of this difference can be retrieved by integrating the product  $P_{\lambda}(X=\rho_C)\times P_{\lambda}(X=\rho_F)$  over the characteristic parameter  $\lambda$ .

With this method, we could determine approximate ages, reddenings, and distances for 10 of the 27 probable or possible open cluster candidates. For another three candidates, at least some of these parameters could be retrieved. The remaining objects are either embedded clusters, or too faint to be studied with the available photometric data.

#### References

- 1. Ivanov, V.D., Borissova, J., et al.: Astron. Astrophys. 394, 1 (2002)
- 2. Froebrich, D., Scholz, A., Raftery, C.L.: Mon. Not. R. Astron. Soc. 374, 399 (2007)
- 3. Koposov, S.E., Glushkova, E.V., et al.: Astron. Astrophys. 486, 771 (2008)
- 4. Glushkova, E.V., Koposov, S.E., et al.: Astron. Lett. 36, 75 (2010)
- 5. Kronberger, M., Teutsch, P., et al.: Astron. Astrophys. 447, 921 (2006)
- 6. Skrutskie, M.F., Cutri, R.M., et al.: Astron. J. 131, 1163 (2006)
- 7. Lawrence, A., Warren, S.J., et al.: Mon. Not. R. Astron. Soc. 379, 1599 (2007)
- 8. Marigo, P., Girardi, L., et al.: Astron. Astrophys. 482, 883 (2008)

# VVV Study of the Young Milky Way Star Clusters: Mercer 35, 69 and 70

Radostin Kurtev, Jura Borissova, Charles Bonatto, Francisco Peñaloza, Valentin Ivanov, Étienne Artigau, Stuart Folkes, Douglas Geisler, Dante Minniti, Philip Lucas, and Stuart Sale

**Abstract** Young massive clusters are usually deeply embedded in dust and gas. They represent excellent astrophysical laboratories for revealing the enigma of star formation processes and the early stages of stellar evolution. Wide-field infrared surveys are a modern tool for studying hidden clusters. "Vista variables in Vía Láctea - VVV" (Minniti et al. New Astron. 15:433, 2010) is an ESO/Chile/VISTA public deep near-IR survey, covering the Galactic Bulge and Southern Galactic disk. This is the next step of our systematic study of the cluster content of the inner Milky Way. Here we present our first analysis of the young hidden clusters Mercer 35, 69 and 70. It is based on VVV and SOFI/NTT  $JHK_S$  photometry and follow-up NIR spectroscopy. All of the investigated clusters are young (t  $\leq$  10 Myr). The basic cluster parameters are obtained from photometry. The follow-up spectroscopy of probable cluster members shows that the brightest star in Mercer 35 presents characteristics of a red supergiant!

R. Kurtev (

) J. Borissova · F. Peñaloza · S. Folkes · S. Sale Universidad de Valparaíso, Gran Bretaña 1111, valparaiso, Chile e-mail: radostin.kurtev@uv.cl

Ch. Bonatto

Universidade Federal do Rio Grande do Sul, Porto Alegre, Brasil

V.D. Ivanov

European Southern Observatory, Chile

E. Artigau

Université de Montréal, Montréal, Canada

D. Geisler.

Universidad de Concepción, Chile

D. Minniti,

Pontificia Universidad Católica, Chile

P. Lucas

University of Hertfordshire, UK

A. Moitinho and J. Alves (eds.), *Star Clusters in the Era of Large Surveys*, Astrophysics and Space Science Proceedings, DOI 10.1007/978-3-642-22113-2\_16, © Springer-Verlag Berlin Heidelberg 2012

110 R. Kurtev et al

# 1 Introduction

Young massive clusters are usually deeply embedded in dust and gas. Some of them are "visible" only in the infrared domain. They also represent excellent astrophysical laboratories for the investigation of the most massive stars and of the early stages of stellar evolution. Wide-field infrared surveys are a modern tool for studying hidden clusters. "Vista variables in Vía Láctea – VVV" [4] is an ESO/Chile/VISTA public deep near-IR survey, covering the Galactic Bulge and Southern Galactic disk where the star formation activity is high. It will take 1,929 h over the next 5 years, covering around 10<sup>9</sup> point sources within an area of 520 sq deg and is well suited to finding and characterising such objects.

This is the next step of our systematic study of the cluster content of the inner Milky Way [1–3]. Here we present our first analysis of the young hidden clusters Mercer 35, 69 and 70. It is based on VVV and SOFI/NTT  $JHK_S$  photometry and follow-up NIR spectroscopy. Our results from the photometry are summarized in Table 1 and Fig. 1a, and from the spectroscopy in Fig. 1b.

#### 2 Results

All of the investigated clusters are young ( $t < 10 \,\mathrm{Myr}$ ).

The follow-up spectroscopy of some of the brightest probable cluster members shows characteristics of supergiant stars. In the Milky Way there are two known massive clusters in the red supergiant (RSG) phase. It is possible that a cluster once thought to be of relatively low mass can turn out to be quite massive on further inspection. Perhaps there are more massive clusters amongst the many clusters that have already been identified (Fig. 1b).

**Table 1** The results of  $JHK_S$  photometry of the target clusters. All distances assume  $R_0 = 8.00 \,\mathrm{kpc}$ 

Mercer 35	Mercer 69	Mercer 70
$E(J - K_S) = 2.4 \pm 0.1$	$E(J - K_S) = 1.5 \pm 0.1$	$E(J - K_S) = 2.0 \pm 0.1$
$A_V(\text{mag}) = 15.1 \pm 0.5$	$A_V(\text{mag}) = 9.5 \pm 0.5$	$A_V(\text{mag}) = 12.8 \pm 0.5$
$(m-M)_0 = 14.0 \pm 0.5$	$(m-M)_0 = 13.4 \pm 0.5$	$(m-M)_0 = 13.0 \pm 0.5$
$dSun(kpc) = 6.3 \pm 1.5$	$dSun(kpc) = 4.9 \pm 1.2$	$dSun(kpc) = 4.0 \pm 1.0$
$dGC(kpc) = 6.8 \pm 1.1$	$dGC(kpc) = 4.5 \pm 0.9$	$dGC(kpc) = 5.0 \pm 0.8$
$x(kpc) = -4.4 \pm 0.9$	$x(kpc) = -3.8 \pm 1.0$	$x(\text{kpc}) = -4.5 \pm 0.8$
$y(kpc) = -5.2 \pm 1.2$	$y(kpc) = -2.5 \pm 0.6$	$y(kpc) = -2.0 \pm 0.5$
$z(pc) = 9 \pm 2$	$z(pc) = 41 \pm 10$	$z(pc) = 40 \pm 10$

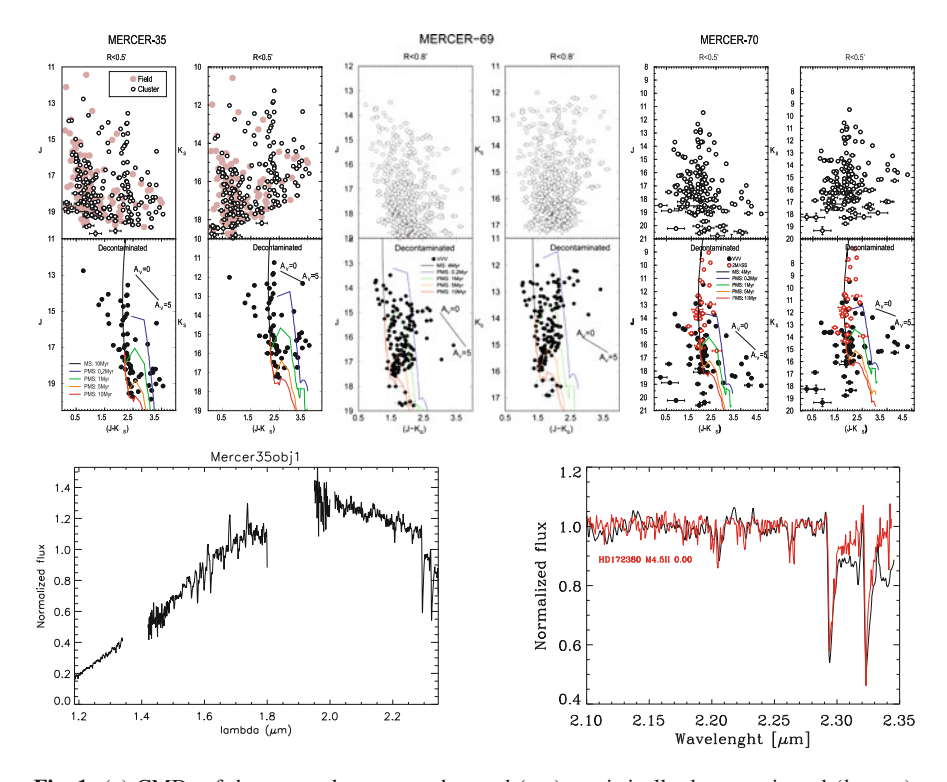


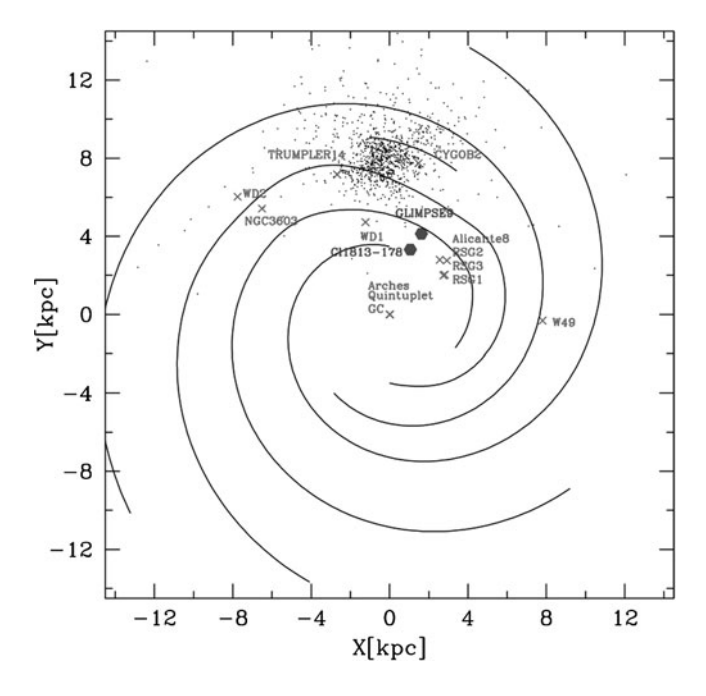
**Fig. 1** (a) CMDs of the target clusters: as observed (*top*), statistically decontaminated (*bottom*). (b) The brightest star of the cluster Mercer 35 shows a typical red supergiant spectrum. The best match is the M4.5 II star HD172380. Spectra obtained with OSIRIS IR camera, SOAR telescope

Acknowledgements RK acknowledges support from Cento de Astrofísica de Valparaíso DIPUV CID03/2006. SF acknowledges funding support from the ESO-Government of Chile Mixed Committee 2009, and from GEMINI Conicyt grant No. 32090014/2009. JB and SS are supported by MIDEPLAN ICM Nucleus P07-021-F. JB acknowledges support from FONDECYT No.1080086.

# References

- 1. Borissova, J., Pessev, P., Ivanov, V.D., et al.: Astron. Astrophys. 411, 83 (2003)
- 2. Ivanov, V.D., Borissova, J., Pessev, P., et al.: Astron. Astrophys. 349, 1 (2002)
- 3. Kurtev, R., Borissova, J., Georgiev, L., et al.: Astron. Astrophys. 475, 209 (2007)
- 4. Minniti, D., et al.: New Astron. 15, 433 (2010)

# Part II Star Formation & Evolution. The Milky Way and Beyond



Galactic distribution of young very massive clusters. From M. Messineo et al., this volume.

# **Optical Surveys of Young Open Clusters**

Estelle Moraux and Jerôme Bouvier

**Abstract** Wide field optical surveys have been proved to be a key tool to study the population of young open clusters. The avent of very large optical CCD cameras over the past 10 years allowed to obtain a complete census of the stellar population in clusters down to the substellar limit. The high efficiency of the cameras combined to their large FOV enable the survey of several hundreds to thousands cluster members in a limited amount of time, allowing in addition the study of their proper motion and variability.

In this contribution I first present recent results on the low mass part of the mass function in open clusters, and discuss whether it depends on local conditions and how it evolves with age. In a second part, I present results obtained by the Monitor project, an unprecedented large scale, high cadence, photometric monitoring survey of young open clusters ideally suited to measure stellar rotation periods and constrain angular momentum evolution models.

### 1 Introduction

A fairly large number of wide-field optical CCD-mosaic cameras have been available to the astronomical community during the last decade. The largest one so far is MegaCam at CFHT with a field of view of  $1\times1$  deg. It consists of  $36\ 2\times4$  K CCDs with a pixel scale of only 0.187"/pixel. Other cameras are about 4 times smaller with a FOV of about 30'  $\times$  30'. For example, there is SuprimeCam on the 8 m class telescope Subaru (34'  $\times$  27', 10 CCD, 0.20"/pixel) or the Mosaic camera on 4 m class telescopes (Mosaic I at NOAO/KPNO and Mosaic II at CTIO/Blanco; 36'  $\times$  36', 8 CCD, 0.26"/pixel). Other wide-field cameras are also available on 2 m

Laboratoire d'Astrophysique de Grenoble, Université Joseph Fourier - CNRS, Grenoble, France e-mail: emoraux@obs.ujf-grenoble.fr

E. Moraux (⋈) · J. Bouvier

116 E. Moraux and J. Bouvier

class telescope (e.g. on the INT/WFC), and of course there is VST at ESO that should be available soon.

Thanks to their very large field of view, these optical cameras are ideal to study nearby open clusters – with little extinction – as it is possible to cover them within a few pointings. A complete census of the cluster population from the stellar domain down to substellar masses (to a few tenths of Jupiter masses) is doable in a relatively small amount of observing time, enabling the study of the mass function in various environments. Moreover the large field of view combined to the camera high efficiency allow to investigate the variability of cluster members to measure rotation periods to constrain the angular momentum evolution, to search for eclipsing binaries to constrain evolutionary models, to look for planetary transits around young stars.

In this contribution, I will highlight some results obtained by our group concerning (1) the mass function of young open clusters that have been derived using wide-field optical cameras (Sect. 2), and (2) the angular momentum evolution of low mass stars focusing especially on the Monitor project (Sect. 3).

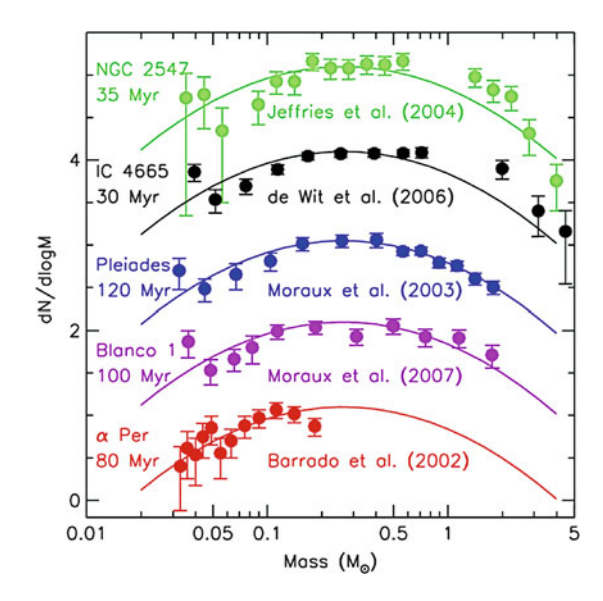
# 2 The Mass Function of Young Open Clusters

# 2.1 A Universal Mass Function for Open Clusters?

Rich and nearby young (10-100 Myr) open clusters are ideal environments to estimate robust mass functions over a wide mass range, from the substellar domain up to massive stars, as most of the sources of uncertainties are reduced. Their youth ensures that brown dwarfs are still bright enough for being easily detected in the optical and a complete census of the cluster population is achievable with the current wide-field cameras thanks to their richness and relative compactness on the sky. After a first phase of photometric selection, bona fide cluster members can be distinguished from interloping field dwarfs using spectroscopic diagnostics of youth, such as lithium or gravity sensitive features. The common proper motion shared by all the cluster's members – a property specific to nearby open clusters – also offers an additional and very powerful criterion to build large samples of confirmed cluster members. Then, masses can be determined relatively easily as cluster members constitute an homogeneous population, at the contrary of the star forming region and galactic field population. Extinction is most often insignificant and scatter in the intrinsic properties (age, distance, metallicity) minimal - nearby cluster age and distance are usually known to better than 20% and sometimes to within a few percent. Cluster member masses can thus be derived converting their luminosity with the help of a unique mass-luminosity relationship delivered by evolutionary models, that are also better constrained and less uncertain for ages > 10 Myr.

Large and unbiased samples of low mass cluster members have been unearthed during the last decade, from which *system* (i.e. not corrected from binarity) present

Fig. 1 The system mass function of young open clusters from low mass brown dwarfs to massive stars, i.e. from  $30M_{Jup}$  to  $3 \, {\rm M_{\odot}}$ . Each cluster MF is fitted by the same log-normal distribution



day mass functions (PDMF) have been derived. Figure 1 show the results obtained for some clusters with an age between 30 to 120 Myr. From 30 Jupiter masses to a few solar masses, the cluster PDMF are all reasonably well fitted by the *same* Scalo-like log-normal distribution

$$\xi_{\rm L}(m) = \frac{dn}{d\log m} \propto \exp\left[-\frac{(\log m - \log m_0)^2}{2\sigma^2}\right],$$

with  $m_0 = 0.25\,\mathrm{M}_\odot$  corresponding to the peak of the distribution and  $\sigma = 0.52$  representing its width. The fact that there is very little evidence for cluster to cluster variation suggests that the cluster MF does not depend much on environmental conditions such as density or turbulence, pointing towards a *universal* initial mass function for open clusters. Moreover, the galactic disk mass function is also very similar ( $m_0 \sim 0.25\,\mathrm{M}_\odot$ ,  $\sigma \sim 0.55$ ; [4]) which is in favour of this argument as the field population consists in majority of stars that were born in cluster or association.

# 2.2 The Dynamical Evolution of Open Clusters

As a cluster evolves, dynamical processes act to deplete its lowest mass members. How the cluster's PDMF relates to the initial mass function is then a matter of concern. It is therefore necessary to investigate the effect of the cluster dynamical evolution on the shape of the mass function. For clusters younger than  $\sim \! 100 \, \mathrm{Myr}$  (or a few crossing times), the fact that all the cluster's PDMF and the field mass function are similar indicate that this effect is negligible, at least in the mass range

118 E. Moraux and J. Bouvier

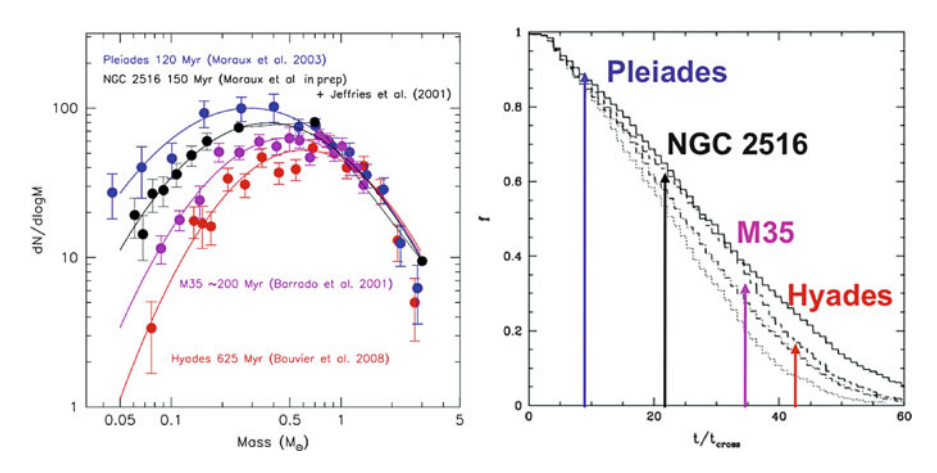


Fig. 2 Left: NGC 2516 ( $\sim$ 150 Myr), M35 ( $\sim$ 200 Myr) and Hyades (625 Myr) PDMF compared to the Pleiades one (120 Myr). The mass functions have been normalized at  $\sim 1 \, {\rm M}_{\odot}$ . Right: Fraction of brown dwarfs remaining in the cluster as a function of crossing time (from [1])

 $0.03-3\,M_{\odot}$ . The shape of the mass function of star forming regions in this mass domain is also consistent with what is found for open clusters, supporting this argument.

For older clusters, we then compared their PDMF to the Pleiades one, taken as the reference (see Fig. 2, left panel). We can clearly see that the mass function is depleted with age at low masses while it does not change for masses larger than  $\sim 0.8 \, M_{\odot}$  and for ages  $\leq 600 \, \text{Myr}$ , which is consistent with the predictions of dynamical evolution models (e.g. [1]; Fig. 2, right panel). We find that the cluster's mass functions can still be fitted by a log-normal distribution but with a peak mass  $m_0$  that increases with age and a decreasing width  $\sigma$  (see also [6]).

We should emphasize that the pertinent parameter to consider for dynamical evolution is not just the absolute age of the cluster but its age relative to its crossing time  $t_{cross}$ . For denser clusters for example, the crossing time is smaller leading to faster evolution. Thus even young ( $\sim 10\,\mathrm{Myr}$ ) clusters can present a deficit of brown dwarfs and low mass stars if they are/were dense. This idea has been developed by [15] who suggested that the peculiar mass function (no objects below 0.1  $\mathrm{M}_{\odot}$ ) and binary properties (no binary with separation larger than 30–50 AU) of the young ( $\sim 9\,\mathrm{Myr}$ ) association  $\eta$ -Cha can be explained by dynamical evolution despite its young age if the initial cluster's configuration was very compact.

#### 2.3 Kinematic Studies

In order to estimate the crossing time ( $t_{cross} = 2R_{\nu}/\sigma_{\nu}$ ) of a cluster and constrain its dynamical state, we need to measure the velocity dispersion of the cluster members as a function of mass with an accuracy better than 1 km/s. This is now becoming possible with proper motion studies using deep wide field optical cluster surveys

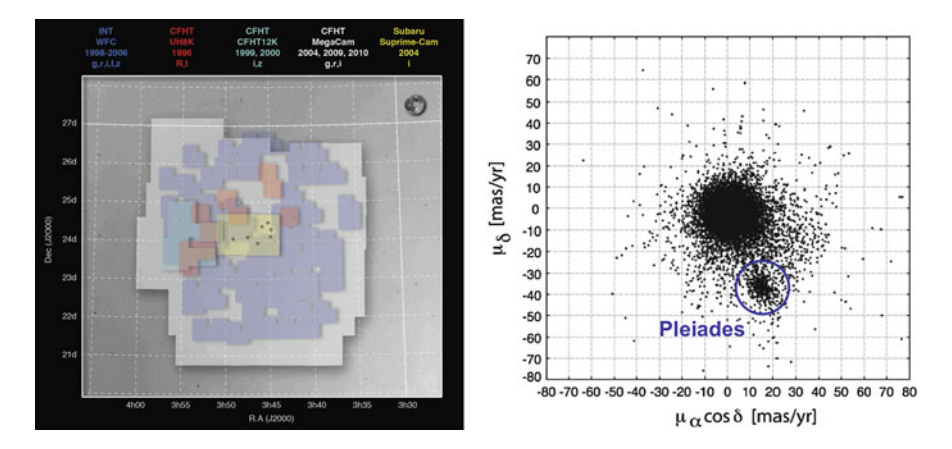


Fig. 3 Left: Coverage of the optical surveys that have been performed in the Pleiades. Right: Preliminary proper motion diagram obtained for the Pleiades. The cluster locus appear clearly around (15,-35) mas/yr. Observations from 3 observatories (CFHT, INT, Subaru) and 5 instruments covering a period of 12 years were used. The final accuracy is better than  $\sim$ 1 mas/yr for bright sources. A total of 520Gb of data was used to build this diagram

that have been performed in the early 2000 as a first epoch. A number of nearby clusters have indeed mean transverse motions of a few tens of mas/yr (e.g. Pleiades, Hyades, Taurus), making it possible to measure their members' motion with an accuracy better than 1 mas/yr (corresponding to 1 km/s at 200 pc) over  $\sim$ 10 years. Proper motion studies are in addition a very powerful tool to distinguish cluster members and in particular to look for objects that have been lost by the cluster due to secular dynamical evolution.

In 2009 and 2010, we observed the Pleiades cluster using MegaCam at CFHT in order to obtain a new epoch for the INT/WFC, CFHT-8K and CFH12K, and Subaru/SuprimeCam data available from the archives. Despite using multi-instrument and multi-wavelength datasets, our preliminary proper motion analysis indicates that with a time baseline of 8–10 years we can reach an unprecedented accuracy, better than 1 mas/yr (< 0.6 km/s at 120 pc) using E. Bertin's AstrOmatic softwares (see Fig. 3) down to i' 23.5.

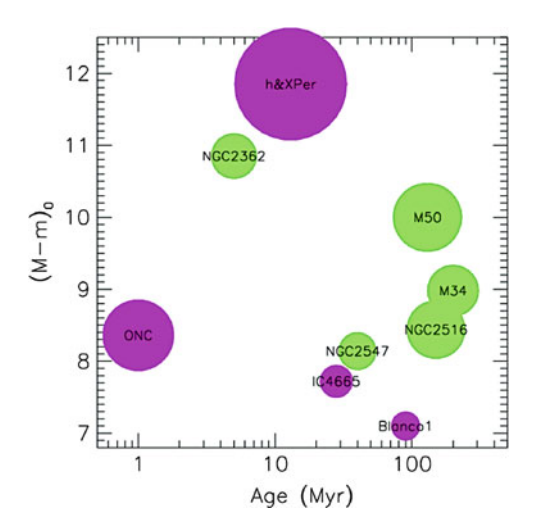
# 3 Stellar Variability

# 3.1 The Monitor Project

Monitor is a large scale monitoring survey of nine young (1–200 Myr) nearby open clusters (see Fig. 4) using worldwide 2–4 m class optical telescopes that started in 2005. Its primary goal is to search for eclipses by very low mass stars, brown dwarfs or planets in the light curves of the lowest mass cluster members (see [2]) and to

120 E. Moraux and J. Bouvier

Fig. 4 Distribution in distance and age of the 9 target clusters. The size of the *circle* representing each cluster scales with the number of monitored cluster members. The color-coding indicates whether we have completed the analysis (*green*) of the rotational periods of the cluster or not (*magenta*)



constrain formation and early evolution models for these objects. The data are also ideally suited to the study of angular momentum evolution in low mass stars, as well as other forms of variability associated with flaring or time-variable accretion.

The large field of view and high efficiency of optical cameras allowed us to monitor several hundreds of low mass stars in each cluster with a time sampling better than 5 min over a few weeks. The light curve analysis revealed periodic modulation due to the presence of cold spots at the surface of the stars and we were able to measure hundreds of rotational periods between 0.2 and 20 days in NGC 2362, NGC 2547, M50, NGC 2516 and M34 [9–12] and [14]. This unprecedented sample combined to other rotational studies from the literature (e.g. ONC, [8]; NGC 2264, [5]; Pleiades, [7]) is bringing strong constraints on angular momentum evolution models and on star-disk interaction (see e.g. [3, 13]). Data around 10–20 Myr are still needed however to better constrain the PMS spin-up models and the disk dissipation timescale.

# 3.2 h & x Persei

The double cluster h &  $\chi$  Persei with an age of 13 Myr is the ideal target for this purpose. Being very rich and compact, we can monitor >10,000 stellar members with a mass between 0.3 and  $1.4\,\mathrm{M}_\odot$  in one MegaCam FOV. This cluster is thus also a very promising target to look for eclipsing binaries since we expect to discover a few tenths of them.

During a first monitoring campaign in Sept.–Oct. 2008 focussing on h Per, we observed this cluster using the 1.5 m telescope at Maidanak (Uzbekistan), 2.6 m at Byurakan (Armenia) and CrAO (Crimea) for a total of >100 h per blocks of 2 h spread randomly over 2 months.

Among about 10,000 h Per photometric candidate members identified from colour-magnitude diagrams, we selected 2287 with light curves containing more than 800 measurements (and up to 986) from CFHT and Maidanak. We chose to perform the period analysis combining only the CFHT and Maidanak datasets, which have the lowest errors and very similar sampling, while the CrAO and Buyrakan datasets, of lower quality, were used to check the reliability of the detected periods.

Periodic signals were searched in the light curves using 3 methods: Lomb-Scargle periodogram, CLEAN-DFT and String-Length (SL). In all cases, we probed a range of periods from 0.2 to 20 days. The phase diagrams were visualized to decide on the reliability of the derived period and, in case the results were discrepant, to decide on the correct period if any. CLEAN proved very reliable to detect the periods of sinusoidal-like light curves, while SL was sometimes, though rarely, found superior for non sinusoidal signals (e.g double-spotted light curves). From the visual inspection of the phase diagrams, we classified 430 objects as clearly periodic and 155 as possibly periodic. The period distribution as a function of mass is shown on Fig. 5 (left panel).

This period sample at an age of 13 Myr combined to previous results at different ages yields a complete view of the rotational history and evolution of low mass stars and brings strong constraints on angular momentum evolution models (see Fig. 5, right panel). In particular, it is found that a weak coupling between the core and the envelope is necessary to reproduce the slow rotators for solar type stars [13]. This results in a strong shear across the radiative/convective boundary while the rapid

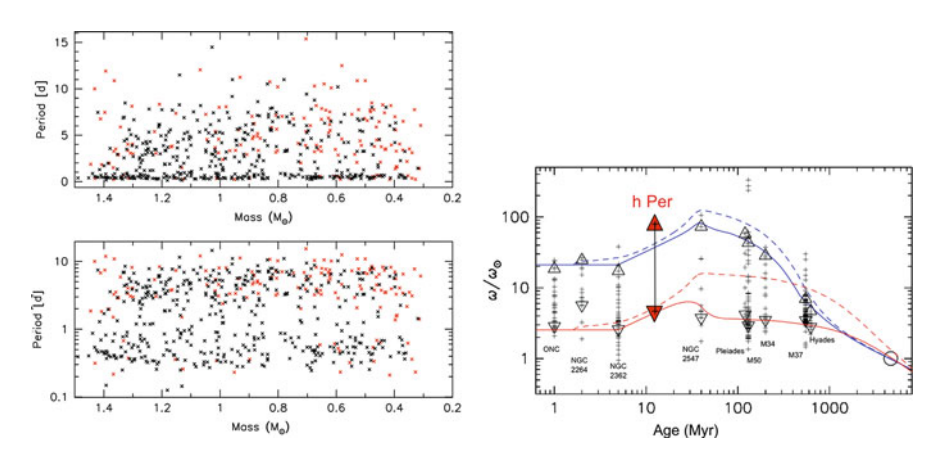


Fig. 5 Left: Periods detected for h Per candidate members as a function of mass (black: robust periods, red: possible periods). Periods are plotted on a linear scale in the upper panel, on a log scale in the lower one. Right: Rotational angular velocity  $\omega$  plotted as a function of time for stars with masses  $0.9 < M/M_{\odot} < 1.1$ . Inverted and direct triangles show the 25th and 90th percentiles of  $\omega$ , used to characterize the slow and fast rotators respectively. Solid lines: modeled evolution of surface rotation for slow (red) and fast (blue) rotators. Dashed lines: rotation of the radiative core. A disk lifetime of 5 Myr is assumed for both models

122 E. Moraux and J. Bouvier

rotators behave more like solid bodies, which may have some impact on lithium depletion and explain the observed scatter of lithium abundance in main sequence solar-type stars [3].

# 4 Summary

To summarize, optical wide-field surveys of young open clusters have unearthed large homogeneous sample of cluster members with the same and precise age, distance and metallicity. This allowed robust estimates of cluster present day mass function from the stellar domain down to  $\sim 30 M_{Jup}$ . Results seem to suggest that there is a *universal* IMF for open clusters that is well represented by a lognormal distribution with  $m_0 \sim 0.25\,\mathrm{M}_\odot$  and  $\sigma \sim 0.52$ , and that these parameters are evolving to larger  $m_0$  and smaller  $\sigma$  when the cluster evolves dynamically resulting in a depletion of brown dwarfs and low mass stars for ages larger than  $\sim 10 t_{cross}$ . High precision proper motion studies are now becoming possible thanks to the large time baseline ( $\sim 10\,\mathrm{years}$ ) with available from the archives, which allow to investigate the kinematics structure of open clusters in preparation to Gaia. Finally, variability studies of cluster members have yielded an unprecedented large number of rotation periods (often as a byproduct of transit search) leading to new important constraints on angular momentum evolution models.

These optical surveys are now being nicely complemented by near-infrared surveys in order to look for planetary mass objects in cluster and estimate the IMF down to a few Jupiter masses, as well as to study the circumstellar disk variability.

#### References

- 1. Adams, T., Davies, M.B., Jameson, R.F., Scally, A.: Mon. Not. R. Astron. Soc. 333, 547 (2002)
- Aigrain, S., Hodgkin, S., Irwin, J., Hebb, L., Irwin, M., Favata, F., Moraux, E., Pont, F.: Mon. Not. R. Astron. Soc. 375, 29 (2007)
- 3. Bouvier, J.: Astron. Astrophys. 489, L53 (2008)
- 4. Chabrier, G.: Publ. Astron. Soc. Pac. 115, 763 (2003)
- 5. Dahm, S.E., Simon, T.: Astron. J. 129, 829 (2005)
- 6. De Marchi, G., Paresce, F., Portegies Zwart, S.: Astrophys. J. 718, 105 (2010)
- 7. Hartman, J. D., Bakos, G. Á., Kovács, G., Noyes, R.W.: Mon. Not. R. Astron. Soc. **408**, 475 (2010)
- 8. Herbst, W., Bailer-Jones, C.A.L., Mundt, R., Meisenheimer, K., Wackermann, R.: Astron. Astrophys. 396, 513 (2002)
- Irwin, J., Aigrain, S., Hodgkin, S., Irwin, M., Bouvier, J., Clarke, C., Hebb, L., Moraux, E.: Mon. Not. R. Astron. Soc. 370, 954 (2006)
- Irwin, J., Hodgkin, S., Aigrain, S., Hebb, L., Bouvier, J., Clarke, C., Moraux, E., Bramich, D.M.: Mon. Not. R. Astron. Soc. 377, 741 (2007)
- Irwin, J., Hodgkin, S., Aigrain, S., Bouvier, J., Hebb, L., Moraux, E.: Mon. Not. R. Astron. Soc. 383, 1588 (2008)

- Irwin, J., Hodgkin, S., Aigrain, S., Bouvier, J., Hebb, L., Irwin, M., Moraux, E., Mon. Not. R. Astron. Soc. 384, 675 (2008)
- 13. Irwin, J., Bouvier, J.: IAU Symp. 258, 363 (2009)
- Irwin, J., Aigrain, S., Bouvier, J., Hebb, L., Hodgkin, S., Irwin, M., Moraux, E.: Mon. Not. R. Astron. Soc. 392, 1456 (2009)
- 15. Moraux, E., Lawson, W.A., Clarke, C.: Astron. Astrophys. 473, 163 (2007)



Maria Messineo starts a general discussion

E. Moraux and J. Bouvier



Jerôme Bouvier makes a point



Hans Zinnecker has a question

# Probing the Low-Mass End of the IMF in Star-Forming Regions: A WIRCam/CFHT Survey

Catarina Alves de Oliveira, Estelle Moraux, Jerôme Bouvier, Andrew Burgess, Hervé Bouy, Chiara Marmo, and Patrick Hudelot

**Abstract** One of the most attempted goals of star formation theories is to determine the dominant process by which brown dwarfs form and the implications of the environment on its outcome. Current theories must be able to reproduce not only the observed shape of the IMF, but predict observable properties of clusters such as multiplicity, mass segregation, frequency and sizes of discs, accretion, etc. The new observational frontier is therefore the detection and characterization of very low mass objects in star forming regions, to confront model predictions from numerical simulations of the collapse of molecular clouds to the observed properties of YSOs. This is the main driver behind a WIRCam large program that has been conducted at CFHT to detect BD with masses between 1 and 30 Jupiter masses in a sample of 6 young clusters. I will present the main results obtained so far for the  $\rho$  Ophiuchi molecular cloud and IC 348, where a spectroscopic follow-up of many of these candidates is being conducted using several facilities (TNG, GTC, NTT, VLT, Gemini) to ascertain their spectral types and masses, and ultimately, to construct the low-mass end of the IMF for those star forming regions.

# 1 Introduction

Although there is a generally accepted theory on how a star forms through the collapse of a molecular cloud core and contracts to the main-sequence [12, 24], two major breakthroughs in the mid-1990s have added a new complexity to the star

C.A. de Oliveira (⋈) · E. Moraux · J. Bouvier · A. Burgess

Laboratoire d'Astrophysique de Grenoble, Observatoire de Grenoble, BP 53, 38041 Grenoble Cedex 9, France

e-mail: Catarina.Oliveira@obs.ujf-grenoble.fr

H Bouy

CAB-LAEFF, Apartado 78, E-28691 Villanueva de la Caada, Madrid, Spain

C. Marmo · P. Hudelot

Institut d'Astrophysique de Paris, 98bis Bd Arago, 75014 Paris, France

A. Moitinho and J. Alves (eds.), *Star Clusters in the Era of Large Surveys*, Astrophysics and Space Science Proceedings, DOI 10.1007/978-3-642-22113-2\_18, © Springer-Verlag Berlin Heidelberg 2012

formation field: the discovery of exoplanets [16,20] and brown dwarfs (BDs, M<75 MJup, [7,19,22]). As brown dwarfs have masses bridging the lowest mass hydrogenburning stars and giant planets, any picture of star and planet formation has to account for them. Their discovery has lead to several formation scenarios: turbulent fragmentation of molecular clouds into very low mass cores [9, 21], collapse and fragmentation of more massive pre-stellar cores, gravitational instabilities in discs [25], premature ejection from pre-stellar cores [23], and photo-erosion of cores [11]. Most theoretical models predict that the formation of brown dwarfs should depend on parameters such as local cloud density, temperature and magnetic field. Yet, observational results so far suggest that the lower IMF, i.e., the ratio of BDs to stars, is fairly independent of local conditions [2, 18]. It is also quite unclear whether these formation scenarios can be extrapolated down into the planetary mass regime  $(M<13M_{Jup})$  [5] or whether isolated planetary mass objects may have other formation channels. This problematic is the main driver behind an on-going large program using the Wide Field IR Camera (WIRCam) at the Canada France Hawaii Telescope (CFHT), originally designed to fully characterize a series of young stellar clusters chosen to represent different environments, and detect brown dwarfs down to a few Jupiter masses.

# 2 The WIRCam/CFHT Survey of Nearby Star-Forming Regions

Using the WIRCam at the CFHT telescope, we conducted a deep near-IR survey of the following nearby star-forming regions: ρ Ophiuchi, IC348, NGC 1333, Serpens, NGC 2264, and λ Ori. The WIRCam is a wide-field camera operating in the near-IR, consisting of four 2048×2048 array detectors, and with a pixel scale of 0.3". The four detectors make a total field of view of approximately 21' in one pointing. All clusters mentioned above were observed in the Y, J, H, and  $K_s$  filters, while IC348 was also observed with two narrowband methane filters,  $CH_4$ -off and  $CH_4$ -on. Depending on the area each cluster occupies on sky, between one and seven pointings were needed to map the entire region. All images were reduced in an analogous way. First, the individual images are processed by the 'I'iwi reductions pipeline at the CFHT, which includes detrending (e.g. bias subtraction, flat-fielding, non-linearity correction, cross-talk removal), sky subtraction, and astrometric calibration. The more detailed reduction is then handled by Terapix [15], the data reduction centre at the *Institut d'Astrophysique de Paris* (France) responsible for carrying out the final quality assessment of the individual images, determining precise astrometric and photometric calibrations, and produce the final stacked images by combining the dither and individual exposures. The photometric calibration of the WIRCam data is done with 2MASS stars in the observed frames as part of the nominal pipeline reduction. To extract the photometric catalogues, we used PSFEx (PSF Extractor), a software tool that computes a PSF model from

well-defined stellar profiles in the image, and the SExtractor programme [4] to compute the photometry for each detected object. Candidates brown dwarfs are then chosen by comparing their colours to those predicted by the evolutionary models from the Lyon group [3, 4], and to previously confirmed members of each cluster. We also make extensive use of multi-wavelength archive data for characterization of the candidates, from the optical (using, for example, Subaru archival images) to the mid-IR using the various public surveys from the *Spitzer* Space Telescope.

# 3 Selection of Results

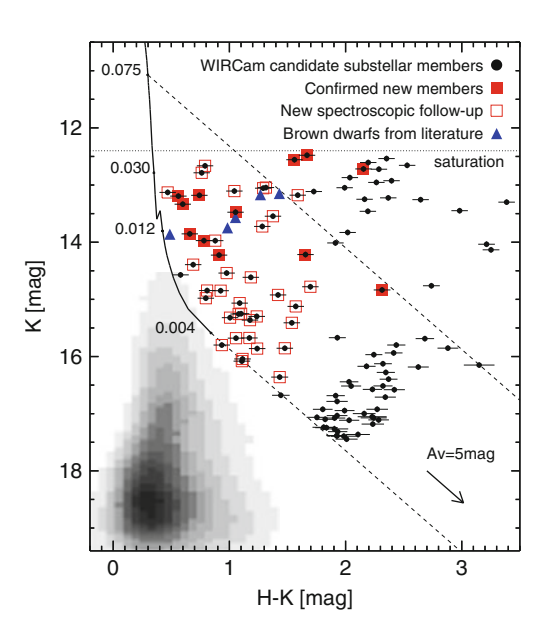
In this section, we will present a selection of results for the young clusters which were firstly studied, the  $\rho$  Ophiuchi cluster [1] and IC 348 [6].

# 3.1 The \( \rho \) Ophiuchi Cluster

The  $\rho$  Ophiuchi cluster is one of the youngest (~1 Myr) and closest star-forming regions (120–145 pc, [13, 14]), with an estimated population of ~300 members [26]. The high visual extinction in the clouds core, with  $A_V$  up to 50–100 mag, make it one of the most challenging regions to study low-mass young stellar objects and before our survey, only 15 brown dwarfs are known in this cluster. With the WIRCam survey, we covered the entire core of the cluster in a total area of ~0.7 deg² down to a completeness limit of J~20.5 and H~K~19.0. According to models, this allows us to detect young objects down to 3  $M_{Jup}$  through 10 mag of  $A_V$ . The final photometric catalogue contains approximately 57,000 objects.

Using the Lyon group models [3,4], we select candidate members if their colours fell redward from the model isochrones in the J vs. J-H, J vs. J- $K_s$ , and  $K_s$  vs. H- $K_s$  colour-magnitude diagrams. From these, only objects that had colours consistent with them being young and substellar in the J-H vs.  $H-K_s$  colour–colour diagram are kept. After removing previously known members from the list, we find 110 substellar candidates, 80 of each had not previously been associated with the cloud. By extensive use of archive multi-wavelength data, we find evidence of mid-IR excess for 27% of the candidates and a variability behaviour consistent with that of YSOs for 15%. To confirm their youth and hence membership, we carried out a pilot spectroscopic follow-up using SofI/NTT and NICS/TNG to acquire low-resolution near-IR spectra. We identify six new brown dwarfs with spectral types ranging from  $\sim$ M6.5 to  $\sim$ M8.25. We also confirm the previously derived spectral type for a very low-mass star close to the substellar limit, and based on the SED constructed from optical to mid-IR photometry, we report the discovery of a candidate edge-on disc around this star. Preliminary results of recent spectroscopic observations using ISAAC/VLT, indicate the discovery of 15 additional brown dwarfs. These include a candidate L0, which according to the models should be close to the deuterium 128 C.A. de Oliveira et al.

Fig. 1 WIRCam/CFHT colour-magnitude diagram for  $\rho$  Oph. Black dots are the candidate members selected from near-IR photometry and squares show the ones followed-up spectroscopically. Triangles show the previously known brown dwarfs within out magnitude limits. The solid line represents the DUSTY 1 Myr isochrone labelled with Solar mass, and the dashed lines the  $\sim$ 75 MJup limit, with increasing amount of visual extinction



burning limit. In an unrelated study, two candidate brown dwarfs from our study have also been confirmed has substellar members [17]. In total,  $\sim$ 23 new brown dwarfs are found in this cluster with our survey, more than doubling the number of previously known substellar members (Fig. 1).

# 3.2 IC 348

The IC 348 young cluster is located at a distance of 300 pc [10] and has an estimated age of 3 Myr. About 360 stellar members are known to date, and assuming a lognormal IMF [8], we thus estimate that this young stellar cluster should host at least 60 members in the substellar regime, double the number of BDs identified so far in this cluster. In fact, a scarcity of brown dwarfs has been claimed to exist in IC 348 in comparison to other star forming regions (e.g. Orion). However, there are several indications that the census of the cluster substellar population is far from complete.

One of the most exciting results from the WIRCam survey, is indeed the discovery of 3 T-dwarf candidates in this cluster, using the deep methane images. After thoroughly analysis of all colour/colour and colour/magnitude diagram analysis, including available optical deep images, two candidates have been rejected for being too bright at optical wavelengths. One good candidate remains though, with an estimated spectral type of T6. Theoretical models suggest a mass of a few  $M_{Jup}$  for this object at 3 Myr. Its methane colours, luminosity, significant extinction and spatial location, are consistent with it being a member of IC 348. With just a few Jupiter masses, this young T-dwarf candidate is one of the youngest, lowest mass

objects found so far in a star-forming region. Furthermore, we find that its frequency is consistent with the extrapolation of current lognormal IMF estimates down to the planetary mass domain.

Using the near-IR imaging data for this cluster, we try to uncover the remaining substellar population. We identified 20 substellar candidates which will be followed-up this Fall with two spectroscopic runs using Osiris/GTC and NIRI/Gemini. The WIRCam study improves upon previous surveys by probing a larger area at an increased sensitivity which we hope will allow us to derive a complete census of the BD population down to  $\sim 7 M_{Jup}$  over a cluster halo with a radius of 17°, corresponding to the largest unclipped radius permitted by our survey.

#### 4 Final Remarks

The first results from our WIRCam/CFHT survey of nearby star-forming regions, demonstrate the success of deep near-IR surveys in uncovering young brown dwarfs down to the planetary regime. The confirmation of the photometric candidates relies, however, on extensive spectroscopic follow-up runs on 8-m class telescopes. These studies reflect a clear need for a multi-object near-IR spectrograph to the European community.

Finally, the scientific return of this large survey will be further expanded with upcoming studies of outflows and discs on the newly found brown dwarf populations, which will provide important constraints to the current brown dwarf formation theories.

**Acknowledgements** We thank Loic Albert and Emmanuel Bertin, for their help with the observations and data reduction of the data for this WIRCam survey. Research supported by the Marie Curie Research Training Network CONSTELLATION under grant no. MRTN-CT-2006-035890.

#### References

- 1. Alves de Oliveira, C., Moraux, E., Bouvier, J., Bouy, H., Marmo, C., Albert, L.: Astron. Astrophys. **515**, 75 (2010)
- 2. Andersen, M., Meyer, M., Greissl, J., Aversa, A.: Astrophys. J. **683**, L183 (2008)
- 3. Baraffe, I., Chabrier, G., Allard, F., Hauschildt, P.: Astron. Astrophys. 337, 403 (1998)
- 4. Bertin, E., Arnouts, S.: Astron. Astrophys. Suppl. 117, 393 (1996)
- 5. Boyd, D., Whitworth, A.: Astron. Astrophys. **430**, 1059 (2005)
- Burgess, A., Moraux, E., Bouvier, J., Marmo, C., Albert, L., Bouy, H.: Astron. Astrophys. 508, 823 (2009)
- 7. Chabrier, G., Baraffe, I.: Astron. Astrophys. **327**, 1039 (1997)
- 8. Chabrier, G.: Publ. Astron. Soc. Pac. 115, 763 (2003)
- 9. Hennebelle, P., Chabrier, G.: Astrophys. J. 684, 395 (2008)
- 10. Herbst, W.: In: Reipurth, B. (ed.) Handbook of Star Forming Regions, Volume I, p. 372 (2008)

130 C.A. de Oliveira et al.

- 11. Kroupa, P., Bouvier, J.: Mon. Not. R. Astron. Soc. 346, 369 (2003)
- 12. Larson, R.B.: Mon. Not. R. Astron. Soc. 161, 133 (1973)
- 13. Lombardi, M., Alves, J.: Astron. Astrophys. 377, 1023 (2001)
- 14. Mamajek, E.E.: Astronomische Nachrichten 329, 10 (2008)
- 15. Marmo, C.: In: Astronomical Society of the Pacific Conference Series, vol. 376, p. 285 (2007)
- 16. Mayor, M., Queloz, D.: Nature 378, 355 (1995)
- 17. McClure, M.K., et al.: Astrophys. J. Suppl. 188, 75 (2010)
- 18. Moraux, E., Bouvier, J., Staufer, J. R., Barrado y Navascues, D., Cuillandre, J.: Astron. Astrophys. 471, 499 (2007)
- 19. Nakajima, T., Oppenheimer, B. R., Kulkarni, S. R., et al.: Nature 378, 463 (1995)
- 20. Oppenheimer, B., Kulkarni, S.R., Matthews, K., Nakajima, T.: Science 270, 1478 (1995)
- 21. Padoan, P., Nordlund, Å Kritsuk, A. G., Norman, M. L., Li, P.S.: Astrophys. J. **661**, 972 (2007)
- 22. Rebolo, R., Zapatero-Osorio, M.R., Martín, E.L.: Nature 377, 129 (1995)
- 23. Reipurth, B. Clarke, C.: Astron. J. 122, 432 (2001)
- 24. Shu, F.H., Adams, F.C., Lizano, S.: Annu. Rev. Astron. Astrophys. 25, 23 (1987)
- 25. Stamatellos, D., Whitworth, A.P.: Mon. Not. R. Astron. Soc. 392, 413 (2009)
- 26. Wilking, B.A., Gagne, M., Allen, L.E.: In: Reipurth, B. (ed.) Handbook of Star Forming Regions, Volume II, p. 351 (2008)



Jayne Birkby and Simon Hodgkin

# Dynamics in the Embedded Phase: Accretion, Collisions, Contraction

Nickolas Moeckel

**Abstract** Numerical studies of the early evolution of star clusters have traditionally been based on full hydrodynamic treatments (hampered by the large computational burden) or a purely gravitational N-body approach (limited by not considering the cluster's natal gas). I will discuss recent work that pushes the N-body techniques toward a more realistic gas treatment. In particular I will focus on the behavior of forming clusters as they accrete gas, leading to compact configurations that are robust to gas expulsion, and in extreme cases to the collisional growth of very massive stars.

#### 1 Introduction

Compared to a cluster-scale hydrodynamic simulation, *n*-bodycodes enjoy a tremendous advantage in the amount of computational resources required to run an experiment. During the weeks or months a current state-of-the-art hydrodynamic simulation of the collapse of a turbulent cloud takes to run, a complete parameter survey can be completed using an *n*-bodycode. The obvious trade off is the inability of the *n*-bodycode to handle gas in any but the crudest approximations.

Thus in order to use *n*-bodytechniques to study the very early, embedded phase of star cluster evolution, care must be taken to use appropriate initial conditions. In particular, spherical, equilibrated stellar distributions bear little resemblance to the filamentary and sub-clustered structure of star forming regions. The forward-looking work of Aarseth and Hills [1] set the stage for considerations of clumpy initial conditions, used by several later authors to investigate the possible dynamical roots of early mass segregation [3, 13, 14].

N. Moeckel (⊠)

Institute of Astronomy, University of Cambridge, Madingley Road, Cambridge CB3 0HA, UK e-mail: moeckel@ast.cam.ac.uk

There is a limit to how much one can gain by playing with initial conditions however, and at some point the need for a gas treatment of some sort will need to be addressed. Gas is, after all, the dominant contributor to the gravitational potential in the embedded phase.

# 2 Adding Accretion to N-Body Codes

A common way to include the bulk effect of an embedding gaseous component in a *n*-bodycode is to include an extra term in the force calculation, associated with the potential of a gas distribution. For the commonly-used Plummer sphere, the additional terms are readily derived and included in the star's motions, e.g. [11,12]. One step toward including a more realistic treatment of gas in *n*-bodycodes is to include some interaction between the stars and the gas beyond this basic gravitational interaction. In the context of star formation, including accretion is a clear choice. In the limit that the gas is motionless the stars will decelerate as they gain mass, and the dynamical evolution of the cluster is altered. This modification to the code NBODY6 [2] was implemented by Moeckel and Clarke [15]. The first application of the code was to study the accretion-driven shrinkage of a forming cluster, leading to high stellar densities and collisions, an idea introduced over a decade ago [5].

# 2.1 Accretion Prescription and Initial Conditions

Our clusters begin their evolution as Plummer spheres with 32,768 ('32 k') stars embedded in a matching background potential identified with the natal gas. The stars begin in the mass range  $0.03-3.0\,\mathrm{M}_\odot$ , with a power-law mass function  $\xi(m) \propto m^{-2.35}$ . For the first Myr of the simulation, the stars grow in mass with a constant mass-doubling time. That is, the shape of the mass function is preserved. After 1 Myr the stars have gained an order of magnitude of mass, so that the mass function spans  $0.3-30.0\,\mathrm{M}_\odot$ . As the stars grow in mass, the mass of the gas potential is globally lowered to conserve mass.

We choose the gas mass such that at the end of the 1 Myr accretion phase, the star formation efficiency is 30%. The accreted gas is assumed to have zero momentum; thus the stars decelerate as they grow in mass. After 1 Myr the gas is removed instantaneously. Many of these choices are plausible but somewhat arbitrary; the idealized nature of these experiments should be kept in mind. Figure 1 shows the relative mass densities of stars and gas at various times in one of the runs. Notable in this plot, between 0.3 and 0.65 Myr the stars begin to dominate the potential at the core of the cluster, which has two consequences: the stars in the stellar-dominated region are able to undergo normal relaxation effects like mass segregation and core collapse; and when the gas is expelled, the stars in the center of the cluster are in a region of higher effective star formation efficiency than the global value of 30%.

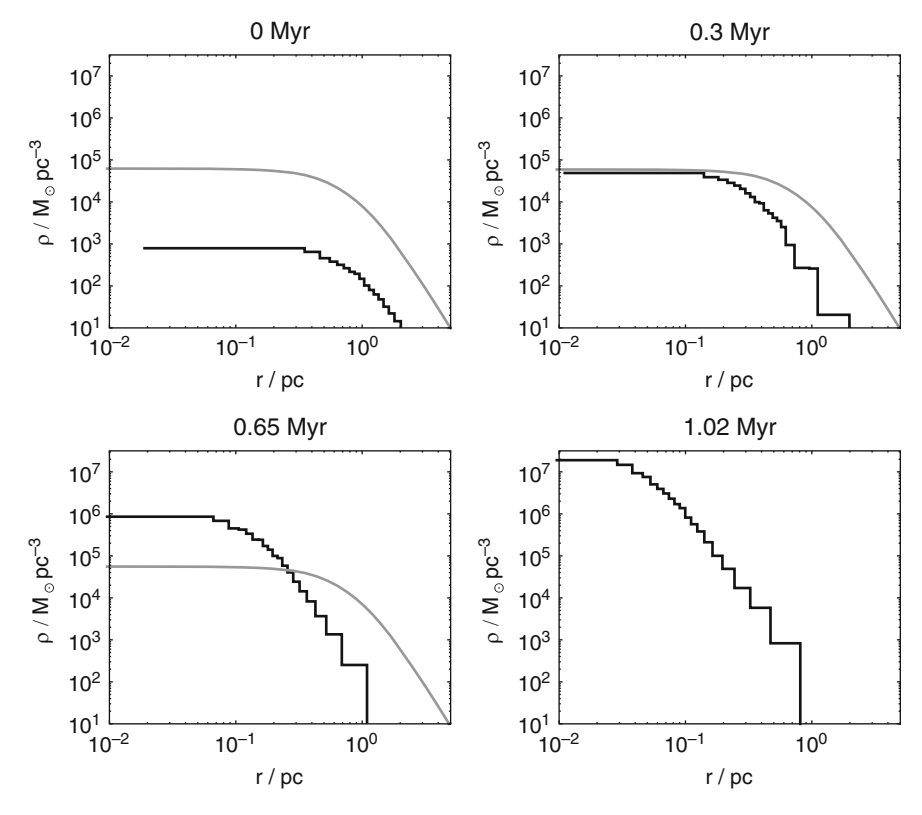


Fig. 1 Mass densities for one of our runs at four times in the cluster's evolution, ranging from the initial conditions to just after the gas is expelled. The *black histogram* shows the stars, while the smooth *gray line* shows the gas density

#### 2.2 Cluster Contraction

As the stars decelerate, they fall into deeper into the cluster center. This results in the stars concentrating in the center of the cluster, seen in the density plots in Fig. 1 and the Lagrangian radii (i.e. the radius enclosing a fixed mass fraction of the stars in a cluster) in Fig. 2. The evolution of the Lagrangian radii in particular show an interesting qualitative change that occurs in the contraction of the clusters.

Focusing on the left panel of Fig. 2, which is the same run as shown in Fig. 1, we see that through much of the accretion phase the cluster is accreting nearly homologously, a result seen in single mass Monte Carlo studies of this cluster accretion process [7]. Some time after the stellar mass dominates, the high mass stars (dark lines) and low mass stars (light lines) begin to diverge. This is the signal of mass segregation and the Spitzer instability [17] driving the cluster to core collapse. In the left panel, this process begins to occur during the accretion phase of the cluster. In the right panel, it begins only after the gas is expelled at 1 Myr.

N. Moeckel

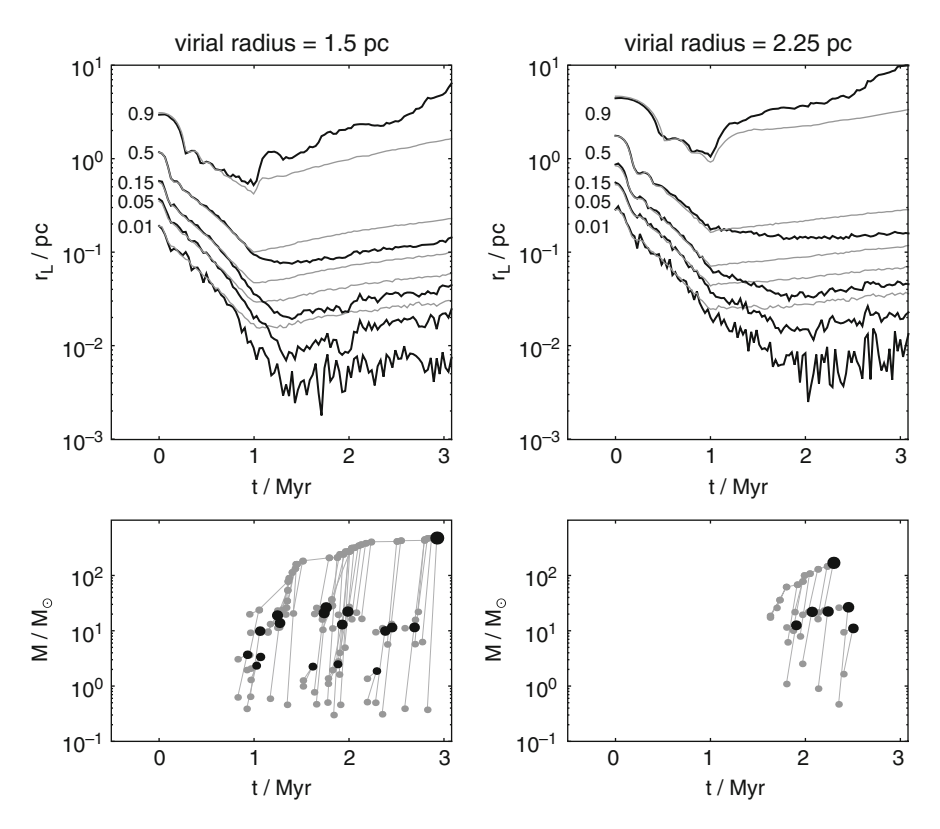


Fig. 2 Top row: Lagrangian radii (i.e. radii enclosing fixed mass fractions, as labeled) for two clusters with different initial radii. The black lines show the Lagrangian radii of the stars in the top third of the mass range, while the light gray lines show the lightest third. Bottom row: collision trees for the same clusters. Light gray dots are collision partners, connected by lines to their product. Larger black dots are still around at the end of the 3 Myr simulation, so they represent the end of a collision chain

The difference lies in the initial virial radii of the clusters. Both clusters evolve to the point seen in Fig. 1 where the stars dominate the potential. The more compact cluster, with an initial virial radius of 1.5 pc compared to 2.25 pc on the right, has a higher stellar density at that point, and consequently the relaxation timescale is shorter. These cluster parameters lie on either side of a dividing line: more compact, and relaxation effects (notably core collapse) have time to manifest themselves during the accretion phase; initially larger, and relaxation effects don't have time to appear until after the gas is expelled. This difference is reflected in the peak density attained, and this is directly related to the collision rate.

## 2.3 Collisions

Collisions between stars begin to occur at an interesting rate compared to star formation timescales once stellar number densities reach  $\sim 10^7$  [6]. While this is a much higher density than seen in the local environment, in these experiments it is easy to attain these densities during core collapse. The bottom row of Fig. 2 shows collision trees for the two simulations shown. In these figures, light gray dots show the time and mass of two stars involved in a collision, and they are joined by lines to the collision product. In these simulations the collisions are ideal and conserve mass and momentum, and there are no stellar evolution effects such as powerful winds from very massive stars; the masses are thus strict upper limits. Larger black dots are those collision products that are still extant at 3 Myr, i.e. they are the end product of a collision chain. Recall that  $30\,\mathrm{M}_\odot$  was the maximum mass reached by accretion; in these experiments any object above that mass was necessarily formed by collisions.

It is immediately apparent that the cluster on the left, starting from a more compact configuration, has had hosted many more collisions, and has an object that has attained a higher mass. There are similarities, however. In both cases the collisions begin just before core collapse (identified visually as the minimum of the innermost Lagrangian radii), and in both clusters a single star undergoes a runaway sequence, dominating the total collisional growth. This occurs in all the simulations we have run, not just the two shown here, and is similar in character to simulations of the collisional growth of potential IMBH progenitors, e.g. [16]. The mass function resulting from this runaway sequence is not smooth. This is evidently not a way to continuously fill in the high end of the stellar mass function, but potentially a way to reach the very high masses associated with some of the more exotic objects known. The generic result of these collision sequences is a dominant object in excess of  $100\,\mathrm{M}_\odot$ , over three times the maximum mass reached by accretion.

Experiments with lower-*n* clusters do not result in the necessary densities for collisions to occur. This is due to the short relaxation times associated with less populous clusters of otherwise similar parameters, and the increased effectiveness of a hard binary in inflating the core. A shorter relaxation time makes the clusters enter core collapse from a less dense configuration, and when a hard binary is formed at the cluster center it rapidly expands the innermost Lagrangian radii. Thus the peak density is lower and experienced for a shorter amount of time, and collisions do not occur.

# 2.4 Expansion

Gas expulsion has long been implicated in the dissolution of clusters [10], and a large body of numerical work has comprehensively explored parameters space, e.g. [4]. A first-order consideration of the problem leads to the star formation efficiency

N. Moeckel

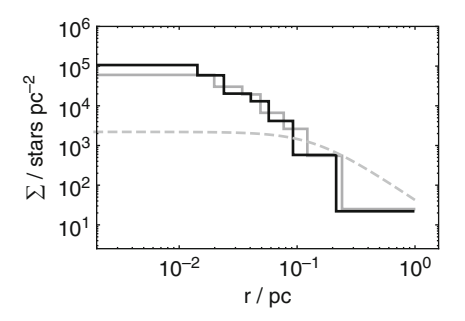


**Fig. 3** Surface density profile at 1 Myr (*gray histogram*) and 2 Myr (*black histogram*) for the cluster in the left column of Fig. 2. The *dashed gray curve* is the surface density of the Arches [8]. All clusters with runaway collision events before or soon after gas expulsion share these high densities

as the key parameter in determining the fate of a cluster after expansion. However, in order to use a single parameter one either makes assumptions about the spatial distribution of the stars and gas and the stars' velocities, or else folds those elements into the word "effective" in "effective star formation rate" [9]. In the case of these clusters, the concentration of stars in the center leads to a locally effective star formation rate much higher than the global 30%.

The result is that the instantaneous expulsion of gas has little effect on the inner cluster; the majority of stars remain bound, and the cluster hardly expands at all. The accretionally-induced contraction of the stellar component of the cluster is thus a means to enhanced cluster survival. This is true for the lower-n clusters as well; while collisions are only to be expected in populous clusters with numbers of order  $10^4$  or higher, the contraction and robustness of the cluster to gas expulsion are seen in all accreting clusters.

The lack of expansion also means that the very high densities that are attained by the accretionally-driven contraction are largely maintained. This is problematic when comparing the simulated clusters to observations. The surface density for clusters with a large number of collisions is an order of magnitude higher than the densest Galactic cluster, the Arches [8] (see Fig. 3). It seems unlikely that this runaway process has played a role in our local universe, although a more sophisticated treatment of the gas expulsion and stellar evolution are required to truly reach that conclusion.

#### **3 Future Directions**

The work discussed here represents a first step at making n-bodytechniques more suitable for studying clusters in the embedded phase. The future of this area must lie in continuing down this path. The most obvious steps are including gas heating

and more sophisticated accretion prescriptions, allowing the gas potential to react to the changing stellar potential in a self consistent way, and most crucially breaking free of spherical symmetry. There remains a great deal of work to be done on cluster dynamics at the transition from gas-dominated to gas-free. Existing hydrodynamic and *n*-bodycodes are not well-suited to statistically meaningful studies of this regime, and the continued development new techniques and methods is the first order of business.

**Acknowledgements** My thanks to the organizers for the invitation, and to Sverre Aarseth for the use of hisGPUs and debugging help during this project.

#### References

- 1. Aarseth, S.J., Hills, J.G.: Astron. Astrophys. **21**, 255 (1972)
- Aarseth, S.J.: In: Gurzadyan, V.G., Ruffini, R. (eds.) The Chaotic Universe, Proceedings of the Second ICRA Network Workshop. Advanced Series in Astrophysics and Cosmology, vol.10. World Scientific (2000)
- Allison, R.J., Goodwin, S.P., Parker, R.J., de Grijs, R., Portegies Zwart, S.F., Kouwenhoven, M.B.N.: Astrophys. J. Lett. 700, L99 (2009)
- 4. Baumgardt, H., Kroupa, P.: Mon. Not. R. Astron. Soc. 380, 1589 (2007)
- 5. Bonnell, I.A., Bate, M.R., Zinnecker, H.: Mon. Not. R. Astron. Soc. 298, 93 (1998)
- 6. Bonnell, I.A., Bate, M.R.: Mon. Not. R. Astron. Soc. 336, 659 (2002)
- 7. Davis, O., Clarke, C.J., Freitag, M.: Mon. Not. R. Astron. Soc. 407, 381 (2010)
- 8. Espinoza, P., Selman, F.J., Melnick, J.: Astron. Astrophys. **501**, 563 (2009)
- 9. Goodwin, S.P., Bastian, N.: Mon. Not. R. Astron. Soc. 373, 752 (2006)
- 10. Hills, J.G.: Astrophys. J. **235**, 986 (1980)
- 11. Kroupa, P., Aarseth, S., Hurley, J.: Mon. Not. R. Astron. Soc. 321, 699 (2001)
- 12. Lada, C.J., Margulis, M., Dearborn, D.: Astrophys. J. 285, 141 (1984)
- 13. McMillan, S.L.W., Vesperini, E., Portegies Zwart, S.F.: Astrophys. J. Lett. 655, L45 (2007)
- 14. Moeckel, N., Bonnell, I.A.: Mon. Not. R. Astron. Soc. 400, 657 (2009)
- 15. Moeckel, N., & Clarke, C.J., MNRAS, 410, 2799 (2011)
- 16. Portegies Zwart, S.F., McMillan, S.L.W.: Astrophys. J. **576**, 899 (2002)
- 17. Spitzer, L.J.: Astrophys. J. Lett. **158**, L139 (1969)

N. Moeckel



Mark Gieles



Sofia Randich and Peter Frinchaboy

# **Unraveling the Initial Conditions of Star Formation in Serpens North**

Ana Duarte-Cabral, Nicolas Peretto, Gary A. Fuller, and Clare L. Dobbs

Abstract The Serpens North Cluster is a nearby low mass star forming region which is part of the Gould Belt. It contains a range of young stars thought to correspond to two different bursts of star formation and so provides the opportunity to study different stages of cluster formation. Here we present recent results based on a detailed analysis of molecular line and dust continuum data of this region. By studying the dynamics, column density and dust temperature structure of Serpens we propose that a cloud-cloud collision has been responsible for the trigger of the most recent episode of star formation. This scenario has been explored using SPH simulations. These simulations are able to successfully explain the similarities and differences observed in the two sub-protoclusters composing Serpens North.

# 1 Dust Continuum View of Serpens North

Located at  $\sim$ 260 pc [16], the optical extinction map of the Serpens Molecular Cloud (MC) covers more than  $10 \, \text{deg}^2$  [1]. However, the majority of the star formation in the cloud is occurring in three clusters covering approximately 1.5 deg<sup>2</sup> [7]. The most active region is the Serpens North Cluster which has a surface density of YSOs

A. Duarte-Cabral  $(\boxtimes) \cdot G.A.$  Fuller

Jodrell Bank Centre of Astrophysics, School of Physics and Astronomy,

University of Manchester, Manchester, UK

e-mail: Ana.Cabral@postgrad.manchester.ac.uk; G.Fuller@manchester.ac.uk

N. Peretto

Service d'Astrophysique, CEA Saclay, France

e-mail: nicolas.peretto@cea.fr

C.L. Dobbs

Max-Planck-Institut für extraterrestrische Physik, Garching & Universitäts-Sternwarte München,

Germany

e-mail: cdobbs@mpe.mpg.de

A. Moitinho and J. Alves (eds.), *Star Clusters in the Era of Large Surveys*, Astrophysics and Space Science Proceedings, DOI 10.1007/978-3-642-22113-2\_20, © Springer-Verlag Berlin Heidelberg 2012

140 A. Duarte-Cabral et al.

of  $222\,\mathrm{pc^{-2}}$ , compared to  $10.1\,\mathrm{pc^{-2}}$  in the rest of the Serpens MC [9]. In this Serpens North cluster (hereafter Serpens), the average gas density is around  $10^4\,\mathrm{cm^{-3}}$  [7] with  $H_2$  column densities greater than  $10^{22}\,\mathrm{cm^{-2}}$  in the cores. The high density of protostars seems to indicate an early stage of evolution where the cluster gas may still be infalling into the cores [13, 17, 18]. The star formation rate in Serpens is  $56\,\mathrm{M}_\odot\mathrm{Myr^{-1}pc^{-2}}$ ,  $\sim 20$  times higher than in the rest of the cloud [9].

Amongst the youngest YSOs found in Serpens there are ten Class 0 and I protostars which are detected in 850  $\mu$ m dust continuum emission (e.g. [3, 12]), hereafter referred to as submillimetre sources (shown on Fig. 1). These are distributed within  $\sim$ 0.2 pc² and divided between two sub-clusters, one to the northwest (NW) and one to the southeast (SE). These submillimetre sources power a number of outflows, which have been studied using several different approaches (e.g., [2, 3, 6, 8, 11]). Figure 1 also shows the Spitzer MIPS 24  $\mu$ m emission tracing young protostars classified as Class I or 0. The oldest objects in the area shown on the image are a few flat spectrum sources [9,14]. The presence of Class II and Class III objects (not shown in Fig. 1) dispersed over a larger area suggests that the region has undergone two episodes of star formation. The first, responsible for these dispersed pre-main sequence stars (the Class II and III sources), occurred about 2 Myr before the most

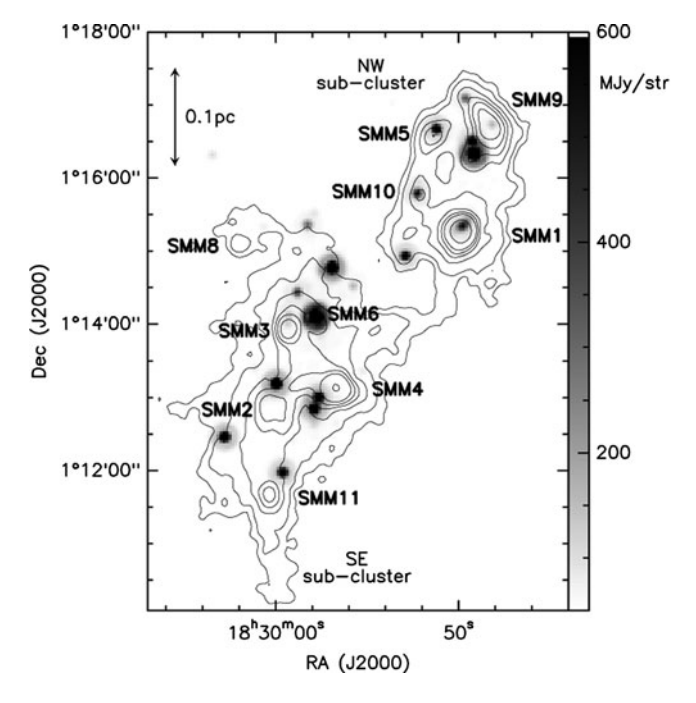


**Fig. 1** Serpens region as seen in 850  $\mu$ m dust continuum emission with SCUBA [3] in contours at 0.4, 0.6, 1, 1.4, 1.8, 2.4 and 5 Jy beam<sup>-1</sup>. The compact 850  $\mu$ m sources are also labeled. In *grey scale* is the 24  $\mu$ m from Spitzer MIPS [10]

recent burst which formed the submillimetre and  $24\,\mu m$  protostars (Class 0, I and flat spectrum sources),  $10^5\,yr$  ago [9, 14].

## 2 Column Density and Gas Temperature in Serpens

We used a large set of CO isotopologue lines obtained with the IRAM 30 m and the JCMT (sub-)millimetre telescopes in order to be able to reconstruct the spatial distribution of the excitation temperature and column density of the gas.

From the dust continuum emission, the volume densities in the Serpens subclusters are typically higher than the critical densities of each of the three transitions observed here. We therefore initially calculated the gas properties assuming LTE (local thermodynamic equilibrium) using a rotation diagram analysis. Despite its uncertainties, the rotation diagram method is robust in retrieving the column density structure and trends throughout the region, as well as the approximate absolute column densities.

The excitation temperature map of the region shows the NW and SE sub-clusters to have different temperature structures. The NW appears very homogeneous with no significant temperature peaks and with temperatures ranging from 9 to 10 K. In contrast the SE region has both higher temperatures, ranging from  $\sim \! 10 \text{ to } 14 \text{ K}$  and a much more peaked distribution. Interestingly, this enhanced temperature in the south does not peak on the SMM protostars but rather between them.

The C<sup>18</sup>O column density map (Fig. 2, right) calculated from the rotation diagram recovers more of the dust structure than the temperature map. Both the south and north sub-clusters are evident as denser regions, even though the dust and gas

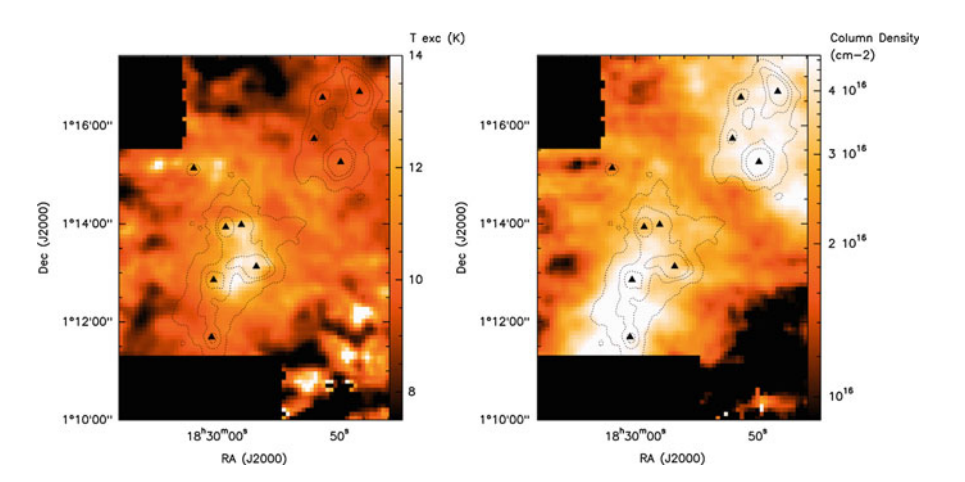


Fig. 2 Maps of the excitation temperature (*left*) and column density (*right*), in colour scale, derived from the rotation diagram method (LTE). The *dotted black* contours show the dust 850  $\mu$ m emission at 0.6, 1.2 and 1.8 Jy beam<sup>-1</sup>

142 A. Duarte-Cabral et al.

column densities peaks are not always coincident, especially in the SE. The mean C<sup>18</sup>O column densities are very similar in the north and the south. The regions with higher gas column density (the entire NW sub-cluster and the filament between SMM11 and SMM2 in the SE sub-cluster) have a lower temperature. Conversely the regions with slightly lower gas column density (between SMM2, SMM4, SMM3 and SMM6 in the SE sub-cluster) have higher temperature. The region south-west of the NW sub-cluster which appears to have a relatively high gas column density seems to have very similar properties to the rest of the NW sub-cluster and yet it is not detected in dust emission. These results are confirmed by non-LTE modeling at some key positions (see [5]).

## 3 Dynamics of Serpens North

On the basis of a study of the line centroid velocity of Serpens, previous studies [15] argued that the region is undergoing global rotation. However, position-velocity diagrams of RA slices along the C<sup>18</sup>O map are incompatible with this interpretation (Fig. 3). For simple rotation we would expect to see a smooth gradient along the velocity axis as the RA changes. This is indeed compatible to what we see, for instance, in the NW sub-cluster (Fig. 3, left panel). On the other hand, we observe two clearly separate velocity components in the southern part of Serpens (Fig. 3, right panel) which merge together when moving to the north of the SE sub-cluster (Fig. 3, central panel). At this point, the two components are barely distinct lines, producing broad, non-gaussian profiles. The SE filamentary structure seen in dust follows this region where the two clouds overlap and merge (see the "dust" lanes on Fig. 3).

A dynamical interaction between two such clouds in the SE sub-cluster, could explain the differences observed in the temperature/column density structure of the

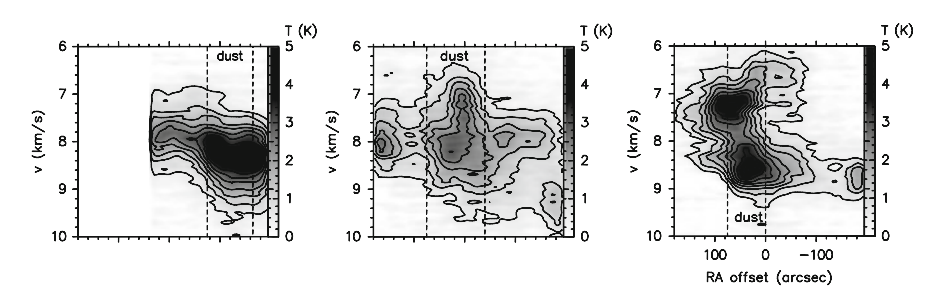


Fig. 3 Position-velocity diagrams of  $C^{18}O$  J = 1 $\rightarrow$ 0 at constant declination: in the NW at 1°15′58″ (*left*) and in the SE at 1°13′28″ (*centre*) and 1°11′48″ (*right*). Right Ascension varies from  $18^h30^m06^s$  to  $18^h29^m46^s$  for all panels. The *dashed lanes* labeled as "dust" represent the regions whose 850  $\mu$ m emission is above 0.6 Jy beam<sup>-1</sup> [4,5]

two sub-protoclusters (cf Sect. 2). Ultimately, it may have been at the origin of this episode of star formation.

#### 4 Dedicated SPH Simulations of Cloud-Cloud Collisions

In order to test the proposal that the structure and star formation in Serpens results from triggering by a cloud-cloud collision we have performed a set of Smoothed Particle Hydrodynamics (SPH) simulations which are compared in detail with the observations. Each of the simulations started with two cylinders, to approximate filamentary clouds, heading toward each other [4]. We tried various initial conditions with different impact parameter, inclination angles, velocity fields and masses. The results from this study support the idea that Serpens' current star formation may, indeed, have been triggered by a collision of two filamentary clouds (Fig. 4).

This model is able to reproduce both the column density structure, a centrally condensed filament aligned in a NW–SE direction, and the two velocity components seen where the collision is occurring, mimicking the SE sub-cluster. This suggests that the SE sub-cluster of Serpens is the direct result of a collision prompting star formation in the collision layer. The same simulations did not, however, produce a second sub-cluster, similar to the NW sub-cluster of Serpens. Therefore, this sub-cluster does not seem to be the direct result of the collision and is most likely just marginally affected by it. This suggestion was already supported by the NW sub-cluster's "well behaved" temperature profile and velocity structure, as well as the uniform age of sources within the sub-cluster. However, the similar stage of evolution of the sources from the two sub-clusters and their proximity, suggests that the two events are not totally independent.

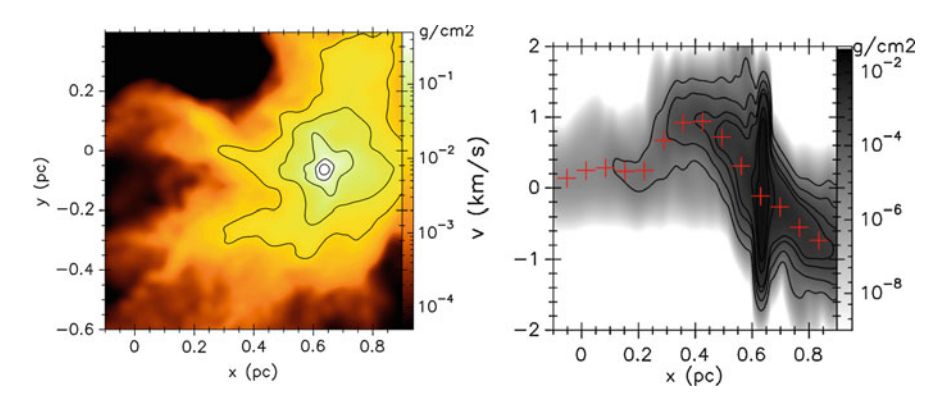


Fig. 4 *Right*: Column density map for the SPH run which we consider to best describe the SE sub-cluster. *Right*: Horizontal PV diagram of the same run, at y = -0.07 pc, showing the column density weighted velocity as red crosses. Figures from [4]

144 A. Duarte-Cabral et al.

A simulation with elongated cylinders and increased masses provides a possible explanation. The presence of a marginally stable region in the northern part of one of the colliding filaments before any interaction between the clouds, can have its collapse quickened by perturbations driven by the cloud–cloud collision.

# 5 Conclusions: Cloud Collision as a Trigger for Star Formation in Serpens

We consider a cloud–cloud collision scenario to be a viable description of the driving of the star formation history in Serpens. Not only can it reproduce the observed velocities and column densities, as it offers a plausible explanation for why the two sub-clusters are so similar and yet so different. The complexity of the region is better explained with such a collision scenario, which is in essence similar to a shear-motion (also suggested by [15]), rather than rotation.

#### References

- 1. Cambrésy, L.: Astron. Astrophys. 345, 965 (1999)
- Davis, C.J., Chrysostomou, A., Matthews, H.E., Jenness, T., Ray, T.P.: Astrophys. J. Lett. 530, L115 (2000)
- 3. Davis, C.J., Matthews, H.E., Ray, T.P., Dent, W.R.F., Richer, J.S.: Mon. Not. R. Astron. Soc. **309**, 141 (1999)
- 4. Duarte-Cabral, A., Dobbs, C.L., Peretto, N., Fuller, G.A.: Astron. Astrophys. 528, A50 (2011)
- Duarte-Cabral, A., Fuller, G.A., Peretto, N., Hatchell, J., Ladd, E.F., Buckle, J., Richer, J., Graves, S.F.: Astron. Astrophys. 519, A27 (2010)
- Eiroa, C., Torrelles, J.M., Gomez, J.F., Sakamoto, S., Hasegawa, T., Kawabe, R., Hayashi, M., Casali, M.M.: Publ. Astron. Soc. Jpn. 44, 155 (1992)
- Enoch, M.L., Glenn, J., Evans II, N.J., Sargent, A.I., Young, K.E., Huard, T.L.: Astrophys. J. 666, 982 (2007)
- Graves, S.F., Richer, J.S., Buckle, J.V., Duarte-Cabral, A., Fuller, G.A., Hogerheijde, M.R., Owen, J.E., Brunt, C., Butner, H.M., Cavanagh, B., Chrysostomou, A., Curtis, E.I., Davis, C.J., Etxaluze, M., Francesco, J.D., Friberg, P., Friesen, R.K., Greaves, J.S., Hatchell, J., Johnstone, D., Matthews, B., Matthews, H., Matzner, C.D., Nutter, D., Rawlings, J.M.C., Roberts, J.F., Sadavoy, S., Simpson, R.J., Tothill, N.F.H., Tsamis, Y.G., Viti, S., Ward-Thompson, D., White, G.J., Wouterloot, J.G.A., Yates, J.: Mon. Not. R. Astron. Soc. 409, 1412 (2010)
- 9. Harvey, P., Merín, B., Huard, T.L., Rebull, L.M., Chapman, N., Evans, N.J. II, Myers, P.C.: Astrophys. J. **663**, 1149 (2007)
- Harvey, P.M., Rebull, L.M., Brooke, T., Spiesman, W.J., Chapman, N., Huard, T.L., Evans II, N.J., Cieza, L., Lai, S., Allen, L.E., Mundy, L.G., Padgett, D.L., Sargent, A.I., Stapelfeldt, K.R., Myers, P.C., van Dishoeck, E.F., Blake, G.A., Koerner, D.W.: Astrophys. J. 663, 1139 (2007)
- 11. Hodapp, K.W.: Astron. J. 118, 1338 (1999)
- 12. Hurt, R.L., Barsony, M.: Astrophys. J. Lett. 460, L45 (1996)
- 13. Hurt, R.L., Barsony, M., Wootten, A.: Astrophys. J. 456, 686 (1996)

- 14. Kaas, A.A., Olofsson, G., Bontemps, S., André, P., Nordh, L., Huldtgren, M., Prusti, T., Persi, P., Delgado, A.J., Motte, F., Abergel, A., Boulanger, F., Burgdorf, M., Casali, M.M., Cesarsky, C.J., Davies, J., Falgarone, E., Montmerle, T., Perault, M., Puget, J.L., Sibille, F.: Astron. Astrophys. 421, 623 (2004)
- 15. Olmi, L., Testi, L.: Astron. Astrophys. 392, 1053 (2002)
- 16. Straižys, V., Černis, K., Bartašiūte, S.: Baltic Astron. 5, 125 (1996)
- 17. Williams, J.P., Myers, P.C.: Astrophys. J. Lett. **518**, L37 (1999)
- 18. Williams, J.P., Myers, P.C.: Astrophys. J. 537, 891 (2000)



Ana Duarte Cabral

A. Duarte-Cabral et al.



Sofia Randich



André Moitinho makes a point

# Do All Stars in the Solar Neighbourhood Form in Clusters?

Eli Bressert, Nate Bastian, and Robert Gutermuth

**Abstract** We present a global study of low mass, young stellar object (YSO) surface densities ( $\Sigma$ ) in nearby (<500 pc) star forming regions based on a comprehensive collection of *Spitzer Space Telescope* surveys. We show that the distribution of YSO surface densities is a smooth distribution, being adequately described by a lognormal function from a few to  $10^3$  YSOs per pc<sup>2</sup>, with a peak at ~22 stars pc<sup>-2</sup>. The observed lognormal  $\Sigma$  is consistent with predictions of hierarchically structured star-formation at scales below 10 pc, arising from the molecular cloud structures. We do not find evidence for multiple discrete modes of star-formation (e.g. clustered and distributed). Comparing the observed  $\Sigma$  distribution to previous  $\Sigma$  threshold definitions of clusters show that they are arbitrary. We find that only a low fraction (<26%) of stars are formed in dense environments where their formation/evolution (along with their circumstellar disks and/or planets) may be affected by the close proximity of their low-mass neighbours.

#### 1 Introduction

It is often stated that most if not all stars form in clusters. This view is based largely on near-infrared (NIR) studies of star-forming (SF) regions within several hundred parsecs of the Sun [27,30]. However, combining high-resolution mid-infrared (MIR) data with the NIR makes YSO identification more robust and less likely to suffer from field star contamination, which leads to better tracing of YSO surface densities.

E. Bressert (⋈) · N. Bastian

University of Exeter, School of Physics, Stocker Road, Exeter EX4 4QL, UK e-mail: eli@astro.ex.ac.uk; bastian@astro.ex.ac.uk

R. Gutermuth

University of Massachusetts, Smith College, Northampton, MA 01063, USA e-mail: rgutermu@smith.edu

E. Bressert et al.

This means that with only NIR imaging, there are large uncertainties in the number of stars at low values of YSO surface densities ( $\Sigma_{YSO}$ ) [8].

With the launch of the *Spitzer Space Telescope* [36] we are now able to differentiate YSOs and contaminating sources based on colour information and hence can study the distribution of YSOs independently of the surface densities. Large field-of-view (FoV) *Spitzer* observations of SF regions [1, 16] found that YSOs extend well beyond the densest groups in their environment and continue to the edge of the survey and presumably, beyond. Several *Spitzer* surveys that cover nearly all the SF regions within 500 pc of the Sun were combined and presented by [7].

The spatial distribution of forming stars, i.e. do they form in clusters, is important for many reasons and here we list several. What spatial distributions of star forming environments lead to Galactic stellar clusters and why do they constitute such a low fraction of the stellar population? Are there multiple discrete modes of star formation, such as clustered and distributed, that manifest themselves as peaks in a surface density distribution (e.g. [8, 33–35])? What fraction of star forming environments are dense enough to affect the YSOs and alter their disk and planet formation/evolution [1, 20], which we refer to as *dense environments*.

Outside the Milky Way we see that star-formation proceeds hierarchically from  $\sim 10\,\mathrm{pc}$  (the resolution limit of most extragalactic surveys) to kpc scales (e.g. [4, 5, 10, 11, 17]). If star formation occurs hierarchically down to 0.1 pc, then it is unlikely, and indeed not expected, that all stars form in gravitationally bound young stellar clusters. The availability of large FoV *Spitzer* surveys of nearby star-forming regions allows us to test how far down in scale this hierarchy proceeds. By hierarchical structure we mean a smoothly varying non-uniform distribution of densities, where denser subareas are nested within larger, less dense areas [13, 32].

In this paper we will investigate (1) whether there is evidence for multimodality in the surface densities of YSOs, (2) what fraction of stars form in dense environments in the local neighbourhood and (3) the relevance of the various cluster definitions provided by [1, 8, 21, 25, 27].

#### 2 Data and Biases

Multiple *Spitzer* surveys were used to generate a comprehensive and statistically significant dataset to investigate the spatial surface density properties of forming stars in the solar neighbourhood. The surveys are the Gould's Belt (GB) survey (Allen et al. in preparation), Orion survey (Megeath et al. in preparation), Cores to Disks (c2d) survey [15], and the Taurus survey [31]. The GB and Orion catalogs have not been publicly released yet. There are more than 7,000 YSO detections in the combined catalogs at distances between 100 and 500 pc.

Spitzer data are necessary for this study as low  $\Sigma_{YSO}$  can be differentiated from field star populations, unlike NIR only studies where field star contamination can be problematic. The comprehensive YSO population represents a global view of the

low-mass star-forming region in the local neighbourhood from low to high surface densities. These *Spitzer* surveys combined represent the most complete census of star formation within 500 pc of the Sun available to date.

Data treatment on distances, exclusion of the central region of the Orion Nebular Cluster, rejection of Class III objects, and potential contaminants are described in [7]. After the data correction process, we have 3857 YSOs remaining to estimate the surface densities presented in this paper.

## 3 $\Sigma_{\rm YSO}$ Distributions

Our primary tool for analysing the surface densities is computing the local observed surface density of YSOs centred on each YSO's position, where  $\Sigma_{\rm YSO} = (N-1)/(\pi D_N^2)$  and N is the Nth nearest neighbour, and  $D_N$  is the projected distance to that neighbour (see [9]). Throughout this work we will adopt N=7, although we note that all results have been tested for N=4-22 and no significant differences were found. Figure 1 shows the surface density distribution of all YSOs in our sample.

In order to see the fraction of YSOs above a given  $\Sigma$  threshold, we show the combined  $\Sigma_{YSO}$  distribution (shown as a cumulative fraction normalised to the number in each combined survey) for the three surveys used in this study in Fig. 1a. Note that the GB/Taurus distribution lies to the left of the c2d survey. This is simply due to the GB/Taurus focusing on lower density regions than c2d. The cumulative distribution for the Orion survey only reaches 0.73 in Fig. 1a and 0.81 in Fig. 1c, where all the surveys have been combined, due to the exclusion of the ONC (see [7]). In Fig. 1c we show the cumulative distribution of all YSOs included in our survey, while in Fig. 1b we split the survey into class I and class II objects.

#### 4 Results

It has been long assumed that two distinct modes of star formation exist for YSOs, "clustered" and "distributed" (e.g. [8, 19, 27]), but the notion has been questioned after *Spitzer* results hinted otherwise [1]. If there are indeed two modes, then we would expect to see a bi- or multi-modal profile in cumulative surface density distribution plots such as Fig. 1a, c. Instead we see smooth and featureless distributions from the low to high stellar surface densities for the c2d, GB, Taurus, and Orion surveys. We find that the  $\Sigma_{\rm YSO}$  distribution of low-mass stars in the solar neighbourhood can be well described by a lognormal function, as seen in Fig. 2, with a peak at ~22 YSOs/pc² and a dispersion  $\sigma_{\log_{10}\Sigma} = 0.85$ .

The spatial distribution of the YSOs in these SF regions is expected to be close to primordial since their YSOs, in particular Class Is and Class IIs, are  $\leq$ 2 Myr old [22, 24]. In order to place stricter constraints on this, we now split the complete

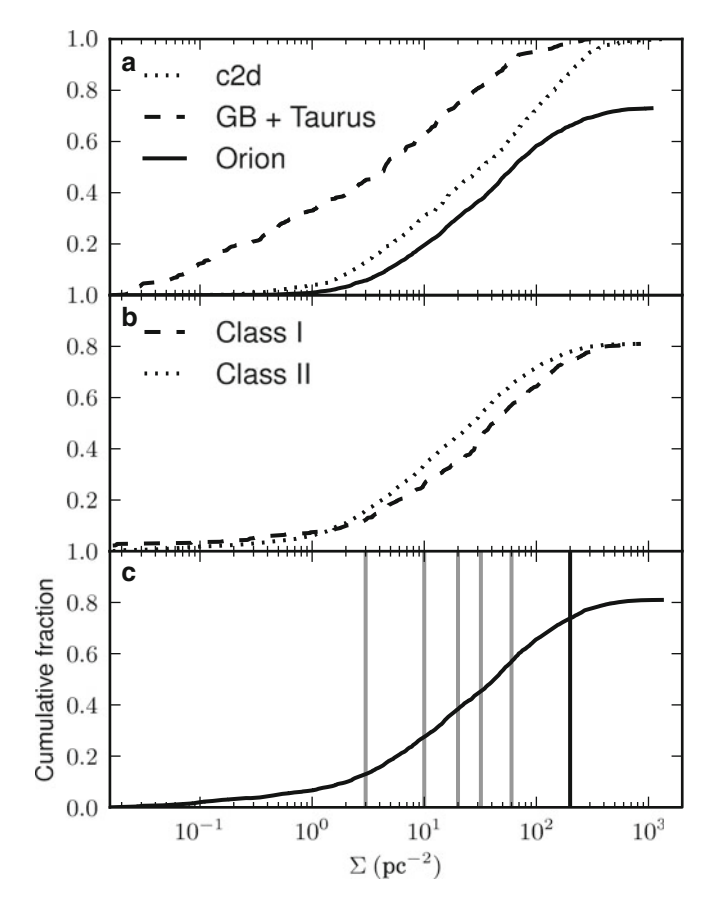
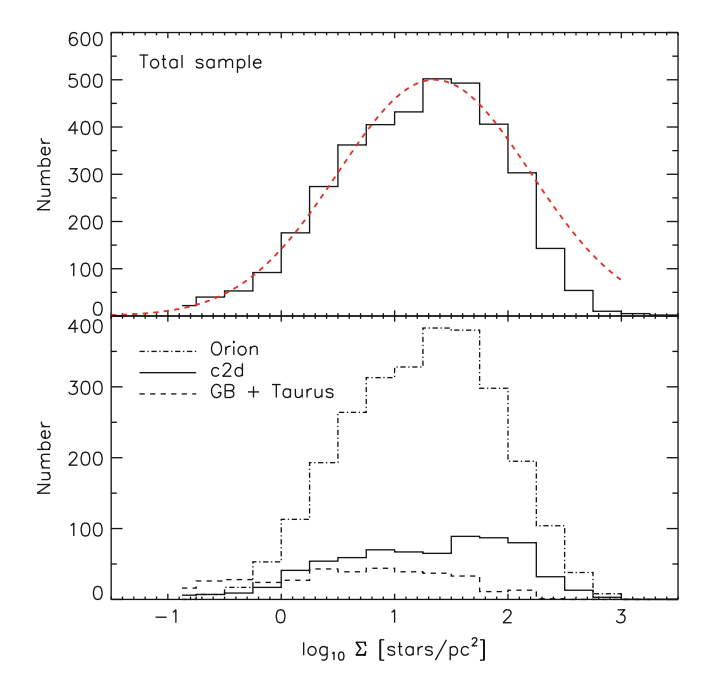


Fig. 1 (a) The cumulative fraction of surface densities for the GB+Taurus, c2d, and Orion surveys. Each SF region included in the distributions has  $N(YSOs) \ge 10$  and a sufficient field-of-view to properly calculate stellar surface densities. The Orion survey stops at 73% for the cumulative fraction since the ONC is excluded. We adopt a 65% disk fraction for all of the SF regions. We normalised each curve by the number of YSOs in each survey. (b) With the GB+Taurus, c2d, and Orion surveys combined we see Class I & II distributions having similar profiles with a small offset in density, showing that we are likely seeing the primordial distribution of the YSOs. (c) With all of the *Spitzer* surveys combined we compare several cluster definitions. The vertical grey lines from left to right are Lada and Lada [27], Megeath et al. (in preparation), Jørgensen et al. [25], Carpenter [8], and [21] stellar density requirements for clusters. These values correspond to 3, 10, 20, 32, and 60 YSOs pc<sup>-2</sup> and intersect the corrected cumulative distribution profile, implying that 87, 73, 62, 55, and 43% of stars form in clusters, respectively. The percentages correlate to what fraction of stars form in "clusters" based on the various definitions. The *black vertical line* is for a dense environment where  $\Sigma \ge 200 \text{ YSOs/pc}^2$ . The fraction of YSOs in a dense environment is <26%



**Fig. 2** *Top panel:* The surface density distribution of the total sample of YSOs in the solar neighbourhood used in this work (*black*). A lognormal function with a peak at  $\sim 22 \text{ YSOs/pc}^2$  and a dispersion  $\sigma_{\log_{10}\Sigma} = 0.85$  is shown as a *dashed line. Bottom panel:* The same as the *top panel* but now broken into the three respective surveys

sample into Class I and II objects, which can be roughly attributed to an age sequence. The cumulative  $\Sigma$  distributions of Class I and II YSOs are shown in Fig. 1b. We see that the two distributions have similar smooth density spectra, however they are slightly offset. The  $\Sigma$  of the Class I/II objects are calculated by finding a YSO's Nth nearest YSO. Once this is done for the YSOs we separate the Class I/II objects.  $\Sigma$  is calculated this way since Class Is and Class IIs are not always spatially distinct from one another [21]. Class IIs are known to be slightly more dispersed than Class Is in high density regions [21] reflecting early dynamical evolution. However, the similar distribution between these classes leads us to conclude that the distribution of observed  $\Sigma$  is mainly primordial in nature.

In Fig. 1c we show five vertical grey lines that refer to the defined densities required for a collection of YSOs to be considered "clustered" [8, 21, 25, 27, 28]. The vertical lines fall on the same featureless slope and do not correspond to any preferred density. The black vertical line, which corresponds to dense environments (as defined in [20]), shows that <26% of YSOs are forming in environments where they (along with their disks and planets) are likely to interact with their neighbours.

E. Bressert et al.

#### 5 Discussion and Conclusions

We conclude that stars form in a broad and smooth spectrum of surface densities and do not find evidence for discrete modes of star formation in the  $\Sigma$  of low mass YSOs in the solar neighbourhood. The observed lognormal surface density distribution is consistent with predictions of hierarchically structured star-formation, which arise from similar structures in molecular clouds [12,14]. Our results suggest that clusters are not fundamental units in the star formation process, but simply the high density tail end of a continuous distribution. A small fraction (<26%) of stars form in dense environments where their formation and/or evolution is expected to be influenced by their surroundings.

By comparing our global surface density distribution with the summary of cluster definitions in [7], we find that the fraction of stars forming in clusters is crucially dependent on the adopted definitions (ranging from  $\sim$ 40 to 90%). Since star/cluster formation happens in a dynamic environment [2, 6, 29] it may be impossible to define what will become a stellar cluster in these early stages, as the final object that remains bound is simply the dynamically mixed part of a larger, initially hierarchical, distribution. In this scenario a cluster can only be clearly defined above the surrounding distribution once it is dynamically evolved where  $t_{age}/t_{cross} > 1$ , as defined by [18].

Star forming environments provide the initial conditions from which star clusters may eventually form, albeit rarely. Since the probability density function of molecular gas varies with environment, as does the tidal field experienced by the SF regions, it is likely that the fraction of YSOs ending up in bound star clusters varies with environment [14] and the observed  $\Sigma_{\rm YSO}$  is not universal. Future investigations will extend this work out to 2 kpc where proto-stellar cores and high-mass SF regions will be included, and testing whether star formation primarily occurs when  $\Sigma_{gas}$  is above a specific threshold (e.g. [3, 23, 26, 27])

**Acknowledgements** We would like to thank the organisers of the JENAM *Star Clusters in the Era of Large Surveys* meeting for arranging the program and inviting us to contribute our work. Additionally, Eli Bressert's trip to the meeting was possible due to the CONSTELLATION network and funds.

#### References

- 1. Allen, L., et al.: Protostars Planets V 361 (2007)
- 2. Allison, R.J., et al.: Astrophys. J. Lett. 700, L99 (2009)
- 3. André, P., et al.: Astron. Astrophys. 518, L102 (2010)
- 4. Bastian, N., et al.: Mon. Not. R. Astron. Soc. 379, 1302 (2007)
- 5. Bastian, N., et al.: Mon. Not. R. Astron. Soc. **392**, 868 (2009)
- 6. Bate, M., Bonnell, I., Bromm, V.: Mon. Not. R. Astron. Soc. 339, 577 (2003)
- 7. Bressert, E., et al.: Mon. Not. R. Astron. Soc. 409, L54 (2010)
- 8. Carpenter, J.M.: Astron. J. 120, 3139 (2000)

- 9. Casertano, S., Hut, P.: Astrophys. J. 298, 80 (1985)
- 10. Efremov, Y.N.: Astron. J. 110, 2757 (1995)
- 11. Elmegreen, B., Efremov, Y.: Astrophys. J. 466, 802 (1996)
- 12. Elmegreen, B.: Astrophys. J. **564** 773 (2002)
- Elmegreen, B., Elmegreen, D., Chandar, R., Whitmore, B., Regan, M.: Astrophys. J. 644, 879 (2006)
- 14. Elmegreen, B.: Astrophys. J. **672**, 1006 (2008)
- 15. Evans, II, N., et al.: Publ. Astron. Soc. Pac. 115, 965 (2003)
- 16. Evans, II, N., et al.: Astrophys. J. Suppl. **181**, 321 (2009)
- 17. Gieles, M., Bastian, N., Ercolano, B.: Mon. Not. R. Astron. Soc. 391, L93 (2008)
- 18. Gieles, M., Portegies Zwart, S.: Mon. Not. R. Astron. Soc. 410, L6 (2010)
- 19. Gomez, M., Hartmann, L., Kenyon, S.J., Hewett, R.: Astron. J. 105, 1927 (1993)
- 20. Gutermuth, R.A., et al.: Astrophys. J. 632, 397 (2005)
- 21. Gutermuth, R.A., et al.: Astrophys. J. Suppl. 184, 18 (2009)
- 22. Haisch, K.E. Jr., Lada, E.A., Lada, C.J.: Astrophys. J. Lett. **553**, L153 (2001)
- Heiderman, A., Evans, N.J. II, Allen, L.E., Huard, T., Heyer, M.: Astrophys. J. 723, 1019 (2010)
- 24. Hernández, J., et al.: Astrophys. J. **671**, 1784 (2007)
- Jørgensen, J.K., Johnstone, D., Kirk, H., Myers, P.C., Allen, L.E., Shirley, Y.L.: Astrophys. J. 683, 822 (2008)
- 26. Johnstone, D., Di Francesco, J., Kirk, H.: Astrophys. J. Lett. 611, L45 (2004)
- 27. Lada, C., Lada, E.: Annu. Rev. Astron. Astrophys. 41, 57 (2003)
- 28. Megeath, T., et al.: (in preparation)
- 29. Moeckel, N., Bate, M.R.: Mon. Not. R. Astron. Soc. 404, 721 (2010)
- Porras, A., Christopher, M., Allen, L., Di Francesco, J., Megeath, T., Myers, P.: Astron. J. 126, 1916 (2003)
- 31. Rebull L.M., et al.: Astrophys. J. Suppl. **186**, 259 (2010)
- 32. Scalo, J.M.: Protostars and Planets II, 201 (1985)
- 33. Strom, K.M., Strom, S.E., Merrill, K.M.: Astrophys. J. 412, 233 (1993)
- 34. Wang, J., Feigelson, E., Townsley, L., Román-Zúñiga, C., Lada, E., Garmire, G.: Astrophys. J. 696, 47 (2009)
- 35. Weidner, C., Kroupa, P. & Larsen, S.S.: Mon. Not. R. Astron. Soc. 350, 1503 (2004)
- 36. Werner, M.W., et al.: Astrophys. J. Suppl. **154**, 1 (2004)

E. Bressert et al.



Rob Jeffries

# **Uncertainties in the Age Scale for Young Open Clusters and Moving Groups**

John R. Stauffer

**Abstract** Young open clusters provide the template data for calibrating nearly all methods of age-dating field stars. Despite the potential for open cluster ages to be quite precise – and despite a large amount of observational effort – the age scale for young open clusters is still controversial, with correction factors of a factor of 2 or more proposed. I will discuss some of the causes for this uncertainty, and touch on the role of future large surveys in helping to resolve the issue.

# 1 Current Cluster Ages and Astrophysical Uncertainties

There has been no recent attempt to, for example, reanalyse all of the available data for the nearby open clusters and derive a set of "best", homogenous ages for those clusters. As a result, one can often find a range of published ages in the recent literature for even the best known clusters. Thus, there is need for improvement even at the level of creating a consistent set of "best" ages for the best known clusters. However, for most clusters, the disagreement is at the factor of two level, and often at only the 50% level. For example, the Pleiades is most often described as having an age somewhere in the 100–150 Myr range. For many purposes, simply being able to sort clusters accurately into an age order is sufficient – and that can be done pretty well.

In any case, for the youngest clusters (age < 5 Myr), a single age is sometimes an over-simplification because there are portions of the "cluster" with clearly different ages. In NGC2264, the "Spokes" (sub-) cluster is claimed to be < 100,000 years old, but "halo" members of NGC2264 are probably a few Myr old. In the Orion Nebula

156 J.R. Stauffer

Cluster, the Trapezium stars may be 1–2 Myr old, but stars are still forming in the BN/KL complex, located only 0.1 pc away (in projection anyway).

In this talk, I will describe the primary age dating techniques for open clusters and moving groups, and briefly outline why their results are uncertain. I will end with my prescription for how to improve the open cluster age scale using data that will likely be acquired in the next decade or so, primarily be the upcoming very large surveys.

### 2 Summary of Open Cluster Age Dating Techniques

The primary open cluster age dating techniques are: (a) Upper Main Sequence turn-off ages; (b) Pre-Main Sequence Turn-on ages; (c) Lithium depletion boundary; and (d) kinematic trace back. Ages can also be estimated from secondary indicators such as rotation periods, chromospheric activity indices (e.g. R'(HK)), coronal activity indices (e.g.  $L_x/L_{Bol}$ ), etc. However, these secondary indices must all be independently calibrated and those calibrations trace back to the primary techniques above.

## 2.1 Upper Main Sequence Turn-Off Ages

This is of course the most venerable of the cluster age dating techniques, with the use of the upper main sequence (UMS) turn-off point as an age indicator dating back more than 50 years [13]. It is a particularly valuable technique because it is applicable to clusters of almost any age. However, because a standard IMF provides few very high mass stars, for ages less than a few tens of Myr the method is only applicable to quite rich clusters.

Speaking as somewhat of an outsider (my own interests are relatively young clusters, where the best ages derive from techniques involving low mass stars), my own view of the UMS turn-off method is that it is in significant need of an update. The last/most-often-quoted UMS turn-off calibration paper is now almost 20 years old [10]. The primary problems contributing uncertainties to the UMS ages then – the amount of convective core overshoot and the possible dependence of this on stellar mass, and the amount of mass loss during the RGB phase – are still the primary sources of uncertainty.

Figure 1 illustrates both the good and the bad in the usage of post-main sequence evolutionary models for age-dating open clusters. The post-main sequence age for Alpha Per is 52 Myr (or less – other theoretical models generally give even younger ages). However, ages derived from fitting PMS isochrones or the lithium depletion boundary (LDB) age yield ages of 75–100 Myr for the cluster. The disagreement is less than a factor of two, but the claimed uncertainties in the UMS and LDB

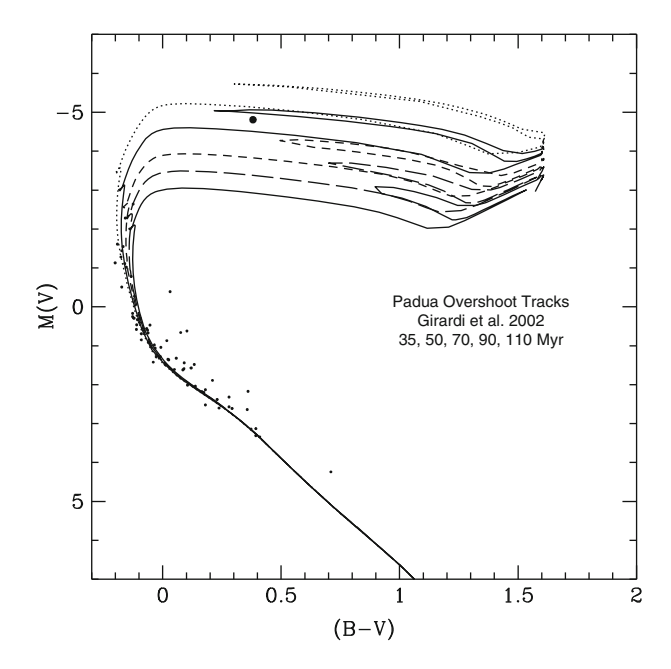


Fig. 1 Color-magnitude diagram for the Alpha Persei open cluster. The object at  $M(V) \sim -5$  is the star Alpha Per – an F supergiant. The location of stars in this part of the HR diagram is a very sensitive function of both mass and age, with this particular set of tracks yielding an age of about 52 Myr for Alpha Per the star (and hence for Alpha Per the cluster, assuming the star is indeed a member of its eponymous cluster)

ages are quite small – implying that one or both of the methods have an additional uncertainty source that is poorly handled in the current generation of models.

#### 2.1.1 Pre-Main Sequence Turn-On and Isochronal Ages

Low-mass stars take tens of millions of years to finish their contraction to the main sequence. Therefore, both the magnitude down to which stars lie on the ZAMS and the displacement of the cluster sequence above the ZAMS faintward of that point can be used as age indicators. This method has been in use for nearly 50 years [4]. The method works quite well at sorting clusters by age, with the youngest cluster being the one whose PMS isochrone lies highest above the ZAMS. However, absolute calibration is made challenging by the fact that – particularly at masses below  $0.6 \ M_{\odot}$  – the theoretical evolutionary models do not accurately yield isochrones whose shapes match empirical isochrones, at least in part due to missing opacities and inadequate treatment of convection by the theoretical models. However, it is probably also true that there are physical processes that affect the SEDs of real low mass stars that simply are not yet generally included in the theoretical models. Young, low mass stars are chromospherically active and have

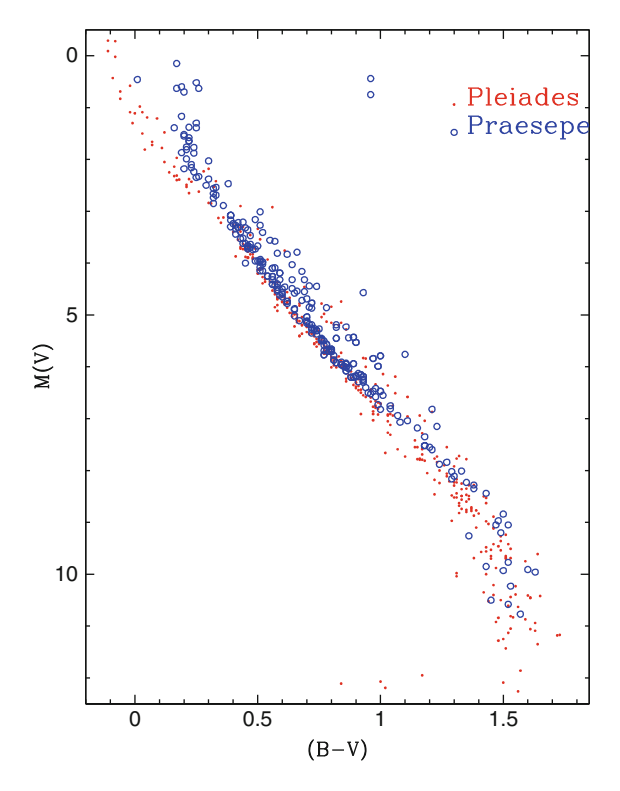


Fig. 2 Color-magnitude diagram comparing stars in the Pleiades (age =  $100 \, \text{Myr}$ ) to stars in the much older Praesepe cluster (age =  $650 \, \text{Myr}$ ). The Praesepe distance modulus has been slightly "fudged" to account for its slightly above solar metallicity. Theoretical models predict that the PMS turn-on point at  $100 \, \text{Myr}$  should occur at about M(V) = 8, and hence the Pleiades stars fainter than that should lie above the Praesepe stars. Instead, the faintest Pleiades stars lie systematically below the Praesepe stars – presumably due to spots and chromospheres causing their B-V colors to be bluer than for the older, comparatively less active Praesepe stars

heavily spotted photospheres - both of which likely make the colors of a young, low mass star different in detail from the colors of an old star of the same mass and effective temperature [16]. Related to this, the strong B fields of young, low mass stars may inhibit convection – resulting in radii and effective temperatures that differ from otherwise similar stars without such B fields [17]. Figure 2 illustrates one part of the problem – showing that the low mass stars in the 100 Myr Pleiades cluster lie **below** the ZAMS defined by the 650 Myr Praesepe cluster stars.

One approach to overcoming this difficulty is to use an empirical isochrone at one age to "tune" the theoretical isochrones and then apply the "tuned" isochrones to clusters of other ages [5]. The better solution for the future is to incorporate the additional physics into the theoretical evolutionary models.

Cluster	Isochr. age	LDB age	Reference
	(Myr)	(Myr)	
IC4665	~25	28	Manzi et al. [9]
NGC2547	~30	35	Jeffries and Oliveira [7]
IC2391	~35	50	Barrado et al. [2]
Alpha Per	50	90	Stauffer et al. [15]
Pleiades	100	130	Stauffer et al. [14]

**Table 1** Clusters with LDB age estimates as of 2010

#### 2.1.2 Lithium Depletion Boundary Ages

This method, originally proposed by [3], is based on the fact that stars below about  $0.065\,M_\odot$  never get hot enough in their cores to burn lithium, while somewhat more massive stars do eventually burn lithium – with the age for lithium ignition being younger for higher mass stars. Because all stars less massive than  $0.3\,M_\odot$  are fully convective, once lithium burns in the core it disappears from the entire star very quickly. Therefore, for the fully convective stars in an open cluster one expects the higher mass stars to show no lithium but that there will be a mass below which all stars retain essentially their primordial lithium abundance. Measurement of this lithium depletion boundary (LDB) in a color-magnitude diagram should therefore be a sensitive function of the age of the cluster. Bildsten in fact argued that the physical processes involved in this mechanism involved very few free parameters, and that the LDB should be a more reliable age estimate than either UMS or PMS isochrone fitting.

The lithium depletion boundary has now been measured in at least five clusters. A comparison of the LDB age to isochronal ages for these clusters is provided in Table 1. At young ages, the LDB and isochronal ages are in reasonable agreement, but for age > 40 Myr, the LDB ages are systematically greater by 30–50%.

There are two operational difficulties with the LDB age-dating method. The first is that the method is only applicable to clusters younger than about 250 Myr – at older ages, the location of the boundary becomes essentially invariant with age, given plausible uncertainties in the observational data. The second is that the method requires obtaining moderately high S/N, moderately high resolution spectra of intrinsically faint stars – even with 8m class telescopes, the requisite spectra can only be obtained for clusters nearer than about 500 pc. Both constraints combine to make it unlikely that a large sample of clusters will ever have their LDB age determined – and therefore one cannot establish a completely independent, LDB-based open cluster age scale. However, one can use the LDB ages as a means to calibrate better the open cluster age scale derived from other methods.

As indicated in Table 1, for age> 40 Myr, the LDB ages are systematically larger than the isochronal ages. This could simply indicate that the isochronal ages are under-estimated. However, two recent papers suggest possible physical reasons for larger than expected uncertainties in the LDB ages. Yee and Jensen [17] argue that because B fields may inhibit convection in low mass stars, the radii and

effective temperatures at a given mass and age will differ from model predictions. Therefore, even if the stellar mass of the LDB can be predicted accurately by theoretical models (as claimed by [3]), the measurables are luminosity and a T(eff) surrogate – and converting those measurables to mass may introduce significant additional uncertainties into the LDB age estimate. Baraffe and Chabrier [1] raise another issue. They show that episodic accretion during PMS evolution can lead to significantly higher central temperatures compared to stars of the same mass and age lacking such accretion. This could make the lithium depletion boundary broader or less distinct.

#### 2.1.3 Kinematic Traceback Ages

This method is not applicable to bound, open clusters – but is applicable to their cousins – young moving groups. Young moving group members are defined as being stars in the solar neighborhood sharing a similar space motion and having a common age (i.e. they were born as a group in a molecular cloud, but the gas was dispersed and the group became unbound). While by definition the members of the group have very similar space motions, it is expected that their motions will differ in detail because of the intrinsic velocity dispersion of the group before it became unbound. Therefore, if one can measure the space motions and distances of the members of a moving group very accurately, it should be possible to trace the locations in space of each star back in time. The age at which the stars were most tightly packed together should then correspond to the age of the group. (or at least the age since the group became unbound).

The advantage of this method is that its basis lies primarily in geometry and not physics. In order to integrate the motions back in time, the method also requires adopting a specific galactic stellar model. However, for relatively young clusters (age<20 Myr), the derived ages are not a strong function of the assumed model.

The group whose age can best be estimated by this method with existing data is the Beta Pic moving group (BPMG). Ortega [11] derives an age of 11 Myr for the BPMG using kinematic traceback, with an expected uncertainty of only about 1 Myr. Mamajek (priv. comm.) derives a very similar kinematic age for the BPMG. This age estimate agrees well with the PMS isochronal age for the BPMG.

A significant difficulty with the kinematic traceback method is that it requires both very accurate membership lists and very accurate observational data (space motions and distances). This difficulty is illustrated by the two published kinematic traceback ages for the TW Hydra moving group  $-8.3\pm0.8$  Myr [12] and  $4.7\pm0.6$  Myr [8]. Both age estimates claim to have very small uncertainties, but the two ages disagree strongly with each other – presumably due to inclusion of nonmembers in one or both studies or to underestimates of the uncertainties in the space motions. The other main problem with this method is that it provides an accurate cluster age only if the age when the cluster became unbound was quite small (say, less than 1-2 Myr).

# 3 The Role of Large Surveys: Towards a Better Calibration of Cluster Ages

The coming tidal wave of data derived from large ground and space-based surveys will certainly provide many possible routes to improving the open cluster age scale. This derives not only from the huge volume of data, but also from the fact that in many cases the data will be both extremely accurate and very homogenous. My current best route towards an improved age scale follows – but other paths may also be equally good.

I would start with the kinematic traceback method and GAIA data. Use the GAIA data to identify all members of the known, nearby young moving groups and accurately measure their space motions (possibly requiring use of ground-based telescopes to determine accurate new radial velocities for these stars). Hopefully, also identify several new young moving groups from analysis of the GAIA data. Derive accurate kinematic ages for these 5–10 young moving groups whose ages will presumably be in the range 10–30 Myr.

Use the GAIA photometry and distances (possibly supplemented with additional photometry from one or more all-sky surveys) to define empirical PMS isochrones for these moving groups. In the best of all worlds, use those empirical PMS isochrones to guide construction of a new set of theoretical models that provide good fits to the empirical isochrones. In a more likely real world, take the best theoretical models of the time and tune them (in a similar fashion to what was done by [5]) so that they match the empirical isochrones.

Use those calibrated PMS isochrones to then determine ages for a large number of clusters over a wider range of ages (e.g. 5–100 Myr), using distances from GAIA and photometry from GAIA, LSST, SkyMapper, Pan-STARRS, etc.

Use data from TESS or ASTRO, proposed NASA Explorer-Class missions that will target a million or more field M dwarfs for exoplanet transit searches, to determine how B fields affect the radii and T(eff) of M dwarfs, and thereby improve the empirical calibration of the LDB ages. Tie the LDB ages to the PMS ages for the clusters with both sets of data.

For all of the above clusters that are old enough and rich enough, use the PMS and LDB age estimates to calibrate the UMS models (i.e. assume the PMS/LDB ages are correct, and adopt overshoot and mass loss parameters that yield UMS turnoff ages that best match the PMS/LDB ages). Accurate UMS ages could then be determined for all of the more distant/older clusters which are not amenable to age estimates from the other techniques.

I will retire long before very much of the above can be accomplished, but I hope that the younger generation will have a good time pursuing this or a similar effort.

J.R. Stauffer

#### References

- 1. Baraffe, I., Chabrier, G., A&A, **521**, 44 (2010)
- 2. Barrado, D., Stauffer, J., Jayawardhana, R.: Astrophys. J. 614, 386 (2004)
- 3. Bildsten, L.: Astrophys. J. **482**, 442 (1997)
- 4. Herbig, G.: Astrophys. J. 135, 736 (1962)
- 5. Jeffries, R. et al.: Astron. Astrophys. **375**, 863 (2001)
- 6. Jeffries, R., Oliveira, J.: Astron. Astrophys. 375, 863 (2001)
- 7. Jeffries, R.D., & Oliveira, J.M., MNRAS, 358, 13 (2005)
- 8. Makarov, V., Gaume, R., Andrievsky, S.: Mon. Not. R. Astron. Soc. 362, 1109 (2005)
- 9. Manzi, S., Radnich, S., de Wit, W., Palla, F.: Astron. Astrophys. 479, 141 (2008)
- 10. Meynet, G., Mermilliod, J.-C., Maeder, A.: Astron. Astrophys. Suppl. 98, 477 (1993)
- 11. Ortega, V.: Astrophys. J. Lett. 575, 75 (2002)
- 12. de la Reza, R., Jilinski, E., Ortega, V.: Astron. J. 131, 2609 (2006)
- 13. Sandage, A.: Ricerche Astronomiche 5, 41 (1958)
- 14. Stauffer, J., et al.: Astrophys. J. Lett. **499**, 199 (1998)
- 15. Stauffer, J., et al.: Astrophys. J. Lett. **527**, 219 (1999)
- 16. Stauffer, J., et al.: Astrophys. J. **593**, 1093 (2003)
- 17. Yee, J., Jensen, E.: Astrophys. J. 711, 303 (2010)



John Stauffer

# **Are There Age Spreads in Star Forming Regions?**

Rob D. Jeffries

**Abstract** A luminosity spread at a given effective temperature is ubiquitously seen in the Hertzsprung–Russell (HR) diagrams of young star forming regions and often interpreted in terms of a prolonged period ( $\geq 10\,\mathrm{Myr}$ ) of star formation. I review the evidence that the observed luminosity spreads are genuine and not caused by astrophysical sources of scatter. I then address whether the luminosity spreads necessarily imply large age spreads, by comparing HR diagram ages with ages from independent clocks such as stellar rotation rate, the presence of circumstellar material and lithium depletion. I argue that whilst there probably is a true luminosity dispersion, there is little evidence to support age spreads larger than a few Myr. This paradox could be resolved by brief periods of rapid accretion during the class I pre main-sequence phase.

#### 1 Introduction

When newly born stars emerge from their natal clouds as class II and class III pre main-sequence (PMS) objects, they can be placed in a Hertzsprung–Russell (HR) diagram. Low-mass ( $<2\,\mathrm{M}_\odot$ ) stars take 10– $100\,\mathrm{Myr}$  to descend the Hayashi track and settle onto the zero-age main-sequence, so the HR diagram can be used, in combination with theoretical models, to estimate individual ages for PMS stars or construct the age distribution of a group of PMS stars. The HR diagrams of young star forming regions (SFRs) usually have an order of magnitude range of luminosity at a given effective temperature ( $T_{\rm eff}$ , see Fig. 1), and this luminosity dispersion is often interpreted as star formation that has been ongoing for  $\geq 10\,\mathrm{Myr}$  within a single

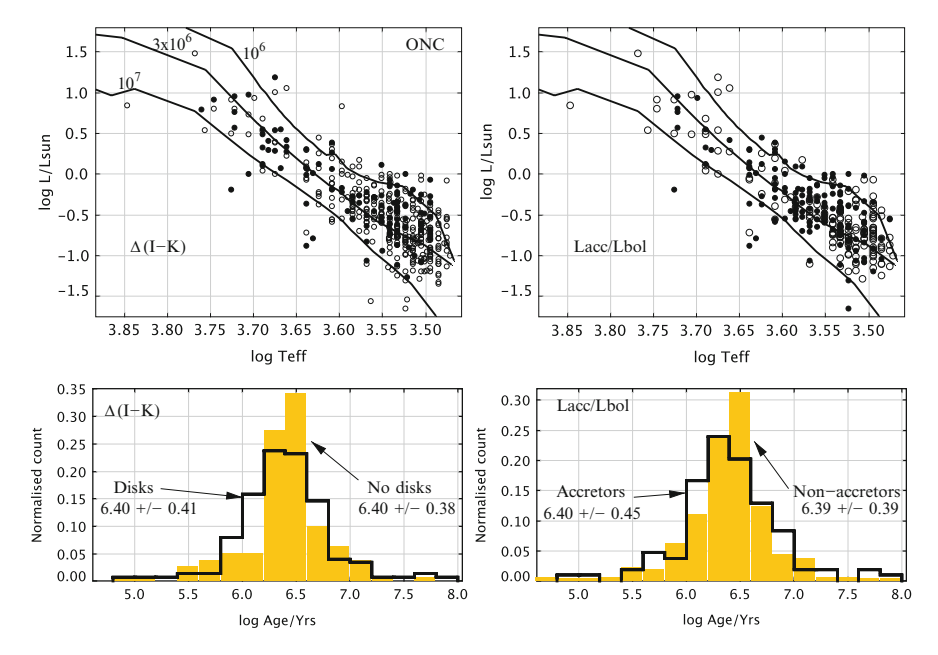


Fig. 1 The HR diagrams and inferred age distributions for samples of stars in the Orion Nebula cluster (ONC, data from [9]). (*Left*) Upper plot shows isochrones (from [31], labelled in Myr) and stars in the ONC separated by infrared excess. Open symbols are stars with  $\Delta(I-K)>0.3$  (data from [16]). Lower diagram shows the age distributions which have identical means and similar dispersions. (*Right*) A similar plot, but the open symbols are stars with  $L_{\text{accrete}}/L_{\text{bol}}>0.1$  (from [9]). Again, the lower plot shows the age distributions of these samples are very similar

SFR or young cluster (e.g. for young, nearby SFRs -[24, 25]; for massive young clusters -[3] or even for resolved star clusters in other galaxies -[8]).

The presence and extent of any age spread is an important constraint on models of star formation. A significant (≥10 Myr) spread would favour a "slow" mode, where global collapse is impeded by, for example, a strong magnetic field (e.g. [33]. Age spreads that were ≤1 Myr however, could be explained by the rapid dissipation of turbulence and star formation on a dynamical timescale (e.g. [10]). The reality or not of age spreads is also important from a practical point of view. Ages from the HR diagram are used to understand the progression of star formation (e.g. triggering scenarios, collect-and-collapse models) and the age-dependent masses estimated from an HR diagram are usually the only way of determining the initial mass function. In this short review, I ask:

- 1. Are the luminosity spreads (at a given  $T_{\text{eff}}$ ) in the HR diagram real?
- 2. If so, do these necessarily imply a wide spread of ages within an individual SFR?

### 2 Luminosity Spreads?

Hartmann (2001) identified many sources of astrophysical and observational scatter that contribute to an *apparent* spread in the luminosities of PMS stars at a given  $T_{\rm eff}$ . These include the likelihood that many "stars" are unresolved multiples; that individual stars may be subject to a range of extinction and reddening; that PMS stars can be highly variable; that the luminosity contributed by accretion processes could vary from star-to-star; that in (nearby) SFRs the stars are at a range of distances; and that placing stars on a HR diagram requires temperature (or spectral type or colour) and luminosity (brightness) measurements which have observational uncertainties. Hartmann concluded that efforts to infer star formation histories would be severely hampered by these effects and that the luminosity and hence age spreads claimed by [25], among others, must be extreme upper limits. [17] showed that it is difficult to verify or indeed quantify luminosity spreads, and hence infer age spreads, unless (a) observational uncertainties are small and (b) both the *size and distribution* of other astrophysical sources of luminosity dispersion are well understood.

One approach to tackle these difficulties is to quantify spreads that could be contributed by individual sources of dispersion and model the outcome. [5] used photometric measurements at more than one epoch to empirically assess the affects of variability on two young SFRs ( $\sigma$  Ori and Cep OB3b) with significant (compared to observational uncertainties) scatter in their colour-magnitude diagrams (CMDs). This approach takes account of correlated variability in colours and magnitudes and the non-Gaussian distribution of variability-induced dispersion. A coeval population was simulated using the observed levels of variability, the likely effects of binarity and observational errors. This model was found to significantly underpredict the observed dispersion. In other words, variability (on timescales of years or less), binarity and observational error could only account for a small fraction of the luminosity dispersion. On the other hand, [32] examined the slightly older Upper Sco SFR and showed that the large observed luminosity spreads could perhaps be entirely explained by a coeval population affected by a combination of observation errors, distance dispersion and binarity. However, the additional dispersion (particularly due to distance uncertainties) was so large in this case that additional scatter equivalent to a real age dispersion of  $\pm 3$  Myr remained a possibility.

A more sophisticated statistical approach has been taken by [8] who, using a maximum likelihood method akin to that proposed by [23], fitted a 2-dimensional synthetic surface density to the CMD of a SFR in the Large Magellanic Cloud. The model includes contributions from unresolved binarity, variability, differential extinction and accretion. These authors conclude that the luminosity spread in the CMD is too large to be accounted for by the "nuisance" sources of dispersion and interpret the additional scatter as a spread in ages of FWHM 2.8–4.4 Myr.

An alternative for investigating the reality of the luminosity dispersions is to examine proxies such as radius or gravity that would be expected to show a

corresponding dispersion, but whose measurement is not so greatly affected by the additional astrophysical sources of scatter. An example is the use of rotation periods and projected equatorial velocities to estimate the projected radii,  $R \sin i$ , of PMS stars in the Orion Nebula cluster (ONC, [19]). These measurements are largely unaffected by binarity, variability, differential extinction, distance or accretion. Assuming that spin-axes are randomly oriented, the distribution of  $R \sin i$  can be modelled to estimate mean radii and the extent of any true spread in radius at a given  $T_{\rm eff}$ . The results confirm that a factor of 2–3 (FWHM) spread in radius exists at a given  $T_{\rm eff}$  and this concurs with the order of magnitude luminosity spread seen in the HR diagram of the same objects.

In summary, although there are few detailed investigations to draw on, the evidence so far suggests that the luminosity spreads seen in SFRs are mostly genuine. Only a fraction of the dispersion can be explained by observational uncertainties, variability, binarity and accretion.

## 3 Age Spreads?

If the luminosity dispersions are genuine, then it is natural to plot a set of HR diagram isochrones, estimate an age for each star and hence infer an age distribution. However it is possible that physical causes other than age could contribute to a real dispersion of luminosity in the HR diagram of young PMS stars. Accretion could perturb the evolution of the central star, inducing a luminosity spread even in a coeval population [34]. To investigate the fidelity of ages deduced from the HR diagram we can compare these ages with those estimated using independent clocks. These include the depletion of photospheric lithium, the evolution of stellar rotation and the dispersal of circumstellar material.

# 3.1 Lithium Depletion

Lithium is ephemeral in the photospheres of young, low-mass stars. Once the central temperature of a star reaches the Li ignition temperature, ( $\sim$ 2.5 × 10<sup>6</sup> K) convective mixing leads to almost complete Li depletion unless the PMS star leaves the Hayashi track and develops a radiative core (see [18]). In principle the level of Li in the atmosphere of a low-mass PMS star is a mass-dependent clock. Palla et al. [26] and Sacco et al. [30] have searched for Li-depleted stars that are bona-fide members of the Orion Nebula cluster and the  $\sigma$  Ori and  $\lambda$  Ori associations. They do find a few such objects (a few per cent of the total) and using models for Li depletion, infer ages for them of >10 Myr, compared to HR diagram ages of 2–5 Myr for the bulk of the PMS population. These observations are consistent with the presence of a small fraction of older objects, co-existing with the bulk of the younger PMS population, arguing in favour of a large age spread.

Whilst this interpretation is possible, there are some problems. First, the bimodal distribution of Li abundances (i.e. most stars are undepleted with a small fraction of extremely Li-depleted objects) does not seem consistent with a smooth underlying distribution of ages and indeed contamination by older, non-members of the cluster has been suggested [27]. Second, although in some (but not all) cases, the Li-depletion age for these stars matches the HR diagram age, they are *not* fully independent age indicators. The central temperature of the star, which controls the Li-burning, will depend on the stellar radius (and hence luminosity in the HR diagram). If for some reason the star had a smaller radius than expected at a given age and therefore appeared older in the HR diagram, its central temperature would *also* be higher and it would have a greater capacity to burn Li.

#### 3.2 Rotation Rates

Young, PMS stars typically rotate with periods of 1–10 d. There is strong evidence that PMS stars with circumstellar disks and active accretion rotate more slowly on average than those without disks (e.g. [7,29]). A widely accepted idea is that stars which are accreting from a disk are braked by the star-disk interaction and held at a roughly constant spin period [28]. Once the disk disperses, or below some threshold accretion rate, the brake is released and the star spins up as it rapidly contracts along the Hayashi track. Thus, the rotation rate of PMS stars should broadly reflect the age of the population – an older population should have fewer strong accretors (see Sect. 3.3), have had more time to spin-up, and hence should contain a greater proportion of fast rotators than a younger population. As the lifetime of accretion is of order a few Myr, then age spreads of 10 Myr should manifest themselves as big differences in the rotation period distributions of the "older" and "younger" populations.

This rotation clock has been investigated by [21]. They divided the PMS populations of several nearby SFRs into "old" (low luminosity) and "young" (high luminosity) samples and compared their rotation period distributions. The null hypothesis that the samples were drawn from the same distribution could be rejected at high significance levels, but the surprising result is that the faster rotating sample is actually the one containing the "young" objects. If the luminosity spreads were truly caused by an age spread, the "disk-locking" model would predict the opposite result. Littlefair et al. interpret this by assuming the populations in each SFR are coeval, but the luminosity spreads are introduced through differing accretion histories which also influence the stellar rotation rate (see Sect. 4).

# 3.3 Disk Dispersal

It is well known that the lifetime of circumstellar material around young PMS stars, traced by the fraction of objects exhibiting infrared excesses or accretion

diagnostics, is on average a few Myr (e.g. [6, 12, 15, 20]). The precise reasons for disk dispersal are still unclear, but if the fraction of stars accreting strongly from a circumstellar disk does decrease with age then we would expect to see fewer active accretors among any older population within a single SFR.

Surprisingly little work has been done in this area. Hartmann et al. (1998) found that mass accretion rates did decline with increasing HR diagram age in Taurus and Chamaeleon. Bertout et al. [4] claimed that accreting classical T-Tauri stars in Taurus appeared significantly younger in the HR diagram than their weak-lined, non-accreting counterparts. On the other hand, Hillenbrand et al. (1998) find no correlation between age and the fraction of PMS stars in the ONC with near-infrared excesses. These studies are difficult because they are afflicted by a number of biases and selection effects.

In preparation for this review I examined a new catalogue of sources in the ONC by [9], which they claim to be complete to very low luminosities. They have estimated the luminosity and effective temperature of stars using a careful star-by-star estimate of accretion luminosity and extinction. Their catalogues give estimated masses and ages based on the models of [31]. Figure 1 shows HR diagrams and deduced age distributions, where the samples have been divided according to (a) whether the I-K excess over a photospheric colour is >0.3 (data from [16]) or (b) whether the accretion luminosity is >0.1  $L_{\rm bol}$ . Neither of these accretion/disk diagnostics shows a significant age dependence within the ONC, the mean ages and age distributions of the subsamples are indistinguishable. I am currently exploring any possible biases (e.g. dependences of age and the likelihood of possessing a disk on position within the cluster) that might explain these results.

Taking the results at face value suggests either: (i) Any true age spreads are much less than the few Myr characteristic timescale for the cessation of accretion and dispersal of circumstellar material and that a star's position in the HR diagram *is not* primarily age dependent. (ii) The scatter in the luminosities caused by the nuisance sources discussed in Sect. 2 is so large that it erases the expected age-dependent decrease in the fraction of stars exhibiting accretion or disk signatures. For the reasons discussed in Sect. 2 I regard this latter possibility as unlikely. In either case (i) or (ii) it would mean that the HR diagram could not be used to claim a large age spread or to estimate the star formation history.

# 4 Episodic Accretion: A Possible Explanation

The idea that early accretion could alter a PMS star's position in the HR diagram and make it appear older have been around for some time (e.g. [22, 34]). Recently it has been realised (e.g. by [11]) that accretion onto very young stars may be transient or episodic, with very high accretion rates ( $\sim 10^{-4} \, \mathrm{M_\odot} \, \mathrm{yr^{-1}}$ ) occurring for brief periods of time ( $\sim 100 \, \mathrm{yr}$ ). "Episodic accretion", which would take place during the early class I T-Tauri phase, has been modelled by [35] and its consequences for the PMS HR diagram are explored by [2]. They find that if the accreted energy

is efficiently radiated away, then a short phase of rapid accretion compresses the PMS star, leading to a smaller radius and lower luminosity. The star will not relax back to the configuration predicted by non-accreting models for a thermal timescale ( $\simeq 20\,\mathrm{Myr}$  for the PMS stars I am discussing), and hence interpreting the HR diagram using non-accreting models would lead to erroneously large ages. A distribution of accretion histories in a coeval SFR could lead to a luminosity spread and the appearance of an age spread. As there may be no connection between accretion rates in the class I phase and later accretion as a class II T-Tauri star this could effectively randomise the ages determined from the HR diagram for young class II and class III PMS stars.

The model may also account for the apparent spin-down of PMS stars with age and for the small proportion of stars which appear to have anomalously high Li depletion. A PMS star with a true age of say 3 Myr, that had been subjected to relatively slow accretion rates during the class I phase would have contracted over 3 Myr from a larger radius and spun-up significantly. A coeval PMS star that had previously accreted at much high rates would already be smaller, less luminous and appear older, but would be relaxing back to its equilibrium configuration on a 20 Myr timescale and so would have undergone very limited contraction and spin-up (Littlefair et al. 2010). The same stars would have smaller radii and higher central temperatures than their slow-accreting counterparts and could therefore burn Li more readily [1].

#### 5 Conclusions

The evidence to date suggests that the luminosity dispersion seen in the HR diagrams of young SFRs has a significant component that cannot be attributed to "nuisance" sources such as binarity, variability and accretion. However, attempts to verify the consequent age spreads implied by the positions of PMS stars in the HR diagram have mixed success. In particular, the rotation rates of PMS stars and the fraction of stars showing active accretion or evidence for circumstellar material within a single SFR do not show the expected decrease with age. "Episodic accretion" potentially resolves this paradox – a very high rate of accretion during the class I phase could drive PMS stars out of equilibrium and towards smaller radii and lower luminosities. A distribution of early accretion rates would effectively scramble ages determined from the HR diagram for a population of class II and class III PMS stars.

If this scenario is borne out by further work, then the traditional HR diagram is a poor tool for estimating the ages of young (<20 Myr) PMS stars and also perhaps for estimating age-dependent masses. Large scale survey work may instead have to rely on less precise but potentially more accurate clocks such as rotation rates or the presence of circumstellar material, although of course these may not be universal and could have significant environmental dependencies.

170 R.D. Jeffries

#### References

- 1. Baraffe, I., Chabrier, G.: Astron. Astrophys. **521**, A44 (2010)
- 2. Baraffe, I., Chabrier, G., Gallardo, J.: Astrophys. J. 702, L27 (2009)
- 3. Beccari, G. et al.: Astrophys. J. 720, 1108 (2010)
- 4. Bertout, C., Siess, L., Cabrit, S.: Astron. Astrophys. 473, L21 (2007)
- Burningham, B., Naylor, T., Littlefair, S.P., Jeffries, R.D.: Mon. Not. R. Astron. Soc. 363, 1389 (2005)
- Calvet, N., Briceño, C., Hernández, J., Hoyer, S., Hartmann, L., Sicila-Aguilar, A., Megeath, S.T., D'Alessio, P.: Astron. J. 129, 935 (2005)
- 7. Cieza, L., Baliber, N.: Astrophys. J. **671**, 605 (2007)
- 8. Da Rio, N., Gouliermis, D.A., Gennaro, M.: Astrophys. J. 723, 166 (2010)
- 9. Da Rio, N., Robberto, M., Soderblom, D.R., Panagia, N., Hillenbrand, L.A., Palla, F., Stassun, K.G.: Astrophys. J. **722**, 1092 (2010)
- 10. Elmegreen, B.G.: Astrophys. J. **530**, 277 (2000)
- 11. Enoch, M.L., Evans, N.J., Sargent, A.I., Glenn, J.: Astrophys. J. 692, 973 (2009)
- 12. Haisch, K. Jr., Lada, E.A., Lada, C.J.: Astrophys. J. 553, L153 (2001)
- 13. Hartmann, L.W.: Astron. J. 121, 1030 (2001)
- 14. Hartmann, L., Calvet, N., Gullbring, E., D'Alessio, P.: Astrophys. J. 495, 385 (1998)
- Hernández, J., Hartmann, L., Calvet, N., Jeffries, R.D., Gutermuth, R., Muzerolle, J., Stauffer, J.: Astrophys. J. 686, 1195 (2008)
- Hillenbrand, L.A., Strom, S.E., Calvet, N., Merrill, K.M., Gatley, I., Makidon, R.B., Meyer, M.R., Skrutskie, M.F.: Astron. J. 116, 1816 (1998)
- 17. Hillenbrand, L.A., Bauermeister, A., White, R.J.: In: van Belle, G. (ed.) 14th Cambridge Workshop on Cool Stars, Stellar Systems and the Sun, ASP Conference Series, vol. 384, 200. San Francisco (2008)
- 18. Jeffries, R.D.: In: Randich, S., Pasquini, L. (eds.) Chemical Abundances and Mixing in Stars in the Milky Way and its Satellites, p. 163. Springer, Heidelberg (2006)
- 19. Jeffries, R.D.: Mon. Not. R. Astron. Soc. 381, 1169 (2007)
- Jeffries, R.D., Oliveira, J.M., Naylor, T., Mayne, N.J., Littlefair, S.P.: Mon. Not. R. Astron. Soc. 376, 580 (2007)
- Littlefair, S.P., Naylor, T., Mayne, N.J., Saunders, E., & Jeffries, R.D., MNRAS, 413, 56L (2011)
- 22. Mercer-Smith, J.A., Cameron, A.G.W., Epstein, R.I.: Astrophys. J. 279, 363 (1984)
- 23. Naylor, T., Jeffries, R.D.: Mon. Not. R. Astron. Soc. 373, 1251 (2006)
- 24. Palla, F., Stahler, S.: Astrophys. J. **525**, 772 (1999)
- 25. Palla, F., Stahler, S.: Astrophys. J. **540**, 255 (2000)
- 26. Palla, F., Randich, S., Flaccomio, E., Pallavicini, R.: Astrophys. J. 626, L49 (2005)
- 27. Pflamm-Altenburg, J., Kroupa, P.: Mon. Not. R. Astron. Soc. **375**, 855 (2007)
- 28. Rebull, L.M., Wolff, S.C., Strom, S.E.: Astron. J. 127, 1029 (2004)
- Rebull, L.M., Stauffer, J.R., Megeath, S.T., Hora, J.L., Hartmann, L.: Astrophys. J. 646, 297 (2006)
- Sacco, G., Randich, S., Franciosini, E., Pallavicini, R., Palla, F.: Astron. Astrophys. 462, L23 (2007)
- 31. Siess, L., Dufour, E., Forestini, M.: Astron. Astrophys. **358**, 593 (2000)
- 32. Slesnick, C.L., Hillenbrand, L.A., Carpenter, J.M.: Astrophys. J. 688, 377 (2008)
- 33. Tassis, K., Mouschovias, T.Ch.: Astrophys. J. 616, 283 (2004)
- 34. Tout, C.A., Livio, M., Bonnell, I.A.: Mon. Not. R. Astron. Soc. 310, 360 (1999)
- 35. Vorobyov, E.I., Basu, S.: Astrophys. J. **650**, 956 (2006)

# The Relevance of X-ray Surveys for the Study of the Properties of Young Open Clusters

Giusi Micela

Abstract Pre-main sequence solar-type stars are at least three order of magnitude more X-ray luminous than mid-aged stars such as the Sun, making X-ray surveys a very powerful tool to study young stars. Specifically X-ray observations of star forming regions or young open clusters are very effective to identify cluster members among the huge number of older field stars present in the same sky region. This capability is very useful in particular to select stars that have already dissipated their disks (weak line type or Class III stars), that cannot be identified with more traditional means such as infrared surveys. As a consequence X-ray surveys are crucial to obtain complete samples needed for the study of global properties of the clusters, such as Initial Mass Functions (IMF) and disk frequency. I will present some examples of such studies with special emphasis on the role of X-ray observations.

#### 1 Introduction

High energy phenomena are common during star formation and at young age. In fact X-ray luminosity decays by 3–4 order of magnitudes from the Pre Main Sequence (PMS) phase to the solar age (e.g. [13]), with most of the evolution occurring starting from the Zero Age Main Sequence (ZAMS).

The evolution of stellar coronal emission is strictly linked to the rotational history of the stars. In fact the X-ray emission is produced by hot plasma in stellar coronae, generated by a dynamo powered by stellar rotation. In turn, winds, channelled by coronal magnetic fields, are responsible for the magnetic braking and for the consequent angular momentum evolution. The star spins down and X-ray emission

G. Micela (⋈)

172 G. Micela

decreases with a continuous feedback mechanism. During this evolution also the corona itself evolves, becoming colder and less dynamical.

In addition to the effects on physics of the outer atmosphere and stellar rotation, the coronal evolution produces important effects in the stellar neighborhood and has important implication for the studies of young stellar populations. For example, during the PMS phase, the copious high energy emission produced by the star ionizes the circumstellar disk, modifying its physical conditions, affecting its evolution and the subsequent planetary formation. Furthermore in the more evolved phase the intense X-ray emission may heat or even (partially) evaporate the atmospheres of close planets [14, 16].

Another important consequence of high activity level of young stars, relevant for the theme of this paper, is the capability of X-ray observations to identify young stars. Indeed, thanks to their intense X-ray emission, young stars dominate the stellar population observed in shallow or intermediate X-ray surveys, specially in the direction of star forming regions.

## 2 X-ray Data of Clusters and Star Forming Regions

The discovery of the relevance of X-ray observations for the study of young stars dates at eighty. The first decade, the Einstein and Rosat age, was a period of discoveries. Most of the star forming regions and clusters within 200 pc were observed. The intense X-ray emission of young stars and their strong variability was observed and the population of Weak line T Tauri Stars (WTTS – pre-main sequence stars with no strong emission lines) was identified for the first time (e.g. [21]).

In the last decade, stellar X-ray astrophysics has entered in a more mature phase: thanks to the large area of XMM and the superb angular resolution of Chandra, it has been possible to probe clusters and massive SFRs up to few kpc, exploring a much larger parameter space, and detecting stars over a larger mass range. The two observatories are very complementary. In fact the large effective area of XMM/Newton makes possible spectral and time analyses relevant for the study of origin of X-ray emission, while the exceptional high spatial resolution of Chandra (fraction of arcsec in the central area of the field of view) allows us to study unambiguously weak sources in very crowded areas as the massive SFRs.

Major results have been obtained on:

- SFR and open cluster morphologies
- · Age spreads and sequential star formation
- Disk frequency
- · Mass segregation
- · Stellar initial mass function

A significant fraction of the exposure time of Chandra and XMM/Newton has been devoted to young star science, with a few large projects dedicated to specially interesting regions. The archives of the two satellites contain now a large number of observations of open clusters and star forming regions, some still not fully exploited.

In the following I will illustrate a couple of examples of X-ray observations to elucidate how the stellar population studies of star forming regions and young open clusters may take advantage of X-ray observations.

## 3 Disk Frequency in Massive Star Formation Regions: The Case of NGC 6611

In this section I will present the study of disk frequency as a function of the environment conditions. In particular I will discuss the analysis of the role of UV radiation from massive stars in evaporating circumstellar disks around nearby stars in NGC 6611, a cluster in the center of the complex of the Eagle nebula.

The region has been studied adopting a multiwavelength approach, with different bands probing different components of stellar systems. In particular the optical band allows determining the stellar properties, infrared observations are the tool to identify disks, and X-rays are used as membership criterion since, as we discussed above, essentially all the X-ray stellar sources in the direction of a SFR may be considered cluster members. We note that X-rays are the most effective way to identify disk-less members that do not present any infrared excess.

Three X-ray observations have been obtained with Chandra (PI: Guarcello). Stars detected in X-rays with optical photometry consistent with the cluster distance and age have been selected as candidate members. Those without NIR excess are our disk-less members, for a total of 1117 selected stars. Their spatial distribution follows very clearly the structure of the cluster [9].

Since disk-less stars have purely photospheric colors, without any contamination due to the presence of a disk, they are an ideal population to determine the main properties of the cluster. Therefore using this sample we have determined a cluster distance of 1,750 pc, an age in the 1–3 Myr range, an average absorption  $< Av > \sim 2.6$  and a core radius of 1.3 pc [7].

Having identified stars with and without disk we are able to derive, in principle without biases, the frequency of disks. Since we want to explore the effect of massive stars on circumstellar disks of low-mass members, we have computed the UV flux emitted from OB stars incident on low-mass members with and without disk. Then we have computed the disk frequency as a function of the incident UV flux. Figure 1 is the resulting histogram in four UV flux bins, where bin size has been chosen to have comparable statistics. While the disk frequency is consistent with being constant in the first three bins, a decrease of disk frequency for the bin at the highest flux is evident. We consider this decrease as the evidence of disk photoevaporation induced by massive stars, that at the NGC 6611 age appears to be relevant up to a distance of 1 pc from the massive stars (the typical distance from an OB star corresponding to the highest UV flux bin).

174 G. Micela

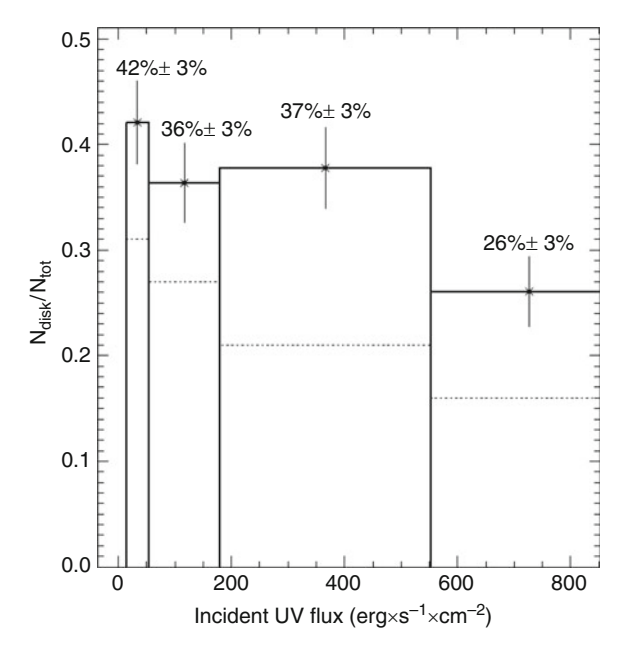


**Fig. 1** Histogram of disk frequency for four bins of different UV incident flux produced by massive stars. Solid line is obtained using Spitzer data, while *dotted line* are data obtained in [7] based only on JHK data. Bin size has been chosen to have comparable statistics in each bin (from [9]

With the multiwavelenght approach outlined above, we have derived a number of results for NGC 6611. In particular the X-ray membership criterion applied to NGC 6611, has allowed us to:

- Identify disk-bearing and disk-less YSOs in the whole Eagle Nebula.
- Observe disk photoevaporation in NGC 6611 close to OB stars (d <1 pc). Photoevaporation is independent from the stellar mass.
- Identify a large scale age gradient with a chronology of star formation in M16 incompatible with large-scale star formation triggering by OB stars.

These results are reported in [7–9].

## 4 Star Formation in the Outer Galaxy

In this section I will present another case in which the X-ray observations have a critical role in assessing the population properties of a young SFR. In particular I will present a project focused on NGC 1893 aiming at studying the processes of star formation in the outer Galaxy.

NGC 1893 is a young cluster at about 12 kpc from the Galactic Center. The region is fairly rich of massive stars [11, 12, 19], with indication of a large PMS

population [17, 20]. Its properties make NGC 1893 a very good target to study the star formation processes in the outer Galaxy, where the conditions should be less conducive to star formation than in the solar neighborhood or in the inner Galaxy: the interstellar radiation field is weaker, prominent spiral arms are lacking and there are fewer supernovae to act as external triggers of star formation. Metal content is, on average, smaller, decreasing radiative losses and therefore increasing cloud temperatures and consequently pressure support.

We have studied the region adopting, as in the case of NGC 6611, a multiwavelength approach, in which different energy bands probe different components of the stellar systems. Also in this case the optical band is used to determine the stellar properties, infrared observations are the tool to measure the disk properties and Xrays are used as membership criterion. In particular we have collected the following observations

- Dolores@TNG:4 (8.6 × 8.6) fields V(10–1000 s), R(10–700 s), I(10–1480 s),  $H\alpha(60-1400 s)$
- Cafos@CalarAlto: 1 (16) field V(15–1500s), R(10–600s), I(10–1500s),  $H\alpha(10-1500s)$
- NICS@TNG:16 (4.2×4.2) fields J(500s), H(600s), K(700s)
- ACIS@Chandra: 17×17 field (0.5–8.0 keV), 450 ksec
- IRAC@Spitzer: mosaic of 26×30 at 3.6, 4.5, 5.8, 8.0

Infrared observations show that the region is rich of star with excesses, indicating the presence of a large population of disk-bearing stars. Figure 2 shows the color-color Spitzer diagram for the stars in the region. Circles identify counterparts of X-ray sources, that occupy both the regions typically populated by Class II and Class III stars, while triangles mark class I stars [3].

X-ray detections have been used to identify cluster members, and those without any excess in infrared have been classified as Class III members. The emission of these stars is exclusively photospheric, implying that their position in the HR diagram is uncontaminated by any other contributions. Therefore the Class III sample may be used, as in the NGC 6611 case, to derive the cluster parameters that will be unaffected by the typical problems related to the disk and/or accretion presence. Figure 3 shows the HR diagram, where the Class III stars clearly mark the cluster locus.

Main results from the analysis of this project include:

- The confirmation that NGC 1893 is a rich cluster with a conspicuous population of PMS stars with 1057 members with circumstellar disk and 391 diskless members [15].
- The derivation of the mean cluster reddening  $E(B-V) = 0.6 \pm 0.1$ , and the cluster distance  $d = 3600 \pm 200$  pc. Note that previous literature values were very uncertain, in a (3,250-6,000) pc interval.
- Class II and III YSOs show very similar age and mass distributions.
- We estimate a disk fraction of about 70% in agreement with that found in cluster of similar age [10].

176 G. Micela

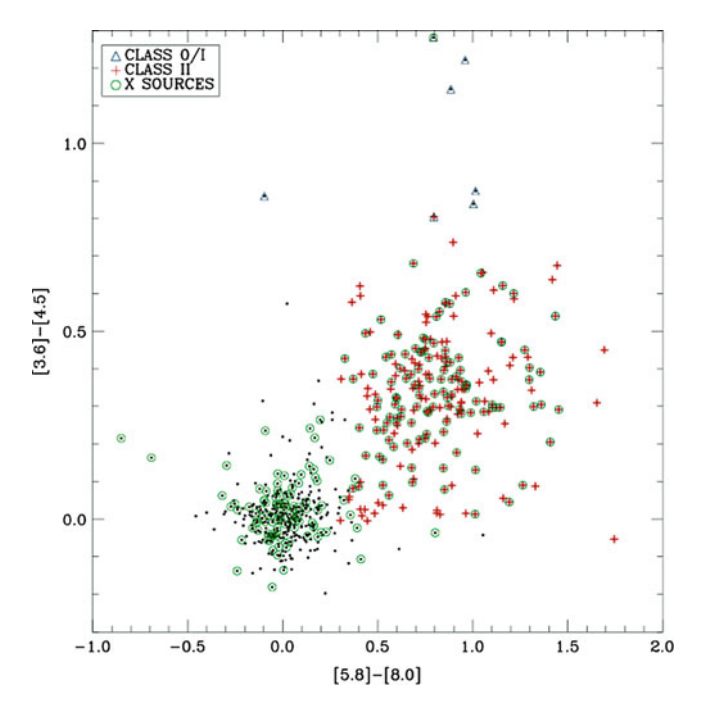


Fig. 2 IRAC col-col diagram: 116 Class II stars identified. Large symbols mark X-ray members [3]

The work is still ongoing and we plan to derive in the next future the Mass Function of the cluster to be compared with that obtained for nearby, coeval clusters. Also for this goal the X-ray selection is a precious tool for a complete member census.

## 5 Disk Frequency in Young Clusters

The results derived from several authors on disk frequency at young age strongly rely on the selection method for disk- and disk-less members. Several diagnostics exist to identify the disk presence or accretion (near infrared for inner disk, far infrared for outer disk,  $H\alpha$ , or UV excess for accretion, etc) that may be not completely consistent. In order to compare different clusters to study age evolution or environment effects, it is needed a uniform disk/accretion indicator. In any case, the class III indicator is always based on X-ray observations.

Table 1 shows a selection of results obtained from several SFRs where column 3 indicates the method used for disk detection. In all the cases X-rays have been used to select Class III stars. Even considering the inhomogeneity of the used methods few peculiar cases with very low disk frequency may be noted. We noticed in

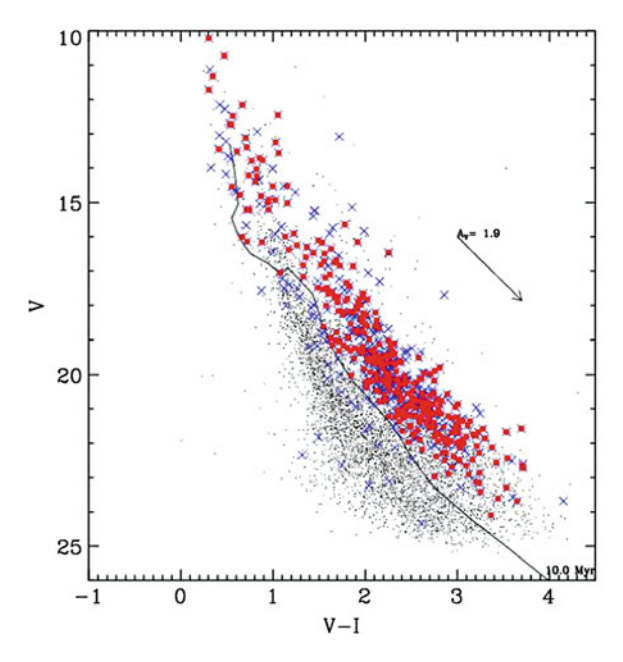


Fig. 3 H-R diagram of NGC 1893: *blue* symbols mark X-ray detections, *red points* are X-ray detections without NIR excess (Class III members – 391 stars). [15]

Table 1 Summary of disk frequency for several clusters. Boldface percentage indicate the cases with anomalous low disk frequency

Names	Age (My)	Disk indicators	Disk frequency (%)	Reference
ONC	1	near-IR, M>1 M <sub>☉</sub>	20.6	[1]
NGC 6611	1	near-IR, M>0.5 ${\rm M}_{\odot}$	35	[9]
Cyg OB2	2	near-IR, M>1 M <sub>☉</sub>	4.4	[2]
NGC 6530	2-3	near-IR, M>0.5 $M_{\odot}$	20	[4]
Tr 16	3	near-IR, M>0.5-1 $M_{\odot}$	15	[1]
NGC 2264	3	Spitzer	38	[18]
NGC 1893	3	near-IR	70	[15]
NGC 2362	5	$H\alpha$ (IR)	5 (12)	[5]
NGC 6231	5–7	near-IR, M>1 Msun	4	[6]

particular the very low disk fraction in Cyg OB2, very rich of massive stars. Other cases with low disk frequency are: NGC 6231, a slightly older cluster that seem to have stopped the star formation process, and NGC 2362, a cluster of similar age, characterized by a short episod of star formation. We stress that in all the cases the class III stars are a substantial fraction of , and in a few cases dominate, the stellar populations in these SFRs.

178 G. Micela

## 6 Summary

In this paper I have discussed some examples of the role of X-ray observations for the study of the low-mass stellar population in young open clusters. In particular I focused on the analysis of disk frequency, for which X-rays are the only tool to select disk-less stars. However this was just an example, in all the cases for which completeness is an issue X-ray observations have an unique role. Examples include the study of the Initial Mass Function, the morphology, the dynamical evolution, the mass segregation, and the star formation history.

Likely only with the exploitation of Gaia data and its capability to measure accurate distances and proper motions, it will be possible to use an alternative method, based on kinematics. However X-rays may be still used to eliminate the residual field contamination.

Chandra and XMM/Newton are doing an excellent job in producing high quality X-ray data of open clusters and SFRs. A wealth of observations are already available (some still to be analyzed), and constitute a precious instrument for the study of star forming regions.

**Acknowledgements** The author acknowledges support by the EC MC RTN CONSTELLATION (MRTNCT2006035890) and by the PRIN-INAF (P.I. Lanza).

## References

- 1. Albacete Colombo, J.F., Damiani, F., Micela, G., et al.: Astron. Astrophys. 490, 1055 (2008)
- 2. Albacete Colombo, J.F., Flaccomio, E., Micela, G., et al.: Astron. Astrophys. 464, 211 (2007)
- 3. Caramazza, M., Micela, G., Prisinzano, L., et al.: Astron. Astrophys. 488, 211 (2008)
- 4. Damiani, F., Prisinzano, L., Micela, G., Sciortino, S.: Astron. Astrophys. 459, 477 (2006)
- 5. Damiani, F., Micela, G., Sciortino, S., et al.: Astron. Astrophys. 460, 133 (2006)
- Damiani, F., Micela, G., Sciortino, S., Harnden, F.R. Jr.: In: Cool Stars, Stellar Systems and the Sun, AIP Conference Proceedings, vol. 1094, 916 (2009)
- 7. Guarcello, M., Prisinzano, L., Micela, G., et al.: Astron. Astrophys. 462, 245 (2007)
- 8. Guarcello, M., Micela, G., Damiani, F., et al.: Astron. Astrophys. 496, 453 (2009)
- 9. Guarcello, M., Micela, G., Peres, G., et al.: Astron. Astrophys. 521, 61 (2010)
- 10. Haisch, K.E.Jr., Lada, E.A., Lada, C.J.: Astron. J. 121, 2065 (2001)
- 11. Marco, A., Bernabeu, G., Negueruela, I.: Astron. J. 121, 2075 (2001)
- 12. Massey, P., Johnson, K.E., Degioia-Eastwood, K.: Astrophys. J. 454, 151 (1995)
- Micela, G.: In: Montesinos, B., Gimenez, A., Guinan, E.F. (eds.) ASP Conference Proceedings, vol. 269, p. 107 (2002)
- 14. Penz, T., Micela, G.: Astron. Astrophys. 479, 579 (2008)
- 15. Prisinzano, L., Sanz Forcada, J., Micela, G., et al., A&A, 527, 77 (2011)
- 16. Sanz Forcada, J., Ribas, I., Micela, G., et al.: Astron. Astrophys. 511, L8 (2010)
- 17. Sharma, S., Pandey, A.K., Ojha, D.K., et al.: Mon. Not. R. Astron. Soc. 380, 1141 (2007)
- 18. Sung, H., Stauffer, J.R., Bessell, M.S.: Astron. J. **138**, 1116 (2009)
- 19. Tapia, M., Costero, R., Echevarria, J., Roth, M.: Mon. Not. R. Astron. Soc. 253, 649 (1991)
- 20. Vallenari, A., Richichi, A., Carraro, G., Girardi, L.: Astron. Astrophys. 349, 825 (1999)
- 21. Walter, F.M.: Publ. Astron. Soc. Pac. 99, 31 (1987)

## **Chandra Observations of Cygnus OB2**

Nicholas J. Wright, Jeremy J. Drake, Janet E. Drew, and Jorick S. Vink

**Abstract** Cygnus OB2 is the nearest example of a massive star forming region, containing over 50 O-type stars and hundreds of B-type stars. We have analyzed two Chandra pointings in Cyg OB2, detecting  $\sim 1,700$  X-ray sources, of which  $\sim 1,450$ are thought to be members of the association. Optical and near-IR photometry has been obtained for ~90% of these sources from recent deep Galactic plane surveys. We have performed isochrone fits to the near-IR color-magnitude diagram, deriving ages of  $3.5_{-1.0}^{+0.75}$  and  $5.25_{-1.0}^{+1.5}$  Myrs for sources in the two fields, both with considerable spreads around the pre-MS isochrones. The presence of a second population in the region, somewhat older than the present-day O-type stars, has been suggested by other authors and fits with the ages derived here. The fraction of sources with inner circumstellar disks (as traced by the K-band excess) is found to be very low, but appropriate for a population of age ~5 Myrs. We measure the stellar mass functions and find a power-law slope of  $\Gamma = -1.09 \pm 0.13$ , in good agreement with the global mean value estimated by Kroupa. A steepening of the mass function at high masses is observed and we suggest this is due to the presence of the previous generation of stars that have lost their most massive members. Finally, combining our mass function and an estimate of the radial density profile of the association suggests a total mass of Cyg OB2 of  $\sim 3 \times 10^4 \, \mathrm{M}_{\odot}$ , similar to that of many of our Galaxy's most massive star forming regions.

N.J. Wright (⋈) · J.J. Drake

Harvard-Smithsonian Center for Astrophysics, 60 Garden Street, Cambridge, MA 02138, USA e-mail: nwright@cfa.harvard.edu

J.E. Drew

Centre for Astronomy Research, University of Hertfordshire, Hatfield AL10 9AB, UK

IS Vink

Armagh Observatory, College Hill, Armagh BT61 9DG, UK

N.J. Wright et al.

## 1 Introduction

Star formation occurs on scales ranging from small star forming regions (SFRs) to the massive superstar clusters seen in merging galaxies, yet our current understanding of star formation is mainly derived from observations of nearby small star forming regions, yet the conditions in these low-mass regions are very different to those found in the massive SFRs that contain hundreds to thousands of OB stars and millions of low-mass stars. High stellar densities, strong stellar winds from OB stars, and a large UV flux are likely to influence the products of the star formation process such as the initial mass function (IMF), the binary fraction, and the properties of proto-planetary disks. Unfortunately the majority of massive SFRs are found at great distances making them difficult to study. The exception to this is Cygnus OB2, which at a distance of 1.45 kpc [5] is the closest known massive SFR, containing  $\sim$ 65 O-type stars and thousands of OB stars [2, 5, 8, 11]. However, the complications of high extinction, a large spatial area, and the inevitable foreground contamination caused by observing in the Galactic Plane have hindered previous attempts to study the low-mass population in the region. To overcome this, we have used Chandra observations to separate the X-ray luminous pre-MS population from the contaminating galactic foreground. Combining these observations with optical and near-IR photometry from recent deep photometric surveys of the Galactic plane we have been able to isolate the pre-MS population in the region.

## 2 Cygnus OB2 Membership and Foreground Contamination

Wright and Drake [15] presented a catalogue of 1696 X-ray sources extracted from *Chandra* observations of two fields in the center of Cyg OB2. The catalogue also includes optical and near-IR photometry from the IPHAS [3], 2MASS [14] and UKIDSS [10] surveys. X-ray selection is highly effective for selecting pre-MS stars, but to remove any remaining foreground contaminants in the catalog we employed the IPHAS  $(r'-H\alpha, r'-i')$  color–color diagram (CCD, Fig. 1) where the main sequence does not redden onto itself but sweeps out an area in the color–color plane (e.g. [3,4]), allowing differently reddened stellar populations to be separated. Employing this method we removed 46 sources ( $\sim$ 3%), leaving a catalog of 1455 high-confidence members of Cyg OB2 that Wright et al. [16] showed was complete to  $\sim$ 1 M $_{\odot}$  (excluding late B and A-type stars that do not all emit X-rays).

## 3 Near-IR Stellar Properties

The integrated properties of the region were studied in the near-IR due to the availability of deep near-IR photometry for the majority of sources. Figure 2 shows (J, J-H) color-magnitude diagrams (CMDs) for sources in the two fields. Pre-MS

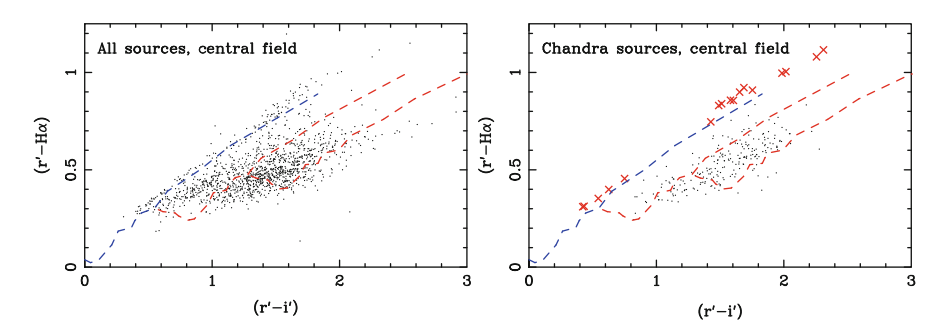
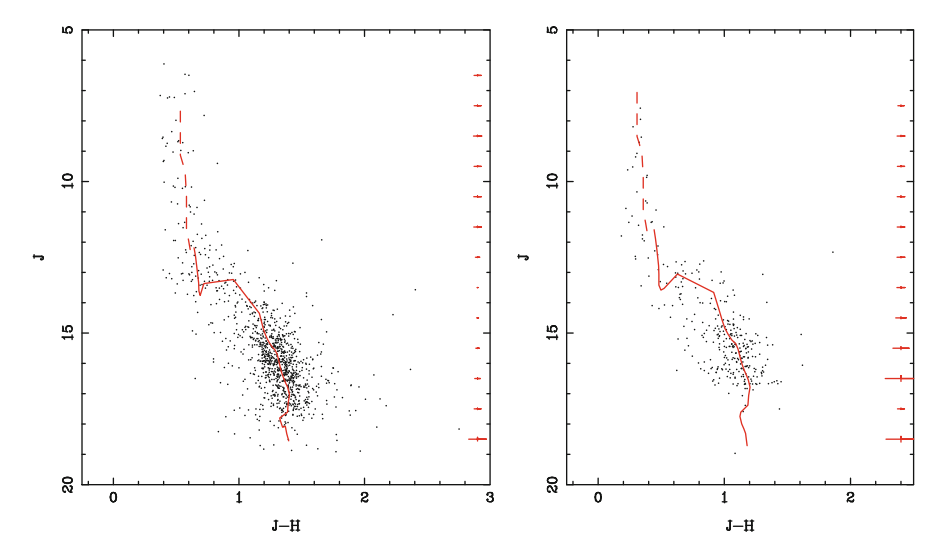


Fig. 1 IPHAS  $(r'-H\alpha, r'-i')$  CCDs for all sources in the *Chandra* observational footprints (*left*) and for sources with *Chandra* associations (*right*). *Blue lines* show unreddened main-sequences [3], while *red lines* are the main-sequence tracks for  $A_V = 4.0$  and 7.0. Sources removed from the catalogue as foreground sources are shown as *red crosses* 



**Fig. 2** Near-IR CMDs for Cygnus OB2 sources in the central (*left*) and north-western (*right*) fields with pre-MS isochrones (*red lines*, [13]) for ages and extinctions of 3.5 and 5.25 Myrs, and  $A_V = 7.5$  and  $A_V = 5.5$ , respectively. Mean photometric errors for each magnitude interval are shown as *red crossed* on the *right* 

isochrones [13] were fit to this data to determine the age and extinction using a simple goodness-of-fit test and weighting each source using its color and magnitude. A bootstrapping technique was used to determine 95% confidence intervals for all fitted quantities. We find different ages for the two fields of  $3.5^{+0.75}_{-1.0}$  and  $5.25^{+1.5}_{-1.0}$  Myrs for the central and north-western fields, respectively. However, the difference between these two ages is within the uncertainties of the two fits.

Figure 3 shows the  $(J - H, H - K_s)$  CCD for the two fields, which was used to identify stars with circumstellar disks based on their near-IR excesses (in the

N.J. Wright et al.

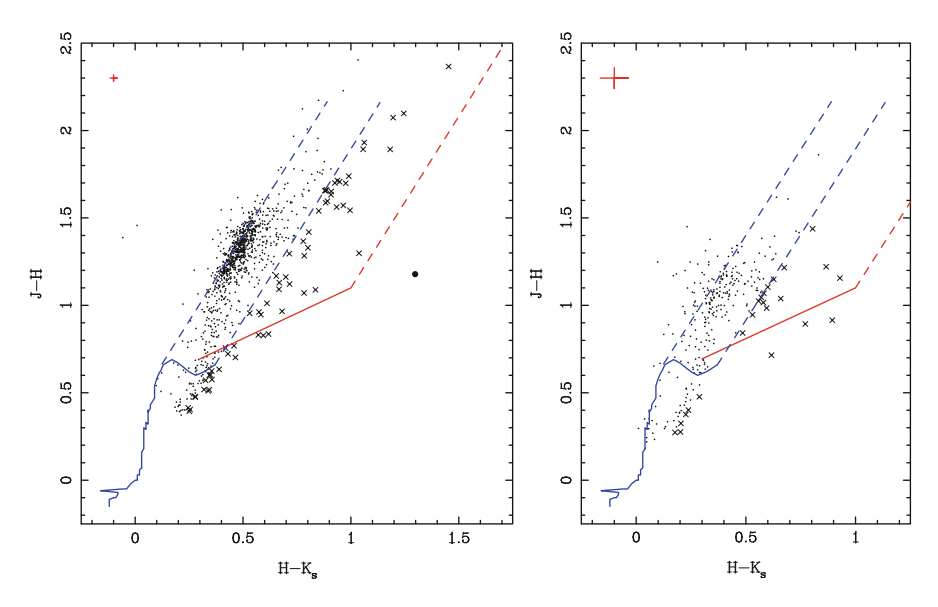


**Fig. 3** Near-IR CCDs for Cygnus OB2 sources in the central (*left*) and north—western (*right*) fields with a main sequence (*blue lines*, [7]), the classical T-Tauri star locus (*red line*, [12]), and reddening vectors (*dashed lines*) shown. Sources falling within the T-Tauri region are marked as crosses and the most highly reddened object in the field is shown as a *large dot*. The mean photometric errors on the two colors is shown in the *top left* corner of each figure in *red* 

absence of longer-wavelength data). We find 63 and 23 sources in this region of the color-color plane, 5.9 and 7.9% of our catalogue in the central and north-western fields respectively. These fractions are significantly lower than that found from near-IR studies of other similar age star forming regions [6], which has previously been suggested as evidence for the impact of environment, particularly the strong UV flux, on the evolution of protoplanetary disks [1]. While our results do support such a theory, with the fraction of circumstellar disks lower in the center of the star forming region where the UV radiation field from OB stars is stronger, the difference is both statistically small and over-simplifies the dynamical and 3-dimensional structure of the region. An alternative explanation is that we are sampling an older generation of star formation as well as the 2 Myr population. A disk fraction of 5-10% is perfectly reasonable for a population with an age of  $\sim$ 5 Myr [6].

## 4 The Stellar Mass Function in Cygnus OB2

Figure 4 shows mass functions (MF) for sources in Cyg OB2, exhibiting a clear power law slope (excluding A and late B-type stars) down to our completeness limit of  $\sim 1 \, \rm M_{\odot}$ , but steepening at higher masses. We fit a slope of  $\Gamma = -1.09 \pm 0.13$  in the combined fields, in agreement with the apparently universal value of

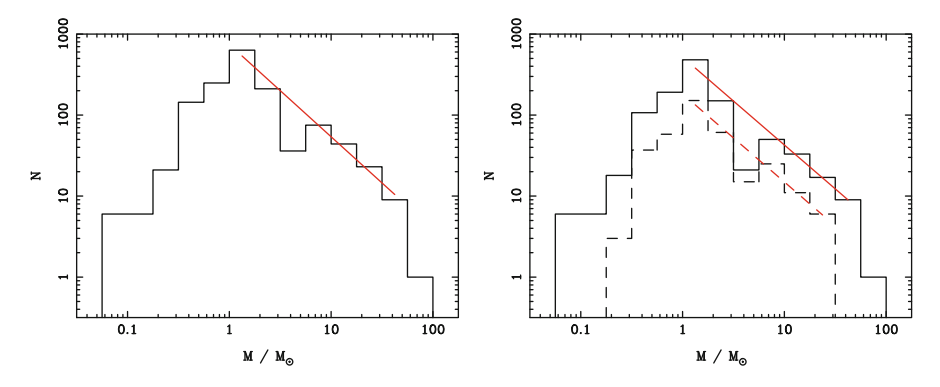


Fig. 4 Mass functions for all sources in Cygnus OB2 with stellar masses derived from near-IR photometry and existing spectroscopic observations. *Left:* MF for both fields combined; *right:* MF for the central (*full line*) and north–western (*dashed line*) fields.  $\chi^2$  fits to the MFs (within the completeness limits) are shown as *red lines* 

 $\Gamma=-1.3$  [9]. When the two fields are considered separately we find negligibly different slopes of  $\Gamma=-1.08\pm0.15$  in the central field and  $\Gamma=-1.09\pm0.10$  in the north-western field. Previous measurements of the MF in Cyg OB2 have mostly been derived from spectroscopy of the massive stars, the most recent measurement by Kiminki et al. [8] resulting in a slope of  $\Gamma=-2.2\pm0.1$ . We find here that the MF is not as steep as this, but confining our sample only to the O-type stars we find a slope of  $\Gamma=-2.72\pm0.52$ , in agreement with this work. We suggest that the steep high-mass slope of the MF is not intrinsic but is a product of the older stellar populations in the region having lost their most massive members, thereby steepening the MF.

## 5 The Age, Star Formation History, and Total Mass of Cygnus OB2

The main constraints on the age of Cyg OB2 have previously been derived from the massive stars in the region. Hanson [5] estimated an age of  $2\pm 1\,\mathrm{Myrs}$  but noted that as the search for OB stars in the region was extended to larger radii the fraction of evolved massive stars increased, contaminating the sample of Cygnus OB2 with non-members. Many of these stars were found to the south of the original association [2] in a region where Drew et al. [4] have since uncovered a population of A-type dwarf stars with an age of 5–7 Myr. We have derived ages of  $3.5^{+0.75}_{-1.0}$  and  $5.25^{+1.5}_{-1.0}\,\mathrm{Myrs}$  for the central and north–western fields, which could suggest a significant age spread across the Cygnus OB2 association. Furthermore, our findings of an age-steepened mass function and a considerably reduced circumstellar disk fraction lend weight to the argument of a previous generation of stars in the region. In such a picture our central field includes the young OB-star dominated association,

N.J. Wright et al.

while the north–western field also includes older stars from a previous generation of star formation. We cannot yet know to what extent there are two distinct generations of stars present, or whether there is a real age spread.

While it is likely that Cygnus OB2 is far from spherically symmetric, we can use a simple King profile to estimate the total size and mass of the association. Fitting a radial profile to our observations and combining it with our mass function (extrapolated down to  $0.01\,M_\odot$  using a multi-stage power-law IMF [9]) we estimate a total stellar mass of  $(3\pm1)\times10^4\,M_\odot$  for the entire association. Such a mass implies that there were originally  $\sim\!75\,$ O-type stars, slightly larger than the currently known number of 65, but supporting our argument that some of the most massive stars have expired. This size is comparable to that of many of the most massive known star forming regions in our Galaxy, confirming the role of Cygnus OB2 as the prime location to study the influence of massive stars on the low-mass stellar population.

### 6 Conclusions

We present an analysis of  $\sim$ 1,450 stellar X-ray sources detected in the Cygnus OB2 association using complementary optical and near-IR photometry. We derive integrated ages, near-IR disk fractions and stellar masses, from which me measure the mass function. Evidence for an age spread, a low disk fraction, and an steep, high-mass slope of the mass function all argue for the presence of an older population of stars in the region. Finally we combine our results to estimate the total mass of the association as  $3 \times 10^4 \, \mathrm{M}_{\odot}$ , comparable to many of our galaxy's most massive star forming regions. The recently completed *Chandra* Legacy Survey of Cygnus OB2 will take this work wider and deeper and will help probe the star formation process in our nearest massive star forming region.

#### References

- 1. Albacete Colombo, J.F., et al.: Astron. Astrophys. 464, 211 (2007)
- 2. Comeron, F., et al.: Astron. Astrophys. **389**, 874 (2002)
- 3. Drew, J., et al.: Mon. Not. R. Astron. Soc. 362, 753 (2005)
- 4. Drew, J.E., Greimel, R., Irwin, M.J., Sale, S.E.: Mon. Not. R. Astron. Soc. 386, 1761 (2008)
- 5. Hanson, M.: Astrophys. J. 597, 957 (2003)
- 6. Hillenbrand, L.A.: in STScI Symp. Ser. 19, 84 (2005)
- 7. Kenyon, S.J., Hartmann, L.: Astrophys. J. Suppl. 101, 117 (1995)
- 8. Kiminki, D., et al.: Astrophys. J. **664**, 1102 (2007)
- 9. Kroupa, P.: Mon. Not. R. Astron. Soc. 322, 231 (2001)
- 10. Lucas, P.W., et al.: Mon. Not. R. Astron. Soc. 391, 136 (2008)
- 11. Massey, P., Thompson, A.B.: Astron. J. 101, 1408 (1991)
- 12. Meyer, M.R., Calvet, N., Hillenbrand, L.A.: Astron. J. 114, 288 (1997)
- 13. Siess, L., Dufour, E., Forestini, M.: Astron. Astrophys. 358, 593 (2000)
- 14. Skrutski, M.F., et al.: Astron. J. 131, 1163 (2006)
- 15. Wright, N., Drake, J.J.: Astrophys. J. Suppl. 184, 84 (2009)
- 16. Wright, N.J., Drake, J.J., Drew, J.E., Vink, J.: Astrophys. J. 713, 871 (2010)

# Young Massive Stellar Clusters in the Milky Way: the Cl1813-178 and GLIMPSE 9 Clusters

Maria Messineo, Ben Davies, Donald F. Figer, Christine Trombley, Elena Valenti, Francisco Najarro, John MacKenty, Karl Menten, R. Michael Rich, Rolf P. Kudritzki, Simon Clark, and Valentiv Ivanov

**Abstract** Most of the stars, if not all, form in clusters, and clusters are generally found in large complexes. However, only a few of such complexes produce young massive clusters. We present first result of an ongoing study to fully map in time and space stellar clusters in two Galactic giant molecular clouds with the aim of understanding how star formation proceeded in the cloud, and of identifying the

M. Messineo (⋈) · K. Menten

Max-Planck-Institut fr Radioastronomie, Auf dem Hgel 69, 53121 Bonn, Germany e-mail: messineo@mpifr-bonn.mpg.de

B. Davies · C. Trombley · D.F. Figer

Rochester Institute of Technology, 54 Lomb Memorial Drive, Rochester, NY 14623-5604, USA

#### E Valenti

European Southern Observatory, Karl Schwarzschild-Strasse 2, D-85748 Garching bei Munchen, Germany

#### F. Najarro

Centro de Astrobiología (CSIC-INTA), Ctra. de Torrejón a Ajalvir km4, 28850, Torrejónde Ardoz, Madrid, Spain

#### J. MacKenty

Space Telescope Science Institute, 3700 San Martin Drive, Baltimore, MD 21218, USA

#### R.M. Rich

Physics and Astronomy Building, 430 Portola Plaza, Box 951547, Department of Physics and Astronomy, University of California, Los Angeles, CA 90095-1547, USA

#### R.P. Kudritzki

Institute for Astronomy, University of Hawaii, 2680 Woodlawn Drive, Honolulu, HI 96822, US

#### S. Clark

Department of Physics and Astronomy, The Open University, Walton Hall, Milton Keynes MK7 6AA, UK

#### V. Ivanov

European Southern Observatory, Ave. Alonso de Cordova 3107, Casilla 19, Santiago 19001, Chile

A. Moitinho and J. Alves (eds.), *Star Clusters in the Era of Large Surveys*, Astrophysics and Space Science Proceedings, DOI 10.1007/978-3-642-22113-2\_26, © Springer-Verlag Berlin Heidelberg 2012

triggering mechanism. The W33 and GAL23.3-0.3 complexes are both located in the inner Galaxy, and are rich of HII regions, supernova remnants, and candidate clusters. The W33 complex contains one of the most massive Galactic stellar cluster with a mass of  $(10^4)~M_{\odot}$ , and an age of 4.5 Myrs. The cluster location at the edge of the molecular complex suggests that this is a secondary episod of star formation. The GAL23.3-0.3 appears to contain much older massive stars (~15 Myr).

## 1 Introduction

An understanding of the mechanisms of formation, evolution, and end state of massive stars is fundamental for the studies of galaxies at all redshifts. Massive stars contribute to the chemical enrichment of the interstellar medium with their strong winds and by exploding as supernovae. Moreover, massive stars are the most luminous stars, can easily be detected in external galaxies, and provide distance estimates; they are the sources of the most energetic phenomena in the Universe, gamma ray bursts (e.g. [20]). Massive stars are typically found in young massive clusters ( $M > 10^3 M_{\odot}$ ). They are usually identified by their ionizing radiation, or by locating massive stellar clusters. Only a few hundred clusters so massive are currently known in the Galaxy [13, 19].

More than 1,500 new candidate stellar clusters have been recently discovered from infrared surveys of the Galactic plane (2MASS, DENIS, SPITZER/GLIMPSE), doubling the number of stellar clusters previously known from optical surveys [6]. Among these candidates, several young clusters rich in massive stars may be hidden [13]. Clusters detected at infrared wavelengths are typically further away than those from optical surveys, therefore sampling a different Galactocentric region. Moreover, with infrared observations it is possible to study obscured/embedded stellar clusters in large complexes, which are the basic units of star formation. By analyzing various episodes of star formation in the same cloud one can identify the triggering mechanism, and locate special conditions that are required for the formation of extremely massive and compact ("starburst") stellar clusters. It is unclear why only a few "starburst" clusters are present in the Milky Way [18], and it is unclear if these clusters form in special environments, and if certain Galactic locations are more favorable to their formation (e.g. the central molecular zone and the endpoints of the Galactic Bar, [4, 13]). Therefore, the availability of large surveys of the Galactic plane at radio and infrared wavelengths opens a golden epoch for detecting and studying new massive clusters in large complexes, and to understand the formation, evolution, and environments of massive stars.

We have ongoing programs to map spatially and temporally the distribution of stellar clusters in two giant molecular clouds, W33 and GAL23.3-0.3, which are rich of HII regions and SN remnants, suggesting the presence of massive episodes of star formation (Fig. 1).

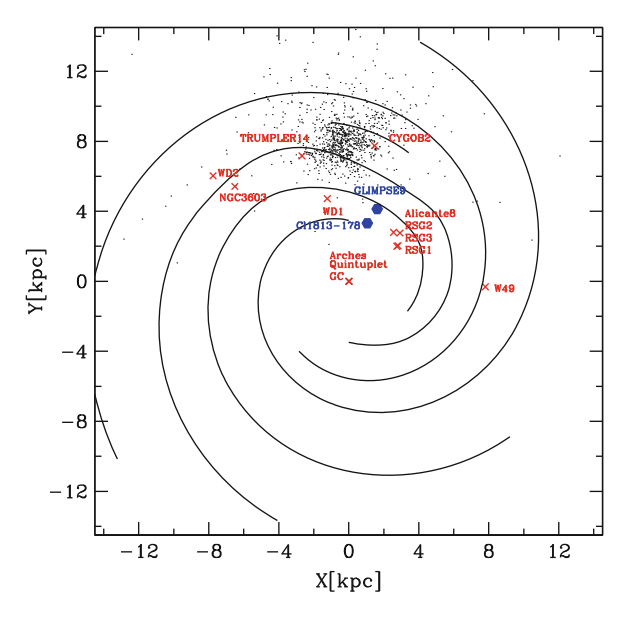


**Fig. 1** Galactic distribution of stellar clusters detected at optical wavelengths (*dots*) taken from [6]. Known young stellar clusters with masses  $> 10^4 \, M_{\odot}$  are shown with crosses [13, 16, 17]. Hexagonal symbols show the location of the Cl1813-178 and GLIMPSE9 clusters, which are discussed in this proceeding. The Galactic center is at (0,0) and the Sun is at (0,8). Spiral arms are taken from [3]

## 2 Stellar Clusters in W33

The main W33 complex is located in the inner Galaxy, at a distance of about 4 kpc, and extends over an area of roughly 29×23 pc [2]. Massive star formation in this complex was already suggested in the 1980s from studies of radio continuum emission and radio recombination lines (e.g. [8]). However, a comprehensive study of its stellar population is still missing. W33A is a well known massive young stellar object [5]. A massive stellar cluster, Cl 1813-178, associated with W33 was reported by [12]. Six other candidate stellar clusters, detected at infrared wavelengths, and possibly associated with the same complex, are listed by [14].

The W33 complex is of particular interest because it hosts also a large number of HII regions and supernova remnants (SNR). The Cl 1813-178 cluster coincides with the SNR G12.82-0.02 and G12.72-0.00 [12], while the BDS2003-115 cluster coincides with the SNR G12.83-0.02 [14].

Cl 1813-178 cluster is on the Western edge of the W33 complex, while W33A and the associated SNR G13.1875+0.0389 are on the Eastern edge of the W33 complex. This confirms that the most recent massive star formation has taken place in several regions in the periphery of the W33 complex. Furthermore, while W33A is still accreting, the Cl1813-178 has an age of about 4.5 Myr. Therefore, star formation in the W33 region covers a large time span [14] (Fig. 2).

M. Messineo et al.

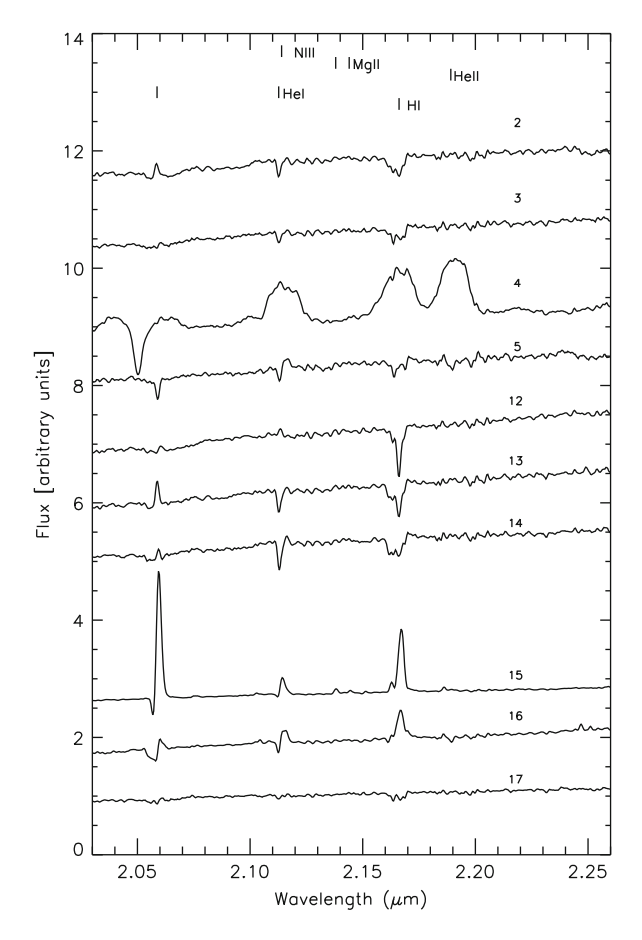


Fig. 2 Examples of K-band spectra of early-type stars detected in the Cl 1813-178 [14]

## 2.1 Cl 1813-178

The Cl 1813-178 cluster was serendipitously discovered as a stellar overdensity in 2MASS images, by combining 2MASS images with radio and X-ray information. The cluster is projected into the G12.72-0.00 and G12.82-0.02 supernova remnants (SNR), and the highly magnetized pulsar associated with the TeV  $\gamma$ -ray source HESS J1813-178.

A near-infrared spectroscopic survey of the brightest cluster members is presented by [14] (See Fig. 2). Among the 61 observed stars, 25 massive stars were detected. Two Wolf–Rayet (WR) stars of type WN7, a candidate luminous blue variable (LBV), and 21 OB stars were identified. Among the OB stars, a O8-O9If star and a O6-O7If star were discovered. Eight of these evolved stars show also X-ray emission, as detected by the Chandra and XMM satellites [7, 9]. The hardness of the X-ray emission from the two WN7 stars strongly suggests binary systems.

Messineo et al. [14] derived an average interstellar extinction of  $A_{\rm K_s}=0.8$  mag and a spectrophotometric distance of  $3.8\pm1.6\,\rm kpc$ , which is consistent with the (stellar) kinematic distance of  $4.8\pm^{+0.25}_{-0.28}\,\rm kpc$ . The mixture of evolved massive stars is reminiscent of other Galactic young massive clusters, such as Westerlund 1, Quintuplet, Galactic center, and Cl 1806-20. By assuming the kinematic distance, the derived values of  $A_{\rm K_s}$ , and bolometric corrections, stellar luminosities were estimated, therefore, stellar masses by comparing the luminosities with evolutionary tracks from the Geneva group [14]. A likely cluster age of 4–4.5 Myr was derived, however, a spread in age of about 1 Myr cannot be excluded. By assuming a Salpeter mass function, a cluster mass of  $1.0\pm0.2\times10^4\,M_\odot$  was obtained. The Cl 1813-178 cluster is a new addition to the list of 14 young massive stellar clusters known in the Milky Way.

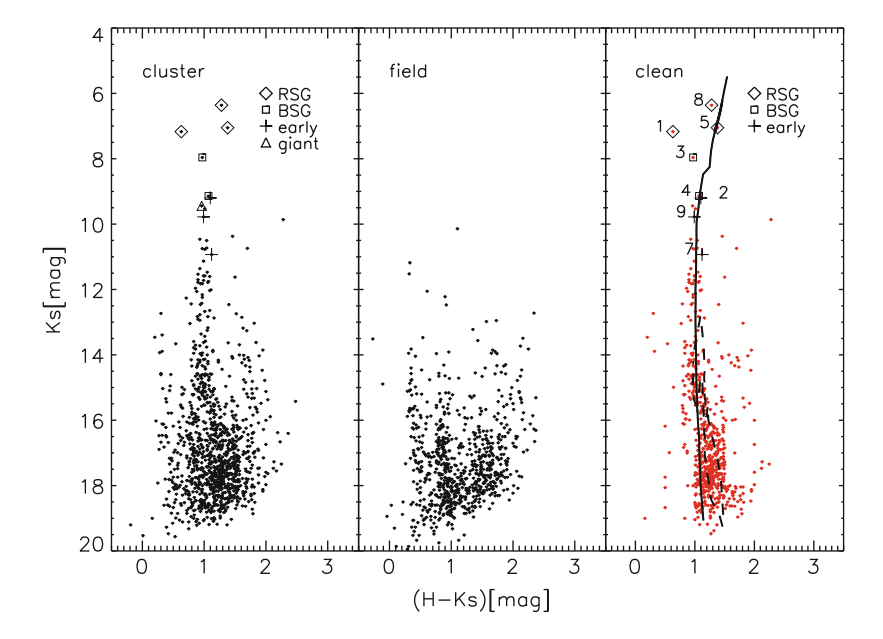


Fig. 3 HST/NICMOS  $H-K_S$  vs.  $K_S$  color-magnitude diagrams (CMD) of the GLIMPSE9 cluster [15]. The cluster CMD is shown on the *left panel*. A CMD of a control field is shown in the *central panel*. A CMD of the cluster field after statistical decontamination is shown in the *right panel*. The *vertical line indicates* an isochrone of 15.0 Myr and solar metallicity from the Geneva group, which was shifted to a reddening of  $A_{K_s} = 1.5$  mag and a distance of 4.2 kpc. *Dotted lines* show isochrones corresponding to a population of 0.5 Myr, and 3 Myr with solar metallicity (Siess et al. 2000). The diamond symbols indicate spectroscopically detected RSGs, while squares indicate BSGs, a plus symbol indicate candidate early-type stars, and triangles giant stars

190 M. Messineo et al.

## 3 Stellar Clusters in the Giant Molecular Cloud GAL23.3-0.3

A study of the GLIMPSE9 cluster, number 9 in the list by [11], is presented in [15]. A well defined cluster sequence appears in the HST/NICMOS  $H-K_{\rm S}$  versus  $K_{\rm S}$  diagram (Fig. 3). Low-resolution K-band spectroscopy reveals three red supergiants (RSG) and two blue supergiants (BSG) among the brightest members. A spectrophotometric distance of  $4.2 \pm 0.4\,{\rm kpc}$  is derived, an average interstellar extinction  $A_{\rm K_S}=1.6\,{\rm mag}$ , and an age between 15 and 27 Myr. A minimum cluster mass of  $1,600 \pm 400 M_{\odot}$  is estimated.

The GLIMPSE9 cluster is located in the direction of the GAL23.3-0.3 giant molecular cloud, and the stellar cluster distance agrees well with that inferred for the complex by [10] and [1], therefore confirming their physical association.

A stellar population possibly associated with the same giant molecular cloud is seen in other regions of the cloud: two regions are associated with the SNR/W41, one region with the SNR G22.9917-0.3583, and another region with SNR G22.7583-0.4917. A program with SINFONI on the VLT is ongoing to observe candidate massive stars in the GAL23.3-0.3 molecular cloud. A preliminary analysis shows the presence of a few RSGs in direction of the SNR/W41 (Fig. 3).

## References

- 1. Albert, J., Aliu, E., Anderhub H., et al.: Astrophys. J. Lett. **643**, L53 (2006)
- 2. Bieging, J.H., Pankonin, V., Smith L.: Astron. Astrophys. 64, 341 (1978)
- 3. Cordes, J.M., Lazio, T.J.W.: ArXiv Astrophysics e-prints, 0207156v3 (2002)
- 4. Davies, B., Origlia, L., Kudritzki R., et al.: Astrophys. J. 696, 2014 (2009)
- Davies, B., Lumsden, S.L., Hoare, M.G., Oudmaijer, R.D., de Wit, W.: Mon. Not. R. Astron. Soc. 402, 1504 (2010)
- 6. Dias, W.S., Alessi, B.S., Moitinho, A., Lépine, J.R.D.: Astron. Astrophys. 389, 871 (2002)
- 7. Funk, S., Hinton, J.A., Moriguchi, Y., et al.: Astron. Astrophys. **470**, 249 (2007)
- 8. Haschick, A.D., Ho, P.T.P.: Astrophys. J. 267, 638 (1983)
- 9. Helfand, D.J., Gotthelf, E.V., Halpern, J.P., et al.: Astrophys. J. 665, 1297 (2007)
- 10. Leahy, D.A., Tian, W.W.: Astron. J. 135, 167 (2008)
- 11. Mercer, E.P., Clemens, D.P., Meade, M.R., et al.: Astrophys. J. 635, 560 (2005)
- 12. Messineo, M., Figer, D.F., Davies, B., et al.: Astrophys. J. Lett. 683, L155 (2008)
- 13. Messineo, M., Davies, B., Ivanov, V.D., et al.: Astrophys. J. 697, 701 (2009)
- 14. Messineo, M., Davies, B., Figer, D.F., et al., ApJ, **733**, 41 (2011)
- 15. Messineo, M., Figer, D.F., Davies, B., et al.: Astrophys. J. **708**, 1241 (2010)
- Negueruela, I., González-Fernández, C., Marco, A., Clark, J.S., Martínez-Nú nez, S.: Astron. Astrophys. 513, A74 (2010)
- Negueruela, I., González-Fernández, C., Marco, A., Clark, J.S.: Astron. Astrophys. 528, A59 (2011)
- 18. Pfalzner, S.: Astron. Astrophys., **498**, L37 (2009)
- 19. Piskunov, A.E., Kharchenko, N.V., Schilbach, E., et al.: Astron. Astrophys. 487, 557 (2008)
- 20. Woosley, S.E., Bloom, J.S.: Annu. Rev. Astron. Astrophys. 44, 507 (2006)

## Multiple Populations in Globular Clusters: The Role of AGB and Super-AGB Stars

Paolo Ventura and Roberta Carini

**Abstract** Spectroscopic and photometric investigations of Globular Cluster stars indicate that these structures are not formed by a simple stellar population, rather they harbour two or three distinct groups of stars, differing in their surface chemical composition. Given that these anomalies are not observed in field stars, these results suggest that some self-enrichment mechanism acted in Globular Clusters, so that new stars are formed from the ashes of the early evolution of stars belonging to the first generation. In this review we focus our attention on the possible role played by stars of intermediate mass, i.e. those objects with mass  $5 \le M/M_{\odot} \le 8$ , that evolve through the thermal pulses phase, and eject into the interstellar medium their envelope, whose chemical composition may have been altered by Hot Bottom Burning experienced by the most massive objects during the quiescent phase of H-burning.

#### 1 Introduction

The spectroscopic and photometric investigations of stars in Globular Clusters (GS) run in the last decades suggested that GC can hardly be considered as simple stellar populations, and that what we observe today is probably the overlapping of more stellar generations, that formed at two or three different epochs, separated by an age gap negligible compared to the total age of the cluster.

On the spectroscopic side, the early discovery that GC giants do not show a uniform surface chemistry, but rather exhibit strong star to star differences among the individual stars [10, 11], was recently confirmed for stars in a less advanced evolutionary stage [7], for which any possible in situ mechanism can be ruled out,

P. Ventuura (⋈) · R. Carini

INAF, Observatory of Rome, via Frascati 33, 00040 Monte Porzio Catone (RM), Italy e-mail: paolo.ventura@oa-roma.inaf.it; roberta.carini@oa-roma.inaf.it

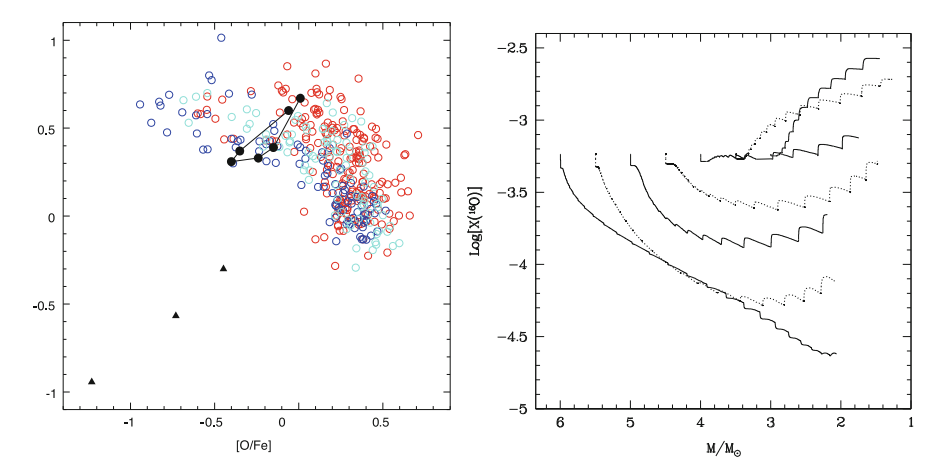


Fig. 1 Left: The oxygen-sodium anticorrelation observed in GC stars (open circles) compared with yields from AGB and super-AGB stars with mass  $5\,\mathrm{M}_\odot \leq M \leq 7.5\,\mathrm{M}_\odot$  (filled circles). Filled triangles indicate the yields from super-AGB stars by [16]. Right: The evolution of the surface content of oxygen in models of intermediate mass during the AGB phase. We indicate for any element X [X/Fe]=Log(X/Fe)-Log(X/Fe) $_\odot$ 

leaving only the difference in the chemistry of the gas from which the stars formed as a plausible explanation. The chemical anomalies define abundance patterns among the chemical species up to Aluminum, the most clear and firmly established of which is the Oxygen-Sodium anticorrelation [3], that has been confirmed to exist (though to different extents) in practically all the GC examined (see the left panel of Fig. 1). Two clear results coming from these investigations are the constancy of the overall content of C+N+O [9], and of the abundances of all the elements heavier than Aluminum, and in particular of the iron content.

Photometrically, recent analysis of Omega Centauri [12] and NGC 2808 [13] have highlighted the presence of multiple main sequences, that can only be interpreted on the basis of a difference in the helium content, the stars in the bluest sequence being more helium rich. This finding nicely fits within the helium enrichment previously invoked to account for the blue clumps and the anomalous morphology of the Horizontal Branches (HB) of the same clusters [6].

The aforementioned findings, and particularly the discovery that stars with the anomalous chemistry involve scarcely evolved objects, still on the main sequence, and thus not capable of any advanced nucleosynthesis beyond the proton-proton chain, pushed the debate towards a self-enrichment mechanism, according to which an early generation of stars evolved rapidly inside the cluster, and ejected into the interstellar medium gas previously processed by advanced p-capture nucleosynthesis, from which new stellar generations have formed.

Among the few candidates proposed so far, we focus on the intermediate masses during their Asymptotic Giant Branch (hereinafter AGB) phase [18]. These stars, whose mass is below  $\sim 6-6.5\,\mathrm{M}_\odot$ , are known to develop a degenerate core made

up of carbon and oxygen soon after the core helium burning phase is concluded, and experience a strong nucleosynthesis at the bottom of their external envelope (commonly named Hot Bottom Burning, HBB) [2, 14] in the following AGB phase, characterized by periodic thermal instabilities, known as Thermal Pulses (hereinafter TP). We also discuss the evolutionary properties of the super-AGB stars, with mass in the range  $\sim 6-8\,{\rm M_\odot}^{-1}$ , that develop a core made up of Neon and Oxygen before undergoing the AGB evolution [15].

#### 2 The AGB Evolution

All stars with mass in the range  $1-6\,M_\odot$  evolve through the AGB phase, during which a CNO burning shell supplies for most of the time the overall energy release, with periodic ignitions of a helium-rich layer below [8]. These stars loose all their external convective mantle before evolving to the White Dwarf stage, and are thus possible efficient polluters of the interstellar environment.

A robust prediction concerning the surface chemistry of this class of objects is that their yields are expected to be enriched in helium, the increase in the helium content increasing with the initial mass. This is a consequence of the second dredge-up, which these stars experience shortly after the consumption of helium in the core, when the surface convective zone penetrates inwards, reaching layers previously touched by CNO burning, and thus enriched in their helium content. The extent of the inwards penetration increases with the core mass. Because this phase is preliminary to the following AGB evolution, the predictions are much more reliable, and less sensitive to all the uncertainties affecting the TP phase.

There are two physical mechanisms by which these stars can alter their surface chemistry:

- In the phases following the thermal pulse, when the CNO burning shell is temporarily extinguished, the base of the convective envelope can penetrate sufficiently inwards to reach layers previously touched by  $3\alpha$  nucleosynthesis, with the consequent carbon enrichment of the whole mantle. This process is known as Third Dredge Up (TDU).
- In more massive AGBs, the bottom of the convective zone becomes so hot as
  to favor HBB conditions: an advanced p-capture nucleosynthesis occurs, with
  the consequent decrease in the surface oxygen, and the increase in the nitrogen
  content. When the temperature exceeds ~ 70 MK, the Ne-Na and Mg-Al chains
  are activated, with the increase in the surface sodium and aluminum, and the
  decrease in the magnesium abundance.

 $<sup>^1\</sup>text{The}$  range of mass involved in the AGB and super-AGB evolution is made uncertain by the core-overshoot during the two major phases of H- and He-burning. In this work we adopted a moderate extra-mixing from the core; the quoted value would be shifted upwards by  $\sim 2\,M_{\odot}$  if overshooting was neglected.

194 P. Ventura and R. Carini

The yields of AGBs depend strongly on which of the two above mechanisms dominates. When HBB is active, we expect to see essentially the signature of p-capture nucleosynthesis, with a constant C+N+O, and, more generally, the abundances of the various elements will reflect the equilibrium values, corresponding to the temperature at the base of the convective zone. On the contrary, TDU favors a rapid increase in the carbon content of the envelope; although this latter can be partly converted into nitrogen in the following quiescent phase of H-burning, the overall C+N+O content increases.

HBB is expected to dominate in the high masses domain: the higher core masses favor higher temperatures at the bottom of the convective zone, thus leading to HBB conditions. Since HBB is commonly accompanied by a rapid increase in the luminosity, these stars are also expected to experience a smaller number of TPs, thus leaving little room for TDU to operate. Lower mass stars, not experiencing HBB, are predicted to live longer and to experience many TDU episodes: their yields will be therefore expected to be carbon rich.

The theoretical modelling of AGB evolution suffers of many uncertainties, associated to the treatment of convection [19], mass loss [20], molecular opacities for C-enriched mixtures [22, 23]. It is however possible to define a qualitative behavior of the yields from AGBs with mass: stars whose initial mass exceeds a threshold value  $M_{thresh}$  will be dominated by HBB, whereas lower masses are dominated by TDU. The value of  $M_{thresh}$  is rather uncertain, and depends essentially on the assumed extra mixing from the core during the two phases of core burning, and on the convective model adopted.

The right panel of Fig. 1 shows the evolution of the surface content of oxygen in stars of different initial mass, ranging from  $3\,M_\odot$  to  $6\,M_\odot$ . We note that stars below  $4\,M_\odot$  are dominated by TDU (oxygen is seen to increase during the evolution), whereas HBB prevails above  $5\,M_\odot$ . Stars in the middle will reflect the effects of both mechanisms.

The efficiency of HBB in stars with mass exceeding  $5\,M_\odot$  can also be seen in the two panels of Fig. 2, that shows the variation of the surface abundance of sodium (Left) and Aluminum (Right) in the same models as in Fig. 1. Note that in the more massive models the early production of sodium due to the combined effects of the second dredge-up and of the early burning of  $^{22}$ Ne is later compensated by the activation of the destruction channel via proton capture by sodium nuclei, which causes the surface abundance of sodium to diminish. These models are expected to produce sodium, but the sodium yields are predicted to be anticorrelated with stellar mass.

## 3 The SAGB Phase

Stars with masses in the range  $6\,\mathrm{M}_\odot < M < 8\,\mathrm{M}_\odot$  ignite carbon in conditions of partial degeneracy and undergo a following phase of thermal pulses, with a degenerate core made up of oxygen and neon [15].

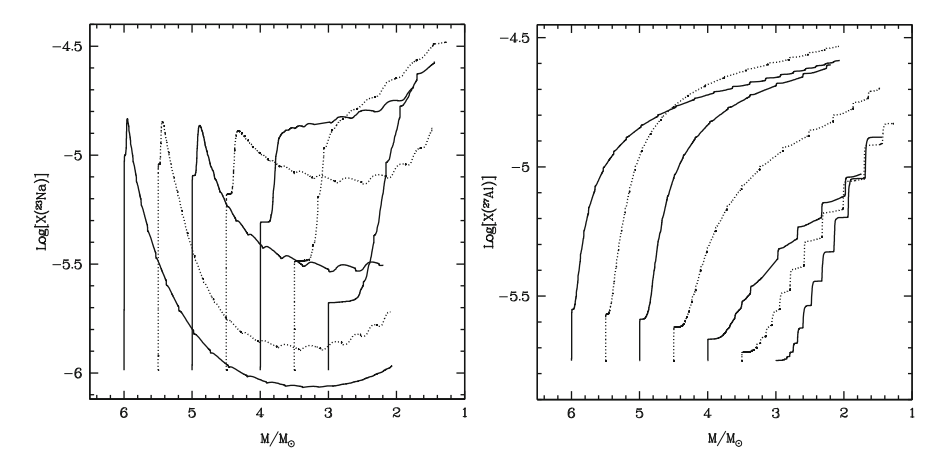


Fig. 2 The same as the *right panel* of Fig. 1, but concerning the evolution of the surface sodium (*left*) and aluminum (*right*)

Their core mass is so high that HBB conditions are easily achieved, independently of the convection model adopted. The most relevant unknown physical ingredient is in this case the treatment of mass loss, as can be inferred by the comparison of SAGB models presented by different research groups. When a mass loss rate scarcely dependent on the luminosity, such as the classic recipe by [17], is adopted, these models are expected to loose their massive envelopes after a long series of TPs, during which the base of the envelope becomes so hot to induce a very advanced p-capture nucleosynthesis, with a drastic reduction of the surface oxygen, and also of the sodium content (see the full triangles in Fig. 1, that indicate the yields predicted in this case). On the contrary, when a treatment of mass loss with a steep increase with the luminosity is used [1], the consumption of the envelope is much faster, and the yields are predicted to be sodium rich (see the filled circles in Fig. 1).

In this latter case we find that the trend between the stellar mass and the degree of nucleosynthesis achieved at the bottom of the convective envelope is reversed: the higher the mass, the less extreme is the chemistry of the yields in terms of the depletion of oxygen and production of aluminum [21]. This can be seen in Fig. 3, that shows the simultaneous variation of the oxygen and sodium mass fraction in models with mass in the range  $6\,\mathrm{M}_\odot < M < 8\,\mathrm{M}_\odot$ . All the models follow he same path, but for increasing mass the evolution is halted earlier, before a very advanced nucleosynthesis can be reached. Note in particular the behavior of the  $8\,\mathrm{M}_\odot$  (indicated with full triangles in the figure), that is predicted to consume the whole envelope when only a modest depletion of oxygen is completed.

196 P. Ventura and R. Carini

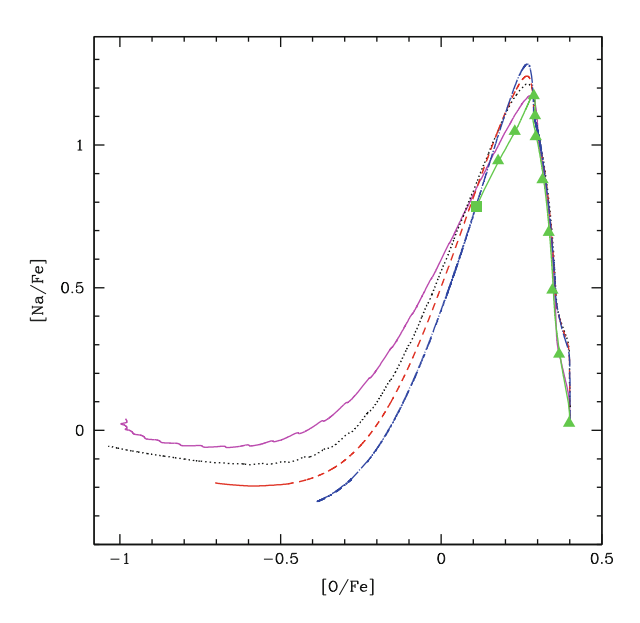


Fig. 3 The simultaneous variation of the surface abundances of oxygen and sodium in models of masses  $6\,M_\odot$  (solid),  $6.5\,M_\odot$  (dotted),  $7M_\odot$  (dashed),  $7.5\,M_\odot$  (dot-dashed) and  $8\,M_\odot$  (full triangles) evolved through the AGB or super-AGB phase. The full square marks the end of the super-AGB evolution of the  $8\,M_\odot$  model

## 4 The Self-Enrichment Scenario by Massive AGBs and SAGBs

The previous sections outlined how the yields by AGBs and SAGBs are uncertain, and are extremely sensitive to the physical description of convection, overshooting, and mass loss. The only exception is the helium manufactured by these stars, that is expected to approach  $\sim 40\%$  for the highest masses investigated. This prediction is rather robust, because the increase in the surface helium is preliminary to the TP phase. The helium enhancement predicted is in excellent agreement with the quantity required to fit the blue main sequences of the most massive GCs, and also to account for the distribution of HB stars in the same structures.

The left panel of Fig. 1 shows that models produced by our group, in which convection is modeled according to the FST prescription and mass loss is treated according to the Blocker's recipe, predict yields of the ejecta that are in good agreement with the chemistry of the stars in Globular Clusters with the most anomalous composition, in terms of oxygen depletion, and aluminum and sodium enhancement.

An appealing explanation for the formation of the population with the anomalous chemistry is that the stars most contaminated are formed directly from the winds of the most massive SGBs, whereas the intermediate chemistries would be the outcome of depletion of this gas with pristine gas survived within the cluster [5].

A problem remains with the mass budget available. The observations indicate the fraction of contaminated stars is  $\sim 50\%$ , whereas the mass budget available from massive AGBs is only  $\sim 10\%$  of the total mass available. A common and plausible explanation that could solve this discrepancy is that the GCs suffers a huge loss of stars from the outskirts of their structure, that preferentially involves stars of the original population, because the new stars with the contaminated chemistry are formed in the central regions, due to radiative cooling of the gas ejected [4,5].

**Acknowledgements** R.C acknowledges financial support from the Observatory of Rome, and from and MIUR/PRIN07 (Chemical composition and multiple populations in Globular Clusters: observations and models; CRA 1.06.07.05)

## References

- 1. Blöcker, T.: Astron. Astrophys. 299, 755 (1995)
- 2. Blöcker, T., Schoenberner, D.: Astron. Astrophys., 244, L43 (1991)
- 3. Carretta, E., Bragaglia, A., Gratton, R.G., et al.: Astron. Astrophys. 505, 117 (2009)
- 4. D'Antona, F., Caloi, V.: Astrophys. J. 611, 871 (2006)
- D'Ercole, A., D'Antona, F., Ventura, P., Vesperini, E., McMillan, S.L.W.: Mon. Not. R. Astron. Soc. 407, 854 (2010)
- D'Ercole, A., Vesperini, E., D'Antona, F., McMillan, S.L.W., Recchi, S.: Mon. Not. R. Astron. Soc. 391, 825 (2008)
- 7. Gratton, R.G., Bonifacio, P., Bragaglia, A., et al.: Astron. Astrophys. 369, 87 (2001)
- 8. Herwig, F.: Annu. Rev. Astron. Astrophys. **43**, 435 (2005)
- Ivans, I.I., Sneden, C., Kraft, R.P., Suntzeff, N.B., Smith, V.V., Langer, G.E., Fulbright, J.P.: Astron. J. 118, 1273 (1999)
- 10. Kraft, R.P.: Publ. Astron. Soc. Pac. 106, 553 (1994)
- 11. Norris, J.E., Cottrell, P.L., Freeman, K.C., Da Costa, G.S.: Astrophys. J. 244, 205 (1981)
- 12. Piotto, G., Villanova, S., Bedin, L.R.: Astrophys. J. **621**, 777 (2005)
- 13. Piotto, G., Bedin, L.R., Andreson, J.: Astrophys. J. 661, L53 (2007)
- 14. Renzini, A., Voli, M.: Astron. Astrophys. 94, 175 (1981)
- 15. Siess, L.: Astron. Astrophys. 448, 717 (2006)
- 16. Siess, L.: Astron. Astrophys. **512**, A10 (2010)
- 17. Vassiliadis, E., Wood, P.R.: Astrophys. J. **413**, 641 (1993)
- 18. Ventura, P., D'Antona, F., Mazzitelli, I., Gratton, R.: Astrophys. J. 550, L65 (2001)
- 19. Ventura, P., D'Antona, F.: Astron. Astrophys. **431**, 279 (2005)
- 20. Ventura, P., D'Antona, F.: Astron. Astrophys. **439**, 1075 (2005)
- 21. Ventura, P., & D'Antona, F., MNRAS, 410, 2760 (2011)
- 22. Ventura, P., Marigo, P.: Mon. Not. R. Astron. Soc. **399**, L54 (2009)
- 23. Ventura, P., Marigo, P.: Mon. Not. R. Astron. Soc. 408, 2476 (2010)

198 P. Ventura and R. Carini



Günther Wuchterl comments on age spreads

# **Chemical Properties of the Open Cluster Population**

Sofia Randich

**Abstract** In the last 15 years the number of open clusters with accurate abundance determination has significantly increased, allowing the investigation of several topics in the context of star formation and evolution, as well as of the formation and evolution of the Milky Way. Here I provide an overview of the chemical properties of the open cluster population. In particular, I will discuss the overall distribution of iron and other elements as a function of cluster age and position in the Galactic disc, focusing on a few recent results.

#### 1 Introduction

Determination of the chemical composition of open star clusters is critical to address a broad variety of astrophysical issues. Measurements of the abundance pattern in star forming regions (SFRs) provide an independent tool to investigate triggered star formation scenarios (e.g., [1, 4] and references therein); to unveil possible common origin of groups, loose associations, and super-clusters (e.g., [5, 21]); to compare the metal content of T Tauri stars around which planets might be forming now, with that of old stars where planets have been detected (e.g., [7, 18]). On the other hand, Galactic open clusters (OCs) are since long recognized as one of the best tools to trace the chemical content of the Galactic thin disc (e.g., [8, 17]); in particular, old clusters can provide reliable information on the status of the disc at epochs earlier than 3–4 Gyr ago, which is crucial for a better comprehension of the overall Galaxy formation and evolution. Finally, accurate knowledge of the cluster metallicity and composition is vital to derive correct ages and masses from isochrone fitting of color-magnitude diagrams, with important implications

200 S. Randich

for empirical determinations of the initial mass function and the study of the secular evolution of stellar properties.

#### 2 Available Measurements

Whereas metallicity can be determined using photometry and low resolution spectroscopy, only high resolution spectra allow deriving accurate abundances of a large number of elements (e.g., [11]). Thanks to the big advancements in instrumentation and, in particular, to availability of efficient, multi-object spectrographs on 8 mclass telescopes, the last 15 years have witnessed major achievements in this field. Significant progress has indeed been made in terms of data quality and accuracy of the measurements; in terms of number of OCs with metallicity determination from high resolution spectroscopy; in terms of coverage in cluster age, distance from the Sun, and Galactocentric distance; in terms of number of elements for which abundances can be determined. Specifically, high resolution metallicities had been derived for less than 15 OCs in 1995 [8], for  $\sim$ 30 clusters in 2000 [11], and for  $\sim$ 40 OCs in 2004 [9]. Now (Nov. 2010), thanks to the contribution of several groups in Europe and the US, not only high resolution [Fe/H] estimates are available for more than 70 clusters, but the cluster sample includes very young close-by SFRs, as well as very distant and old OCs. Also, besides iron, accurate abundances are now routinely obtained for  $\alpha$ , Fe-peak, and neutron capture (s- and r-process) elements.

## 3 The Iron Distribution

In Fig. 1 we show the metallicity distribution of OCs. The figure shows that they cover the [Fe/H] range from about three times below solar ([Fe/H] = -0.5) to [Fe/H]  $\sim$ 0.2, with a small tail of super metal-rich clusters. The average is [Fe/H] = -0.04, with a dispersion of the order of 0.2 dex. The median is [Fe/H] = -0.03, while the 25th and 75 percentiles are [Fe/H] = +0.06 and -0.2, respectively.

## 3.1 Age-Metallicity Relation

The lack of an age-metallicity relation for the OC population has been known since at least 15 years [8]. The current and updated large sample of clusters with high quality [Fe/H] measurements allows us to re-address the issue, based on larger statistics and higher quality data. In Fig. 2 we plot [Fe/H] as a function of age for the clusters shown in Fig. 1 and SFRs with available metallicity determination. This, at variance with previous studies, allows us to extend the age interval to very young clusters. The figure confirms the lack of a relationship between metallicity and age;

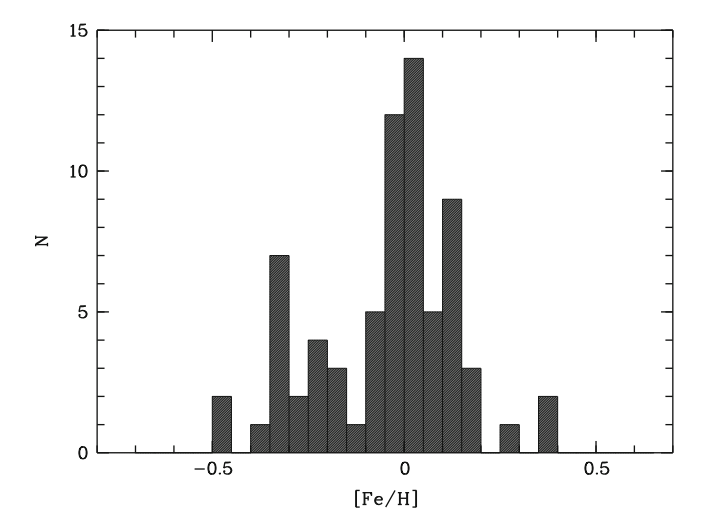


**Fig. 1** Overall metallicity distribution of OCs. The histogram is derived using [Fe/H] from various sources in the literature. Specifically, metallicities for most of the clusters are taken from the compilation of [12], with the update of [13]. To these we added another few OCs not considered in [12] and [13]. The sample shown in the figure does not include SFRs and young associations

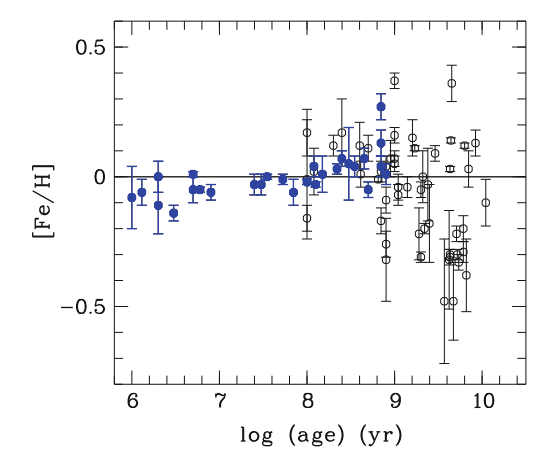


Fig. 2 [Fe/H] as a function of age for the clusters shown in Fig. 1 and SFRs. Metallicities for these were taken from [18] ( $\rho$  Oph, Chamaeleon, Lupus, Corona-Australis), [1] (ONC, Orion OB1b), [7] (Taurus), Biazzo et al. ([2]  $-\lambda$  Ori, 25 Ori). Ages of the OCs were taken from [12] and [13], or derived consistently. *Filled blue circles* indicate clusters closer than 500 pc to the Sun. The *horizontal line* indicates the solar [Fe/H]

namely, old OCs do not have systematically lower [Fe/H] than younger ones and actually several old clusters are present with a solar or above solar [Fe/H] content. The figure however shows that clusters younger than about 1 Gyr are characterized by a much smaller dispersion than older clusters and that very few of the former have

202 S. Randich

a significantly subsolar iron content (e.g., [Fe/H] < -0.2). More quantitatively, OCs older than 1 Gyr have a mean metallicity [Fe/H]<sub>av.</sub> =  $-0.08 \pm 0.20$ , while for the younger ones we find [Fe/H]<sub>av.</sub> =  $0.01 \pm 0.11$ , i.e., a similar average, but a factor of two smaller dispersion.

Is the lack of metal-poor young clusters real or due to some observational bias? Figure 2 indeed shows that most of the clusters younger than 1 Gyr have distances from the Sun below 500 pc. This suggests that we might be missing metal-poor young clusters, which would be located at farther distances from the Sun, while the young cluster population with available metallicity only samples the solar neighborhood.

## 3.2 Star Forming Regions and Young Associations

In very recent years significant progress has been achieved in the determination of the abundance pattern of low-mass (T Tauri) members of SFRs and young associations ([1] and references therein). Whereas until a few years ago metallicity measurements were scarce and yielded discrepant results, high quality determination for about 10 SFRs are now available. These data show that none of the regions sofar studied has a metallicity above solar; most surprisingly, most of them have a slightly sub-solar metallicity, with the Orion Nebula Cluster being the most metalpoor one ([Fe/H] =  $-0.14\pm0.04$ ). Also, SFRs younger than 10 Myr have on average a lower [Fe/H] than young OCs with ages in the range 10–150 Myr (see Fig. 2). Both the SFR and young cluster samples are relatively small and additional homogeneous measurements are needed. With this caveat in mind, Biazzo et al. noted that, given the young age of the clusters, stellar migration is unlikely the reason for the possible difference in the [Fe/H] distributions of the OCs and SFRs. Hence, this difference is likely to reflect a difference in the interstellar gas from which members of SFRs and young clusters formed. This in turn must be a relic of the process of star formation in the solar neighborhood, rather than an effect of chemical evolution, given the short timescales involved and the fact, that in any case chemical evolution would yield that the younger regions (i.e., the SFRs) are more metal-rich than the older clusters.

Furthermore, the homogeneous study of the abundance pattern in Orion by Biazzo et al. (2011, in preparation), also allowed them to eventually exclude significant group-to-group variations in  $\alpha$  elements, which would be the signature of local enrichment due to Supernova explosion.

Finally, the lack of metal-rich SFRs represents a puzzle within the context of the metallicity-planet connection, since, as well known, gas giant planets are preferentially found around metal-rich stars. On the one hand, as suggested by [18] this might mean that metal-rich stars hosting gas giant planets have migrated into the solar neighborhood from the inner parts of the Galaxy, where the probability of forming planets would therefore be higher (see also discussion in [7]). On the other hand, the lack of metal-rich T Tauri stars in SFRs, might indicate that the probability of finding newly formed planets around them is low.

## 4 Radial Metallicity Gradient

Radial abundance gradients and their evolution with Galactic age are among the most critical empirical constraints that one can put on the star formation history in the Galactic disc, the initial mass function, gas flows, and, more in general, on Galactic chemical evolution models For instance, the variation with time (or lack thereof) of the iron abundance gradient is the consequence of the disc formation process and different predictions (e.g., time-flattening evolution or the opposite) are made by different models (e.g., [3, 16]). Several studies of OCs have addressed the issue of the metallicity gradient, but no final agreement on both its shape and its time evolution has been reached sofar. It is now commonly accepted that a gradient is present, i.e. [Fe/H] decreases with increasing Galactocentric distance (R<sub>GC</sub>). This is normally explained in most Galactic evolution models by assuming different infall and star formation rates for the inner and outer disc. However, three different interpretations are proposed on the empirical side for the exact shape and slope of the gradient; each of the three implies different scenarios of inner disc vs. outer disc evolution. Twarog et al. [20] suggested that the decreasing trend is the result of two different plateaus, one around solar metallicity and for R<sub>GC</sub> below 10 kpc, and a second one, with a metallicity around [Fe/H] = -0.3, for larger  $R_{GC}$  values. [15] instead conclude that the gradient is consistent with a rather shallow slope  $(\sim -0.05 \pm 0.01 \text{ dex kpc}^{-1})$  and with a gentle change around 12 kpc, where the gradient becomes flat. Finally, [12] and [13] –see also Fig. 3) suggest a steeper slope

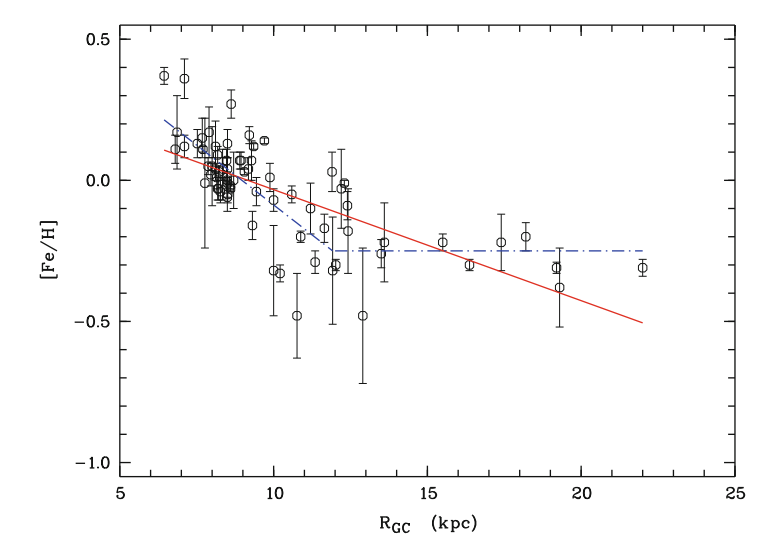


Fig. 3 [Fe/H] as a function of the Galactocentric distance. The latter has been derived adopting a solar  $R_{GC}$  equal to 8.5 Kpc (see [12]). The *red solid line* represents the best fit to all points, assuming a single slope ( $-0.04\pm0.005~{\rm dex~kpc^{-1}}$ ); the *blue dashed line* instead indicates the fit up to 12 kpc (slope equal to  $-0.085\pm0.01~{\rm dex~kpc^{-1}}$ ) and a flat gradient for larger radii

(of the order of  $-0.1 \, dex \, kpc^{-1}$ ) up to a given radius, after which the distribution becomes flat. We believe that the current sample of OCs and, in particular, the inclusion in the sample of the tree clusters located at small radii [13], confirm a steep slope for the inner clusters and a flattening afterwards, with a rather abrupt transition. Available data, in particular the paucity of OCs with  $R_{GC}$  between 12 and 15 kpc, do not allow constraining the exact radius where the change of slope, and thus the transition between inner and outer disc, occur.

Also, it is not yet ascertained whether there is an evolution of the gradient with age. Whereas [12] and [13] found hints of evolution, with the gradient becoming flatter at younger ages, the sample of young clusters at large  $R_{GC}$  and in the inner part of the disc is still small. Additional measurements are therefore needed to draw firm conclusions on this issue.

### 5 Other Elements

The abundances of  $\alpha$ , Fe-peak, and neutron capture elements and their ratios to Fe are crucial to get insights on the importance of stars with different masses and evolutionary lifetimes in the heavy element enrichment of the interstellar medium, as well as to put constraints on stellar yields. As mentioned in the Introduction, in recent years a significant step forward has been made in measurements of abundances of several OCs. The main results are discussed below.

Several recent studies have compared [X/Fe] ratios in OCs with the pattern of field stars (e.g., [10, 13, 15, 19]). All these studies concur that OCs show a rather homogeneous [X/Fe] abundance pattern, although some scatter is present, most likely due to random and systematic measurement uncertainties. Both the Fepeak and the  $\alpha$  elements show, within uncertainties, close-to-solar ratios and are consistent with the distribution of field stars in the thin disc. Interestingly, [5] and [1] found that young nearby clusters and SFRs are also characterized by a solar abundance pattern, suggesting that the solar neighborhood has undergone very little (if any) chemical evolution since the formation of the Sun.

#### 5.1 Abundance Gradient

All the elements show a [X/H] gradient very similar to the iron gradient; in other words, the trend of [X/Fe] with  $R_{GC}$  is flat, although at any given  $R_{GC}$  a rather large dispersion of [X/Fe] values is seen. This result is consistent with Galactic chemical evolution models, since the gradient is determined for all elements by the radial dependence of the star formation rate and infall. Claims were made that clusters at large  $R_{GC}$  might show some enhancement in  $\alpha$ -elements (e.g., [22]), which was interpreted as due to a different star formation history in the outer parts of the disc

and, in particular, to accretion of enriched material. Friel et al. [10] suggest that the enhancement is instead consistent with the [O/Fe] vs. [Fe/H] trend for field stars (higher O for lower [Fe/H]) and with the under-solar metallicity of the outer clusters.

## 5.2 Age Evolution

Similarly to iron, most of the other elements do not show any age evolution and old OCs are characterized by the same abundance pattern as younger ones [15]. Two exceptions are however found which are discussed below.

Oxygen. Friel et al. [10], based on their own measurements for six clusters and on a compilation of data from the literature, found that oxygen appears enhanced in old OCs with respect to young ones. They suggested that this might be due to the fact that older clusters have formed from material more enriched by Type II SNe than younger counterparts. However, they caveat that systematic effects in oxygen abundance determination might play a role; the trend should therefore be confirmed based on a larger and more homogeneous oxygen dataset.

s-process elements. D'Orazi et al. [6] determined barium abundances in a sample of  $\sim$ 20 clusters. Surprisingly, they found that an age-metallicity relationship does hold for this s-process element, since young clusters are characterized by systematically higher [Ba/Fe] ratios than older ones. Their results were based on stars that have inherited Ba from previous generations and have not produced it yet; thus the enhancement must be due to enrichment of the interstellar medium from which the stars formed. D'Orazi et al. [6] showed that their chemical evolutionary model could reproduce the observed trend only by introducing different Ba yields from low-mass AGB stars. In particular, they needed an overproduction of Ba in stars with masses between 1 and 1.5  $M_{\odot}$ . If the enhancement of Ba in young clusters is real and not due to systematic effects (like., e.g., NLTE due to chromospheric activity of young stars), the same enhancement should be observed for other s-process elements. For this reason, we measured additional s-process elements; namely, yttrium and zirconium, belonging to the first peak of the heavy element abundance distribution, along with lanthanum and cerium, which belong to the second peak of the same distribution (Maiorca et al., in preparation). Note that none of the lines used for the analysis is known to suffer from NLTE effects. In Fig. 4 we plot [Ce/Fe] as a function of cluster age. Similarly to the results for Ba, the figure clearly shows that Ce increases with decreasing stellar age; in particular, [Ce/Fe] is around solar (or below) for clusters older than 1 Gyr, while it is enhanced by  $\sim 0.2 - 0.3$  dex for the younger counterparts. Similar behaviour is seen for Y, Zr, and La. This not only confirms the results of [6], but knowledge of the [X/Fe] vs. age pattern for different elements allows putting further constraints on the efficiency of the s-process in lowmass stars.

206 S. Randich

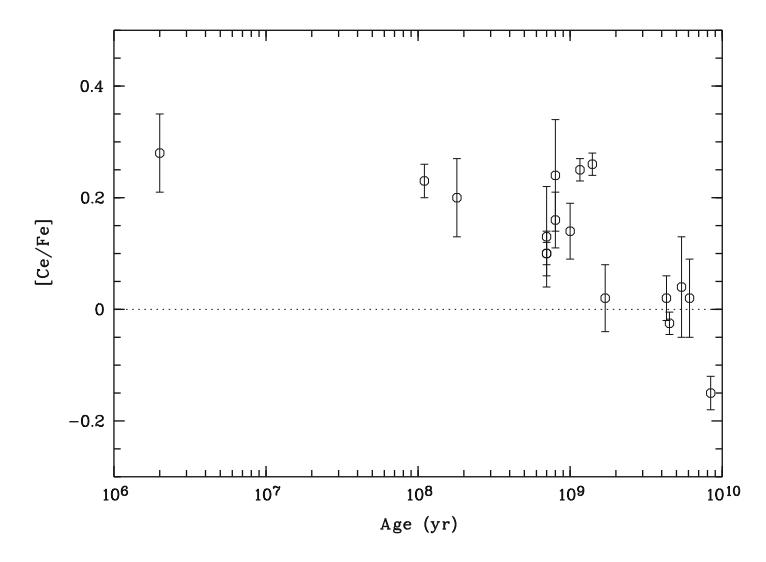


Fig. 4 Ratio of cerium over iron ([Ce/Fe]) as function of cluster age for a sample of clusters studied by Maiorca et al. (in preparation). The horizontal line denotes the solar ratio

## References

- 1. Biazzo, K., Randich, S., & Palla, F., A&A, 525, 35 (2011)
- 2. Biazzo, K., Randich, S., Palla, F., & Briceño, C., A&A, 530, 19 (2011)
- 3. Chiappini, C., Matteucci, F., Romano, D.: Astrophys. J. 554, 1044 (2001)
- 4. Cunha, K, Lambert, D.L.: Astrophys. J. 426, 170 (1994)
- 5. D'Orazi, V., Randich, S.: Astron. Astrophys. 501, 553 (2009)
- 6. D'Orazi, V., Magrini, L., Randich, S., et al.: Astrophys. J. 693, L31 (2009)
- 7. DOrazi, V., Biazzo, K., & Randich, S., A&A, **526**, 103 (2011)
- 8. Friel, E.D.: Annu. Rev. Astron. Astrophys. 33, 381 (1995)
- Friel, E.D.: In: Chemical Abundances and Mixing in Stars in the Milky Way and its Satellites, ESO Astrophysics Symposia, p. 3 (2006)
- 10. Friel, E.D., Jacobson, H.R., Pilachowski, C.A.: Astron. J. 139, 5 (2010)
- 11. Gratton, R.: ASP Conf. 198, 225 (2000)
- 12. Magrini, L., Sestito, P., Randich, S., Galli, D.: Astron. Astrophys. 494, 95 (2009)
- 13. Magrini, L., Randich, S., Zoccali, M., et al.: Astron. Astrophys. 523, 11 (2010)
- 14. Maiorca, E., Randich, S., Busso, M., Magrini, L., & Palmerini, S., ApJ, 736, 120 (2011)
- 15. Pancino, E., Carrera, R., Rossetti, E., Gallart, C.: Astron. Astrophys. 511, 56 (2010)
- 16. Portinari, L., Chiosi, C.: Astron. Astrophys. 350, 827 (1999)
- 17. Randich, S., Bragaglia, A., Pastori, L.: ESO Messenger 121, 18 (2005)
- 18. Santos, N.C., Melo, C., James, D.J., et al.: Astron. Astrophys. 480, 889 (2008)
- 19. Sestito, P., Bragaglia, A., Randich, S. et al.: Astron. Astrophys. 488, 943 (2008)
- 20. Twarog, B.A., Ashman, K.M., Anthony-Twarog, B.J.: Astron. J. 114, 2556 (2009)
- 21. Viana Almeida, P., Santos, N.C., Melo, C., et al.: Astron. Astrophys. 501, 965 (2009)
- 22. Yong, D., Carney, B., Teixeira de Almeida, M.L.: Astron. J.130, 597 (2005)

## Deep and Extended Multiband Photometry of the Galactic Globular Cluster M71

Alessandra Di Cecco, Giuseppe Bono, Matteo Monelli, Peter B. Stetson, Rosa Becucci, Scilla Degl'Innocenti, Pier G. Prada Moroni, and Roberto Buonanno

**Abstract** We present the preliminary results of the ground-based (MegaCam@ CFHT) and space-based (ACS@HST) photometry for the Galactic globular cluster M71. By comparing data and theory, we found that the age  $(11.0 \pm 1.5 \, \text{Gyr})$  of M71 agrees well with the bulk of the more metal poor globular clusters.

#### 1 Introduction

The age of the globular clusters (GCs) provides key information concerning the epoch of the Galaxy's birth. In particular, the metal-rich GCs are considered essential age tracers for investigating the formation of the Galactic halo, thick disk and bulge. M71 is one of the most metal-rich ([Fe/H] = -0.73, [5]) GCs and it is located at low Galactic latitude ( $l = 56.74^{\circ}$ ,  $b = -4.56^{\circ}$ ). This cluster is affected by a moderate reddening (E(B-V) = 0.25), a low mass, and a low central density ( $Log(\rho_c) \simeq 3 L_{\odot} pc^{-3}$ ). In a previous investigation based on Ströngrem photometry, [4] found that this cluster is  $\sim$ 2 Gyr younger than the the bulk of the more metal poor GCs.

A.D. Cecco (⊠)

ESO, Karl Schwarzschild Strasse 2, D-85738 Garching, Germany

e-mail: adicecco@eso.org

G. Bono · R. Buonanno G., UniToV, via della Ricerca Scientifica 1, 00173 Rome, Italy

M Monelli

IAC, C/ Via Lactea, 38205 San Cristobal De La Laguna, Tenerife, Spain

P.B. Stetson

DAO-HIA, NRC, 5071 West Saanich Road, Victoria, BC V9E 2E7, Canada

R. Becucci · S. Degl'Innocenti · P.G. Prada Moroni Department of Physics, University of Pisa, Largo B. Pontecorvo 2, 56127 Pisa, Italy

A. Moitinho and J. Alves (eds.), *Star Clusters in the Era of Large Surveys*, Astrophysics and Space Science Proceedings, DOI 10.1007/978-3-642-22113-2\_29, © Springer-Verlag Berlin Heidelberg 2012

A.D. Cecco et al.

#### 2 Dataset and Results

We used ground-based data acquired with MegaCam@CFHT (FoV:  $1^{\circ}$  x  $1^{\circ}$ , scale: 0.187''/pixel) and space data from ACS@HST (FOV:  $202'' \times 202''$ , scale: 0.05''/pixel). The complete MegaCam data consists of 50 dithered images, taken in the 5 SDSS bands: u', g', r', i', z' (see [2] for details). Up to now, we used the images acquired by the two central chips (total FoV:  $7' \times 35'$  around the cluster center) in four bands (g', r', i', z'). The space data came from HST archive and were acquired in the F814W and F606W bands. For each frame we performed PSF photometry using

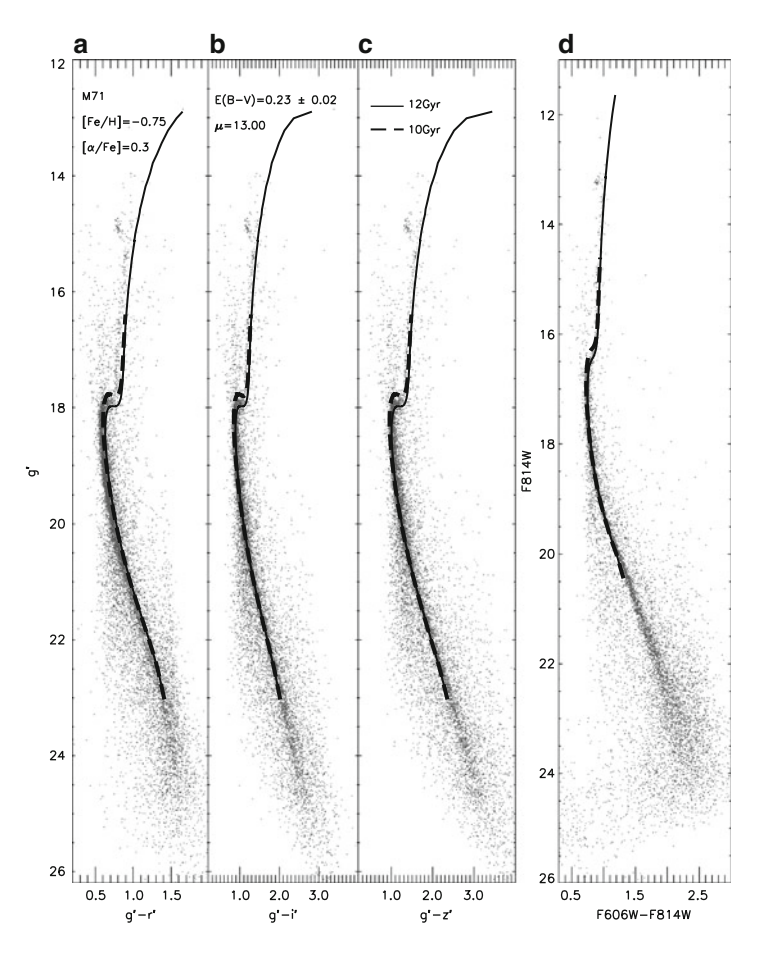


**Fig. 1** CMD of the GC M71. Panels (a), (b), (c) show the CFHT data. Panel (d) shows ACS data. The *dashed* and the *solid lines* show 10 and 12 Gyr cluster isochrones at fixed chemical composition

<sup>&</sup>lt;sup>1</sup>GO: 10775, PI: Sarajedini

DAOPHOT IV and ALLSTAR [6]. Individual catalogs of the chips were rescaled to a common reference system using DAOMATCH/DAOMASTER and then we ran ALLFRAME [7] on the entire dataset. The calibration curves were estimated by using ~2,000 local standard stars from [1]. The color-magnitude diagrams (CMDs) for the CFHT data are plotted in panels (a), (b), (c) of Fig. 1. The ACS data are shown in panel (d) of Fig. 1. The overplotted isochrones were calculated at fixed chemical composition ([Fe/H] = -0.75, [ $\alpha$ /Fe] = 0.3, Y = 0.255; see [3] for a more detailed discussion concerning the adopted input physics). By adopting the same true distance modulus ( $\mu$  = 13.00) and the reddening value (E(B-V) =  $0.23 \pm 0.02$ ) within current uncertainties, we found that the age of M71 is 11.0  $\pm$  1.5 Gyr in all the CMDs of Fig. 1. It is interesting to note that the age found for M71 is, within the uncertainties, similar to the age obtained for one of the most metal poor GCs (M92, [3]) by using the same theoretical framework.

- 1. Clem, J.L., VandenBerg, D.A., Stetson, P.B.: Astron. J.134, 1890 (2007)
- 2. Clem, J.L., Vanden Berg, D.A., Stetson, P.B.: Astron. J.135, 682 (2008)
- 3. Di Cecco, A., Becucci, R., Bono, G., et al.: Publ. Astron. Soc. Pac. 122, 991 (2010)
- 4. Grundahl, F., Stetson, P.B., Andersen, M.I.: Astron. Astrophys. 395, 481 (2002)
- 5. Harris, W.E.: Astron. J.112, 1487 (1996)
- 6. Stetson, P.B.: Publ. Astron. Soc. Pac. 99, 191 (1987)
- 7. Stetson, P.B.: Publ. Astron. Soc. Pac. 106, 250 (1994)

# Chromospheric Activity and Lithium Abundance in NGC2516

Angela E. Messina, Alessandro C. Lanzafame, and Innocenza Busà

**Abstract** We present new measurements of lithium abundance and chromospheric activity in the NGC2516 open cluster using FLAMES-VLT archive data. These supplement existing data and provide new information on the spread of lithium abundance and the chromospheric activity index  $R'_{\rm HK}$  at approximately the Pleiades age. Comparison with theoretical models and with other observational data for the lithium abundances of NGC2516 shows that the hotter stars in our sample have a higher lithium depletion than average. Finally, the chromospheric activity index  $R'_{\rm HK}$ , compared to other know cluster data, seems to give a lower chromospheric age than the one provided from lithium abundance.

## 1 Data Source and Analysis

The data of this work consist of archive VLT/FLAMES spectra of the open cluster NGC 2516. Spectra around the CaII H & K lines cover the range between 385.4 and 404.9 nm, with a resolution R $\sim$ 19,600. Spectra around the lithium doublet cover the wavelength range between 643.8 and 718.4 nm, with R  $\sim$  8,000. The calculation of the lithium abundance and of the chromospheric index of  $R'_{HK}$  is described in [6].

A.E. Messina (⋈) · A.C. Lanzafame

Dipartimento di Fisica e Astronomia, Sezione Astrofisica, Università di Catania,

INAF - Osservatorio Astrofisico di Catania, Via S. Sofia 78, 95123 Catania, Italy e-mail: angela.messina@oact.inaf.it

I Busà

INAF - Osservatorio Astrofisico di Catania, Via S. Sofia 78, 95123 Catania, Italy

212 A.E. Messina et al.

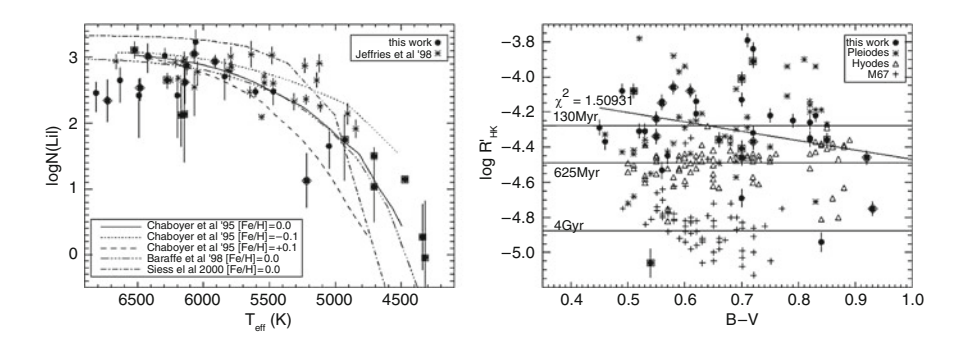


Fig. 1 Lithium abundances vs  $T_{eff}$  (left) together with data from [3] and a comparison with theoretical models [1,2,7] at 150 Myr. The chromospheric activity index  $\log R'_{HK}$  vs B-V (right) is compared with clusters of different age and the  $\log R'_{HK}$  vs. age empirical relation (all from [5]). A linear fit to NGC 2516 members data are also shown. In both figures, diamonds indicate binaries and squares not members

### 2 Comparison with Theory and Other Data

The derived lithium abundance supplemented by data from [3] have been compared with theoretical models at 150 Myrs (Fig.1, left panel). The models of [1] and [2] (with -0.1 < [Fe/H] < 0) agree quite well with the data; the model of [7] shows a deficient depletion for star hotter than 5,000 K and an excessive depletion for cooler stars. The hotter stars in the sample show a higher Li depletion, somewhat correlated to their relatively lower  $v \sin i$ .

The log  $R'_{\rm HK}$  dependence on B-V is compared with other clusters (Fig.1, right panel) and with the log  $R'_{\rm HK}$  vs. age empirical relation of [5]. The log  $R'_{\rm HK}$  points are just above the age of Pleiades (130 Myr), and their media give a chromospheric age of  $\sim$ 120 Myrs, in the range of 0.5 < B-V < 0.9.

**Acknowledgements** Angela E. Messina thanks the EAS for the grant support, which made the participation at this meeting possible.

- 1. Baraffe, I., Chabrier, G., Allard, F., Hauschildt, P.H.: Astron. Astrophys. 337, 403 (1998)
- 2. Chaboyer, B., Demarque, P., Pinsonneault, M.H.: Astrophys. J. 441, 876 (1995)
- 3. Jeffries, R.D., James, D.J., Thurston, M.R.: Mon. Not. R. Astron. Soc. 300, 550 (1998)
- 4. Jeffries, R.D., Thurston, M.R., Hambly, N.C.: Astron. Astrophys. 375, 863 (2001)
- 5. Mamajek, E.E., Hillenbrand, L.A.: Astrophys. J. 687, 1264 (2008)
- 6. Messina, A.: PhD Thesis, University of Catania (2010)
- 7. Siess, L., Dufour, E., Forestini, M.: Astron. Astrophys. 358, 593 (2000)

# A Deep Photometric Survey of the Double Cluster h & $\chi$ Per

Cátia V. Cardoso, Estelle Moraux, and Jerôme Bouvier

**Abstract** We performed a deep multi-band photometric survey of the central regions of the young ( $\sim$ 13 Myr) and very rich double cluster, h &  $\chi$  Persei, extending the membership down to the boundary region between stellar and substellar domain (0.07M $_{Sun}$ ). We used data from CFHT (WIRCAM and MEGACAM) in I, Y, J, H and Ks bands. To select the candidate members we produced CMDs that we compared with the isochrones, and previous known members from photometric, spectroscopical, X-ray, proper motion, disk and H alpha emission studies. We selected several thousand candidate members in h &  $\chi$  Persei, down to late M dwarfs in a field of view of 20 by 20 arcmin for each cluster.

h &  $\chi$  Persei is a young very dense double cluster (e.g., Mayne et al. [5] through pre-main sequence isochrone fitting derived an age of 13 Myr; Currie et al. ([2], presented the most complete spectroscopic study of this double cluster 11,000 stars, ongoing X-ray study by Caramazza et al.).

Using data from CFHT (WIRCAM and MEGACAM) in I, Y, J, H and Ks bands and additional known candidate members from other studies (e.g. [2]) we made a candidate member selection based on the BT-Settl isochrone model [1].

To estimate our completeness and saturation levels we compared our observations to the Besançon Galactic Models. To obtain an estimate of the cluster parameters we fitted a King profile [4] to the two clusters simultaneously plus a field contamination, rc and rt are the core radius and tidal radius, respectively. The cluster centre was derived by Bragg and Kenyon [3], because due to saturation of

C.V. Cardoso (⊠)

University of Exeter, EX4 4QL, Exeter, UK

e-mail: catia@astro.ex.ac.uk

E. Moraux · J. Bouvier LAOG, Grenoble, France

e-mail: estelle.moraux@obs.ujf-grenoble.fr; Jerome.Bouvier@obs.ujf-grenoble.fr

214 C.V. Cardoso et al.

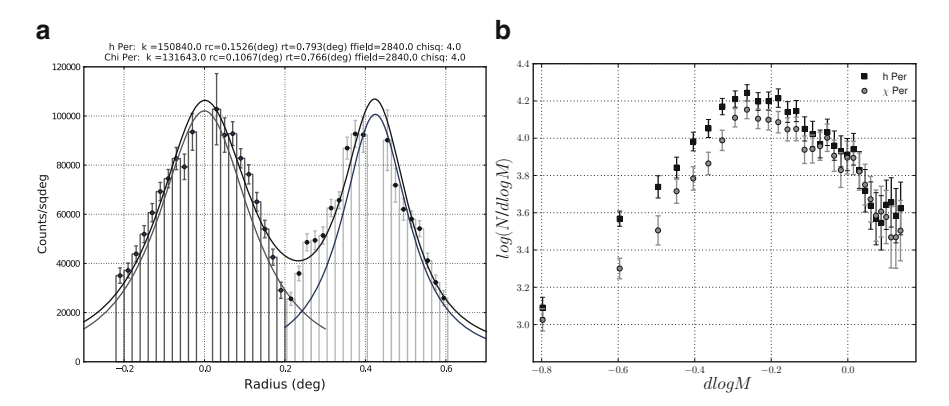


Fig. 1 (a) Radial star density profile, with the double King profile fitted to the data. h Per on the *left* and  $\chi$  Per on the *right*. The central bins were removed because of incompleteness due to the presence of bright stars in the field. This profile was calculated in a horizontal strip across the centre of the two clusters to minimize the contamination differential due to the presence of the companion cluster. (b) h Per (*black squares*) and  $\chi$  Per (*grey circles*) Stellar Mass Function. In our candidate selection we estimate to be complete to  $\sim 0.1 M_{Sun}$ 

bright stars in the core region we have a limited precision. The area covered by our observations does not allow us to constrain both the tidal radius and the field stars density. We estimated the tidal radius using equation (10) of Pinfield et al. [6], that assumes a circular orbit of the cluster around the Galactic centre, we have taken the cluster mass values from [2]. The estimate of the field contamination derived using the King profile was negligible. So in this preliminary work we will be presenting an uncorrected for field contamination stellar mass function.

With our multi-band photometric study we have selected 16,000 candidate cluster members down to brown dwarfs ( $\sim$ 0.06  $M_{Sun}$ ). We have estimated from King profiles the cluster extent and concentration. We presented preliminary results of the deepest Stellar Mass Function for h &  $\chi$  Persei down to 0.1  $M_{Sun}$ 

**Acknowledgements** We would like to thank the people from Terapix (P. Hudelot, E. Bertin), the people from the Monitor project (J. Irwin) and F. Allard for the BT-Settl models. This work is funded in part by the European Commission Sixth Framework Programme Marie Curie Research Training Network CONSTELLATION (MRTN-CT-2006-035890).

- 1. Allard, F.: Astron. Astrophys. **500**, 93 (2009)
- Currie, T., Hernandez, J., Irwin, J., Kenyon, S.J., Tokarz, S., Balog, Z., Bragg, A., Berlind, P., Calkins, M.: Astrophys. J. Suppl. 186, 191 (2010)
- 3. Bragg, A.E., Kenyon, S.J.: Astrophys. J. 130, 134 (2005)
- 4. King, I.: Astrophys. J. 67, 471 (1962)
- 5. Mayne, N.J., Naylor, T., Littlefair, S.P., Saunders, E.S., Jeffries, R.D.: Mon. Not. R. Astron. Soc. 375, 1220 (2007)
- 6. Pinfield, D.J., Jameson, R.F., Hodgkin, S.T.: Mon. Not. R. Astron. Soc. 299, 955 (1998)

# A Detailed Spectroscopic Analysis of the Open Cluster NGC 5460

Luca Fossati, Colin P. Folsom, Stefano Bagnulo, Jason Grunhut, John Landstreet, Oleg Kochukhov, Claudia Paladini, and Gregg A. Wade

**Abstract** In stellar astrophysics, the study of the atmospheres of early-type stars plays a very special role since they display a variety of different phenomena, such as diffusion of chemical elements. To understand the actual role of all these physical phenomena, it is important to seek constraints from observations and for this purpose open cluster stars are particularly interesting they have: the same original chemical composition and age, and accurate age determinations. Here we present the results obtained for the stars observed in NGC 5460 with the FLAMES multiobject spectrograph of the ESO VLT. We find that the abundance of several elements increases with temperature between 7,000 and 10,500 K and decreases from 10,500 to 13,000 K. No correlation between abundance and  $v \sin i$  was found.

## 1 Introduction, Abundance Analysis and Results

The chemical compositions of early-type field stars have been studied by several authors, but the published results tend to be inhomogeneous and not easy to combine. Our goal is to determine abundance patterns in early-type cluster members of different ages. Therefore, we performed a large observational campaign obtaining spectroscopy of a large number of early-type stars in a sample of ten open clusters, homogeneously distributed in age from  $\log t = 6.8$  to  $\log t = 8.9$ . The observed clusters and the instruments used for the observations are presented in [4].

All our results regarding the Praesepe open cluster are published in [2,3,6]. This work is dedicated to the analysis of NGC 5460, that we observed with the FLAMES

L. Fossati (⋈)

Department of Physics and Astronomy, Open University, Walton Hall,

Milton Keynes MK7 6AA, UK e-mail: l.fossati@open.ac.uk

C. Paladini

Institut für Astronomie, Universität Wien, Türkenschanzstrasse 17, 1180 Wien, Austria e-mail: claudia.paladini@univie.ac.at

L. Fossati et al.

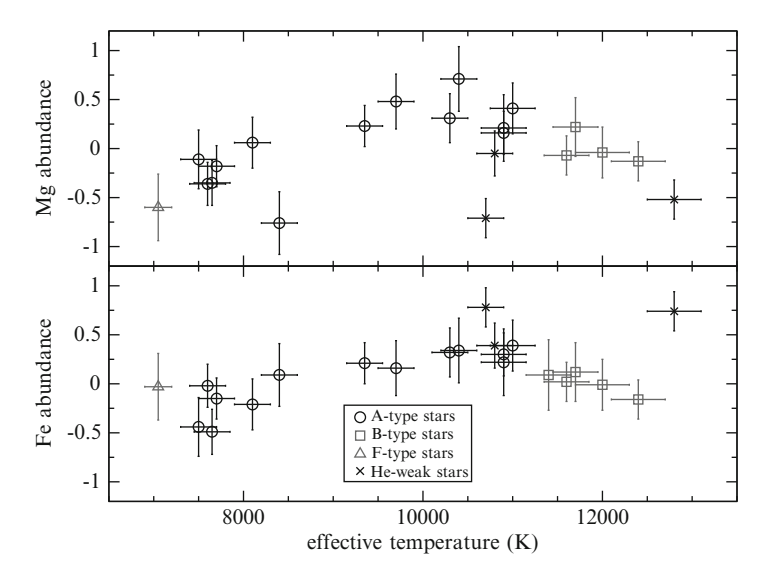


Fig. 1 Abundances relative to the Sun [1] of the most analysed elements as a function of  $T_{\rm eff}$  for B- (open squares), A- (open circles), F-type (open triangles) and He-weak stars (crosses)

multi-object spectrograph at the ESO VLT. Parameter determination and abundance analysis were performed making use of the methodology, codes and tools described in [2,3].

Figure 1 displays the abundances of Mg and Fe against  $T_{\rm eff}$ : the abundance increases with  $T_{\rm eff}$  up to  $T_{\rm eff}{\sim}10{,}500\,{\rm K}$  and decreases for higher temperatures. A linear fit shows that these correlations are significant for both Mg and Fe.

Further analysis allows us to conclude that errors in the parameters produced such trends. We also find it to be unlikely that our LTE approximation could be the source of the abundance correlations with  $T_{\rm eff}$  for both Mg and Fe [5, 7], while diffusion processes could be responsible for the correlations observed.

- Asplund, M., Grevesse, N., Sauval, A.J.: In: Barnes, T.G., Frank, N. (eds.) Cosmic Abundances as Records of Stellar Evolution and Nucleosynthesis, ASP Conference Series, vol. 38, p. 25 (2005)
- Fossati, L., Bagnulo, S., Monier, R., Khan, S.A., Kochukhov, O., Landstreet, J., Wade, G., Weiss, W.: Astron. Astrophys. 476, 911 (2007)
- Fossati, L., Bagnulo, S., Landstreet, J., Wade, G., Kochukhov, O., Monier, R., Weiss, W., Gebran, M.: Astron. Astrophys. 483, 891 (2008)
- Fossati, L., Bagnulo, S., Monier, R., Khan, S.A., Kochukhov, O., Landstreet, J.D., Wade, G.A., Weiss, W.W.: Contributions of the Astronomical Observatory Skalnate Pleso, 38, 123 (2008)
- Fossati, L., Ryabchikova, T., Bagnulo, S., Alecian, E., Grunhut, J., Kochukhov, O., Wade, G.: Astron. Astrophys. 503, 945 (2009)
- 6. Fossati, L., Mochnacki, S., Landstreet, J., Weiss, W.: Astron. Astrophys. 510, A8 (2010)
- 7. Przybilla, N., Butler, K., Becker, S.R., Kudritzki, R.P.: Astron. Astrophys. 369, 1009 (2001)

# A Kinematic Study of Open Clusters: Implications for Origin

Dave Vande Putte, Thomas P. Garnier, Ignacio Ferreras, Roberto Mignani, and Mark Cropper

**Abstract** The Galactic population of Open Clusters provides an insight into star formation in the Galaxy. The open cluster catalogue by Dias et al. Astron. Astrophys. 389, 871 (2002) is a rich source of data, including kinematic information. This large sample made it possible to carry out a systematic analysis of 481 open cluster orbits, using parameters based on orbit eccentricity and separation from the Galactic plane. These two parameters may be indicative of origin, and we find them to be correlated. We also find them to be correlated with metallicity, another parameter suggested elsewhere to be a marker for origin in that high values of any of these two parameters generally indicate a low metallicity ([Fe/H] Solar < -0.2 dex). The resulting analysis points to four open clusters in the catalogue being of extra-Galactic origin by impact of high velocity cloud on the disk: Berkeley 21, 32, 99, and Melotte 66, with a possible further four due to this origin (NGC 2158, 2420, 7789, IC 1311). A further three may be due to Galactic globular cluster impact on the disk i.e of internal Galactic origin (NGC 6791, 1817, and 7044).

## 1 Open Cluster Database and Orbit Calculations

Orbit calculations require values for the six positional and velocity parameters. Several large compilations exist, and we chose DAML [1], Version 2.10. It lists 1787 OCs, and the required information is available for 481 clusters, of which 111 also have metallicity data. These subsets of DAML constituted our database for this work. The orbits are generated as described in [2], using an analytical model of the Galactic potential.

D.V. Putte (⋈) · T.P. Garnier · I. Ferreras · R. Mignani · M. Cropper Mullard Space Science Laboratory, UCL, Dorking, RH5 6NT, UK e-mail: dwvp@mssl.ucl.ac.uk

D.V. Putte et al.

### 2 Orbit Analysis

The orbital parameters are the maximum height above the plane  $(z_{max})$ , and  $\eta$ which is the orbit width in the disk plane, divided by the average orbit radius in the disk plane. The larger these parameters, potentially the more unusual the origin of the cluster. We find the orbital parameters to be correlated between them, and to be correlated with decreasing metallicity. We set the threshold for unusual origin at  $z_{max} > 0.9$  kpc,  $\eta > 0.5$ , and metallicity [Fe/H] < -0.2 dex, based on the probability distributions of these parameters in the selected database. Thirty-five clusters meet at least one criterion for unusual origin. Clusters Berkeley 21, 32, 99, and Melotte 66 are the only ones satisfying all three criteria. In addition to mergers, alternative explanations could account for the origins of these OCs. For example, Berkeley 21, 32, 99, and Melotte 66 could result from low metallicity, extra-Galactic high velocity clouds in the halo being shocked by a Globular Cluster. NGC 2158, 2420, 7789, and IC 1311 meet the metallicity and criteria, so could also be due to these causes. NGC 6791, 1817, and 7044 meet the  $\eta$  criterion and have metallicities near Solar, so they could be due to a Globular Cluster shocking the disk, and imparting a motion that is not circular. Nine other clusters meet only the metallicity criterion, and could thus be due to a merger with a body containing these clusters, or with the clusters being caused by merger. Another 15 clusters meet one criterion only, but the remainder of their relevant data do not permit conclusions about their origin.

#### 3 Conclusion

Orbital and metallicity analysis of the Open Clusters in DAML provides a tool for suggesting a variety of OC formation mechanisms. Eight clusters may be the result of Globular Cluster impacts with low metallicity, high altitude extra-Galactic high velocity clouds: Berkeley 21, 32, 99, Melotte 66, NGC 2158, 2420, 7789, IC 1311. Globular clusters impacting gas clouds in the disk could have produced three further Open Clusters: NGC 6791, 1817, 7044. Another eleven that meet only the metallicity criterion could be the result of mergers. Another fifteen satisfy one criterion for unusual origin, but data are not sufficient to reach a conclusion on origin. Time has been granted to spectroscopically observe seven of the top eight candidates for unusual origin. The full list of cluster candidates is given in Table 4 of [2].

- 1. Dias, W.S., Alessi, B.S., Moitinho, A., Lépine, J.R.D.: Astron. Astrophys. 389, 871 (2002)
- Vande Putte, D., Garnier, T., Ferreras, I., Mignani, R., Cropper, M.: Mon. Not. R. Astron. Soc. 407, 2109 (2010)

# The Luminosity Function of Globular Clusters Used As a Distance Indicator

Daniela Villegas, and the ACS Fornax Cluster Survey team

**Abstract** We report on the results of a study of the properties of the globular cluster luminosity function (GCLF) as a distance indicator, performed using the homogeneous data set provided by the ACS Virgo and Fornax Cluster Surveys. The relative Virgo–Fornax distance modulus derived from our study is systematically lower than the values derived by other distance indicators and in particular is 0.2 mag lower than the value obtained by using surface brightness fluctuation measurements on the same data-set. Overall, the results discussed here indicate that the GCLF parameters vary continuously and systematically as a function of galaxy luminosity (i.e., mass) and may be influenced by the cluster environment as suggested by cosmological simulations.

#### 1 Context

This contribution summarises the results of a study of the globular cluster luminosity function (GCLF) of 132 early-type galaxies [5]. We aimed to perform a precise test of the use of the turnover magnitude of the GCLF ( $\mu$ ) as a distance indicator by comparing the relative distance between the Virgo and Fornax clusters derived using this method to the one derived from a surface brightness fluctuations (SBFs) analysis performed on the same data-set.

Each of the 132 galaxies included on this study was observed with ACS during a single HST orbit, as part of the ACS Virgo Cluster Survey [2] and the ACS Fornax Cluster Survey [4]. The globular cluster system of each galaxy was studied using a maximum likelihood approach to model the intrinsic GCLF using a Gaussian distribution after accounting for contamination and completeness effects.

D. Villegas (⊠)

European Southern Observatory, Karl Schwarzschild Str. 2, 85748 Garching, Germany e-mail: dvillega@eso.org

#### 2 Results

The main results of this study can be summarised as follows:

- Using the GCLF turnover magnitude as a distance indicator on this very homogeneous data set, we derive a relative distance modulus between the Virgo and Fornax clusters of  $0.21 \pm 0.04$  mag, which is 0.21 mag lower than the one derived using SBF measurements of the same data  $(0.42 \pm 0.03, [1])$ .
- Setting the relative Virgo—Fornax distance as that given by SBF implies a difference in the value of  $\mu$  in the two closest clusters of galaxies, suggesting that this quantity is influenced by the environment in which a globular cluster system is formed and evolves. The observed discrepancy in the absolute magnitude of the GCLF turnover in Virgo and Fornax can be accounted for if the globular cluster systems in the Fornax cluster were on average 3 Gyr younger than those in Virgo.
- We performed numerical simulations in order to determine how much of the observed dispersion in the value of  $\mu$  is intrinsic. These simulations considered the three main factors driving the spread: cluster depth, measurement errors, and the intrinsic scatter in the turnover magnitude. The simulations allow for an additional dispersion of 0.21 mag in the case of Virgo and 0.15 mag for the Fornax cluster, that cannot be accounted for by the cluster depth or the observational errors alone, and therefore corresponds to an intrinsic dispersion in the value of  $\mu$ .
- The measured GCLF turnover is found to be systematically fainter for low luminosity galaxies, showing a  $\sim$ 0.3 mag decrease in dwarf systems, although we suffer from large uncertainties in that galaxy luminosity regime. This might be at least partly accounted for by the effects of dynamical friction.
- Overall, we find that GCLF parameters vary continuously and systematically as a function of galaxy luminosity (i.e., mass) and may be inuenced by the cluster environment as suggested by cosmological simulations [3].

- 1. Blakeslee, J.P., et al.: Astrophys. J. **604**, 556 (2009)
- 2. Côté, P., et al.: Astrophys. J. Suppl. 153, 223 (2004)
- 3. De Lucia, G. et al.: Mon. Not. R. Astron. Soc. **366**, 499 (2006)
- 4. Jordán, A.: Astrophys. J. Suppl. 169, 213 (2007)
- 5. Villegas, D., et al.: Astrophys. J. **717**, 603 (2010)

# **Chemical Properties of the Hipparcos Red Clump**

Eduardas Puzeras and Gražina Tautvaišienė

**Abstract** *Hipparcos* data have allowed the identification of a large number of clump stars in the solar neighbourhood. We discuss our present knowledge of their distributions of metallicities, CNO abundances, carbon isotope ratios and memberships of the first ascent giants and helium-core-burning stars.

#### 1 Introduction

The *Hipparcos* catalog ([4]) contains about 600 clump stars with parallax error lower than 10%. This accuracy limit corresponds to a distance of about 125 pc within which the sample of clump stars is complete. Now it is important to investigate their distributions of masses, ages, colors, magnitudes and metallicities, which may provide useful constraints to chemical evolution models of the local Galactic disk.

C, N, O, and Fe abundances in Galactic clump stars were recently investigated by means of high-resolution spectroscopy. Abundances of iron peak elements in a sample of 62 red clump stars were investigated by [5]. For a subsample of 34 stars [6] have determined abundances of carbon, nitrogen, oxygen and  $^{12}$ C/ $^{13}$ C isotope ratios. Abundances of C, N and O in 177 clump giants of the Galactic disk were determined by [3]. A sample of 63 red clump stars, mainly located in the southern hemisphere, was investigated by [1]. A spectroscopic analysis of a sample of nearby giants, with red clump stars among them, was done by [2]. From this study we have selected 138 red clump stars.

Institute of Theoretical Physics and Astronomy, Vilnius University, A. Gostauto 12, LT-01108, Vilnius, Lithuania

e-mail: eduardas.puzeras@tfai.vu.lt; grazina.tautvaisiene@tfai.vu.lt

E. Puzeras (⋈) · G. Tautvaišienė

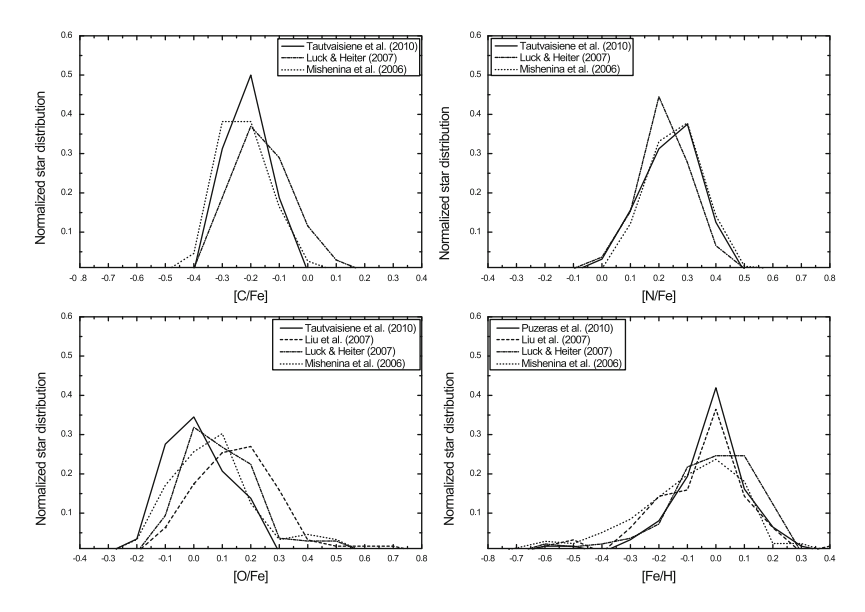


Fig. 1 C, N, O, and Fe abundance distributions in the samples of Galactic clump stars investigated by [1,3-6] and [2]

#### 2 C, N, O, and Fe Abundance Distributions

Up to date analyses of clump stars of the Galaxy show the following characteristics: [Fe/H] range from +0.4 to -0.7 dex with the majority of stars concentrated at solar metallicity value with a scatter of  $\pm 0.2$  dex; [C/Fe] range from -0.4 to 0.1 dex with the maximum at -0.25 dex; [N/Fe] range from 0.0 to +0.5 dex with the maximum at +0.25 dex; [O/Fe] range from -0.2 to 0.3 dex with the maximum number of stars around the solar value.

According to  $^{12}\text{C}/^{13}\text{C}$  isotope ratios determined by [6], the investigated stars fall into two groups of helium-core-burning and first accent giants in almost equal numbers. In the paper by [3], according to nitrogen abundance values, there were found 21 clump giants, about 54 clump candidates and about 100 usual giants.

- Liu, Y.J., Zhao, G., Shi, J.R., Pietrzyński, G., Gieren, W.: Mon. Not. R. Astron. Soc. 382, 553 (2007)
- 2. Luck, R.E., Heiter, U.: Astron. J. 133, 2464 (2007)
- Mishenina, T.V., Bienaymé, O., Gorbaneva, T.I, Charbonnel, C., Soubiran, C., Korotin, S.A., Kovtyukh, V.V.: Astron. Astrophys. 456, 1109 (2006)
- 4. Perryman, M.A.C.: ESA-SP, 404, 231 (1997)
- Puzeras, E., Tautvaišienė, G., Cohen, J.G., Gray, D.F., Adelman, S., Ilyin, I., Chorniy, Y.: Mon. Not. R. Astron. Soc. 404, 1225 (2010)
- Tautvaišienė, G., Edvardsson, B., Puzeras, E., Barisevičius, G., Ilyin, I.: Mon. Not. R. Astron. Soc. 409, 1213 (2010)

# **Chemical Composition of a Kinematically Identified Stellar Group in the Milky Way**

Edita Stonkutė, Gražina Tautvaišienė, Birgitta Nordström, and Renata Ženovienė

**Abstract** We present the preliminary results of a project aimed at high resolution spectral analysis of stars in a kinematically identified stellar group, suspected to belong to a remnant of a disrupted satellite galaxy. The 16 stars analysed by now have a metallicity around -0.7 dex, an average isochrone age of about 12 Gyr, their chemical composition is homogeneous and distinct from the Galactic disk dwarfs. This provides further evidence of their common and maybe extragalactic origin.

#### 1 Introduction

The formation and evolution of the Milky Way is quite complex and still not fully understood. Helmi et al. [4] have used a homogeneous data set of about 14.500 F- and G-type stars from the Nordström et al. catalogue [5], which has complete kinematic, metallicity and age parameters, to search for signatures of past accretions in the Milky Way. There were found three groups of stars which in so called APL space cluster around a region of roughly constant eccentricity, they have distinct metallicity [Fe/H] and age distribution, providing hints of their common origin [4].

From high-resolution spectra obtained with the FIES spectrograph at the Nordic Optical Telescope, La Palma, we measured abundances of oxygen,  $\alpha$ -elements and other heavier chemical elements in stars belonging to the third group identified by Helmi et al. [4]. The method of analysis can be found in our previous paper [8].

Institute of Theoretical Physics and Astronomy, Vilnius University, A. Gostauto 12, LT-01108, Vilnius, Lithuania

e-mail: edita.stonkute@tfai.vu.lt; grazina.tautvaisiene@tfai.vu.lt; renata.zenoviene@tfai.vu.lt

B. Nordström

Niels Bohr Institute, Copenhagen University, Juliane Maries Vej 30, DK-2100, Copenhagen, Denmark

e-mail: birgitta@astro.ku.dk

E. Stonkutė (⋈) · G. Tautvaišienė · R. Ženovienė

224 E. Stonkutė et al.

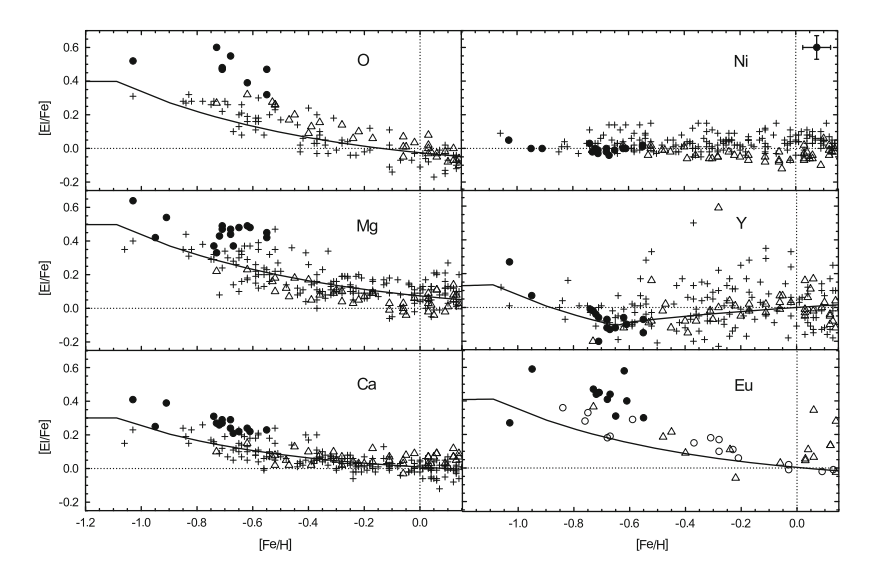


**Fig. 1** Chemical element abundances for our program stars (*black dots*). The data for the Milky Way disk dwarfs by [3] (*plus signs*), [1] (*open triangles*) and [2] (*open circles*). The Galactic chemical evolution models by [6,7] are shown with *solid lines* 

## 2 Detailed Chemical Composition

From the detailed chemical composition of the stars investigated we see that the sample is chemically homogeneous (Fig. 1). The average value of [Fe/H] for the 16 stars investigated in this study is -0.7 dex. Abundances of oxygen,  $\alpha$ -elements and the r-process element europium are overabundant in comparison to the Galactic disk dwarfs [1–3] and the modeled trends [6,7]. The distinct chemical composition of the stars is providing further evidence of their common and maybe extragalactic origin.

- 1. Bensby, T., Feltzing, S., Lundström, I., Ilyin, I.: Astron. Astrophys. 433, 185 (2005)
- 2. del Peloso, E.F., da Silva, L., Porto de Mello, G.F.: Astron. Astrophys. 434, 275 (2005)
- 3. Edvardsson, B., Andersen, J., Gustafsson, B., et al.: Astron. Astrophys. 275, 101 (1993)
- 4. Helmi, A., Navarro, J., Nordström, B., et al.: Mon. Not. R. Astron. Soc. 365, 1309 (2006)
- 5. Nordström, B., Mayor, M., Andersen, J., et al.: Astron. Astrophys. 418, 989 (2004)
- 6. Pagel, B.E.J., Tautvaišienė, G.: Mon. Not. R. Astron. Soc. **276**, 505 (1995)
- 7. Pagel, B.E.J., Tautvaišienė, G.: Mon. Not. R. Astron. Soc. 288, 108 (1997)
- Stonkuté, E., Nordström, B., Tautvaišienė, G.: Chemical Abundances in the Universe: Connecting First Stars to Planets. In: Chunga, K., Spite, M., Barbuy, B. (eds.) IAU Symp., vol. 265, p. 376. Cambridge University Press, Cambridge (2010)

# Star Disk Interaction in T Tauri Stars: Analysis of the MgII Lines

Fátima López Martínez and Ana Inés Gómez de Castro

**Abstract** The Mg II resonance doublet is produced in the cromosphere of T Tauri Stars (TTSs) at 2795/2802 Å. The Mg II feature is the strongest in the near-ultraviolet spectra of TTSs. These profiles display a broad emission with a central narrow absorption. In some profiles blueshifted absorption is observed overimposed to the broad emission indicating the presence of a wind. The narrow central absorption is produced in the interstella/circumstellar medium. Henceforth, the Mg II is a fundamental tracer of the TTSs atmospheres and circumstellar environments.

### 1 Study of MgII Lines in T Tauri Stars

There are 73 observations of the MgII lines in TTSs in the International Ultraviolet Explorer (IUE) and Hubble Space Telescope (HST) data archive. This provides an excellent sample to study the environment of TTSs. The profiles of 19 TTSs have been studied, some of them have more than one observation. The observations from the HST have been carried out with the instruments STIS (with filter/grating E230M) and HRS (filter/grating G270M). The IUE observations are obtained in the high dispersion mode.

Most of the stars have strong IR excesses, pointing out the existence of circumstellar disks. Stars cover a broad range of masses, but the most of them have ages of around  $10^6$  years (approximately the inner disk dispersal time). The MgII profiles are shown in Fig. 1.

F. López Martínez (⋈) · A.I. Gómez de Castro

S.D. Astronomía y Geodesia, Facultad CC Matemáticas, University of Complutense,

E Â- 28040 Madrid, Spain

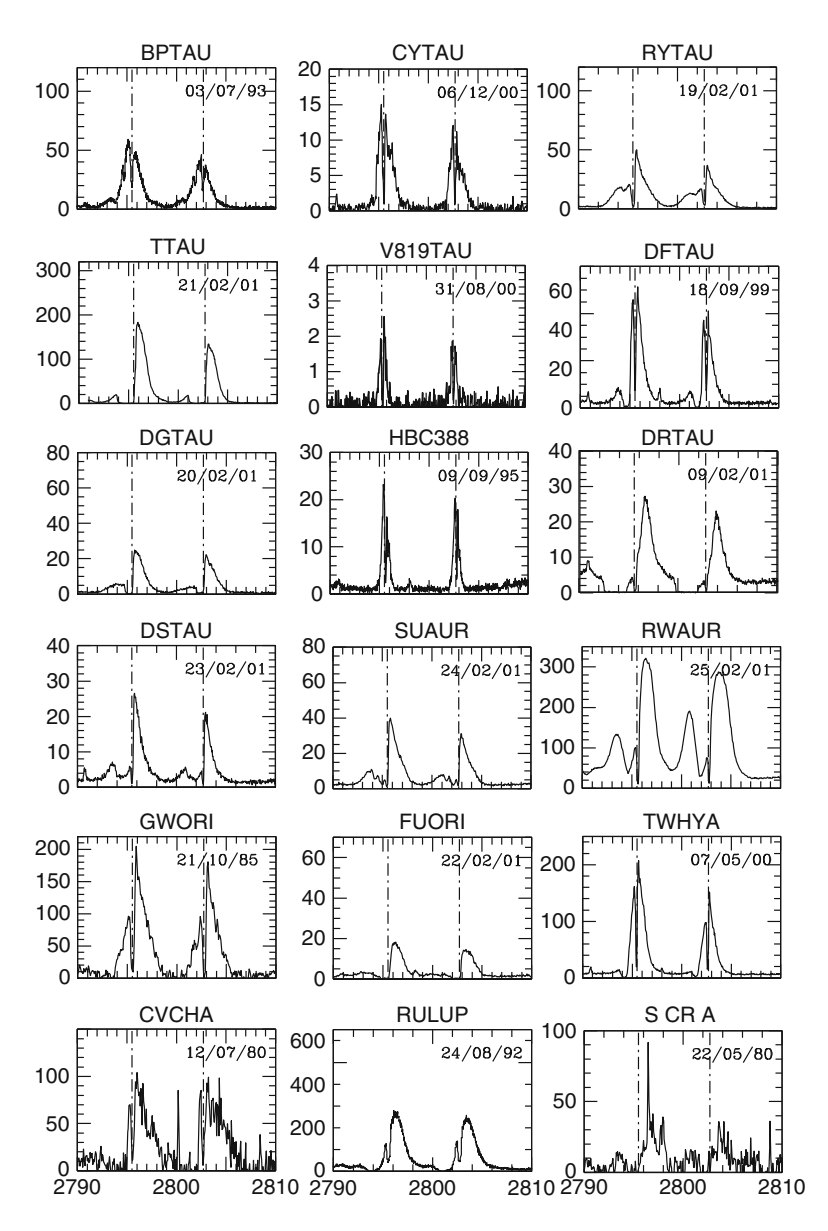


Fig. 1 Profiles

# **Indication of Mass Segregation in LMC Star Clusters**

Grigor B. Nikolov, Mary Kontizas, Anastasos Dapergolas, Maya K. Belcheva, Valeri Golev, and Ioannis Bellas-Velidis

**Abstract** In this contribution we present our investigation on mass segregation in selected LMC star clusters. As a diagnostic of mass segregation we use: (1) Colour-magnitude diagrams at various distance from each cluster centre; (2) Radial-density profiles at various magnitude ranges; and (3) comparison with dynamical models which provide core-radius, a measure of a cluster's compactness.

#### 1 Results

We construct the number-density profiles for 6 Large Magellanic Cloud (LMC) clusters of various age based on WFPC2 images from the HST archive. The dependence of the derived from model fitting [1] core-radius with magnitude as presented in Table 1 is used to trace mass segregation. In the investigated clusters here we see trend in two clusters already suspected in mass-segregation, NGC 1711 [3] and NGC 2157 [2]. For NGC 1711 and NGC 2157 there is clearly a trend of increasing core-radius with magnitude. Clusters NGC 1898, NGC 2031, NGC 2157

G.B. Nikolov (⋈) · V. Golev

Astronomy Department, Faculty of Physics, Sofia University, St Kliment Ohridski,

BG-1164 Sofia, Bulgaria e-mail: gnikolov@phys.uoa.gr

M. Kontizas · M.K. Belcheva

Dpt. of Astrophysics, Astronomy and Mechanics, National and Kapodistrian

University of Athens, GR- 15784 Athens, Greece

A. Dapergolas · I. Bellas-Velidis

IAA, National Observatory of Athens, GR-11810 Athens, Greece

<sup>&</sup>lt;sup>1</sup>http://archive.stsci.edu

228 G.B. Nikolov et.al

Table 1 Derived core-radius for each magnitude bin

Name	mag	$r_c$	Name	mag	$r_c$
NGC 1711	15–16	$8.61 \pm 3.66$	NGC 2011	15–16	$0.07 \pm 8.39$
	16–17	$7.09 \pm 0.54$		16-17	$7.89 \pm 1.76$
	17-18	$12.38 \pm 0.98$		17-18	$15.00 \pm 0.61$
	18-19	$12.21 \pm 0.63$		18-19	$9.89 \pm 0.76$
	19-20	$10.27 \pm 0.61$		19-20	$6.80 \pm 3.69$
	20-21	$15.27 \pm 0.10$		20-21	$10.64 \pm 0.49$
	21-22	$13.29 \pm 1.24$		21-22	$9.31 \pm 1.81$
	22-23	$11.88 \pm 0.51$		22-23	$15.60 \pm 1.33$
	23-24	$16.28 \pm 0.39$		23-24	$10.75 \pm 2.23$
NGC 1984	15-16	$3.82 \pm 1.55$		24-25	$14.38 \pm 0.67$
	16-17	$3.92 \pm 0.85$	NGC 1898	16-17	$19.44 \pm 6.01$
	17-18	$7.62 \pm 1.05$		17-18	$3.66 \pm 2.04$
	18-19	$7.38 \pm 1.90$		18-19	$2.64 \pm 2.98$
	19-20	$8.91 \pm 0.71$		19-20	$7.49 \pm 0.47$
	20-21	$6.01 \pm 0.37$		20-21	$10.95 \pm 0.43$
	21-22	$7.85 \pm 0.92$		21-22	$13.01 \pm 0.62$
	22-23	$3.28 \pm 1.07$		22-23	$13.17 \pm 0.30$
	23-24	$2.00 \pm 2.27$	NGC 2214	16-17	$5.63 \pm 1.21$
NGC 2031	16-17	$6.79 \pm 0.56$		17-18	$14.75 \pm 2.18$
	17-18	$5.34 \pm 0.35$		18-19	$11.55 \pm 0.75$
	18-19	$11.92 \pm 0.39$		19-20	$11.45 \pm 0.50$
	19-20	$12.86 \pm 0.40$		20-21	$10.15 \pm 0.32$
	20-21	$14.02 \pm 0.27$		21-22	$15.18 \pm 0.20$
	21-22	$11.51 \pm 0.58$		22-23	$14.35 \pm 0.41$
	22-23	$18.60 \pm 0.85$		23-24	$14.79 \pm 0.99$
	23-24	$17.84 \pm 0.69$		24-25	$10.40 \pm 0.20$
	24-25	$20.58 \pm 0.58$			

and NGC 2214 also indicate presence of mass segregation, unlike NGC 1984 and NGC 2011.

**Acknowledgements** G. Nikolov and V. Golev appreciate the financial support by the bulgarian National Science Fund through grant DO 02-85 and through DO 02-362. M. Belcheva ackkowledges financial support from EC FP6 RTN ELSA.

- 1. Elson, R.A.W., Fall, S.M., Freeman, K.C.: Astrophys. J. 323, 54 (1987)
- 2. Fischer, P., Pryor, C., Murray, S., Mateo, M., Richtler, T.: Astron. J. 115, 592 (1998)
- 3. Subramaniam, A., Sagar, R., Bhatt, H.C.: Astron. Astrophys. 273, 100 (1993)

# **Carbon and Nitrogen As Tracers of Stellar Evolution in Red Clump Stars of Open Clusters**

Gražina Tautvaišienė and Šarūnas Mikolaitis

**Abstract** The carbon and nitrogen abundances, C/N and especially carbon isotope ratios  $^{12}\text{C}/^{13}\text{C}$  are key tools for stellar evolution studies. In this presentation we overview available up to date analyses of C and N abundances in red clump stars of open clusters along with our recent results obtained for the open clusters NGC 6134 and IC 4651. The clump stars have accumulated all chemical composition changes, which have happened during their evolution along the giant branch and during the helium flash, thus are very trustful sources of information. A comparison of the observational data with theoretical models of stellar evolution shows that processes of extra-mixing in stars of 2–3  $M_{\odot}$  turn-off masses are larger than predicted.

#### 1 Introduction

Carbon and nitrogen are important products of nucleosynthesis processes in stellar interiors, and the evidence of their abundance variation during stellar evolution is a signature of physical mixing processes between the atmosphere and deeper layers of a star. Such abundance alterations may be well traced in open clusters. They provide a unique possibility for investigation of a number of stars of nearly the same age, distance and origin, as open cluster stars are claimed to be formed in the same protocloud of gas and dust. Open clusters have a high reliability of mass, distance, evolutionary phase and abundance determinations.

In this contribution, we overview results of recent high-resolution ( $R \approx 80,000-30,000$ ) spectral studies in which red clump stars of open clusters were analyzed: abundances of carbon, nitrogen and  $^{12}\text{C}/^{13}\text{C}$  isotope ratios were

Institute of Theoretical Physics and Astronomy, Vilnius University, A. Gostauto

12, LT-01108, Vilnius, Lithuania

e-mail: grazina.tautvaisiene@tfai.vu.lt; sarunas.mikolaitis@tfai.vu.lt

G. Tautvaišienė (⋈) · Š. Mikolaitis

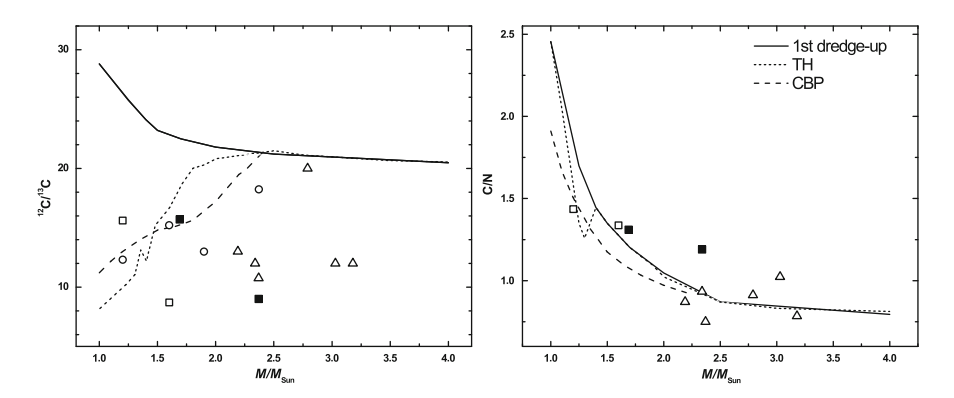


**Fig. 1** The averaged carbon isotope ratios (*left*) and carbon to nitrogen ratios (*right*) in clump stars of open clusters as a function of stellar turn-off mass. Results from [4,5] are marked by *filled squares*; from [6] – *open triangles*; from [7,8] – *open squares*; from [3] – *open circles*. The models of the 1st dredge-up and thermohaline mixing are taken from [2] and shown by *solid and dotted lines*, respectively. The CBP model of extra-mixing by [1] is plotted as a *dashed line* 

investigated in NGC 6134 and IC 4651 by [4,5]; in M 67 and NGC 7789 – by [7,8]; in open clusters NGC 3532, 5822, 6134, 6281, 6281, 6633 and IC 4756 – by [6]. Gilroy [3] obtained  $^{12}$ C/ $^{13}$ C ratios in NGC 752, 2360, 2682 and IC 4756 open cluster red clump stars.

## 2 Comparison of Observational Data with Theoretical Models

In Fig. 1, we compare observational data with the theoretical model of extramixing called "cool bottom processing" (CBP, [1]) and the most recent model of thermohaline mixing (TH, [2]). The comparison shows that processes of extramixing in stars of 2–3  $M_{\odot}$  turn-off masses are larger than predicted by theoretical stellar evolution models.

- 1. Boothroyd, A.I., Sackmann, I.J.: Astrophys. J. **510**, 232 (1999)
- 2. Charbonnel, C., Lagarde, N.: Astron. Astrophys.in press, arXiv1006.5359 (2010)
- 3. Gilroy, K.K.: Astrophys. J. **347**, 835 (1989)
- 4. Mikolaitis, Š., Tautvaišienė, G., Gratton, R., Bragaglia, A., Carretta, E.: Mon. Not. R. Astron. Soc. 407, 1866 (2010)
- Mikolaitis, Š., Tautvaišienė, G., Gratton, R., Bragaglia, & A., Carretta, E., Mon. Not. R. Astron. Soc., 413, 2199 (2011)
- 6. Smiljanic, R., Gauderon, R., North, P., Barbuy, B., Charbonnel, C., Mowlavi, N.: Astron. Astrophys. 502, 267 (2009)
- 7. Tautvaišienė, G., Edvardsson, B., Tuominen, I., Ilyin, I.: Astron. Astrophys. 360, 499 (2000)
- 8. Tautvaišienė, G., Edvardsson, B., Puzeras, E., Ilyin, I.: Astron. Astrophys. 431, 933 (2005)

### **Observations of the IMF in Clusters**

Joana Ascenso and João Alves

**Abstract** The Initial Mass Function (IMF) is a seemingly a universal outcome of the star formation process. Over the last five decades it has been measured in young clusters and associations, in old globulars and in the field, in the Milky Way and in neighboring galaxies, covering regions spanning a wide range of physical conditions. The result is always similar: a Salpeter-like mass distribution for the higher masses and a subsequent flattening for lower masses. As we analyse more distant and dense clusters, however, our ability to measure the IMF properly becomes severely hampered by crowding.

#### 1 Introduction

The determination of the IMF of any population depends on our ability to detect its members and to determine masses. Mass is not a direct observable, hence the difficulty of deriving accurate and consistent IMFs for different regions, having to rely heavily on assumptions and on the knowledge of other properties like distance and age that are, by themselves, very challenging to ascertain. The previous step – detecting the cluster's members – may be as hampering or more to the determination of the mass function. I will focus on the problem of completeness and how it impacts the study of stellar clusters. Details on the IMF in clusters can be found in recent excellent reviews by, e.g., [2–8].

Centro de Astrofísica da Universidade do Porto, Rua das Estrelas, 4150-762 Porto, Portugal e-mail: jascenso@astro.up.pt

Institute of Astronomy, University of Vienna, Türkenschanzstrasse 17, 1180 Vienna, Austria e-mail: joao.alves@univie.ac.at

J. Ascenso (⋈)

J. Alves

J. Ascenso and J. Alves

#### 2 The Problem

Our ability to detect all stars in a cluster determines the accuracy of our IMF. Stars can go undetected for several reasons, both observational and characteristic of the star forming region itself.

### 2.1 Sensitivity

The most obvious consequence of having time-limited observations is that we cannot detect objects fainter than some brightness limit, compromising our ability to sample the IMF in the lowest mass range.

#### 2.2 Resolution

Resolution is a limiting factor in all observations. The first consequence of not being able to resolve (visual) multiples is that the luminosities of "individual" objects, that actually comprise two or more stars are overestimated, counting as more massive stars. This will affect the shape of the IMF, mostly in the low-mass end, especially if using logarithmic mass bins. The other consequence is one of demographics: blending stars means we lose cluster members.

#### 2.3 Variable Extinction and Nebula

Other factors influence the completeness in embedded clusters. Variable extinction, for example, cannot be avoided, and in most cases clusters have also bright and variable nebulas permeating the stellar distribution. This causes problems of variable completeness across the field, either by dimming the brightness of the stars, or by reducing the contrast between the background and the objects, overall lowering the ability to detect faint stars.

#### 3 A Solution

The best way to estimate the completeness of a given sample is to perform artificial stars experiments. These consist in adding artificial stars of different brightnesses to the observed cluster image and trying to recover them with the correct brightness using the exact same method used for the detection and photometry of the science

stars [1]. Knowing the completeness limit of a sample will delimit the mass range over which one feels confident that the IMF is fully sampled, but this information can be used further to correct their sample of incompleteness by dividing the observed mass function by the completeness profile (e.g. [9], but see also discussion in [1]).

Using synthetic clusters, we found that thorough completeness tests provide reasonable completeness corrections for incompleteness due to sensitivity and resolution. In particular, for seeing limited images of a  $10^4~M_{\odot}$  cluster at 3 kpc, we push the confidence limit by 4 mag in the K-band, accurately correcting the luminosity function up to the 20% completeness limit. Although many authors have done this in the past, this procedure had never been validated before. We find that the success of these corrections depend greatly on the completeness assessment method and on the individual cluster properties, hence the recommendation to model each cluster observed rather than to apply the completeness corrections blindly.

- 1. Ascenso, J., Alves, J., Lago, M.T.V.T.: Astron. Astrophys. 495, 147 (2009)
- 2. Bastian, N., Covey, K.R., Meyer, M.R.: Annu. Rev. Astron. Astrophys. 48, 339 (2010)
- Chabrier, G.: The Initial Mass Function 50 Years Later. In: Corbelli, E., Palla, F., Zinnecker, H. (eds.) Astrophysics and Space Science Library, vol. 327, 41. Springer, Dordrecht (2005)
   Clarke, C.J.: Astrophys. Space Sci. 324, 121 (2009)
- 5. Elmegreen, B.G.: Starbursts: From 30 Doradus to Lyman Break Galaxies. In: de Grijs, R., González Delgado R.M. (eds.) Astrophysics and Space Science Library, vol. 329, 57 (2005)
- 6. Elmegreen, B.G.: In: The Evolving ISM in the Milky Way and Nearby Galaxies (2005)
- 7. Lada, C.J. Lada, E.A.: Annu. Rev. Astron. Astrophys. 41, 57 (2003)
- 8. Luhman, K.L.: Star Formation at High Angular Resolution, In: Burton, M.G., Jayawardhana, R., Bourke, T.L. (eds.) IAU Symposium, vol. 221, 237 (2004)
- 9. Stolte, A., Grebel, E.K., Brandner, W., Figer, D.F.: Astron. Astrophys. 394, 459 (2002)

J. Ascenso and J. Alves



Joana Ascenso, Ana Cabral and Paula Brochado



João Alves

# Dynamical Evolution of Rotating Globular Clusters with Embedded Black Holes

Jose Fiestas and Rainer Spurzem

**Abstract** The dynamical evolution of globular clusters with embedded black holes is investigated. The interaction between the black hole and stellar component in rotating clusters is followed by using NBody and 2D + 1 Fokker–Planck numerical techniques. The models can reproduce the Bahcall–Wolf solution  $f \propto E^{1/4}$  ( $n \propto r^{-7/4}$ ) inside the zone of influence of the black hole in a relaxation time scale. We explore the system dissolution due to mass-loss in the presence of an external galactic tidal field.

#### 1 Method and Results

Total disruption and accretion of stars inside disruption radius is realised by ( $\Gamma$  is a magnification factor in order to accelerate performance)

$$r_{\rm d} \sim \Gamma r_{\star} (M_{\rm bh}/m_{\star})^{1/3} \tag{1}$$

Zentrum für Astronomie, University of Heidelberg, Mönchhofstrasse 12-14, 69120 Heidelberg, Germany

e-mail: fiestas@ari.uni-heidelberg.de

R. Spurzem

Zentrum für Astronomie, University of Heidelberg, Mönchhofstrasse 12-14, 69120 Heidelberg, Germany

National Astronomical Observatories of China, Chinese Academy of Sciences, Beijing 100012,

e-mail: spurzem@ari.uni-heidelberg.de

J. Fiestas (⊠)

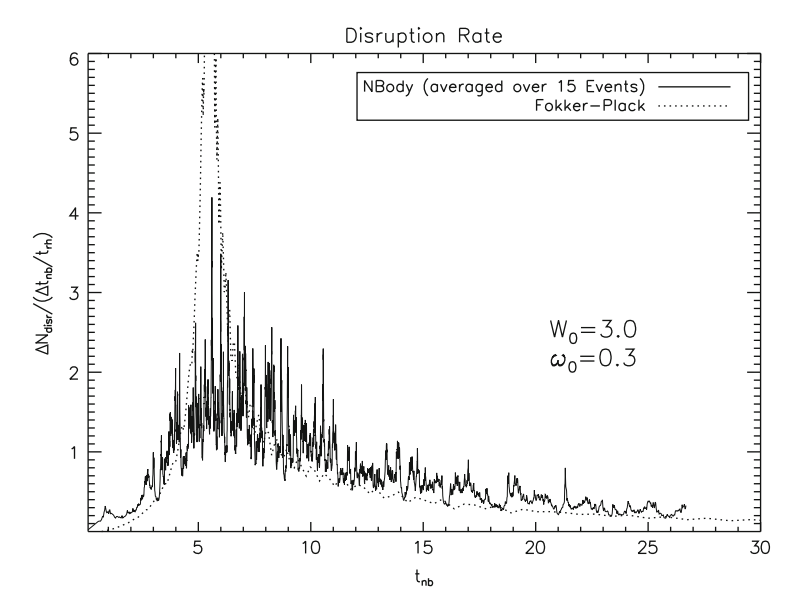


Fig. 1 Disruption rates realized in NBody (thick lines) and Fokker–Planck rotating (King) models (thin lines) including stellar accretion at the BH tidal radius [2]

The gravitational dominance of the central BH over the surrounding stars vanishes at a radius defined by

$$r_{\rm h} = \frac{GM_{\rm bh}}{\sigma_c^2} \tag{2}$$

We use initial rotating King models with the parallel NBODY6++ [3], implemented with total stellar accretion [2] and the PHIGPU code, performed in 85 nodes of a GPU hardware at the **Laohu** cluster (NAOC, Beijing), which makes possible high particle number simulations ( $N \sim 10^6$ ) in a reasonable computing time (days to few weeks). N-body results have been calibrated with our own developed 2-D+1 orbit-averaged Fokker–Planck model [1] (Figs. 1 and 2).

Acknowledgements We thank the SPP 1177 and the special funds of Chinese Academy of Sciences for the use of the GPU cluster in Beijing.

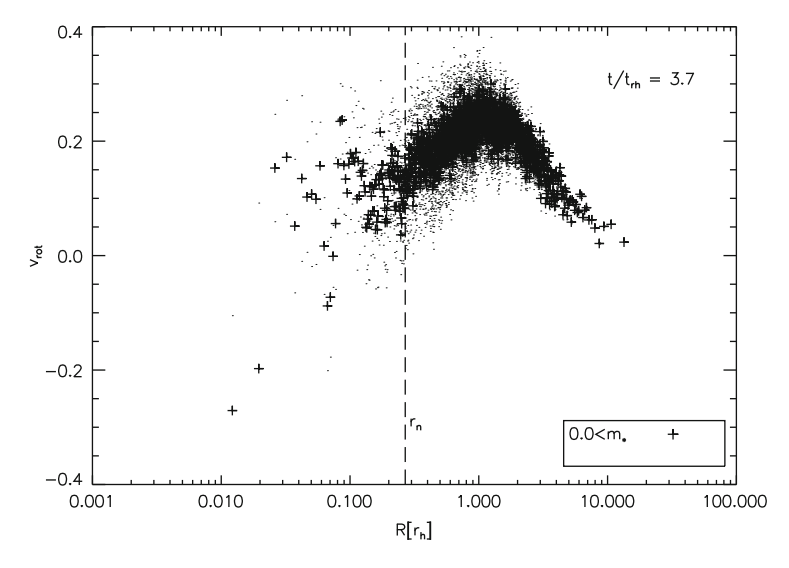


Fig. 2 Evolved rotational velocity profile. Model:  $W_0 = 3.0$ ,  $\omega_0 = 0.9$ . The cluster rotates as initially in the outer parts and develops rotation in the inner parts. Some stars develop counter-rotation. The influence radius is shown with the vertical *dashed-line* 

- 1. Fiestas, J., Spurzem, R.: Mon. Not. R. Astron. Soc. 405, 194 (2010)
- 2. Fiestas, J., Porth, O., Berczik, P., Spurzem, R.: submitted to Mon. Not. R. Astron. Soc. (2011) arXiv:1108.3993
- 3. Spurzem, R.: Comp. Appl. Maths. 109, 407 (1999)

# Stellar Populations in the Super Star Clusters NGC 3603 and 30 Doradus

Loredana Spezzi, Giacomo Beccari, Guido De Marchi, Francesco Paresce, Marco Sirianni, Morten Andersen, Nino Panagia, and the WFC3 SOC

**Abstract** We highlight the main results of a multi-wavelenght study of the super star clusters NGC 3603 and 30 Doradus, recently observed with Wide Field Camera 3 (WFC3) on board the HST.

#### 1 Context

NGC 3603 and 30 Doradus are massive young (e.g., few Myr) clusters located in the Galaxy ( $d\approx7$  kpc) and in the Large Magellanic Cloud ( $d\approx52$  kpc), respectively. Because of their relative proximity, the copious numbers of massive O-type stars together with large numbers of lower-mass stars, still associated to gas and dusty nebulosities left over from the parental cloud, these clusters represent small-scale resolved prototypes of the star-burst clusters commonly seen in active galaxies and, as such, represent an ideal opportunity to shed light on the many unclear facets of the star formation mechanism (see, e.g., [3]).

We conducted a multi-wavelength survey of NGC 3603 and 30 Doradus with new WFC3 on board the HST in the UV, optical and near-IR combining the use of broad-band and narrow-band filters. For a detailed description of these observations and the data reduction procedure we defer the reader to [1,2].

L. Spezzi (⊠) · G. Beccari · G. De Marchi · M. Sirianni · M. Andersen ESA, Space Science Department, Keplerlaan 1, 2200 AG Noordwijk, The Netherlands e-mail: lspezzi@rssd.esa.int

F. Paresce

INAF-Istituto di Astrofisica Spaziale e Fisica Cosmica, Via P. Gobetti, 101, I-40129 Bologna, Italy

N. Panagia

Space Telescope Science Institute, Baltimore, MD 21218, USA

240 L. Spezzi et al.

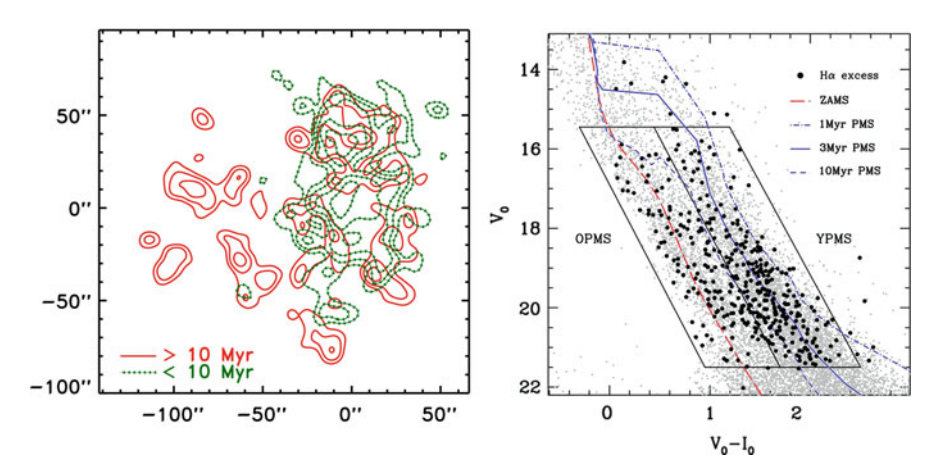


**Fig. 1** Left: Density contour plots of the two populations of PMS stars in 30 Doradus, separated by  $\sim$ 10 Myr. The youngest population (dotted line) is clearly more centrally concentrated than the older population (solid line), whereas the latter dominates the eastern portion of the field [2]. Right: Hα excess emission stars in NGC 3603 (black dots) are shown on the color-magnitude diagram (CMD). As expected, most of the objects lie in the canonical PMS region of the CMD (YPMS, box on right-hand side). Surprisingly, a number of sources are located on or near the ZAMS (OPMS). The two populations are well separated by a 10 Myr PMS isochrone [1]

### 2 Highlights

The unprecedented photometric capabilities and the resolving power of the new WFC3 camera allowed us to find, for the first time, clear evidence of multiple stellar populations in both clusters with an age spread of 1 to 20–30 Myrs. The spatial distributions of the cluster stars indicate that the older population is more widely and uniformly distributed over the cluster field than the much clumpier younger population (Fig. 1, left). A reasonable separation of the main components of these populations can now be made by the use of their  $H\alpha$  excess (Fig. 1, right), a good indicator of their pre-main sequence (PMS) status, allowing a better understanding of the stellar mass function and its evolution in time.

**Acknowledgements** This paper is based on Early Release Science observations made by the WFC3 Scientific Oversight Committee. We are grateful to the Director of the Space Telescope Science Institute for awarding Director's Discretionary time for this program.

- 1. Beccari, G., et al.: Astrophys. J. 720, 1108 (2010)
- 2. De Marchi, G., et al. arXiv:1106.2801
- 3. Portegies Zwart, S.F., et al.: Annu. Rev. Astron. Astrophys. 48, 431 (2010)

# **Dynamical Expansion of Star Clusters**

**Mark Gieles** 

**Abstract** Most globular clusters have half-mass radii of a few pc with no apparent correlation with their masses. This is different from elliptical galaxies, for which the Faber-Jackson relation suggests a strong positive correlation between mass and radius. Objects that are somewhat in between globular clusters and lowmass galaxies, such as ultra-compact dwarf galaxies, have a mass-radius relation consistent with the extension of the relation for bright ellipticals. Here we show that at an age of 10 Gyr a break in the mass-radius relation at  $\sim 10^6 M_{\odot}$  is established because objects below this mass, i.e. globular clusters, have undergone expansion driven by stellar evolution and hard binaries. From numerical simulations we find that the combined energy production of these two effects in the core comes into balance with the flux of energy that is conducted across the half-mass radius by relaxation. An important property of this "balanced" evolution is that the cluster half-mass radius is independent of its initial value and is a function of the number of bound stars and the age only. It is, therefore, not possible to infer the initial massradius relation of globular clusters and we can only conclude that the present day properties are consistent with the hypothesis that all hot stellar systems formed with the same mass-radius relation and that globular clusters have moved away from this relation because of a Hubble time of stellar and dynamical evolution.

#### 1 Introduction and Results

The half-mass radius of old globular clusters in the Milky Way depends only weakly on mass [7]. A negative correlation between radius and mass is found for the clusters in the outer halo [1,6]. Because this is also found for extra-galactic globular

242 M. Gieles

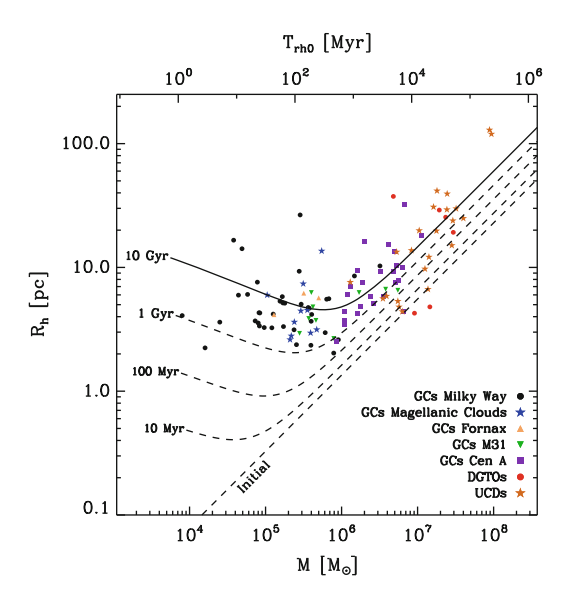


Fig. 1 Mass M, and half-mass radius  $R_{\rm th}$ , values for hot stellar systems. The lines show the evolution of the mass-radius relation using the extension of the Faber–Jackson relation as initial conditions. At an age of 10 Gyr the objects with  $M \lesssim 10^6 {\rm M}_{\odot}$  (globular clusters) have evolved to a constant relaxation time-scale and this is why their mass-radius relation is different from the more massive Ultra Compact Dwarf galaxies (UCDs) and Dwarf Globular Transition Objects (DGTOs), whose mass-radius relation is still close to the initial one

clusters [4] the mass-radius relation, or lack thereof, is an important aspect of the fundamental plane relations of globular clusters [5].

Here we consider the expansion of star clusters driven by mass loss due to stellar evolution and hard binaries and we present a description for the radius evolution including both effects, based on results of N-body simulations [2]. Combining scaling relations for the (adiabatic) expansion of clusters because of stellar evolution with relations for expansion due to 2-body relaxation we present a simple formula for the radius evolution as a function of initial mass, radius and age (equations (6) and (7) in [2]). Applying this result to a Faber–Jackson type initial mass-radius relation (the representation in units of mass and radius are taken from [3]) we show that at an age of 10 Gyr a break occurs at  $\sim 10^6 {\rm M}_{\odot}$ (see Fig. 1). This break can be thought of as the boundary between collisional systems and collision-less systems.

- Baumgardt, H., Parmentier, G., Gieles, M., Vesperini, E.: Mon. Not. R. Astron. Soc., 401, 1832 (2010)
- Gieles, M., Baumgardt, H., Heggie, D.C., Lamers, H.J.G.L.M.: Mon. Not. R. Astron. Soc. 408, L16 (2010)

- 3. Haşegan, M., et al.: Astrophys. J. 627, 203 (2005)
- 4. Jordán, A., et al.: Astrophys. J. **634**, 1002 (2005)
- 5. McLaughlin, D.E.: Astrophys. J. **539**, 618 (2000)
- 6. van den Bergh, S., Mackey, A.D.: Mon. Not. R. Astron. Soc. 354, 713 (2004)
- 7. van den Bergh, S., Morbey, C., Pazder, J.: Astrophys. J. **375**, 594 (1991)

# The Metallicity Gradient in the Galactic Disk Revealed by Cepheids and Open Clusters

Patricia Cruz and Jacques R.D. Lépine

**Abstract** We have collected results from individual observations of metallicities of Cepheids and open clusters from the literature in order to investigate the [Fe/H] gradient in the Galactic disk. We re-computed the distances of the Cepheids based on the period-luminosity and period-intrinsic color relations, and the distances of open clusters with more precise ways of computing the effect of interstellar extinction. The data obtained were analyzed using the short distance scale of the galactocentric distance of the Sun,  $R_0 = 7.5 \,\mathrm{kpc}$ . We have concentrated our study on the Galactic distributions of [Fe/H]. We discuss the existence of a sudden step down in metallicity at a galactic radius of about  $8.6 \,\mathrm{kpc}$ , followed by a relatively flat region, and we report the existence of an azimuthal gradient. The same break in the metallicity gradient was previously presented by other authors, and it has been detected in samples of other objects as well. We also discuss two different hypotheses for this feature, which both are based on the connection between the spiral structure and star-formation rate of the Galaxy.

## 1 Introduction and Analysis

Cepheids and open clusters have been used as tracers of the Galactic structure and evolution. Their value lies in the accuracy of distance determination, metal content and age, that provide information about the Galactic disk. Many works have

P. Cruz (⊠)

Departamento de Astrofísica, Centro de Astrobiología (CAB/INTA-CSIC), PO BOX 78, 28691 Villanueva de la Cañada, Madrid, Spain

e-mail: pcruz@cab.inta-csic.es

J.R.D. Lépine

Instituto de Astronomia, Geofísica e Ciências Atmosféricas, Universidade de São Paulo (IAG/USP), Rua do Matão 1226, Cidade Universitária, São Paulo, SP, Brazil e-mail: jacques@astro.iag.usp.br

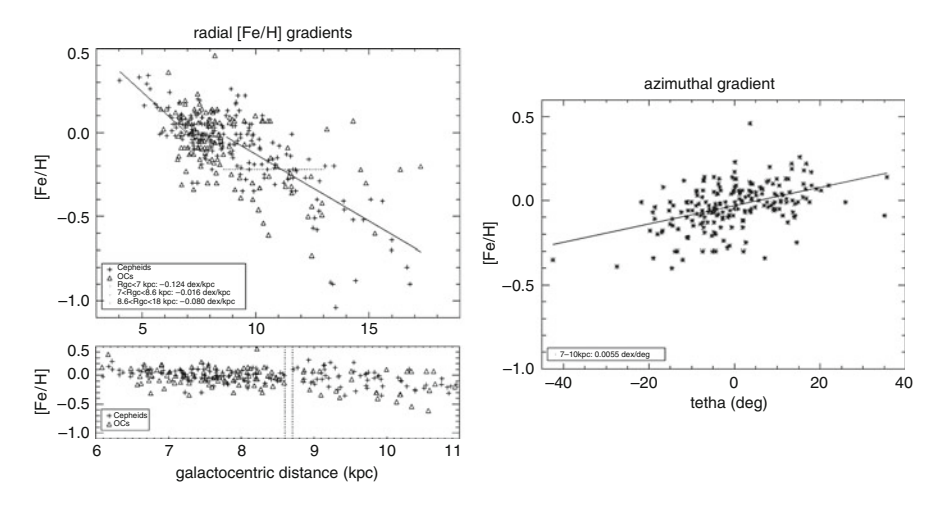


**Fig. 1** Left: (Top) [Fe/H] distribution with new values of  $R_{GC}$ . (Bottom) The gap near  $R_{GC} = 8.6$ . Right: Azimuthal gradient of [Fe/H]

confirmed the existence of a chemical gradient in the Galactic disk, although there is still no agreement between the results. The aim of this study is to investigate the evidence of a sudden discontinuity, a possible multi-modal gradient, and their connection to the corotation pattern. The data considered for this study was a set of 214 Cepheids and 133 open clusters from the literature.

Metallicity gradients based on the sample have been presented by several authors adopting different values of  $R_0$ . The galactocentric distances of the sample were re-calculated assuming  $R_0 = 7.5\,\mathrm{kpc}$  [3], and the new distribution of [Fe/H] reveals the existence of a gap, near to  $R_{GC} = 8.6\,\mathrm{kpc}$ , that divides the sample. The distribution shows that the inner region of the disk have a steeper gradient, followed by a "plateau" at solar vicinity. The gradient is shallower towards greater distances. With that in mind, it seems necessary to separate the [Fe/H] distribution in three distinct zones, considering a multi-modal gradient. The gradients are  $(d\,\mathrm{[Fe/H]}/dR_{GC})$ :  $R_{GC} < 7\,\mathrm{kpc}$ :  $-0.124\,\mathrm{dex/kpc}$ ,  $7 < R_{GC} < 8.6\,\mathrm{kpc}$ :  $-0.016\,\mathrm{dex/kpc}$ , and  $R_{GC} > 8.6\,\mathrm{kpc}$ :  $-0.080\,\mathrm{dex/kpc}$ . We have found an azimuthal gradient, with a slope of  $0.0055\,\mathrm{dex/deg}$ . The range of  $7 < R_{GC} < 10\,\mathrm{kpc}$  was chosen to reduce the dispersion caused by the scatter in metallicity (Fig. 1).

#### 2 Discussion

A metallicity gradient based on Cepheids and open clusters is presented for recalculated values of  $R_{GC}$ . The new [Fe/H] distribution reveals some important features. There is a marked minimum in the density of objects at 8.6 kpc. The gradient is better described by a multi-modal function, which confirms the results

of [2] and others. A possible explanation for our results is associated to the corotation point, at 8.3 kpc [1], that generates a gap of gas and a minimum of star formation – that we believe to have been observed at 8.6 kpc. This gap of gas is expected to be quite large (1 kpc), creating two isolated regions, which could be the reason of the gradient discontinuity.

We report for the first time the existence of an azimuthal gradient of metallicity, revealed by Cepheids and open clusters. The increase of Fe abundance shown here could represent a possible enrichment of the gas when it passes through the spiral arms, or even be due to a combination of radial flow and rotation of the Galaxy. The existence of this azimuthal gradient shows the importance of galaxys spiral structure in the history of stellar formation. We will search for [O/H] gradients found with other tracers, aiming to find patterns similar to those presented in this work.

- 1. Amôres, E.B., Lépine, J.R.D., Mishurov, Y.: Mon. Not. R. Astron. Soc. 400, 1768 (2009)
- 2. Andrievsky, S.M., Luck, R.E., Martin, P., Lépine, J.R.D.: Astron. Astrophys. 413, 159 (2004)
- 3. Lépine, J.R.D., Dias, W.S., Mishurov, Y.: Mon. Not. R. Astron. Soc. 386, 2081 (2008)

# Spitzer's View of NGC2264's Circumstellar Disk Population

Paula S. Teixeira, Charles J. Lada, Massimo Marengo, and Elizabeth Lada

**Abstract** We present a *Spitzer* study of the pre-main sequence population of the young cluster NGC 2264. The disk population is divided into three classes, based on individual spectral energy distributions: optically thick disks, in a homologous manner depleted or anemic disks, and radially depleted transition disks. Our analysis indicated that there may be two distinct evolutionary paths; disks evolve from optically thick to anemic via the first path, and from optically thick to transition in the second. Most of the disks seem to follow the first path. It is yet unknown what physical mechanism triggers this evolutionary differentiation – it could be directly connected to the nature of planet formation within the disk.

# 1 The Pre-main Sequence Population of NGC 2264

NGC 2264 is a rich star forming region, <5 Myr old, located at  $\sim800\pm100$  pc away in the Monoceros constellation, and is hierarchically structured [3]. Its pre-main sequence (PMS) population was first identified by [8] and has been extensively

P.S. Teixeira (⊠)

European Southern Observatory, Karl-Schwarschild-Strasse 2, 85748 Garching bei Müenchen, Germany

e-mail: pteixeir@eso.org

C.J. Lada

Harvard Smithsonian Center for Astrophysics, 60 Garden Street, Cambridge, MA 02138, USA e-mail: clada@cfa.harvard.edu

M. Marengo

Department of Physics and Astronomy, Iowa State University, 12 Physics Hall, Ames, Iowa 50011-3160, USA

e-mail: mmarengo@iastate.edu

E. Lada

Department of Astronomy, University of Florida, 211 Bryant Space Science Center, Gainesville, FL 32611-2055, USA

e-mail: lada@astro.ufl.edu

A. Moitinho and J. Alves (eds.), *Star Clusters in the Era of Large Surveys*, Astrophysics and Space Science Proceedings, DOI 10.1007/978-3-642-22113-2\_45, © Springer-Verlag Berlin Heidelberg 2012

250 P.S. Teixeira et al.

studied since (see review by [2]). We re-visited this cluster to better characterize the PMS population and explore disk evolution using the *Spitzer* Space Telescope. NGC 2264 was observed by the *Spitzer* InfraRed Array Camera (IRAC) and by the Multiband Imaging Photometer for SIRTF (MIPS). We used data from the Guaranteed Time Observations programs 37 (P.I.: G. Fazio) and 58 (P.I.: G. Rieke).

#### 2 Disk Evolution

We built spectral energy distributions (SED) for 1,404 sources that were detected in all four IRAC bands (3.6, 4.5, 5.8, and 8  $\mu$ m). The sources were classified, according to their SED slope following [4], into sources with (1) optically thick disks (OTD), (2) anemic disks (AD), (3) transition disks (TD), and (4) naked photospheres. We found 377 sources that have circumstellar material: 271 OTD, 116 AD, and 5 TD. The spatial distribution of these three groups of sources is quite distinct: the sources with OTDs are mostly embedded and preferentially located in two regions of the cluster (near IRS 1 and in the Spokes cluster). Sources with ADs and TDs, on the other hand, were not embedded and are spatially distributed throughout the region in a more uniform manner. All these facts indicate that sources with OTDs are less evolved than the other two groups of sources. We placed the sources on H-R diagrams after careful dereddening to quantify this result. We found that there is a wide spread in the H-R diagrams, however, the median age of sources with optically thick disks is 1 Myr younger than the median age of sources with either anemic or transition disks. We therefore postulate that there are two evolutionary paths OTDs can follow, namely, one where they are in a homologous manner depleted throughout their entire radial extent (ADs), or another where they are radially depleted, i.e., the inner disk disappears at a faster pace than the outer disk (TDs). Interestingly, the fraction of sources with TDs is  $\sim 10\%$ , similar to the fraction of FGKM stars that host giant planets within 30 AU [1]. We refer the reader to [5,6] and [7], where we explain in detail all of these results.

- 1. Butler, R.P., et al.: Astrophys. J. 646, 505 (2006)
- 2. Dahm, S.E.: Handbook of Star Forming Regions, vol. I, 966. San Francisco, CA: ASP (2008)
- 3. Lada, C.J., Lada, E.A.: Annu. Rev. Astron. Astrophys. 41, 57 (2003)
- 4. Lada, C.J., et al.: Astron. J. 131, 1574 (2006)
- 5. Teixeira, P.S., et al.: Astrophys. J. Lett. **636**, L45 (2006)
- 6. Teixeira, P.: Ph.D. Thesis, Universidade de Lisboa, Portugal (2008)
- 7. Teixeira, P.S., Lada, C.J., Marengo, M., Lada, E.A.: Astron. Astrophys.(submitted) (2010)
- 8. Walker, M.F.: Astrophys. J. Suppl. **2**, 365 (1956)

# **Super Star Clusters in IR-Luminous Interacting Galaxies: The NIR Luminosity Function**

Petri Väisänen, Zara Randriamanakoto, Stuart Ryder, and Seppo Mattila

**Abstract** We present a pilot study of a larger on-going survey to detect SSCs in LIRGs using *K*-band Adaptive Optics imaging. We show the first significant sample of NIR luminosity functions of extragalactic SSCs, which appear to be significantly shallower than typical power-law slopes determined from optical studies of lower IR-luminosity systems. We also present the first brightest cluster vs. star-formation rate of the host galaxy relation derived in the NIR.

## 1 Introduction

Very massive ( $10^3$  to  $10^7$   $M_{\odot}$ ) young "super star clusters" SSCs, have been found in large numbers in strongly star-forming interacting galaxies. Can the most massive ones only form in those extreme conditions? How do the galaxy properties affect the outcome? What is their subsequent evolution and life, which ones survive and perhaps end up as (old) globular clusters? These questions are studied in our ongoing survey of a few dozen strongly star-forming galaxies using near-IR Adaptive Optics (AO). The galaxies are at distances ranging from 40 to 180 Mpc, span the range from starbursts to ULIRGs, and are at various stages of merging, interaction,

P. Väisänen (⋈) · Z. Randriamanakoto

South African Astronomical Observatory, P.O. Box 9, Observatory 7935, Cape Town,

South Africa

e-mail: petri@saao.ac.za; zara@saao.ac.za

S. Ryder

Australian Astronomical Observatory, Epping, NSW 1710, Australia

e-mail: sdr@aao.gov.au

S. Mattila

Tuorla Observatory, University of Turku, FI-21500 Piikkiö, Finland

e-mail: sepmat@utu.fi

or isolation. VLT/NACO is used for the main survey, and here we report a pilot study using the Gemini/ALTAIR/NIRI instrument [4,5]. Both instruments deliver a spatial resolution of  $\approx 0.1$ ", and the data are very well complemented with existing HST optical data for many of the targets. As a first step to analyze the SSC populations we construct their luminosity function (LF), which can then be used to constrain e.g. the cluster initial mass functions and SSC formation and disruption models.

# 2 The NIR Luminosity Function and Brightest SSC Versus SFR

We performed aperture photometry on point sources in the complex background conditions of the galaxies along with relevant completeness corrections and blending simulations. The resulting SSC candidate number counts are fitted with a power-law of the form  $\Phi(L)dL \propto L^{-\alpha}dL$ . The fitted power-law indexes are typically  $\alpha \approx 1.6 \pm 0.2$  for our initial sample of galaxies (Fig. 1). This is significantly shallower than most slopes observed in the optical, which tend to be close to two (e.g. [3]). Our LF slope could perhaps indicate mass-dependent disruption of the SSCs, or environment and/or SFR dependent cluster IMFs: most other determinations are from less luminous IR-galaxies. [1] recently derived a similar slope for the LIRG Haro 11. We stress that these results will soon be checked with a larger sample and (even) more careful photometric completeness and blending analysis and modelling.

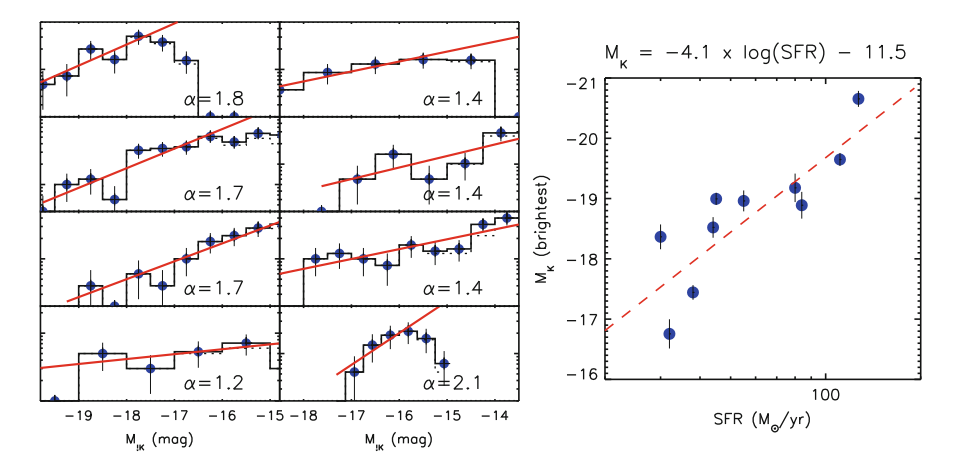
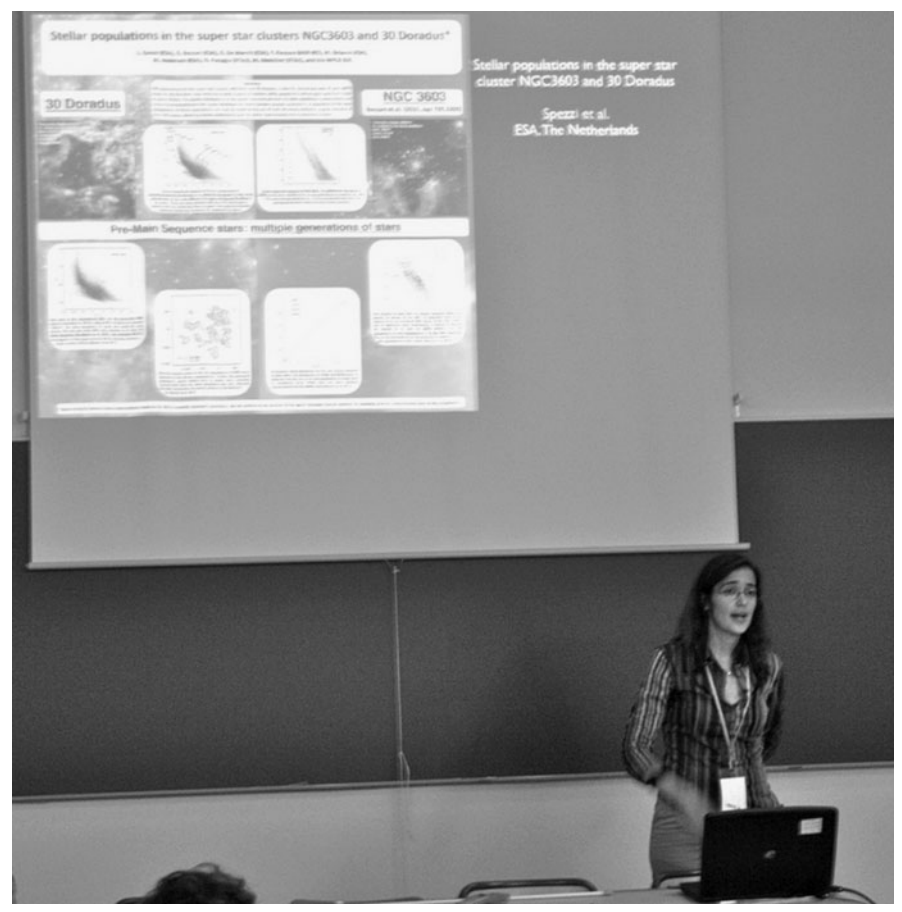


Fig. 1 Left: preliminary K-band SSC LFs in our pilot sample. Points and histograms show the completeness corrected SSC number counts against  $M_K$  absolute magnitude, and the *straight* (red) lines the weighted least-squares fit with the index  $\alpha$  indicated. Right: the relation between the brightest SSC in the galaxy vs. the host galaxy SFR determined from its IR luminosity. The dashed line shows the best fit to the data points, and the relation is also shown at the top

We also looked for a relation between the brightest K-band SSC vs. the SFR of the host galaxy. This is the first such relation derived for a NIR SSC sample, and is similar to equivalent relations in the optical (e.g. [2]). We note that these relations indicate that the V-K colour of the brightest SSC reddens with SFR.

- 1. Adamo, A., et al.: Mon. Not. R. Astron. Soc. 407, 870 (2010)
- 2. Bastian, N.: Mon. Not. R. Astron. Soc. 390, 759 (2008)
- 3. Elmegreen, B.G., Efremov Y.N.: Astrophys. J. 480, 235 (1999)
- 4. Randriamanakoto et al.: 2011, in prep.
- 5. Väisänen, P., et al.: Mon. Not. R. Astron. Soc. 384, 886 (2008)



Paula Teixeira



Loredana Spezzi makes a comment



Mark Casali and Janet Drew

# **Populations of Variable Stars in Open Clusters**

Richard I. Anderson, Nami Mowlavi, and Laurent Eyer

**Abstract** We present our work in progress that explores links between properties of variable star populations and their host open clusters. Information from WEBDA and the Dias catalog [2] has been considered. We explain the context, consider open cluster red giants as tracers of a Galactic age-metallicity relationship, and outline the intended future direction and prospects of this project.

### 1 Context

Open clusters (OCs) can be seen as snapshots probing stellar evolution as a function of age and metallicity. The variable star content of an OC may depend on these (and further) parameters. Thus, there exists great potential for providing stringent constraints on stellar evolution theory by investigating how variable star populations differ among OCs. The following information is particularly useful in this respect: instability strip boundaries and (im-)purity; relative variable star fractions; variability properties; metallicity; memberships; multiple star fractions.

We consider published literature on variable star studies in OCs. As a first step, we take information from two sources: the WEBDA OC database and Dias OC catalog [2]. While WEBDA is not a variable star database, it does provide some information on certain types of stars, e.g. periodic variables or red giants (RGs). RGs can be considered (candidate) variable stars, since different kinds of variability occur during the RG phase, and many RGs exhibit solar-like oscillations (e.g. [3]).

R.I. Anderson  $(\boxtimes) \cdot L$ . Eyer

Observatoire de Genève, Université de Genève, 51 Ch. des Maillettes, CH-1290 Sauverny, Switzerland

e-mail: richard.anderson@unige.ch

N. Mowlavi

ISDC, Observatoire de Genève, Université de Genève, 16 Ch. d'Ecogia, CH-1290 Versoix, Switzerland

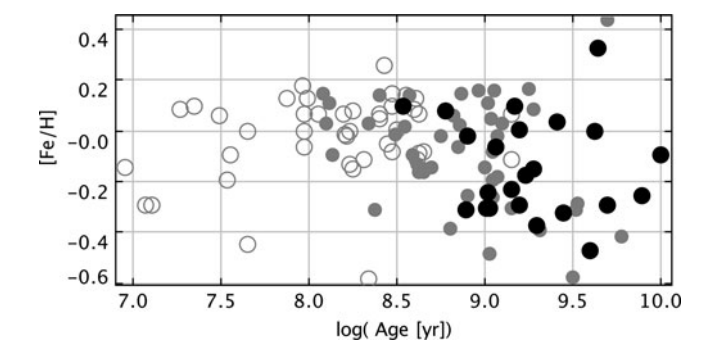


Fig. 1 [Fe/H] against age for OCs with RGs. Data from WEBDA and [2]. Binned number of RGs,  $N_{\rm RG}$ , indicated in *greyscale*. Open circles:  $N_{\rm RG} < 10$ ; grey filled circles:  $10 \le N_{\rm RG} \le 50$ ; black filled circles:  $N_{\rm RG} > 50$ . Some entries may be erroneous: e.g. Ruprecht 97 ([Fe/H]/log(age) = -0.59/8.34) is actually close to solar metallicity [1]

Additionally, RGs are ideal to determine abundances or binary fractions (e.g. [5] to [4]). Finally, since cluster membership can be reliably determined for RGs, chemical abundance measurements from open cluster red giants can contribute to the understanding of the age-metallicity relationship, cf. Fig. 1: older OCs harbor more RGs and show a larger spread in [Fe/H].

## 2 Outlook

As a next step, we will carefully check the references in WEBDA and [2] (e.g. for cluster ages, since automatic age determinations are prone to errors due to presence of Blue Stragglers or contamination from non-members), and continue by considering additional sources. Supplementary data from archives or new observations, e.g. abundance determinations for individual clusters, will help to complete the picture. The inhomogeneity of the information investigated poses a major challenge, e.g. since systematic uncertainties may vary between sources. Nevertheless, we are confident that stellar evolution will benefit from combining published literature results from studies on stellar variability in OCs in such a systematic way.

**Acknowledgements** This research has made use of: the WEBDA database (www.univie.ac.at/webda), operated at the Institute for Astronomy of the University of Vienna; NASA's Astrophysics Data System Bibliographic Services; the SIMBAD database, operated at CDS, Strasbourg, France; the VO tool TOPCAT (www.starlink.ac.uk/topcat).

- Clariá, J.J., Piatti, A.E., Mermilliod, J.-C., Palma, T.: Astronomische Nachrichten, 329, 609 (2008)
- 2. Dias, W.S., Alessi, B.S., Moitinho, A., Lépine, J.R.D.: Astron. Astrophys. 389, 871 (2002)
- 3. Hekker, S., Kallinger, T., Baudin, F., De Ridder, J., Barban, C., Carrier, F., Hatzes, A.P., Weiss, W.W., Baglin, A.: Astron. Astrophys. **506**, 465 (2009)
- 4. Mermilliod, J.-C., Andersen, J., Latham, D.W., Mayor, M.: Astron. Astrophys. 473, 829 (2007)
- 5. Mermilliod, J.-C., Mayor, M.: Astron. Astrophys. 219, 125 (1989)

# Tracing the Structure of the Perseus Arm with IPHAS

Roberto Raddi, Janet E. Drew, Stuart E. Sale, Danny Steeghs, and the IPHAS Consortium

**Abstract** Research aiming to describe the spiral structure of the Milky Way disc has to confront both difficulties in obtaining distances and the high interstellar extinction found in the Galactic plane. We present a study of a section of the Perseus Arm, between Galactic longitudes  $(120^{\circ}, 140^{\circ})$  and Galactic latitudes  $(-1^{\circ}, +4^{\circ})$ , including a number of young clusters. Determination of physical parameters of young stellar objects (YSO) and mapping of the A-star surface density are used to analyse evidence of young structures (typically  $10-100 \,\mathrm{Myrs}$  old) defined in space.

### 1 Introduction

The anatomy of the Perseus Arm has been investigated in a recent census of known open clusters [2]. Several star formation sites – typically at a distance of  $\sim 2-3$  kpc – present evidence of multiple phases of star formation on large and/or small spatial scales, lasting up to  $\sim 20$  Myr [1] and [4]. With a line of sight generally free of a significant density of foreground stars, a wide area study of the Perseus Arm is made possible by the comprehensive reach of a survey like the INT/WFC Photometric H $\alpha$  Survey of the Northern Galactic Plane (IPHAS) [3]. A large scale search for emission line objects both associated with recent star formation (Herbig Ae/Be, classical T Tauri stars) or  $\sim 10-30$  Myr old clusters (classical Be stars) can be used as a powerful tool to produce a precise "radiography" of the age/spatial

R. Raddi (⋈) · J.E. Drew

Centre for Astrophysic Research - STRI, University of Hertfordshire, College Lane Campus, Hatfield, AL10 9AB, UK

e-mail: r.raddi1@herts.ac.uk

S. Sale · D. Steeghs · the IPHAS Consortium

Universitad de Valparaiso - Pontificia Universidad Católica de Chile, University of Warwick, CV4 8UW, UK

http://www.iphas.org

260 R. Raddi et al.

profile of the Arm. [7] proved the efficiency of IPHAS photometry in picking  $H\alpha$  emitters out of the crowd. As the IPHAS colours themselves do not distinguish among different classes of emission line stars, spectroscopic follow-up observations are needed to achieve this (see e.g. [6]).

# 2 Data Analysis and Discussion

About 300 H $\alpha$  emitters (13  $\leq r' \leq$  17) have been observed out of a sample of 338 emission line candidates in the area, with  $\Delta\lambda \sim$  6 Å at FLWO/FAST. 73 have been re-observed at INT/IDS and NOT/ALFOSC, with  $\Delta\lambda \sim$  2–4 Å and S/N > 20. The latter spectra have been typed by comparing them with templates from the INDO–US library. Interstellar reddening has then been determined for this same subset, by dereddening the spectra against appropriate model atmospheres (Castelli & Kurucz, ATLAS9).

To place each of our sample of stars with a reliable spectral type along its sight-line, we used the algorithm MEAD, described in [5]. MEAD derives line of sight extinction curves from IPHAS photometry, by using large numbers of field non-emission stars (early-A to mid-K). Preliminary work has shown the expected gathering of Perseus Arm young stars towards recent star formation loci. Further investigation has to be done on a more numerous and sparser population of – more likely – classical Be stars, to determine their relationship with the Arm. A further 27 spectra, collected at INT/IDS in Oct. 2010, will enhance coverage of the surveyed area.

We are also examining the A star surface density across the region, in order to locate young structures. This may provide a further tool to interpret the organization and uncover eventual clustering of  $\sim 10$ –100 Myr old population (a figure and more discussion can be found in Drew et al. in this volume).

**Acknowledgements** RR acknowledges the support of a University of Herfordshire studentship.

- 1. Carpenter, J.M. et al.: Astrophys. J. Suppl. 130, 381 (2000)
- 2. de La Fuente Marcos et al.: New Astron. 14, 180 (2009)
- 3. Drew, J.E. et al.: Mon. Not. R. Astron. Soc. 362, 753 (2005)
- 4. Oev et al.: Astron. J. 129, 393 (2005)
- 5. Sale, S.E. et al.: Mon. Not. R. Astron. Soc. **392**, 497 (2009)
- 6. Vink, J.S. et al.: Mon. Not. R. Astron. Soc. 387, 308 (2008)
- 7. Witham, A.R. et al.: Mon. Not. R. Astron. Soc. 384, 1277 (2008)

# Setting up the T35 Telescope at Sierra Nevada Observatory for Detecting Variable Stars in Open Clusters

Susana Martín-Ruiz, Francisco J. Aceituno, and Juan Gutiérrez Soto

**Abstract** The T35 is a 14" telescope installed at the Sierra Nevada Observatory (Granada, Spain). This telescope is equipped with a large format CCD camera for detecting AF-type pulsating stars in the open clusters. In order to test the accuracy of V measurements obtained with T35, we observed one of the target variable stars using the uvby photometer at the 90-cm telescope. Here, we compare the light curves obtained in both photometries.

#### 1 Motivation

The advantage of studying pulsating stars in open clusters is that they offer us additional constrains for testing the stellar models respect to the isolated stars. Therefore, systematic observations of a significant sample open clusters are necessary to detect stellar variability. In order to carry out this project, we need a telescope of modest aperture (30–40 cm) with a wide field CCD camera to reach the desired S/N in a reasonable time.

The T35 telescope is located at the Sierra Nevada Observatory (SNO) (2,896 m altitude). It is a 35.5-cm Schmidt–Cassegrain telescope with a  $4,008 \times 2,762$  CCD Camera. The field of view is  $31.70 \times 21.14$  arcmin with a scale of 0.2475 arcsec per pixel. Detailed information on T35 can be found in [3].

Instituto de Astrofísica de Andalucía - CSIC, Glorieta de la Astronomía s/n 18008 Granada (Spain)

e-mail: susana@iaa.es; fja@iaa.es; jgs@iaa.es

S. Martín-Ruiz (🖂) · F.J. Aceituno · J.G. Soto

262 S. Martín-Ruiz et al.

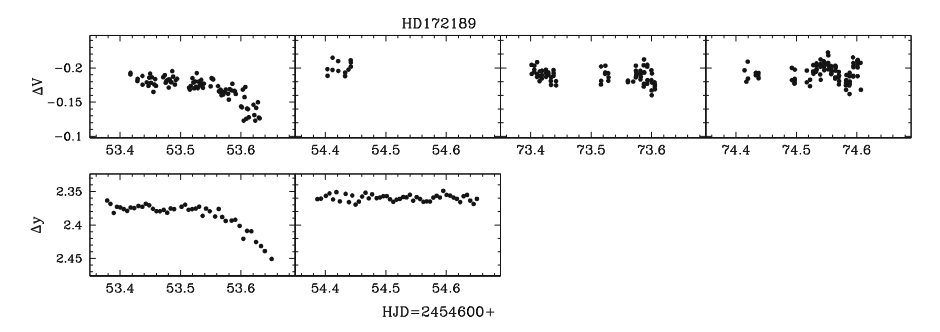


**Fig. 1** Light curves of the binary star HD 172,189 in the V-Johnson filter obtained with the T35 telescope (top) and in the y-Strömgren filter obtained with the 90-cm telescope (bottom)

### 2 Observations and Results

In order to test the precision of measurements, we observed the variable star HD 172,189, member of the open cluster IC 4,756. HD 172,189 (V = 8.85 mag, A2) is an eclipsing binary with a  $\delta$  Scuti pulsating component [1, 2]. This star is a perfect target for probing the accuracy of variability in and out of eclipse. The observations with T35 were performed during four nights using UVBI Johnson filters. In order to achieve a signal-to-noise of more than 1,000 in the V-filter, an integration time between 6 and 8 s was used depending on the night. Image reduction was carried out using the MaxIm DL package and HD 172,248 (V = 8.97 mag, B9) was choosen for the comparison star. The binary star was also measured during the first two nights using the *uvby* multicolour photometer at the SNO 90-cm telescope, with HD 172,365 ( $V = 6.40 \,\text{mag}$ , F8) as the comparison star. Figure 1 shows both light curves in the V-Johnson and y-Strömgren bands. As can be seen, despite the precision of y data (4–5 mmag) being around 4 mmag better than V data, the V measurements are good enough for detecting amplitudes up to a hundredth of a magnitude. Better results can be obtained if, in addition to observing with better atmospheric conditions, telescope tracking is optimized. To solve this problem, an external auto-guiding system is being implemented.

- 1. Creevey, O.L., Uytterhoeven, K., Martín-Ruiz, S., et al.: Astron. Astrophys. 507, 901 (2009)
- Martín-Ruiz, S., Amado, P.J., Súarez., J.C., Moya, A., Arellano Ferro, A., Ribas, I., & Poretti. E.: Astron. Astrophys. 440, 711 (2005)
- 3. Martín-Ruiz, S., Aceituno, F.J., Abril, M., et. al.: Advances in Astronomy, Article ID 869810 **2010**, 42, (2010)

# The Substellar Population of the $\sigma$ Orionis Cluster

Victor J.S. Béjar, Karla Peña-Ramírez, and Maria R. Zapatero Osorio

Abstract We present a deep I, Z photometric survey ( $I_{\rm compl} = 22\,{\rm mag}$ ) covering a total area of  $1.12\,{\rm deg^2}$  in the  $\sigma$  Orionis cluster. Using I, I-Z color-magnitude diagrams, we have selected 165 photometric candidates ( $I=16-24\,{\rm mag}$ ), which correspond to a mass interval from 0.11 down to 0.006  ${\rm M_{\odot}}$ . Using J-band photometry, we have found that 120 of 147 candidates within the completeness of the survey ( $\sim 80\%$ ) follow the infrared photometric sequence of the cluster; we will consider them as likely members. Using J, H, K-band data from UKIDSS and mid-infrared data from IRAC/Spitzer, we have found that 6-11% of the bona fide candidates have near-infrared flux excesses, and about  $34\pm 8\%$  show mid-infrared flux excesses, probably related to the presence of disks. We have determined that the mass spectrum from 0.11 to 0.013  ${\rm M_{\odot}}$  is a rising function that can be represented by a power-law distribution ( ${\rm dN/dm} \sim m^{-\alpha}$ ) with an exponent  $\alpha=0.4-1.1$ .

## 1 Search and Candidate Selection

We have obtained a deep IZ photometric survey ( $I_{compl} = 22$ ) covering a total area of  $1.12 \deg^2$  in the  $\sigma$  Orionis cluster (352 pc, 2–4 Myr; [4, 5]). Details of the observation can be found in Table 1. From I, I - Z color–magnitude diagrams, we have selected 165 candidates in the magnitude range I = 16–24. According to evolutionary theoretical models [1], they have estimated masses in the range of 0.11– $0.006 \, M_{\odot}$  for the age of 3 Myr. J-band photometry (See Table 1) of candidates within the completeness magnitude of the survey (I = 16–22 mag.) allows us, using

V.J.S. Béjar (⊠) · K. Peña-Ramírez

Instituto de Astrofísica de Canarias, La Laguna (Tenerife), Spain

e-mail: vbejar@iac.es

M.R.Z. Osorio

Centro de Astrobiología (CSIC-INTA), Torrejón de Ardoz, Madrd, Spain

V.J.S. Béjar et al.

Table 1         Observing log
-------------------------------

Telescopes	Instruments	Plate scale	Band	Exp. time	Observation dates
INT	WFC	0.33 ("/pix)	IZ	3×1,200 s	1998 Nov 12, 13
					1998 Sep, 1999 Jan-Dec,
TCS	CAIN-II	1.00 ("/pix)	J	60–1,000 s	2000, Jan, Feb
3.5 m CAHA	Omega'	0.40 ("/pix)	J	1,000 s	1998 Oct 16

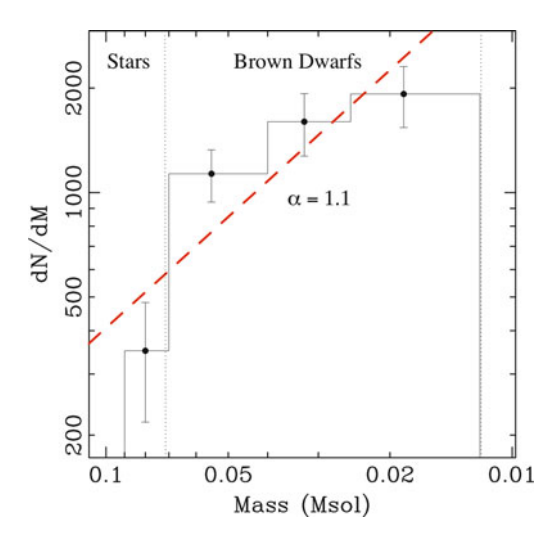


**Fig. 1** Mass spectrum (dN/dm) for the 3 Myr isochrone from the Lyon group. The best power-law fit (m<sup> $-\alpha$ </sup>) with  $\alpha = 1.1$  is represented by the red line. The separation between stars, brown dwarfs and planetary-mass objects is shown by vertical dashed lines. Data points error bars are Poissonian

an I, I-J color–magnitude diagram, to determine that 120 of 147 ( $\sim$ 80%) follow the infrared photometric sequence of the cluster and hence, they are considered as bona fide cluster member candidates.

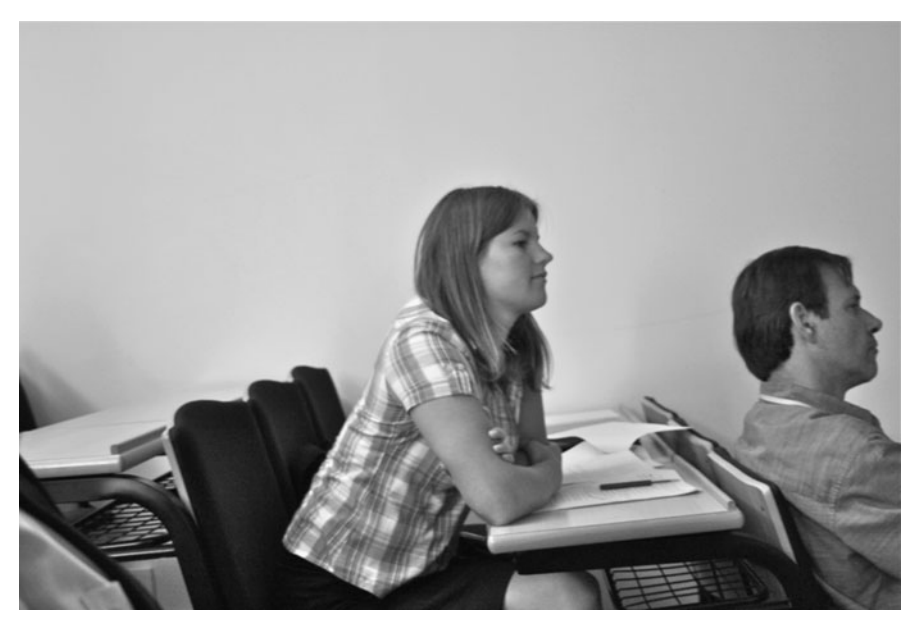
# 2 Disk Frequency and the Substellar Mass Function

Using the available *JHKs* photometry from the UKIDSS catalogue and 3.6, 4.5, 5.8 and 8.0  $\mu$ m photometry from the IRAC/Spitzer data, we have built different colorcolor diagrams to identify sources with flux infrared excesses. We found that 6–10 of 93 bona fide candidates present near-infrared excesses (6–11%) and 21 over 61 (34 $\pm$ 8%) show mid-infrared excesses. This flux excesses are probably related to the presence of disks, most of them transition disks.

We have obtained the mass spectrum (dN/dm) from the I-band luminosity function and the mass-luminosity relations given by theoretical models [1], using color and Teff-spectral type relations and bolometric corrections from [2, 3] to

transform Teff and luminosities into observables (see Fig. 1). The mass spectrum is a rising function from 0.11 to 0.013  $M_{\odot}$  and can be represented by a power law  $(dN/dm{\sim}m^{-\alpha})$  with  $\alpha=0.4-1.1$ .

- 1. Baraffe, I., et al.: Astron. Astrophys. 337, 403 (1998)
- 2. Golimowski, D.A., et al.: Astron. J. 127, 3516 (2004)
- 3. Leggett, S., et al.: Astrophys. J. 548, 908 (2001)
- 4. Perryman, M.A.C.: Astron. Astrophys. 323, L49 (1997)
- 5. Zapatero Osorio, M.R., et al.: Astron. Astrophys. 384, 937 (2002)



Edita Stonkutė and Eduardo Martín

V.J.S. Béjar et al.



Daniela Villegas



Hans Zinnecker